Recommendations for Surface Treatment for Virginia Inverted T-Beam Bridge System

Rebecka L. Gilbertson

Thesis submitted to the faculty of the Virginia Polytechnic Institute and State University in partial fulfillment of the requirements for the degree of

Master of Science
In
Civil Engineering

Carin L. Roberts-Wollmann, Chair
Matthew H. Hebdon
Ioannis Koutromanos

May 9th, 2018
Blacksburg, VA

Keywords: Inverted T-Beam, Accelerated Bridge Construction, Horizontal Shear, Concrete Surface Roughening, Push-off Tests

Recommendations for Surface Treatment for Virginia Inverted T-Beam Bridge System

Rebecka L. Gilbertson

ABSTRACT

This thesis investigates the impact of interface surface treatment methods for use in the Virginia Inverted T-Beam bridge system. The specific system consists of precast beams with thin bottom flanges placed next to one another, with a cast-in-place slab on top. Previous research has shown that the strength of this system after cyclic loading is highly dependent upon the shear strength of the interface between the precast and cast-in-place sections, especially for the adhesion-based connection configuration. The approval of this bridge system for use in bridges with high daily traffic volumes hinges on the verification of its strength and durability for a 50-year lifespan.

The shear strength of ten different surface textures was tested using push-off tests to determine which interface roughening methods would prove adequate for use in the bridge system. The strength was found to depend on both the amplitude and the geometry of the undulations on the beam-to-slab interface. Using this information, a texture was selected for a new trial of the adhesion-based connection configuration, and a test specimen was constructed. After completing cyclic loading to simulate the design life of the bridge, it was found that the system achieved a strength similar to previous monotonically loaded specimens. It was concluded that the bridge is safe for use in high daily traffic areas provided that a surface roughening with adequate shear strength is used.

Recommendations for Surface Treatment for Virginia Inverted T-Beam Bridge System

Rebecka L. Gilbertson

GENERAL AUDIENCE ABSTRACT

The Virginia Inverted T-Beam bridge system was initially designed to be more durable and economical than other types of bridges. The bridge is constructed by arranging prefabricated beams side-by-side across the span before placing fresh concrete overtop. In the most economical version of the system, the only connection between the beams is the newly placed concrete. For the beams and topping to act together, the bond between them must be strong. Roughening the surface of the prefabricated beams increases the strength of the bond, although different roughening patterns achieve different levels of strength. Past tests of the bridge system have utilized inadequate roughing patterns which lead to low bridge failure loads after many loading cycles. This low-cost configuration is currently only approved for use in low daily traffic areas.

The goal of this research was to determine a roughening pattern that would result in a high bridge failure load which would allow the low-cost configuration to be approved for high daily traffic areas. Several roughening patterns were investigated and the patterns producing the highest shear strengths were determined. The best pattern was chosen to be used for the bridge configuration and a sub-section of the bridge was constructed. This specimen was subjected to a loading protocol that simulated the traffic that an actual bridge would be subjected to over its life span. The failure load was then measured and found to be high enough to warrant the use of the specific system in high daily traffic areas.

ACKNOWLEDGEMENTS

Dr. Carin Roberts-Wollmann, thank you for your guidance throughout this project and my graduate level education. Dr. Matthew Hebdon and Dr. Matthew Eatherton, thank you for being wonderful resources throughout this project. Dr. David Mokarem, thank you for the tremendous amounts of help and advice that you have given me, both in the lab and in the classroom. Mr. Brett Farmer and Mr. Dennis Huffman, thank you for always lending me your experience and never getting too annoyed at my constant stream of questions. Mrs. Deborah Cooper, thank you for always being supportive, caring, and willing to help.

Logan Perry, Vishali Vasudevan, and every other graduate student I know: thank you for casting concrete, making rebar cages, assembling formwork, laughing with me, and being amazing people.

Mom and Dad, thank you for raising me to believe in myself and my dreams.

Austin, thank you for helping me water my concrete and for being my safe harbor.

TABLE OF CONTENTS

LIST OF FIGURES

LIST OF TABLES

CHAPTER 1: INTRODUCTION

1.1 Motivation and Background

Currently, one quarter of the 600,000 bridges in the United States are in need of repair or replacement, according to a report by the Federal Highway Administration (FHWA) [1]. Traditional forms of bridge construction, such as fully cast-in-place bridges, consist of construction done only on site which can lead to long periods of traffic disruption if a bridge needs to be replaced. Accelerated Bridge Construction (ABC) is a method by which the amount of time spent working on site is reduced, and the most common form of ABC utilizes Prefabricated Bridge Elements and Systems (PBES). PBES can be anything prefabricated from beams and deck panels to whole bridge substructures.

Some forms of PBES like adjacent box beams, which can be seen in Figure 1.1, have been known to have issues with joints between precast elements. The joints are a shear key initially filled with grouted that can crack over time under normal shear loads from traffic. These cracks allow for reduced load transfer between the elements, which can produce excessive deflections and lead to cracks propagating through the topping material. Cracking in the bridge driving surface allows for the ingress of chloride laden water with can lead to deterioration of the structure. There is a need for a form of PBES that is quick and easy to construct on site that does not suffer from these same joint issues.

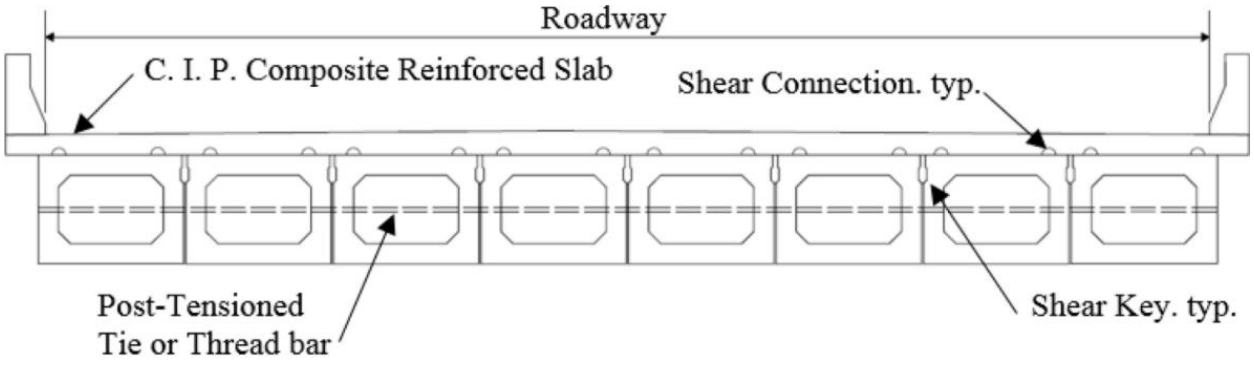

Figure 1.1: Adjacent box beam bridge design (Used with permission of ASCE [2])

In an attempt to discover new and better forms of PBES, the American Association of State Highway and Transportation Officials (AASHTO) sent a group of engineers to other countries in 2004 [3]. One system was observed in France; it was called the "Poutre-dalle," or beam-slab, and was an inverted T-beam system that also served as the formwork for the cast-in-place topping slab. The cross-section of this beam is shown below in Figure 1.2. Between 2005 and 2012, research was completed at the University of Minnesota to refine the system for use in short to medium span bridges. Alterations were made to the beam configuration, including exchanging the 180-degree hooks for 90-degree ones. The altered beam can be seen below in Figure 1.3. A total of twelve bridges were constructed in Minnesota and it was determined that the system was susceptible to shrinkage cracks, as well as transverse and longitudinal cracks. Construction of the beams with the protruding hooks was also expensive and difficult. It was concluded that the benefits did not outweigh the costs, and that more research and refinement was needed to make the system practical and economical.

Figure 1.2: Poutre-dalle system in France, 2004 (Used with permission of Matière [4])

Figure 1.3: Changes to Poutre-dalle done in Minnesota (Used with permission of MnDOT [5])

In 2012, work began at Virginia Polytechnic Institute and State University (Virginia Tech) to refine this system for the Virginia Department of Transportation (VDOT). Changes were made to the reinforcing arrangement and the straight webs with hooks were replaced with textured, sloped webs, creating the Virginia Inverted T-Beam Bridge system. Two variations of the system exist: one with the reinforcement within the web of each precast beam welded together to form a steel connection between bridge beams, and one without any connection between the webs, termed the "no-connection connection" [3]. This configuration will be referred to as the adhesion-based connection in this research. The dimensions and typical reinforcement specifications for the system can be seen in Figure 1.4.

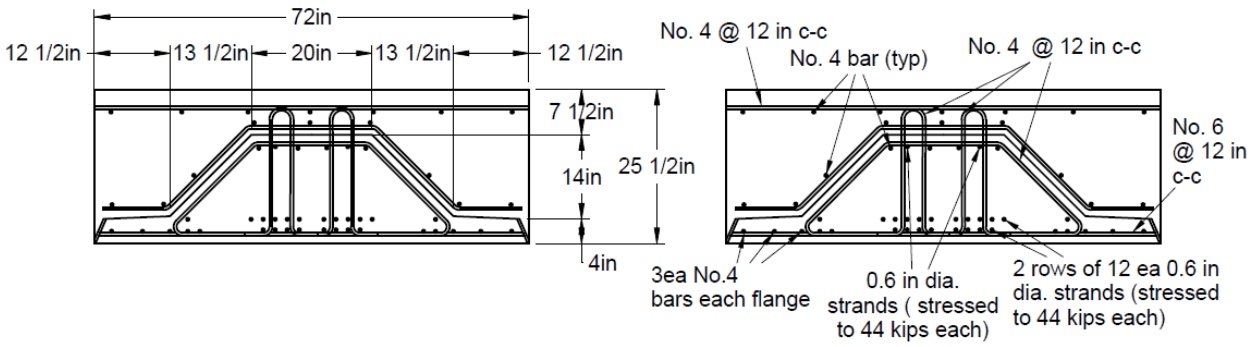

Figure 1.4: Virginia Inverted T-Beam bridge system dimensions (left) and reinforcment specifications (right) (Used with permission of Dr. Roberts-Wollmann [6])

Tests were done by Menkulasi in 2014 that verified that both variations performed adequately under monotonic loads, and as a result two bridges were built in Virginia using these systems. The welded flange system was approved for use in a high average daily traffic (ADT) bridge, but the adhesion-based connection was only approved for low ADT use as there were some questions raised about how the purely bond-based connection would fare after a design life's amount of loading cycles [7]. To verify the strength of the systems throughout the whole design life, cyclic tests were performed by Edwin in 2017 on both the welded connection and adhesion-based connection transverse sub-assemblage specimens. The results verified the strength of the welded connection post-cycling, but the performance of the adhesion-based connection was insufficient. The subpar performance of the specimen was attributed to inadequate surface roughening on the precast beams, and further research into surface roughening techniques for this system were recommended [8].

1.2 Objective and Scope

The objective of this research is to determine the characteristics of surface textures that provide adequate shear strength to the make the adhesion-based connection type of Virginia Inverted T-Beam bridge system viable for use in high ADT bridges. The scope of the research includes:

- Testing ten surface roughening configurations with 30 horizontal shear push-off tests
- Cyclic and ultimate failure load testing a transverse sub-assemblage Virginia Inverted T-Beam specimen, constructed using a confirmed surface roughening.

The surface roughening configurations that were selected reflect common textures that are currently in use by precast concrete manufacturers today. The types that were examined varied from raked, to formed, to exposed aggregate. Characteristics of each type, such as spacing and pattern, were modified as well. This allowed for a set of recommendations to be prepared on what surface roughening characteristics produce higher shear strengths. A surface texture that had proven strong through the horizontal shear push-off tests was then used to manufacture the sub-assemblage specimen. A cyclic test was done to simulate service level loading for the design life of the bridge, and then an ultimate failure load test performed to determine if the ultimate capacity of the bridge throughout its design life is adequate to be used for high ADT bridges.

1.3 Organization

The body of this report begins with a review of relevant literature, including any necessary background information, past research, and pertinent sections of building codes for both horizontal shear push-off tests and the Virginia Inverted T-Beam bridge system. Then the methods and materials used for construction and testing of both the push-off specimens and the sub-assemblage specimen are described. The results of both types of tests are then given and discussed. Finally, a summary of the previous sections is given along with conclusions and recommendations that were derived from the results.

CHAPTER 2: LITERATURE REVIEW

2.1 Organization

This chapter contains background information on both topics of this report: horizontal shear transfer in composite members and the Virginia Inverted T-Beam bridge system. The first section concerns horizontal shear transfer in composite members and contains a general description, relevant work, and a discussion of current recommendations for determining the adequacy of an interface roughening. The second section contains information regarding the Virginia Inverted T-Beam bridge system, including a discussion of the benefits of accelerated bridge construction, a history of the project, and a synopsis of previous work done to advance the system.

2.2 Horizontal Shear Transfer in Composite Members

Currently, only very basic recommendations are available that describe how to roughen concrete surfaces to achieve adequate shear transfer across cold-joint interfaces. This section describes current knowledge and research related to horizontal shear transfer to show that a need for an in-depth investigation into surface roughening characteristics is necessary. No research has been done thus far that compares the shear strength of different surface roughening types and characteristics without reinforcement across the shear interface.

2.2.1 General Description

The combination of precast girders and cast-in-place slabs, a composite system, is a popular way of constructing bridges as it allows for the use of precast concrete girders, which decreases the amount of time that it takes to construct a bridge as compared to fully cast-in-place bridges. Unlike other prefabricated systems, such as adjacent box beams, which suffer from issues originating from exposed deck joints, a composite system features a cast-in-place slab which limits the number of exposed joints between precast sections. An example of a composite system is shown in Figure 2.1.

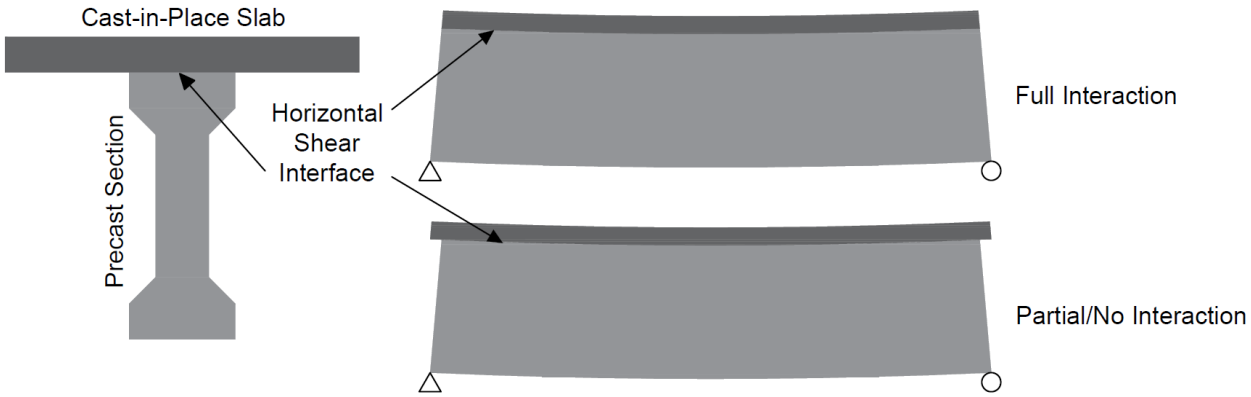

Figure 2.1: Composite concrete bridge system with horizontal shear interface

The weakest link in a composite system is at the cold-joint, which is prone to shear failures which are brittle and undesirable. To ensure that the composite bridge can perform as one section, the interface between the precast section and cast-in-place slab must have adequate ability to transfer shear. The shear stress at the can be calculated using elastic beam theory equation:

$$v_h = \frac{VQ}{Ib_v}$$

v_h = horizontal shear stress
V = vertical shear force at section
Q = first moment of area of the portion above interface with respect to the neutral axis
I = moment of inertia of the compostite cross section
b_v = width of interface

Force is transferred across the joint through a combination of cohesion between the surfaces, shear friction, and reinforcement dowel action. Different opinions exist on how to calculate the contributions of each component and building codes are currently used to determine the total horizontal shear capacity of an interface.

2.2.2 Relevant Work

This section describes completed work that pertains to horizontal shear transfer and push-off tests. The work done before 2011 was summarized from the descriptions provided in “Analysis of the AASHTO LRFD Horizontal Shear Strength Equation” (Lang, 2011). Lang had performed

research on past work to create a database of all known push-off tests performed by researchers and compare the results to predictions made using the AASHTO LRFD equation [9]. Work that was done during and after 2011 was summarized from the original source material. For all of the studies, a summary of the work is provided and further information can be found in the original publication.

Hanson (1960) performed 62 push-off tests and full beam tests to investigate the shear strength between precast beams and cast-in-place slabs. The characteristics of the push-off tests were varied in three categories: the number of stirrups across the interface, the use of adhesive bond agents, and the selected surface roughening. The types of surface roughening tested were smooth, rough, keyed, bare smooth aggregate, and bare rough aggregate. Hanson determined that how the precast interface is handled influences the baseline shear strength, and then increasing the amount of reinforcing adds strength. It was found that keys did not effectively change the shear strength [10].

Saemann and Washa (1964) studied the effect that the location of the neutral axis has on shear transfer, as well as other factors such as surface roughness, amount of reinforcement, shear keys, and concrete strength. Forty-two beams were constructed with different lengths and attributes, and tested in four-point bending. It was found that the shorter beams failed in shear and the longer ones in tension, except for the shorter beams with higher reinforcing ratios which failed in combined tension and shear. Saemann and Washa found that the surface roughness did not influence longer beams, but that on shorter beams a rougher surface translated to higher shear strength [11].

Hofbeck, Ibrahim, and Mattock (1969) produced 38 push-off tests to study how cracks along a shear interface affect the shear strength. The number of reinforcing stirrups across the interface varied from zero to six in number and from 1/8 in. to No. 5 in size, and the concrete strengths were also varied. Selected specimens were pre-cracked, and then the specimens were tested under incremental loading. Hofbeck, Ibrahim, and Mattock found that the shear strength mostly depended upon the amount of reinforcement across the interface, and that pre-cracking the specimens had a negative effect on the ultimate shear strength [12].

Mattock, Johal, and Chow (1975) studied the effect that the presence of a moment has on shear transfer across an interface. A total of 27 push-off tests were completed, some tested with applied moments and others with pure tension. Mattock, Johal, and Chow found that the presence of a moment does not affect the shear transfer across an interface if reinforcing steel is present in the tension zone. The research suggested that the shear capacity could be accurately approximated by two different equations but that both should be limited to a maximum of $0.3f'_c$ [13].

Mattock, Li, and Wang (1976) investigated the effect of lightweight concrete on the horizontal shear capacity of a specimen. Several types of lightweight concretes were tested as well as the strength of the concrete, amount of reinforcing across the interface, and if the specimen was pre-cracked or not. Mattock, Li, and Wang found that lightweight concretes have less shear capacity than normal weight concrete, and that the type of lightweight concrete does not matter. Equations different from those for normal weight concrete were recommended for use with lightweight concrete [14].

Walraven and Reinhardt (1981) aimed to refine finite element models to correctly model shear interactions. A set of experiments were completed to determine the effects of reinforcing ratio, reinforcing bar size, angle of reinforcing, surface roughening, and concrete strength. All the specimens were pre-cracked along the interface and tested vertically. Walraven and Reinhardt determined that the size of bar did not affect the shear strength, only the reinforcing ratio matters, and that the ideal angle for the reinforcement was 135 degrees [15].

Bass, Carrasquillo, and Jirsa (1989) studied how varying different aspects of a shear interface would affect shear transfer under cyclic loading. 33 push-off tests were constructed with both sides placed at separate times, and the varied aspects were the interface treatment, the amount and geometry of reinforcing across the interface, and the concrete strengths on either side. Five different interface treatments were used: untreated, heavily sandblasted, chipped, shear keys, and epoxy bonding. Bass, Carrasquillo, and Jirsa found that shear strength increased as the amount of

reinforcement and embedment depth increased, but that the type of interface treatment did not influence the shear strength at displacements over 0.2 in. [16].

Loov and Patnaik (1994) attempted to determine if the ACI shear equation could be streamlined and did so by completing 16 beam tests with varied concrete strength, clamping force, and flange length. The beams were constructed to have a precast section with a roughened surface and a cast-in-place slab. The clamping force was achieved by altering the amount of steel and width of the web. The single point loading tests produced mostly shear failures which allowed Loov and Patnaik to generate a new equation for shear capacity [17].

Choi (1996) examined how the use of powder-driven nails as a surface treatment affected the shear strength of the specimen. Four slabs were constructed as test specimens, with the interface sandblasted to various degrees and between zero and two nails installed in the surface. Choi concluded that the number of nails installed had a direct effect on the shear strength and that the level of sandblasting did not [18].

Kamel (1996) tested 63 push-off specimens as part of a study of composite bridge systems. The interface treatments that were tested included smooth debonded, smooth bonded, rough unbonded, rough bonded, and debonded keys. The interface was reinforced with deformed bar stirrups, threaded rod, or no ties. Kamel concluded that the deformed bars were more effective than the treaded rod, and that the debonding sealant did contribute to an increase in shear strength resulting from additional adhesion [19].

Valluvan, Kreger, and Jirsa (1999) performed a total of 16 push-off tests to examine how well the ACI shear equation estimates shear strength for precast surfaces with cast-in-place slabs. The amount of reinforcing, level of normal force, and concrete strength were varied. Loading was either simple ultimate failure testing or cyclic. Valluvan, Kreger, and Jirsa found the ACI equation to be very conservative where sustained normal force was provided and so a new equation was suggested [20].

Patnaik (2001) examined the applicability of the ACI shear equation in predicting the shear capacity with a smooth interface. A total of 24 beams of two types were tested: T-beams and rectangular beams. The concrete strength and the amount of reinforcement were varied within the specimens. The beams were loaded at a single point in the center of the beam and tests revealed that the strength of the concrete had an inconsequential effect on the shear capacity, but the amount of reinforcing across the interface did. Patnaik suggested equations for the calculation of shear capacity for smooth interfaces [21].

Kahn and Mitchell (2002) investigated the applicability of the ACI building code shear friction equation for high strength concrete. Fifty push-off tests were constructed with varying interface conditions (un-cracked, pre-cracked, and cold-joint smooth or roughened), different high concrete strengths, and between zero and eight legs of No.3 size stirrups. Kahn and Mitchell concluded that the ACI equation was conservative for high strength concrete and proposed an alternative equation that is more accurate for high strength concrete [22].

Kahn and Slapkus (2004) studied the shear interface of high strength T-beams with precast webs and cast-in-place flanges. The webs were all constructed of 12,000 psi concrete with exposed aggregate interface treatment and between five and seven stirrups. The flanges were constructed of either 7,000 psi or 11,000 psi concrete, and it was found that all the beams with lower strength concrete flanges failed in shear, while the beams with higher strength failed in flexure. Kahn and Slapkus found that the AASHTO shear equation underestimated the shear strength by more than six times [23].

Banta (2005) investigated the performance of the shear interface between ultra-high-performance concrete (UHPC) and lightweight concrete, placed at separate times. Two aspects of the 24 push-off specimens were varied: the interface treatment and amount of reinforcement present across the interface. Up to six legs of No. 3 reinforcing bars were across the interface of each specimen, and one of four interface treatments was used (smooth, keyed, deformed, or chipped). During testing, the horizontal load was applied gradually and a large concrete block was used to produce the necessary normal force. Banta concluded that the chipped surface was the best interface treatment of the four tested [24].

Scott (2010) examined how the use of different concrete densities affects the shear strength with 36 push-off tests. Some specimens had lightweight concrete used for the bottom (precast) section and the top (cast-in-place) section, whereas others only had a lightweight top or were all normal weight concrete. All specimens had a raked interface and the reinforcing ratio was varied. Scott observed that specimens with lightweight concrete had higher cohesion values than normal weight specimens, but that specimens that were all normal weight concrete had higher post-fracture strengths than specimens with any lightweight concrete if reinforcement was provided [25].

Sells (2012) researched the effects that utilizing self-consolidating concrete could have on the shear strength of precast members. Twenty push-off tests were constructed to test different concrete type, concrete strength, several aggregates, and percentage of the volume of aggregate. Both conventional concrete specimens and self-consolidating concrete specimens were created with each aggregate type and strength. All the specimens were cast monolithically and did not have reinforcing across the shear interface. The specimens were tested vertically and it was found that the compressive strength of the concrete had a small effect on the shear strength. Sells concluded that the type of aggregate had the largest effect on shear strength. It was also found that with higher strength concrete, aggregate interlock contributes less to the horizontal shear strength as the initial crack propagates through the aggregate as the paste can be stronger than the aggregates themselves. Ultimately, Sells determined that self-consolidating concrete does have adequate shear strength for precast sections [26].

Shaw (2013) studied how lightweight concrete alters the shear strength that can be achieved across a cold joint interface. Thirty-six push-off specimens were tested with various concrete unit weights, concrete strengths, and either a smooth or roughened interface. All specimens were constructed with the same amount of reinforcing steel across the interface. The accuracy of both the ACI design equation and the PCI Design Handbook were tested as compared to the results of the tests. Tests were done with loading vertically and it was found that the flanges were susceptible to failing before the shear interface. A form of confinement for the flanges was developed, which used prestressing to constrict the flanges in both perpendicular directions to the load direction. After the addition of the prestressing, the flanges would not fail before the shear

interface. Shaw found that the unit weight of the concrete used to construct the specimen did not have a significant effect on the shear strength of the interface [27].

Krc (2015) investigated the effect that lightweight aggregates have on the shear strength between precast members and cast-in-place slabs. A total of 28 push-off tests were constructed, either cast in two phases with a cold joint or with both sides cast at the same time. Those specimens that were constructed in two phases had either a roughened interface or a smooth one, and those that were cast as one piece were either pre-cracked or left un-cracked prior to testing. The lightweight concrete used was either sand lightweight or all lightweight, and three different types of lightweight aggregates were tested: expanded shale, expanded slate, and expanded clay. Normal weight specimens were constructed as a control group. All specimens had the same reinforcing ratio across the interface. The specimens were loaded vertically with special care taken to confine the flanges as they were prone to premature failure with the selected testing setup. Krc determined that the specimens cast as one piece showed higher strength when a higher unit weight of concrete was used, independent of the pre-cracked attribute. It was concluded that specimens cast in two phases with roughened interfaces showed an increased shear strength with increasing unit weight, but that smooth interface specimens did not benefit from higher unit weights and had an overall lower shear strength [28].

Soltani (2016) researched a new procedure for calculating shear capacity as part of a larger report on horizontal shear. A four-point bending method was adapted for use to investigate horizontal shear interaction between precast members and cast-in-place slabs. Sixteen specimens were created, half in the classic push-off style and the other half in a V-notched style which would be tested in four-point bending. The interface for both specimen types was made to be 4 in. by 8 in. and each specimen was either made to have a smooth treatment or a roughened treatment that had a 0.25 in. amplitude. All specimens had 4 No. 3 bars across the interface. The push-off specimens were tested vertically, using an actuator to apply the load to one end and the floor as a reaction at the other. The v-notched specimens were also loaded vertically, with load points and supports points located such that no moment was produced across the interface. Soltani found that loading and applying normal force to v-notched specimens is more difficult than for push-off tests, but that the construction of the specimens was easier as the reinforcing

was much simpler. The shear strength values for both specimen types were measured to be within 5% for specimens with roughened surfaces [29].

2.2.3 AASHTO LRFD Bridge Design Specification

As of the eighth edition of the AASHTO LRFD Bridge Design Specification, section 5.7.4—Interface Shear Transfer—Shear Friction provides guidance for designers on how to design members for shear transfer across an interface. The following equation is given to calculate the shear strength, under the requirement that minimum shear reinforcement has been provided:

$$V_{ni} = cA_{cv} + \mu\left(A_{vf}f_y + P_c\right) \leq \min\begin{Bmatrix} K_1 f'_c A_{cv} \\ K_2 A_{cv} \end{Bmatrix}$$

V_{ni} = nominal interface shear resistance (kip)
c = cohesion factor*
A_{cv} = area of concrete considered to be engaged in interface shear transfer; = $b_{vi}L_{vi}$ ($in.^2$)
b_{vi} = interface width considered to be engaged in shear transfer (in.)
L_{vi} = interface length considered to be engaged in shear transfer (in.)
μ = friction factor*
A_{vf} = area of interface shear reinforcement crossing the shear plane within the area A_{cv}
f_y = yeild stress of reinforcement but design value not to exceed 60 (ksi)
P_c = permanent net compressive force normal to the shear plane; 0.0 if force is tensile (kip)
K_1 = fraction of concrete strength available to resist interface shear*
f'_c = specified 28day compressive strength of the weaker concrete on either side of the interface (ksi)
K_2 = limiting interface shear resistance*
$*$ −Value given for different interface characteristics

The cohesion and friction factors (c, μ, K_1, and K_2) are given for different interface characteristics. The values for many different scenarios are given in section 5.7.4.4 of the AASHTO specification; the scenarios for normal weight concrete are as follows:

For "a cast-in-place concrete slab on clean concrete girder surfaces, free of laitance with surface roughened to an amplitude of 0.25 in.":

$$c = 0.28\ ksi$$

$$\mu = 1.0$$

$$K_1 = 0.3$$

$$K_2 = 1.8\ ksi\ for\ normal\ weight\ concrete$$

For “normal weight concrete placed against a clean concrete surface, free of laitance, with surface intentionally roughened to an amplitude of 0.25 in.”:

$$c = 0.24\ ksi$$
$$\mu = 1.0$$
$$K_1 = 0.25$$
$$K_2 = 1.5\ ksi$$

For “normal weight concrete placed against a clean concrete surface, free of laitance, but not intentionally roughened”:

$$c = 0.075\ ksi$$
$$\mu = 0.6$$
$$K_1 = 0.2$$
$$K_2 = 0.8\ ksi$$

The values for “concrete anchored to as-rolled structural steel by headed studs or by reinforcing bars where all steel in contact with concrete is clean and free of paint” were not included in this section [30].

2.2.4 ACI 318

As of the 2014 version of ACI 318 “Building Code Requirements of Structural Concrete”, the only guidance for designers on how surface treatment affects the horizontal shear capacity of a section is in Table 16.4.4.2 – Nominal horizontal shear strength. The table allows that if a section has more shear reinforcement across the interface than minimum and that the cast-in-place “Concrete (is) placed against hardened concrete (that has been) intentionally roughened to a full amplitude of approximately ¼ in.” then the lesser result of the following two equations shall be used to compute shear capacity:

$$V_{nh} = \lambda\left(260 + 0.6\frac{A_v f_{yt}}{b_v s}\right) b_v d \ \ or \ \ 500 b_v d$$

$V_{nh} = nominal\ horizontal\ shear\ strength$
$\lambda = lightweight\ concrete\ factor$
$A_v = area\ of\ sheaer\ reinforcement$
$f_{yt} = tensile\ yeild\ stress\ of\ reinforcment$

$b_v = width\ of\ the\ concrete\ surface$
$s = spacing\ of\ reinforcement$
$d = distance\ from\ extreme\ compression\ fiber\ to\ centroid\ of\ tension\ reinforcement;\ \geq 0.8h$

This equation attributes 260λ psi to cohesion of the concretes if the precast interface has been roughened to a ¼ in. amplitude, but no guidance was provided about the frequency or shape of the grooves [31].

2.2.5 The fib Model Code for Concrete Structures

The 2010 version of the fib Model Code defines various was to determine the characteristics of surface roughening and then uses these to assign cohesion and shear friction values to each surface. In section 6.3, the code outlines two ways to determine the category of roughness that an interface falls under: mean roughness and mean peak-to-valley height. The mean roughness method compares the mean profile line, or the average height of the surface over the whole sample length, to the average deviation from the mean line, or the average of the absolute values of the deviation of the profile height from the mean line over the whole sample length. The mean peak-to-valley height averages the difference between the highest peak and lowest valley for several sample lengths. These methods place the surface roughness into one of four categories: very smooth, smooth, rough, and very rough.

Once a category has been determined, the following equation is used to determine the shear resistance of the texture:

$$\tau = \tau_a + \mu\sigma_c$$

$\tau = shear\ resistance$
$\tau_a = cohesion\ value$
$\mu = coefficient\ of\ friction$
$\sigma_c = confining\ stress\ (constant)$

For the cohesion value, rough surfaces are allotted a bond value between 1.5 and 2.5 N/mm2 (220 to 360 psi) whereas very rough surfaces are given between 2.5 and 3.5 N/mm2 (360 to 500 psi). The coefficient of friction given for the smooth category is between 0.5 and 0.7, rough is from 0.1 to 1.0, and very rough is from 1.0 to 1.4 [32].

2.3 Virginia Inverted T-Beam Bridge System

2.3.1 Accelerated Bridge Construction (ABC)

According to the Federal Highway Administration's (FHWA) 2011 publication, "ABC is bridge construction that uses innovative planning, design, materials, and construction methods in a safe and cost-effective manner to reduce the onsite construction time that occurs when building new bridges or replacing and rehabilitating existing bridges" [1].This method of construction aims at reducing total construction time and thus decreasing the period for which alternative traffic patterns are necessary. Reducing the impact of bridge construction is necessary as one quarter of the 600,000 bridges in the United States need some form of repair or replacement. The more bridges that can be constructed using ABC, the lower the onsite construction time and the less the overall disruption to traffic patterns [1].

The most common form of ABC is the use of Prefabricated Bridge Elements and Systems (PBES). The FHWA defines PBES as "structural components of a bridge that are built offsite, or near-site of a bridge, and include features that reduce the onsite construction time and mobility impact time that occur from conventional construction methods" [1]. PBES elements include bridge decks, beams, piers, and abutments/walls. PBES systems can range from superstructures (beam and deck combinations) to complete bridges with both superstructure and substructure. Constructing the elements or systems off site requires smaller traffic disruptions than fully cast-in-place methods and allows for increased levels of quality control. Limiting the amount and difficulty of work necessary to install the PBES elements or systems is a key to diminishing onsite construction time even further [1].

2.3.2 Project History

The information in this section was obtained from Fatmir Menkalasi's report titled "The Development of a Composite Concrete Bridge System for Short-to-Medium-Span Bridges," published in 2014 [3]. A more in-depth history can be found in the original publication.

Tasked to explore what types of PBES were being used in other countries, AASHTO sent a team of engineers to Japan and Europe in 2004. A system called the Poutre-Dalle (meaning beam-

slab) was being used in France at the time. It combines precast inverted T-beams with a cast-in-place slab. Figure 2.2 shows the inverted T-beam portion of the system. The beams are placed adjacently such that there is no gap between the flanges, allowing for the beams to simultaneously be formwork for the cast-in-place slab. The cast-in-place slab is connected to the precast beams through the hooked reinforcing bars that extend over the flanges of the inverted T-beams, thus the system acts as a composite slab after completion. This system eliminates the issue of reflective cracking due to concentrated loading that afflicts other systems in use for short-to-medium span bridges.

Figure 2.2: Poutre-Dalle (beam-slab) bridge system seen in France in 2004 (Used with permission of Matière [4])

After the tour, a Poutre-Dalle inspired system was used in Minnesota to construct two bridges. Engineers exchanged the 180° hook bars for 90° hooks that allowed for the installation of a reinforcing cage with longitudinal reinforcement above the joint, shown below in Figure 2.3. From 2005 to 2012, research was performed at the University of Minnesota to improve the performance with respect to surface cracking. By 2012, a total of twelve bridges had been constructed in Minnesota. The system was shown to be susceptible to shrinkage cracking as well as longitudinal and transverse cracking, although it performed much better than other systems with respect to reflective cracking. The conclusion of the work was that the difficulty of

constructing precast sections with transverse reinforcement protruding from the flanges was not worth the small increase in performance that is gained, and thus more research was recommended.

Figure 2.3: Minnesota inverted T-beam with 90-degree hooks and longitudinal reinforcing cage above joint (Used with permission from MnDot [3])

2.3.3 Most Recent Work

Menkulasi

Menkulasi (2014) performed ultimate failure load testing on transverse sub-assemblage specimens with varied cross-sectional shapes and connection type between precast sections. The cross-sectional shape used in the Minnesota bridges, with vertical webs, was tested alongside a second shape, with tapered webs which is shown in Figure 2.4. It was hypothesized that the

tapered sides would provide a higher bond strength between the precast section and the cast-in-place slab. The hope was that, by increasing the bond strength, the 90-degree hooked bars would no longer be necessary, thus making construction of the inverted t-beams much easier and cheaper. The connection types tested were straight sided webs with hooked bars, tapered webs with welded flanges, and tapered webs without welded flanges, termed the "no-connection connection" or adhesion-based connection. The tapered webs were intentionally roughened with a straight-sided texture to a ¼ in. amplitude.

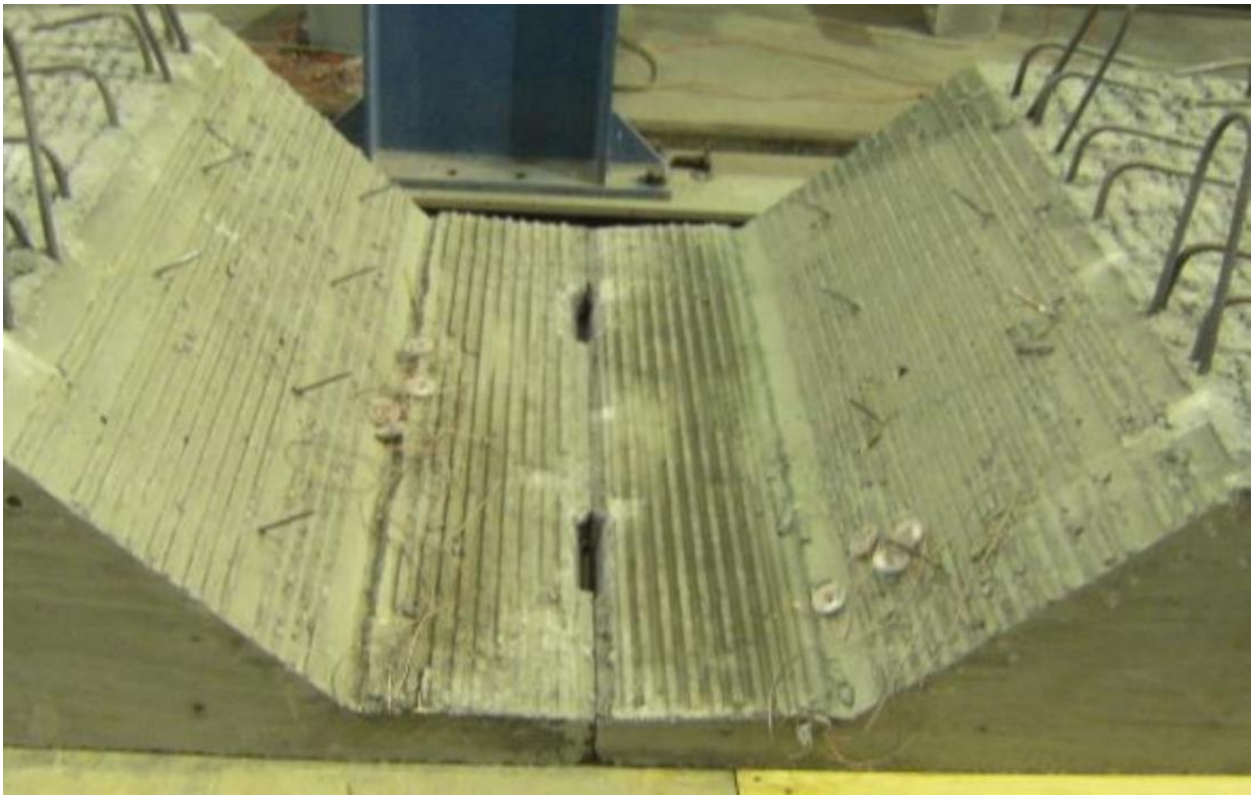

Figure 2.4: Inverted T-Beam with tapered webs (Used with permission of Menkulasi [3])

Testing revealed that all specimen configurations "performed well at service load levels" as they all had cracking loads well above the 25 kip threshold [3]. The specimens cracked as similar loads, even the one relying solely on concrete bond to provide the precast to cast-in-place connection. The ultimate failure load values and profiles of the specimens were varied. The highest load achieved was 300 kips by the specimen with welded flanges, and the lowest was 90 kips by the adhesion-based connection specimen. Despite achieving a lower load than the welded connection, the adhesion-based connection did achieve an adequate failure load, and it was

decided that further iteration of this connection type would be beneficial. By altering the reinforcing steel arrangement within the precast and cast-in-place members, a much higher ultimate load of 240 kips was achieved, proving that the cost-effective adhesion-based connection is sufficient under monotonic loads. Cyclic testing was recommended to determine if repeated loading could result in cracks that would change the performance of the adhesion-based connection [3].

Edwin

Edwin (2017) carried out cyclic testing followed by ultimate failure load testing on one welded connection type and one adhesion-based connection type inverted T-beam sub-assemblage. The objective of these tests was to prove that the adhesion-based connection would still perform adequately in large loading scenarios despite possible damage caused by a 50 year design life on a high average daily traffic (ADT) volume bridge. A total of 3,650,000 cycles of 30 kips were applied to simulate 200 fully loaded semi-trucks per day, which is consistent with VDOT statistics for high ADT bridges. These cycles were performed at 2 Hz and the applied load had a minimum of 10 kips to reduce the amount of vibrations generated by the loading. Both specimens were constructed identically other than the reinforcing and procedures that are necessary to achieve either connection type. A cross-hatch type surface texture, shown in Figure 2.5, was selected to be applied to the sloped web and flange sections of the precast members as it could potentially provide adequate shear strength in two directions.

Figure 2.5: Cross hatch surface roughening constructed for both cyclic tests performed by Edwin (Used with permission of Edwin [8])

Some issues occurred during construction, such as concrete with inadequate strengths and failure of formwork during concrete placement, though the main concern had to do with the forming of the surface texture. The decision was made to cut the texture into plywood sheeting and then cover the plywood with plastic sheeting before casting to make the formwork removal easier. After removal, it was found that the plastic had rounded out the edges of the texture, making the corners less angular. Testing revealed that the adhesion-based connection specimen had a lower cracking load, 40 kips, and a lower ultimate load, 63 kips, than those tested by Menkulasi in 2014, possibly due to the smooth surface texture. For the welded connection specimen, cracking began at 100 kips and ultimate failure was at 194 kips, also much lower than that tested previously by Menkulasi. It was theorized that the surface texture created was inadequate and could have caused both specimens to have lower strength. Further research into what aspects of a surface texture affect its adequacy and retesting of the sub-assemblages was recommended [8].

CHAPTER 3: METHODS AND MATERIALS

3.1 Organization

This chapter describes the methods and materials used to construct and tests both the horizontal shear push-off specimens and the Virginia Inverted T-Beam sub-assemblage specimen. The push-off specimens will be discussed first, and the sub-assemblage specimen second. Details are included for both specimen types that relate to the surface treatments selected, specimen details and construction, and testing apparatus and sequence.

3.2 Horizontal Shear Push-off Specimens

3.2.1 Selected Surface Treatments

A total of 30 specimens were constructed with three specimens for each of the ten textures examined. Roughening type, spacing, and other characteristics were varied amongst the textures. Table 3.1 summarizes the selected surface textures and their corresponding characteristics. The name of the texture can be found in the first column, with the second stating the amplitude of the texture and the third stating the spacing between repeating features of the texture. Column four states, in the case of formed textures, the de-bonding agent used during the casting process. The last column lists the specimen names that are associated with that surface texture. The specimen names were created so that the information pertinent to each specimen would be easily discernable from the name. Figure 3.1 shows an example specimen name with each of the components labeled.

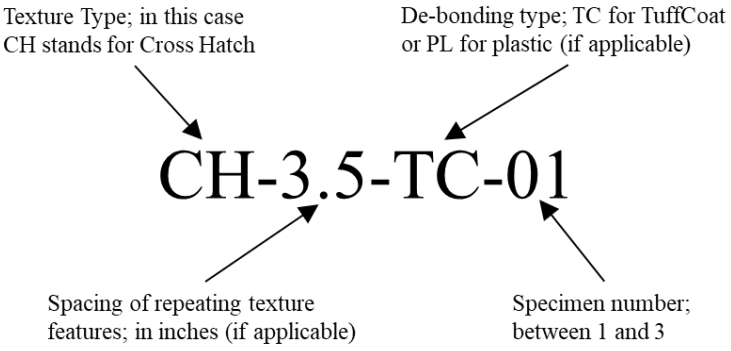

Figure 3.1: Specimen naming scheme explained

Table 3.1: Summary of selected surface texture attributes and specimen names

Texture Name	Amplitude (in.)	Spacing (in.)	De-bonding	Specimen Names
Raked	0.25	1	---	RK-1-01
				RK-1-02
				RK-1-03
		2	---	RK-2-01
				RK-2-02
				RK-2-03
		3	---	RK-3-01
				RK-3-02
				RK-3-03
Rectangular Grooves	0.25	1	TuffCoat®	RG-1-01
				RG-1-02
				RG-1-03
Trapezoidal Grooves	0.25	1.5	TuffCoat®	TG-1.5-01
				TG-1.5-02
				TG-1.5-03
		3	TuffCoat®	TG-3-01
				TG-3-02
				TG-3-03
Cross Hatch	0.25	3.5	TuffCoat®	CH-3.5-TC-01
				CH-3.5-TC-02
				CH-3.5-TC-03
			Plastic	CH-3.5-PL-01
				CH-3.5-PL-02
				CH-3.5-PL-03
Square Knobs	0.25	2.5	TuffCoat®	SK-2.5-01
				SK-2.5-02
				SK-2.5-03
Exposed Aggregate	Theoretical: 0.25 (Actual: 0.1875)	---	---	EA-01
				EA-02
				EA-03

Diagrams of the details for each texture are shown in Figure 3.2. The drawings include top-down views and cross-section views of each texture. Dimensions are given for all aspects necessary to reproduce the texture. There is only one type of cross hatch pictured as the formwork used for each is the same and all differences originate from the selected de-bonding method. The textures have been depicted with the amplitude formed by removing material from the concrete surface, although it is believed that forming the texture by raising parts of the surface is also valid. In the

production of the specimens for this work, some were produced by removing material, and others by raising the surface, depending on which was more easily achieved for that texture type. A more in-depth discussion of how each texture was produced for this research is provided within section 3.2.3 Specimen Construction.

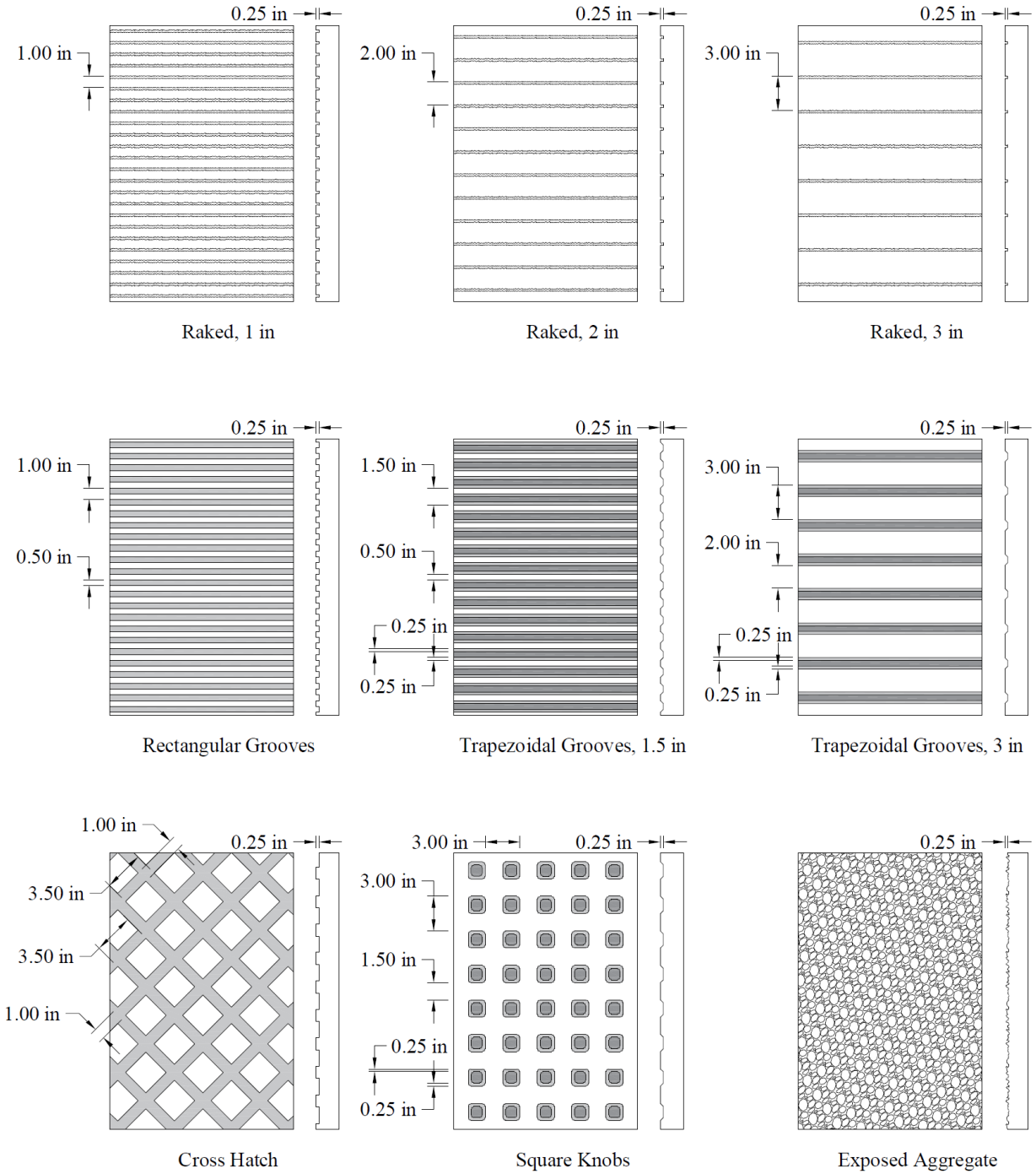

Figure 3.2: Details for selected surface textures

3.2.2 Specimen Detailing

The horizontal shear push-off specimens for this research were constructed in accordance with those built by Jana Scott at Virginia Tech in 2010 [25]. This configuration was selected as the laboratory technicians were experienced with how these types of specimens were best constructed.

Geometry

The specimens are comprised of two sections: a bottom that simulates a precast section, and a top that simulates a cast-in-place slab. Both sections are 16 in. thick "L" shapes with the same dimensions, shown in Figure 3.3. The two sections are joined along their long sides, or leg, leaving a 4 in. gap between the short side, or chimney, and the end of the leg, as shown in Figure 3.4. The interface between the two section measures 16 in. by 24 in. for a total of 384 in.^{2}.

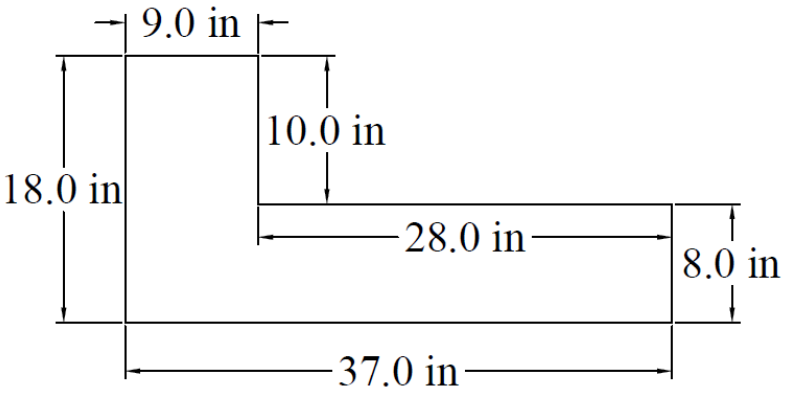

Figure 3.3: Dimensions of horizontal shear push-off specimen sections

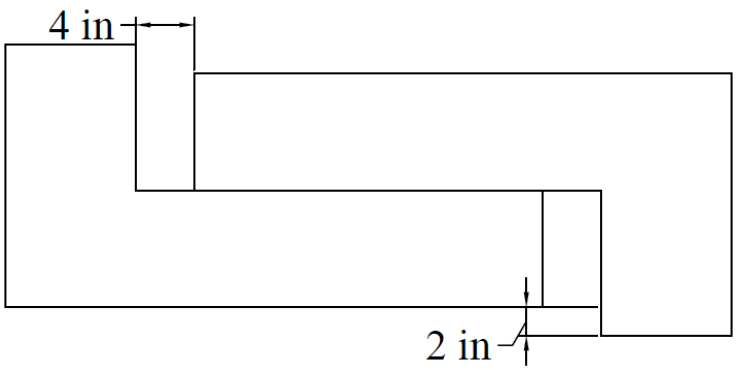

Figure 3.4: Dimensions of joined horizontal shear push-off sections

Reinforcement

There is no reinforcement across the shear interface of these specimens, so the only reinforcing present is each section's individual cage. Each cage is "L" shaped, just like the sections, and the cages for both the top and bottom are identical. Each cage is made up of two main bar assemblies, two center bars, three leg stirrups, and three chimney stirrups. The main and center bars are No. 4 bars, and the stirrups are No. 3 bars. A minimum of 1 in. of cover was provided to all bars and A615 Grade 60 reinforcing steel was used. Cross-sectional views of the reinforcing cages can be seen in Figure 3.5 and more details about the cages including dimensions and bend diameters can be found in Appendix A. This size of reinforcing used for the main bars in this cage has been reduced by one size from those used by Scott (2010) as the loads expected to be achieved in the testing process are much lower without reinforcement across the shear interface.

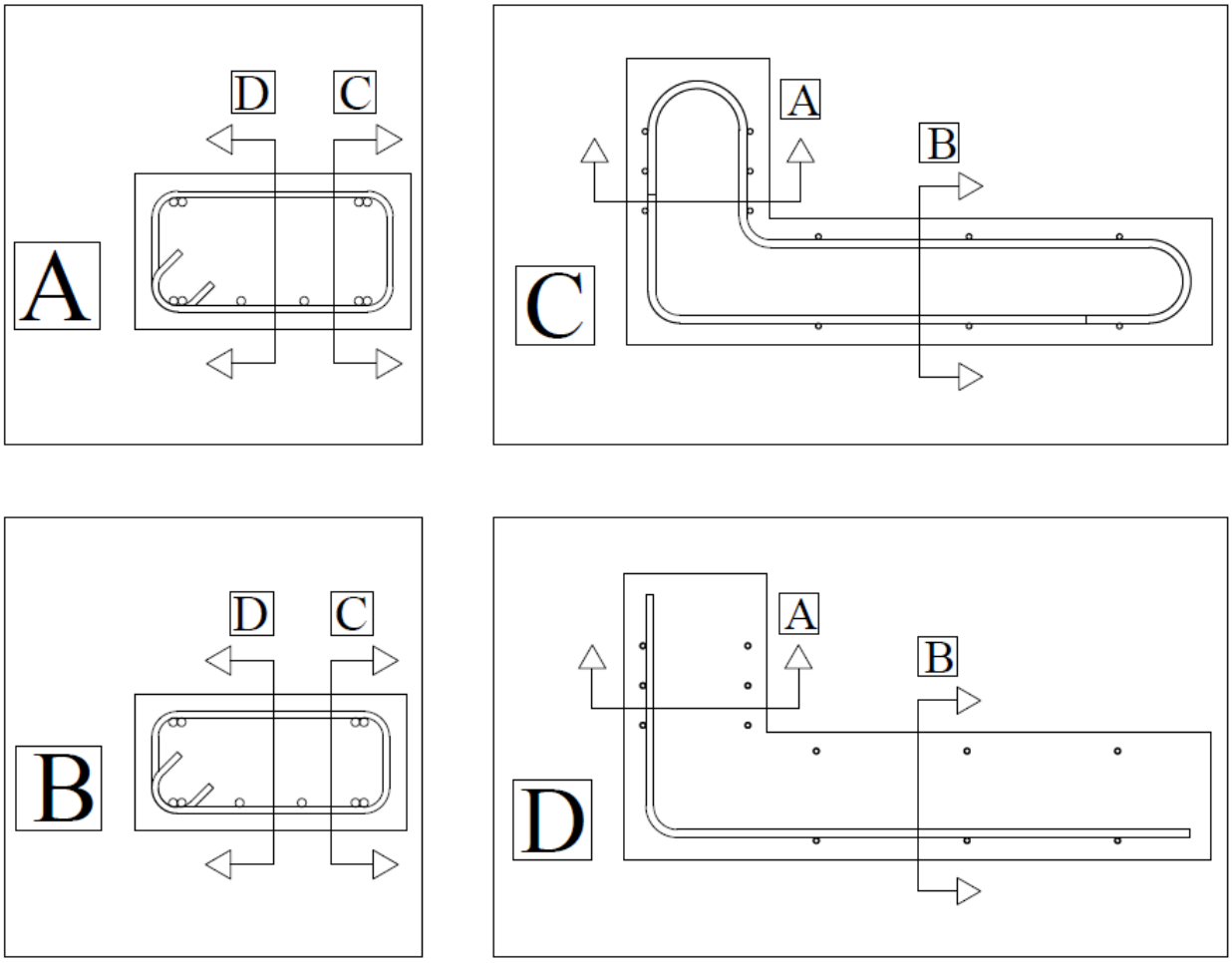

Figure 3.5: Cross-sectional views of the horizontal shear push-off specimen reinforcing cages

Concrete Specifications

The specimens are meant to simulate the precast concrete beams of the Virginia Inverted T-Beam bridge system, so the same concrete that was used for the precast and cast-in-place parts of the sub-assemblage tests performed by Menkulasi (2014) and Edwin (2017) were used for these specimens. The bottom section was specified to be constructed from an 8000 psi concrete mix. The concrete was ordered from Conrock, a local concrete provider, and contains silica fume and water reducer. The top section was specified to be constructed from a 4000 psi concrete mix, that was also obtained from Conrock. The 4000 psi mix contains fly ash as well as water reducer. Both mixes were specified to have at least 5% air content and between 5 and 7 in. of slump. Mix designs for both concrete mixes can be found in Appendix B.

3.2.3 Specimen Construction

The 30 specimens were cast in three batches, six specimens in the first batch and 12 in the second and third. Each batch of specimens required two concrete placement days, one for the bottom section and one for the top.

Formwork Details

The formwork was designed using pictures of formwork that was utilized by Scott (2010), which can be found in the original report [25]. The walls of the formwork are constructed from ¾ in. plywood that is supported by 2x4 supports, as seen in Figure 3.6. The top surface of the leg side of the bottom form was left open to allow for the formation of the textured surface. The gap between the end of the leg of the bottom section and the chimney of the top section was achieved by use of foam blocks. Foam insulation board was trimmed to size and stacked to achieve the 4 in. space. Foam was chosen as it is easy to trim and could be removed in chunks if it had adhered to the concrete. The use of wooden blocks to create the gap had been tested, but it was found that the wood had swelled during casting and became very hard to remove.

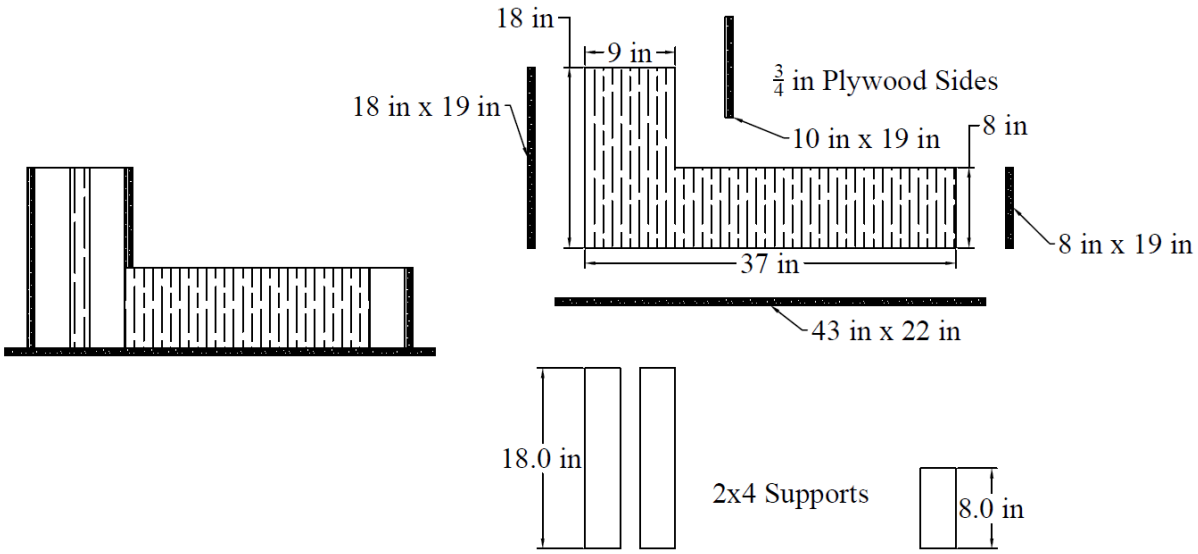

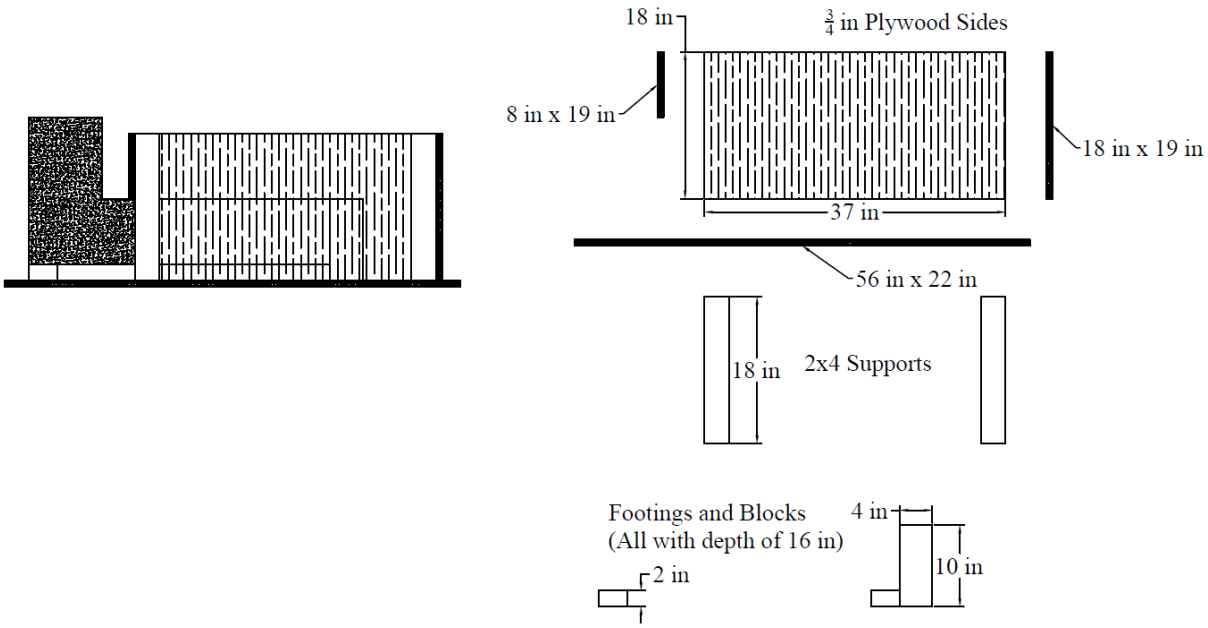

Figure 3.6: Formwork for horizontal shear push-off specimens

Construction Sequence

The first step taken in constructing the horizontal shear push-off specimens was to tie the reinforcing cages. This was done with steel tying wires using a manual wire twister. Both parts of the main bars were tied together first, and then they were connected to the leg stirrups. One chimney stirrup was installed so that then the center bars could be tied in, and then the last two chimney stirrups were connected. After the rebar cages were assembled, the formwork for the bottom section was constructed, making sure to thoroughly secure the plywood to the 2x4 supports. Any exposed screws were covered with duct tape to prevent concrete from filling the screw slots. The reinforcing cages were then installed in the forms using chairs to achieve the correct cover, and all the forms placed on plastic sheeting to protect the floor. Figure 3.7 shows the forms ready for cast day.

Figure 3.7: Forms and reinforcing for push-off specimens prepared for placement of bottom section concrete

The placement of the concrete for the bottom section took place in two steps. First, the leg portion of the form was filled and consolidated by use of a vibrator. The level of the concrete was ensured to be even across the exposed portion of the leg and within the chimney section. This lift of concrete rested for a period of no more than 20 minutes while work continued with the other specimens. In the case of specimens that were to receive formed textures, this time was used to install the textured plywood on the exposed surface of the leg. The chimney was then filled with concrete and consolidated, the extra pressure helping to force the concrete further into the textured plywood. In the case of specimens that were treated after casting, such as raked surfaces, the resting period helped the concrete to settle such that the chimney could be filled without concrete slumping out through the exposed top of the leg. After the chimney was filled for these specimens, all the exposed surfaces were finished with a trowel. More information about the formation of the surface textures is provided in the Surface Roughening Method section.

The bottom sections were moist cured for 7-days after the initial placement. A moist cure was achieved by laying wet burlap over each specimen after the concrete had reached initial set and rewetting it daily. Plastic was placed over the wet burlap to hold in as much moisture as possible. Once the moist cure had finished, the forms were removed from the specimens and they were then prepared for the placement of the second section.

The forms for the top section placement were constructed around the bottom section and the foam blocks inserted. To maintain clear separation between the top and bottom of the specimen, the forms for top section were tightened on to the bottom section by use of prestressed pencil rod. Small holes were drilled in both wide sides of the formwork and 3/8 in. rod was threaded through. It was determined that the area occupied by the foam would be the easiest place to thread the rod through as the foam was soft and it would not disturb the specimen itself. One end of the pencil rod was secured with an end cap, and the other end had an end cap placed, but not tightened, and then the hand tensioner placed. The hand tensioner grips the rod and is rotated along its central screw to increase its length, tensioning the rod. The end cap was then secured and the hand tensioner removed. The equipment used for prestressing the rods is shown below in Figure 3.8. Caulk was also used to seal the bottom section to the wooden formwork.

Figure 3.8: Equipment used for pretensioned pencil rod placement; (left) end caps with securing screw, (center) pencil rod inserted through end cap, (right) 1-ton hand tensioning system

The reinforcing cage was inserted into the form for the second section and chairs were used to obtain adequate cover. Figure 3.9 shows the forms ready for the second cast.

Figure 3.9: Forms and reinforcing for push-off specimens prepared for placement of top section concrete

The placement of the concrete for the top section consisted of wetting the previously placed concrete to standard surface dry, filling the form with fresh concrete, and consolidating. The exposed surface was troweled and then the seven-day moist curing process was commenced after initial set was reached. The formwork was removed after the moist cure was finished and the specimen was let to cure for at least 28-days before testing occurred.

Surface Roughening Methods

There were three categories of surface roughening that required different production methods in this research: raked surfaces, exposed aggregate, and manufactured textures. The raked surfaces were produced by way of handmade rakes constructed from 7-wire prestressing strand, as that is what is commonly done at precast concrete plants. The individual wires of the strand served as the tines of the rake and were spread out and trimmed to achieve the required spacing. When used, the rake was placed at one edge of the finished concrete surface prior to initial set and pulled across to create 0.25 in. grooves at the specified spacing. The three rakes that were constructed are shown in Figure 3.10.

Figure 3.10: Rakes made from 7-wire prestressing strand with one, two, and three in. spacing of tines (left to right)

The exposed aggregate surfaces were produced using a simple method that only requires a spray bottle of water and a soft brush. After the concrete surface was cast and finished, water was misted over the surface until the surface looked as if bleed water had collected on the surface. The surface was left to rest until there was no water sitting on the surface (concrete was still moist), and then the misting was repeated. These steps were iterated until the exposed surfaces that were not being treated had stiffened, approximately an hour. The surface was then rinsed heavily and softly brushed until the aggregate had been exposed. This process increases the water-to-cement ratio of just the very surface layer of concrete paste such that it is easily brushed away while the subsurface paste is unaltered. The possible amplitude of the exposed aggregate depends greatly upon the size of the aggregate as at least 50% of each aggregate needs to be anchored in concrete paste to create a sufficiently strong surface texture. Since the mix design used for the bottom section of the specimens in this research was a typical mix used by precast plants, the aggregate was smaller and only a 3/16-in. amplitude could be achieved.

The manufactured textures were produced using ¾-in. plywood that was carved with the desired pattern. Plywood sheets were cut to be large enough to cover the exposed surface area plus some overhang on all sides. The patterns were sketched out on the plywood, leaving a 4 in. gap that

corresponds to the area between the end of the top section leg and bottom chimney. A router was used to carve out the patterns and a combination of mortising and v-groove router bits, shown in Figure 3.11, were used to achieve the correct shapes.

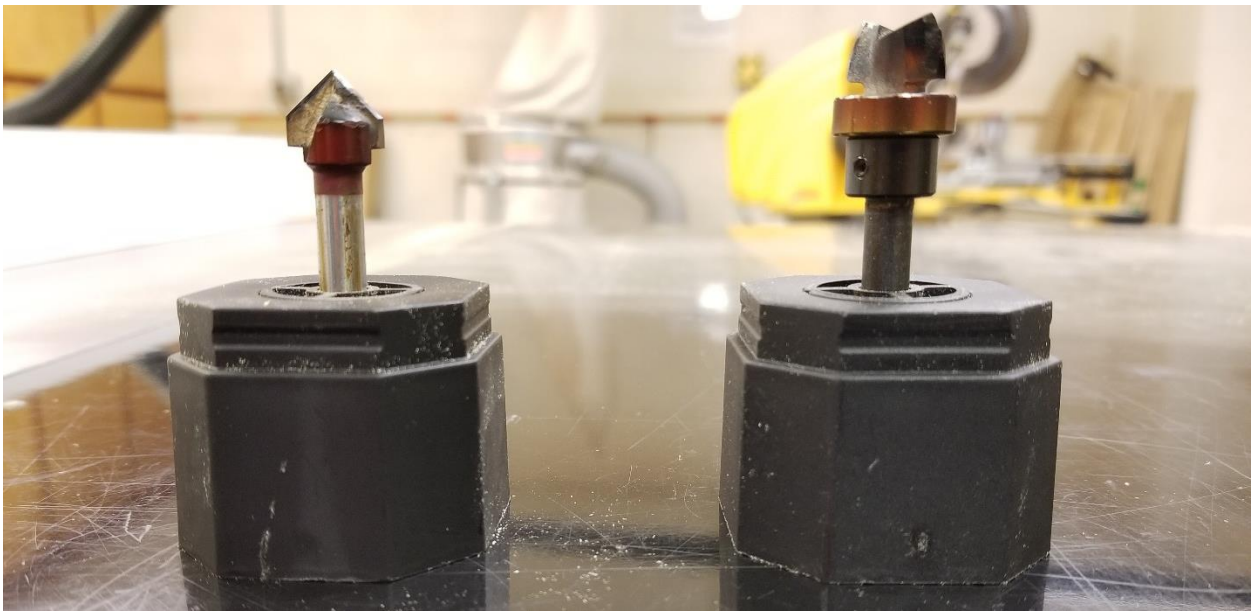

Figure 3.11: (Left) v-groove router bit, (right) mortising router bit

During casting, these patterned plywood boards were pressed into the exposed portion of the leg of the bottom specimen section to form the manufactured textures, but a de-bonding method was needed to help release the plywood from concrete after forming. The carved plywood on its own has open grains that allow for the ingress of wet concrete, resulting in a significant bond between the form and concrete which leads to difficult form removal. One method of closing off these open wood grains is to place plastic sheeting between the form and the concrete during placement. This method was used by Edwin (2017) and was found to produce the rounded textures that were believed to be the cause of a lowered shear strength in a Virginia Inverted T-Beam sub-assemblage test specimen [8].

An alternative method for closing off the wood grains was devised that uses TuffCoat® from Rhino Linings Corporation, a pick-up truck bed liner. The “elastomeric polyurea hybrid lining” is applied using an air sprayer and dries within minutes, according to the company’s specification sheet which can be found in Appendix C [33]. The coating comes in a dual cartridge containing two components that are combined in the mixing straw before being sprayed

onto the surface. The application temperature is important to the quality of the coating so it was found that the cartridge should be microwaved for 30 to 60 seconds, depending on the storage temperature, and shaken thoroughly before being applied. A uniform coating is key to achieving the best formwork release, so a twice-over approach was taken to ensure that all the corners in each textured surface had been covered. First, the coating was applied at a 45-degree angle to the surface where the plywood was set, careful to move the sprayer consistently to achieve a solid black coating where the spray could reach. Then, the coating was applied at a 135-degree angle to that same surface, coating any corners that had been hidden to the first spray. Before concrete placement, formwork release oil was applied to each coated texture. Figure 3.12 shows the equipment necessary for the application process and Figure 3.13 shows how the twice-over approach.

Figure 3.12: TuffCoat® application supplies; (top-left) TuffCoat® dual cartridge, (top-center) mixing straw, (top-right) air sprayer with air hose attachment, (bottom) full assembly

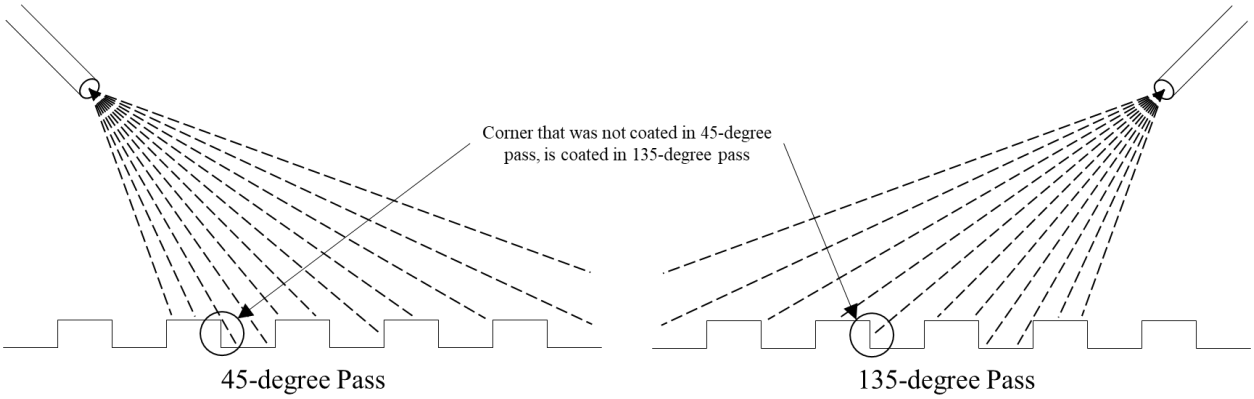

Figure 3.13: Method of applying TuffCoat® to coat all corners of textured plywood

Issues Faced During Construction

The first issue involved ill-consolidated concrete in the chimney sections of some specimens. The concrete that was delivered for the placement of the first set of bottom sections was already very stiff when it arrived, most likely due to the delivery being in the afternoon on a very hot summer day. Because of this, consolidating the concrete was very difficult especially while we were placing the concrete for the chimneys as they were last and the concrete had become more stiff as worked progressed. When the formwork was removed from the specimens, it was found that some of the chimneys had very severe honeycombing with exposed reinforcing and would be unusable for testing purposed. It was decided that the six specimens that had the worst honeycombing would be discarded, all of which were from two texture types, and reduce our initial scope from 36 specimens to 30 specimens. A few specimens needed patching with high strength grout, as shown in Figure 3.14, but the damage was concentrated on parts of the chimney that was not going to be in contact with the testing apparatus. The subsequent concrete deliveries were always scheduled in the morning as it was cooler then, to try to avoid issues with the concrete setting up quickly.

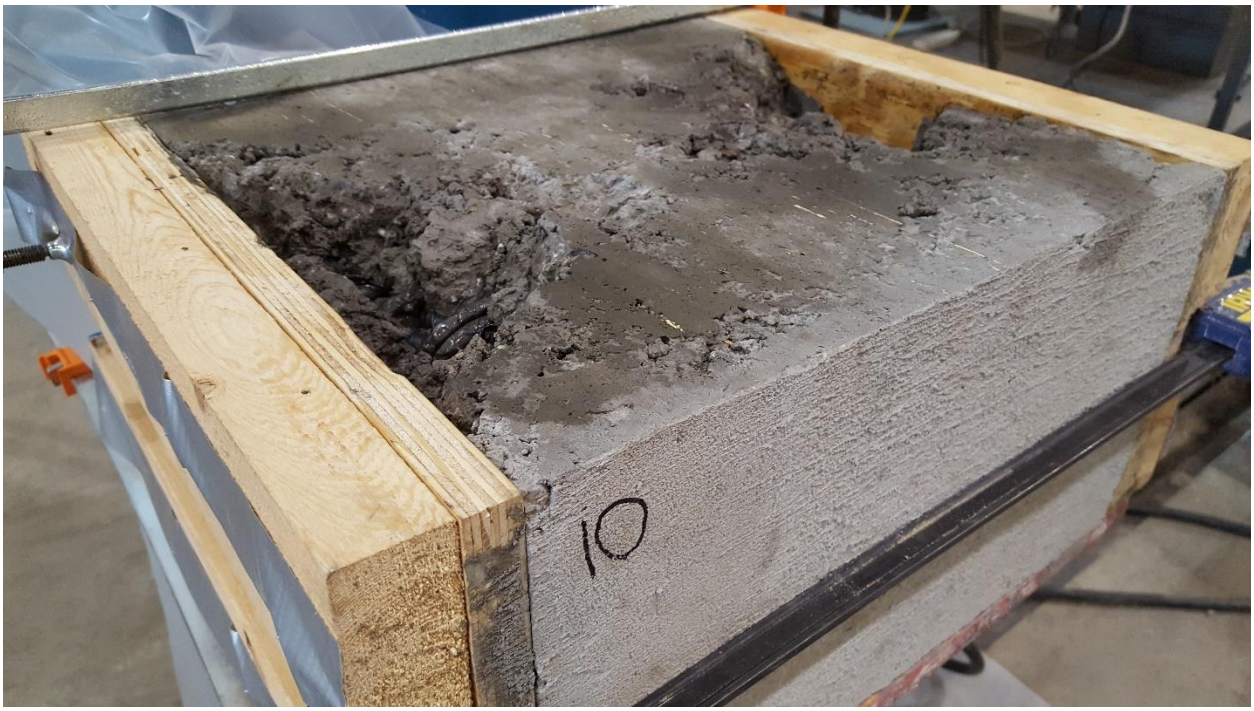

Figure 3.14: Specimen prepped for patching with high strength grout

The second issue was with the creation of the rectangular groove manufactured texture. In the past, this texture had been known to be very hard to produce cleanly with the best success taking place when the time was spent to chisel out the plywood form from the formed concrete. This method is very time consuming and was ruled out as a possible method for this research. It was hoped that the addition of a TuffCoat® surface was enough to create a clean removal, but it was not. Figure 3.15 shows the bottom section of a specimens during removal of the textured plywood. About half of each rectangular groove was torn off with the form, and the plywood was left behind in the other half. This occurrence is consistent with the other two specimens with this pattern. These specimens were not discarded as about 50 percent of the texture was still intact and the question was raised about how differently the damaged texture would perform from expected.

Figure 3.15: Result of removal of textured plywood form for rectangular grooves

3.2.4 Testing Apparatus

To test the horizontal shear strength across the interface of the specimens, two forces need to be generated: a lateral force and a normal force, as shown in Figure 3.16. The lateral force is applied directly in line with the interface on one end of the specimen and the other end is fixed against a support. The normal force is applied orthogonally to the interface over the length of the interface and is equal to 10 percent of the lateral force or expected shear strength. This force simulates normal dead and live loading on the interface and helps to compensate for any effects from eccentricity of the load.

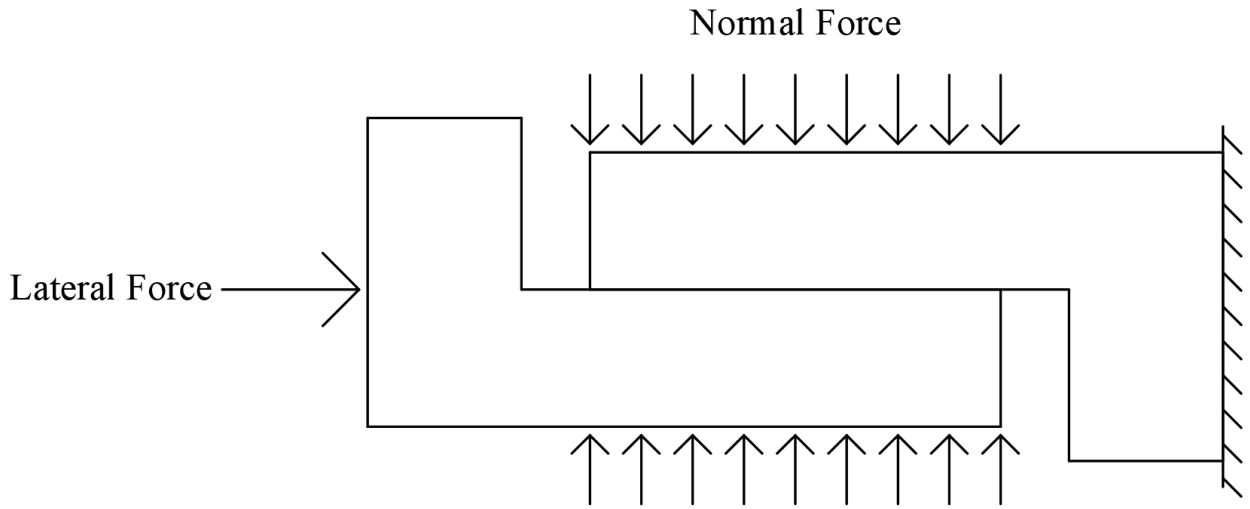

Figure 3.16: Loading on a horizontal shear push-off specimen during testing

The test set-up for this research uses a hydraulic cylinder to apply the lateral force and a steel harness for the normal force. To achieve the lateral force, an abutment was secured to the strong floor with eight 1 in. diameter A325 bolts and then a 200-ton Enerpac® RR-20013 hydraulic cylinder was bolted to the face of the abutment. The cylinder applies pressure directly to a 200 kip load cell which is suspended from the specimen by way of a fabricated steel "backpack". The bottom section of the specimen is resting on three 2 in. rollers which allow for movement of the bottom relative to the top during testing. The top section is resting against the other abutment, which was secured to the strong floor with eight 1 in. diameter A325 bolts. The set-up can be seen in Figure 3.17. The chimney of the top section is not in contact with the floor.

Figure 3.17: Horizontal shear push-off specimen testing apparatus

The normal force was created by a steel harness that was constructed of four one in. threaded steel rods and 2 in. x 1 in. x 0.1875 in. A36 steel channels welded in the configuration shown in Figure 3.17. Each rod had a strain gauge installed that was calibrated to associate the strain read by the gauge with the tension force in the rod. The rods were suspended between the top and bottom channels with a nut at either end, and these nuts were tightened to induce tension in the rods. They were tightened until one-quarter of the total normal force was generated in each rod. During the test, the change in the normal force due to dilation of the crack was tracked to ensure that large increases in force weren't occurring when the interface broke. To reduce any translation of the top channel in relation to the bottom channel, which would also result in an increase in normal force, greased plates were installed between the specimen and bottom channels to allow the channel to slide with the top channel during specimen failure. During testing it was found that the channels were excessively deflecting from the rod loads and so 3/8 in. plate was added to the top of each channel to make them rectangular tubes, which greatly increased the stiffness of the harness.

The instrumentation used for this test included the four rod strain gauges, the load cell, and four linear variable differential transformers (LVDTs) to measure the relative movement between the top and bottom sections. The LVDTs were mounted using two bracket pieces, which were attached by drilling into the concrete, inserting a wall hanging anchor, and then screwing the brackets into place. The bracket configuration was chosen specifically such that the instrumentation would not be crushed in the case of a large deformation. Figure 3.18 shows the LVDTs and how they were installed.

Figure 3.18: Horizontal Shear Push-off Specimen LVDT configuration and attachment method

3.2.5 Testing Sequence

After the specimen had been placed in the apparatus and instrumentation attached, the rods were tightened to the specified normal force. In this research, the shear strength of the specimens was assumed to be 150 kips, and so the applied normal force was 1.5 kips or 0.375 kips in each rod. Readings of instrumentation were commenced then the hydraulic cylinder was engaged with the load cell and specimen, and the piston extended gradually so that the load increased at an appropriate consistent rate. The specimen was loaded until the interface experienced shear failure, which was evident by both the loud popping noise heard and the sudden increase in displacement between the sections. After the shear failure, the cylinder was reengaged to determine the residual shear strength of the specimen and to observe if any dilation of the crack occurred. The cylinder was then disengaged and the interface of the failed specimen was inspected. Each test took on average five minutes from the first engagement of the hydraulic cylinder to final disengagement.

3.3 Virginia Inverted T-Beam Sub-Assemblage Specimen

3.3.1 Specimen Detailing

One Virginia Inverted T-Beam sub-assemblage specimen was constructed with the adhesion-based connection configuration that was tested by both Menkulasi (2014) and Edwin (2017). As explained in Menkulasi (2014), the sub-assemblage specimen was designed to test the connection between the precast beam's sloped sides and flanges and the cast-in-place slab [3]. A section was selected from a larger bridge assembly which included two precast beams, each with a corresponding wheel load, which can be seen in Figure 3.19. The details for the specimen were obtained from Edwin (2017) and the only alteration was to the surface roughening method selected for the shear interface, which was the 1.5 in. trapezoidal grooves [8].

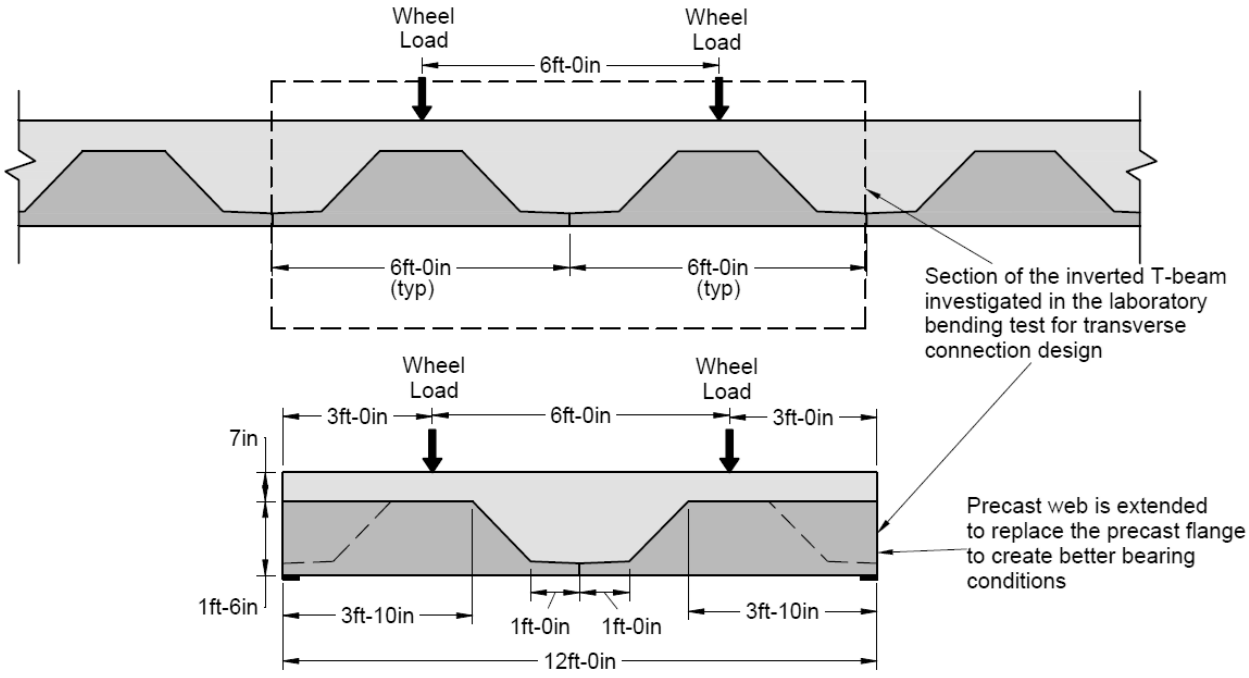

Figure 3.19: Virginia Inverted T-Beam sub-assemblage specimen as a section of a larger bridge assembly (Used with permission of Dr. Roberts-Wollmann [6])

Geometry

The completed specimen is 12 ft. long, 4 ft. wide, and 25.5 in. deep, and contains three distinct sections: two precast beams and a cast-in-place slab. The precast beams have been altered such that only one side of each has the sloped web and flange with texture, as only one interface

region is to be studied and altering the shape makes for easier construction. The specimen geometry is shown in Figure 3.20. When the beams are exposed to harsh weather conditions, a ¾ in. chamfer is included on either side of where the beam flanges join as drip guards to prevent chloride-laden water droplets from advancing along the underside of the beams and causing issues with corrosion. Drip guards are not necessary for the purposes of this research and so were not included in the precast beams created for the sub-assemblage specimen.

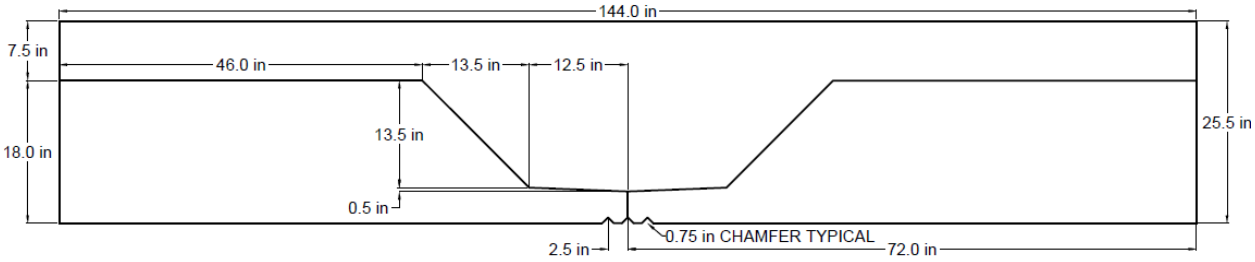

Figure 3.20: Dimensions of Virginia Inverted T-Beam sub-assemblage specimen sections (Used with permission of Dr. Roberts-Wollmann [6])

Reinforcing

The reinforcing design used in this research was consistent with that used by Edwin (2017) [8]. Three separate reinforcing cages were constructed for the specimen, two for the precast beams and one for the cast-in-place slab, which is shown in Figure 3.21. All reinforcement was A615 Grade 60. Reinforcing bar lifting loops were also included in the precast beam reinforcing cages that penetrated through the cast-in-place slab and stuck out from the top surface of the specimen so that it could be maneuvered using an overhead crane. The positions of the lifting loops are shown in Figure 3.22. Further information about the reinforcing details and quantities used can be found in Appendix A.

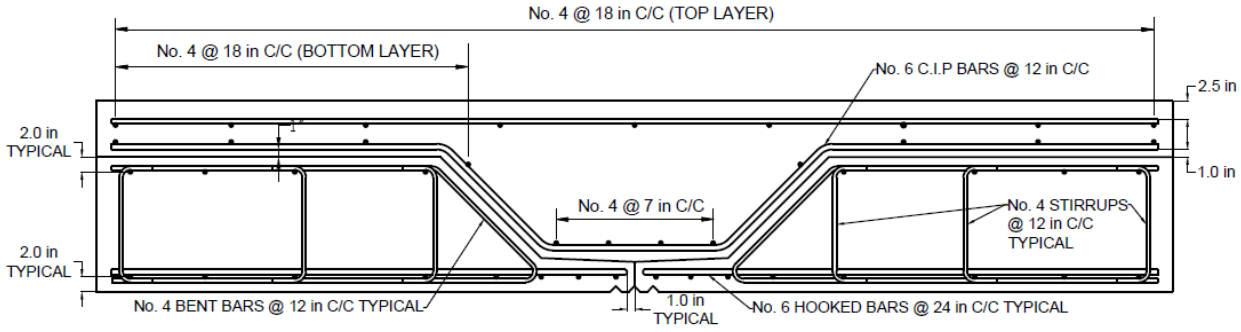

Figure 3.21: Reinforcing details for Virginia Inverted T-Beam sub-assemblage specimen (Used with permission of Dr. Roberts-Wollmann [6])

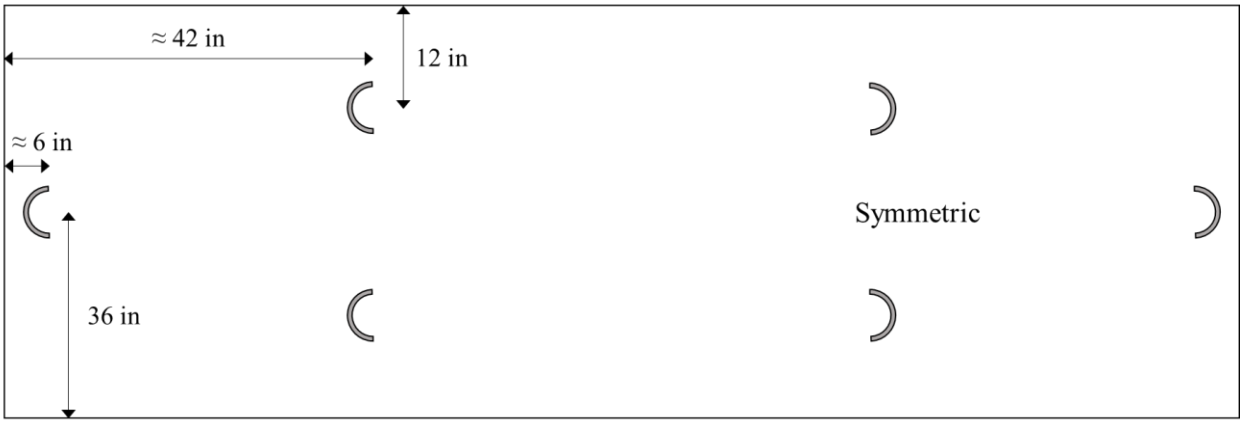

Figure 3.22: Location of lifting loops for Virginia Inverted T-Beam sub-assemblage specimen

Concrete Specifications

Due to issues with the quality of concrete that was received during the horizontal shear push-off specimen construction, the concrete supplier was changed for the sub-assemblage specimen. Chandler concrete provided both an 8000 psi mix for the precast beams and a 4000 psi mix for the cast-in-place slab. The 8000 psi mix contained slag cement as well as a high range water reducer, and the 4000 psi mix contained fly ash. Both mixes were specified to have at least 5% air content and between 5 and 7 in. of slump. Mix designs for both concrete mixes can be found in Appendix B.

Embedded Instrumentation

The instrumentation plan for this test was consistent with that of Edwin (2017). A total of six strain gauges were installed on the reinforcing cages of the sub-assemblage specimen, two in each precast beam and two in the cast-in-place slab. The strain gauges in the precast sections were located on the No. 6 hooked bars, 15.5 in. away from the end of the flange on the inner legs, and the strain gauges in the cast-in-place slab were on the bent bars, directly over the flange joint. The locations of each strain gauge can be seen in Figure 3.23. The strain gauges used were type WFLA-6-11-3LT gauges from Tokyo Sokki Kenkyujo Company. Installation of the gauges was consistent with the company's guidelines using cyanoacrylate adhesive. Extra protection was provided to the gauges as they can be easily damaged during concrete placement, especially when consolidation by vibrator is performed. The strain gauge wires were strung out of the

specimen by way of the rebar. The protection and wire stringing process is shown in Figure 3.24. Some of the strain gauge wires needed to be extended to reach the data acquisition system, so changes in gauge factor were accounted for using the equations provided by the manufacturer, which can be found in Appendix C.

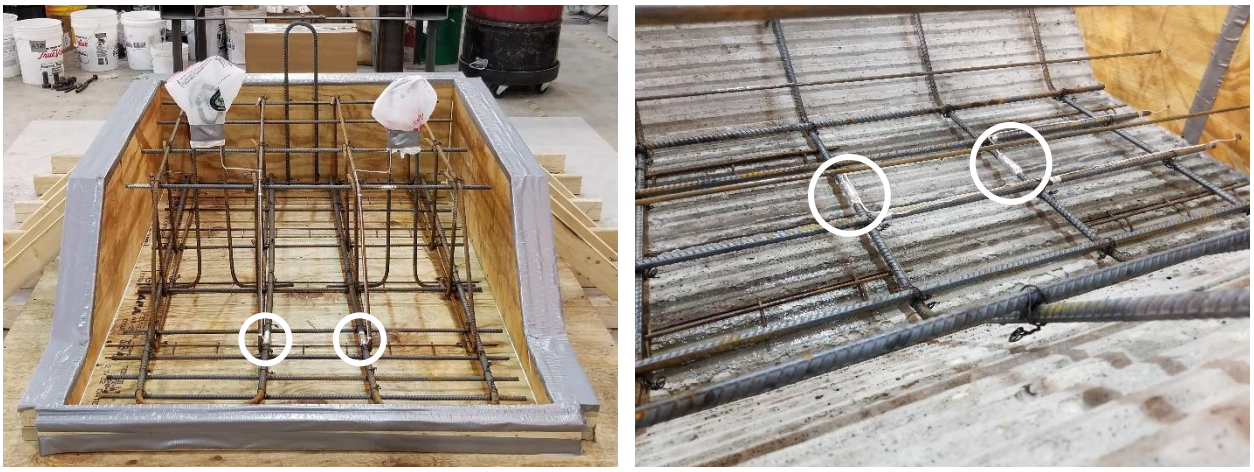

Figure 3.23: Locations of embedded strain gauges in Virginia Inverted T-beam sub-assemblage specimen

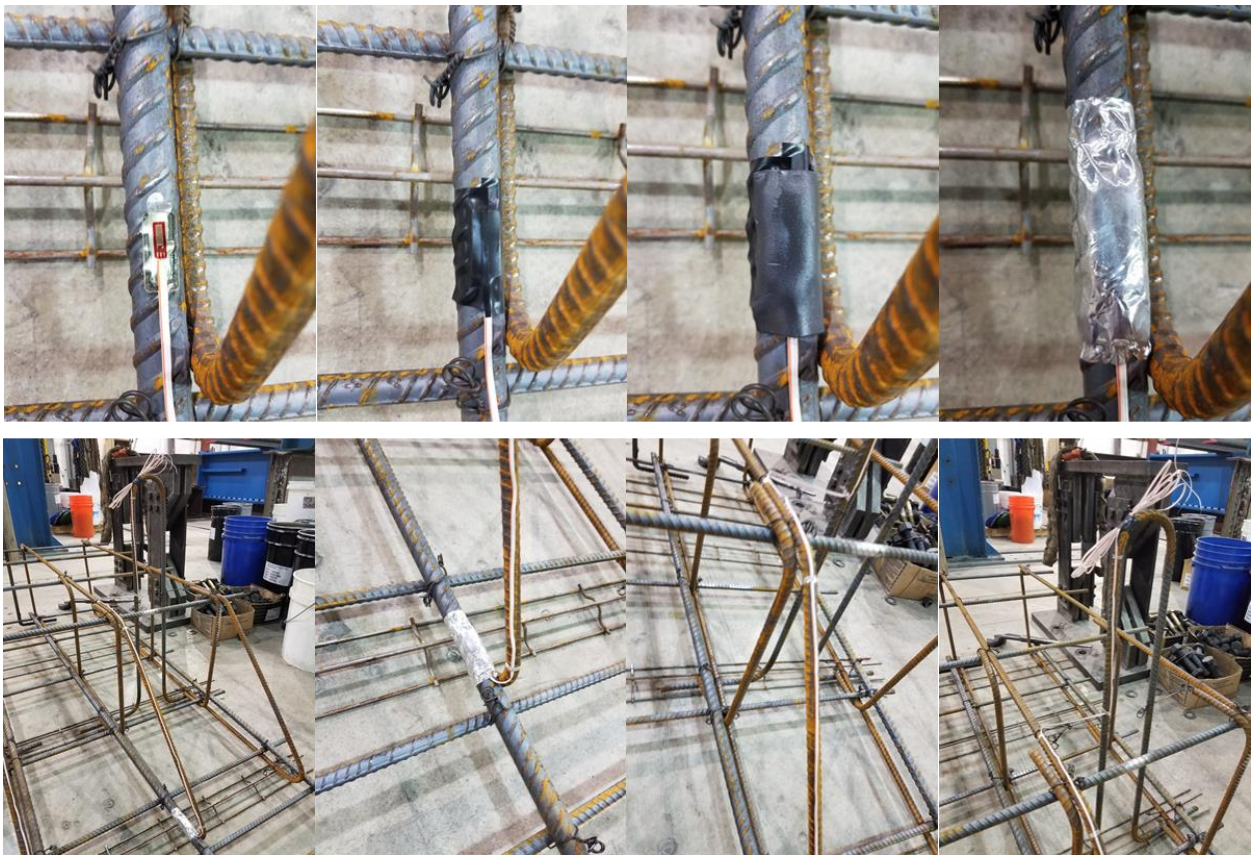

Figure 3.24: (Top) protecting strain gauge with duct tape, neoprene rubber tape, and foil tape; (bottom) stringing the strain gauge wires out of the specimen

3.3.2 Specimen Construction

The specimen was constructed in two casts, one for the precast members, and then one for the cast-in-place slab. The time between the cast of the beams and the slab would have ideally been seven days, but scheduling issues with the lab space/equipment meant that only four days could be provided between placing the concrete for the beam and the slab.

Formwork Details

The formwork used to construct the specimen was based off formwork used by Edwin (2017) but changes were made to prevent the type of formwork rupture that occurred when constructing those specimens [8]. The walls and platform were fabricated from ¾ in. plywood and 2x4 studs, and secured using mostly 2 ½ in. drywall screws although longer screws were used to secure the wall pieces together. The formwork was constructed such that the walls from the first concrete placement could be converted into the part of the formwork for the second concrete placement. Lateral support was provided by a combination of diagonal kickers and prestressed pencil rod, which was used previously for the horizontal shear push-off specimen formwork. The walls and kickers were secured to the studs within the platform.

The top of the flange and the sloped web surfaces required special formwork to create the formed surface roughening. The formed surfaces were created using the same methods that were used to make the textures for the horizontal shear push-off specimens, and then studs were added to the backs to support the textured surfaces during casting. A small strip of the form was left open at the end of each flange so that it could be ensured that concrete had filled the whole flange. Small textured formwork strips were made to cover the gap during placement after concrete had begun to flow out through the opening. Small burp-holes were made with a drill bit in the textured flange lid to allow for air bubbles to escape during consolidation. Images of the formwork can be seen in Figure 3.25 through Figure 3.27. Figure 3.25 shows the fit of the formwork walls being checked before the positioning was finalized, Figure 3.26 shows the formwork before the placement of the concrete for the precast beams, and Figure 3.27 shows the formwork before the placement of the concrete for the cast-in-place slab.

Figure 3.25: Testing the sub-assemblage formwork fit without lateral supports; (left) formwork for precast beams; (right) formwork for cast-in-place slab

Figure 3.26: Formwork for sub-assemblage specimen before placement of concrete for precast beams; (left) kickers and pencil rod have been installed; (right) supported textured form pieces

Figure 3.27: Formwork for sub-assemblage specimen before placement of concrete for cast-in-place slab after installation of upper forms and extra pencil rod

Construction Sequence

After the formwork for the precast beams was constructed as discussed in the previous section and coated with form oil, the reinforcement cages were constructed and installed in the formwork, using chairs to produce the specified cover. The strain gauges were installed and protected as previously discussed. The edges of the formwork were covered in duct tape, the removal of which would produce clean edges so that the second level of formwork fit correctly. All screws and pencil rod end caps necessary for deconstruction of the formwork were taped over and then the textured formwork was installed. The textured formwork for the sloped webs was secured with a prestressed pencil rod that connected to the opposite formwork wall as well as many long screws into the vertical walls.

On cast day, the concrete was placed in one beam form and consolidated using a vibrator until concrete was flowing out all the way across the gap at the end of the flange, then the textured gap piece was installed. The specimen was then filled the rest of the way, taking extra care to consolidate the sloped web and flange areas to remove as many air bubbles as possible. The specimen was leveled off and the exposed surface was raked with a 1 in. spacing. The process was repeated for the other specimen.

Twenty-four hours after placing the concrete, the textured forms were removed. The revealed surface was well formed and relatively free of bubbles. There was no excessive deflection of the formwork, which meant very clean lines. The formed interface surface can be seen in Figure 3.28.

Figure 3.28: Formed interface surface on Virginia Inverted T-Beam sub-assemblage specimen

The specimen was moist cured with wet burlap and plastic for four days before the cast-in-place slab was poured. The beam sections were pushed together, the formwork rebuilt and the extra pieces for the cast-in-place slab added, and then the formwork was oiled. The reinforcing cage was constructed and installed using chairs, and the strain gauges installed and protected. On cast day, the precast concrete was cleaned to ensure a surface free of debris and laitance and was moistened to a standard surface dry. The concrete was placed and consolidated with a vibrator. The surface was leveled and finished, making sure that there was enough room between the lifting loops and the concrete surface to attach the lifting equipment. The cast-in-place slab was moist cured for seven days and then allowed to cure at normal air temperature and moisture for 21 days before testing began.

3.3.3 Testing Apparatus

The test frame and load schedule used in this research is the same as that used by Edwin (2017) except for the actuator used and changes made to the lateral bracing provided to the actuator [8].

Test Frame and Load Application

Two types of loading were performed on the sub-assemblage specimen: cyclic and ultimate failure. For the cyclic loading, a 55 kip MTS® 244.31 hydraulic actuator was used to apply a

compressive load to a spreader beam which would load two bearing pads evenly. This set-up resulted in two point-loads being applied to the specimen through rubber bearing pads, which simulates the tires of a loaded semi-truck. For the ultimate failure test, the same set-up was used, but the actuator was switched for a 200-ton Enerpac® RR-20013 hydraulic cylinder and 250 kip load cell.

Figure 3.29 shows the test set-up. The specimen is supported on two W14x90 stiffened beams, spaced 12 ft. center-to-center, which were connected to the strong floor using four 1 in. diameter A325 bolts. A ¼ in. rubber bearing pad was placed between the specimen and support beams to decrease any wearing or stress concentrations that could occur if the specimen were to bear on just the edge of the beams. Two 9 in. by 18 in. by 2.5 in. bearing pads were placed on top of the specimen, centered along the short side, 3 ft. from the end and spaced 6 ft. center-to-center. A W14x120 stiffened spreader beam was centered on top of the bearing pads to spread the load from the actuator. The actuator was supported from the top by two W21x62 columns with two W21x62 crossbeams that have parts of the flanges removed to fit along the columns. The columns were bolted to the strong floor with four 1 in. diameter A325 bolts, and the crossbeams were connected to each column with six 7/8 in. diameter A325 bolts. The actuator was mounted to the crossbeams with a custom steel mount, featuring eight 7/8 in. diameter bolts. Two 4x4x3/8 angles were used to brace the actuator, one on either side of the columns, and shorter pieces of 2.5x2.5x1/4 angle connected the two long angles to the actuator. The angles were connected to the columns with two 7/8 in. bolts on each side, to the shorter pieces with a 7/8 in. bolt on either end, and to the actuator with 8 1in. bolts. Four 1 in. plates were placed under the actuator, on the crossbeam, and clamped into place. These plates allowed for the extension of the actuator to be varied such that damage didn’t occur to the cylinder of the actuator during the cycling.

Figure 3.29: Test set-up for Virginia Inverted T-Beam bridge system sub-assemblage specimen

Instrumentation

A total of 18 instruments were used for the sub-assemblage tests: six wire potentiometers (wire pots), six LVDTs, and six strain gauges. The wire pots were arranged along the bottom of the specimen, along the median, to measure the deflection of the specimen. They were affixed by attaching metal sheets to the bottom of the specimen with epoxy and then placing magnetic hooks to the end of the wire. The LVDTs were placed on the long side of the specimen to measure if and how much the interface cracks and opens during testing. They were attached to the specimen using the same method discussed in section 3.2.4 of this report. A diagram of the wire pot and LVDT locations can be seen in

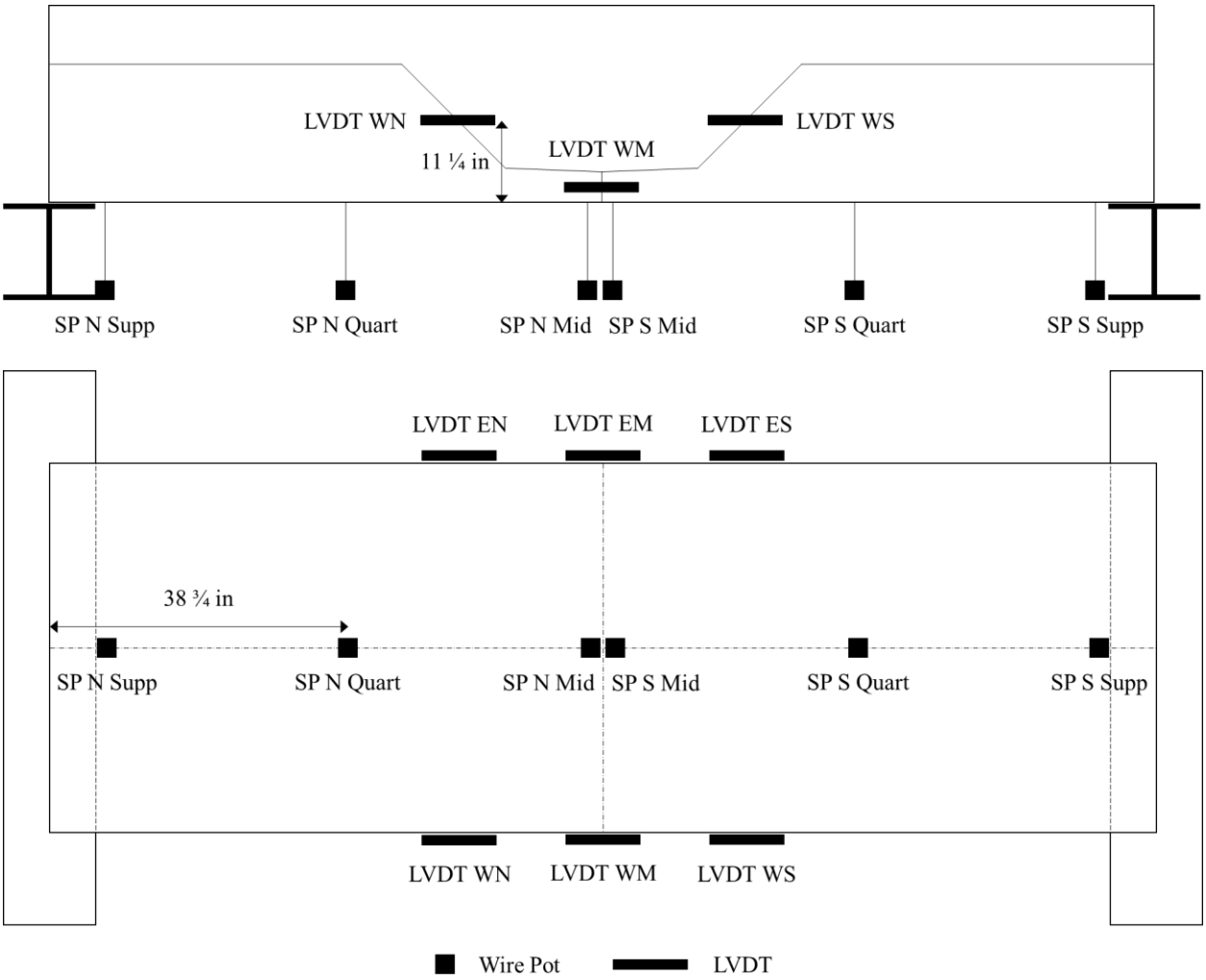

Figure 3.30, and installation details can be seen in Figure 3.31. The strain gauges were installed in the areas previously discussed in section 3.3.1.

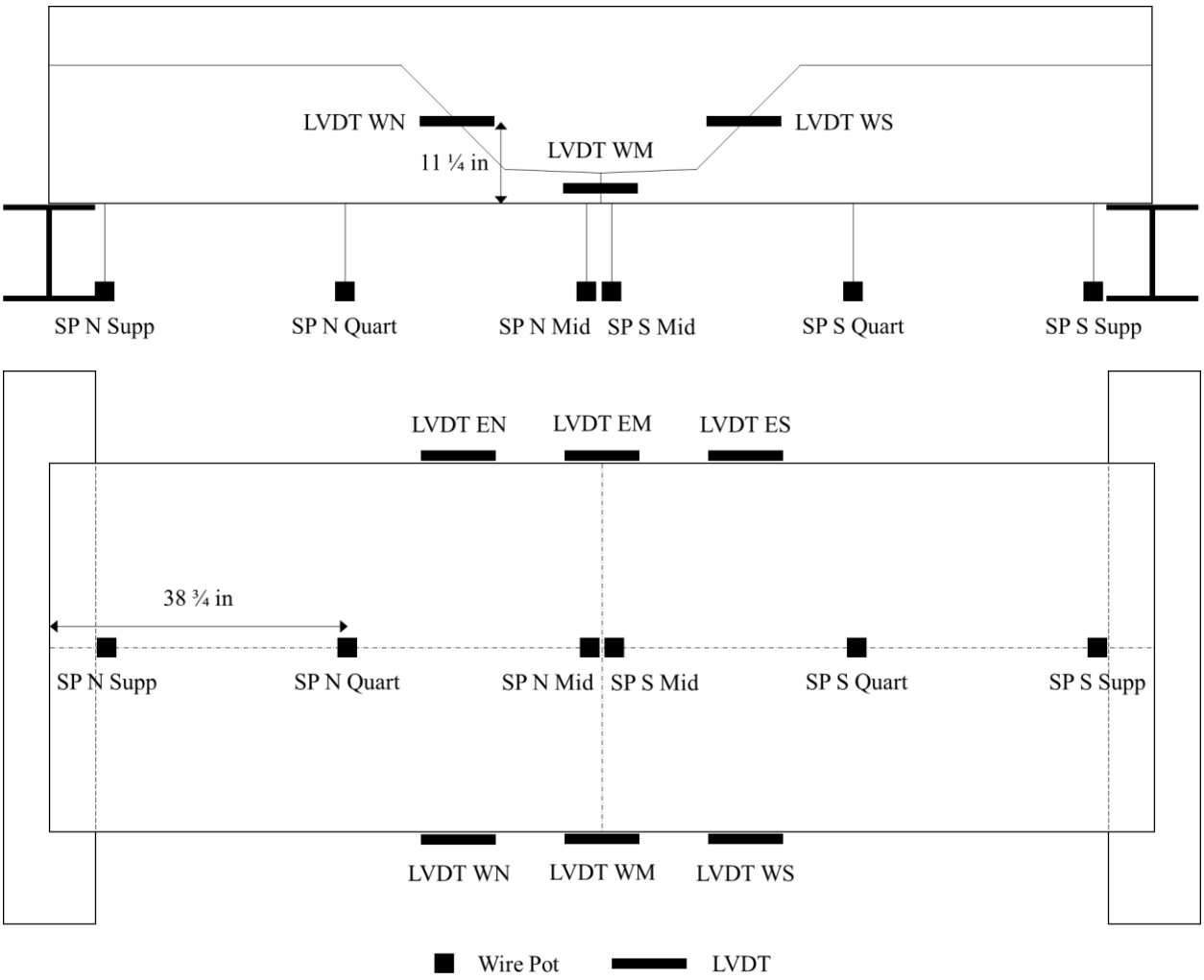

Figure 3.30: Diagram of wire pot and LVDT locations on sub-assemblage specimen

Figure 3.31: (Left) installation of wire pot with magnetic hook; (right) installation of LVDT

3.3.4 Testing Sequence

Cyclic Testing

The sub-assemblage specimen underwent 3,650,000 cycles of 30 kips. The cycles were performed at 2.75 Hz and the minimum load during the cycles was 3 kips. The minimum was not set to zero to prevent uplift of the actuator from the spreader beam. The cycling was stopped at certain intervals to perform monotonic tests where a cycle was performed manually and readings were taken. Each monotonic test took between three and four minutes to complete, which helped to decrease any delays between the applied load and the deflection of the system. The monotonic tests were performed at approximately the following amount of cycles: 0, 10, 100, 1000, 10,000, 100,000, 300,000, and every 200,000 cycles until 3,650,000.

Ultimate Failure Load Testing

After completion of the cyclic testing, the specimen was tested to ultimate failure. Before loading began, the specimen was inspected for any visible cracking. The test then began and the load was raised to 30 kips, where the load was held and the specimen was again inspected. The test proceeded in 10 kip intervals, pausing to look for cracking each time, until the specimen was no longer able to hold additional load. Readings from the instrumentation were taken continuously throughout the loading process.

CHAPTER 4: RESULTS AND DISCUSSION

4.1 Organization

This chapter contains both the results from the tests that were completed and discussions of those results. The first section is about the horizontal shear push-off specimens, including the strength of the concrete used to construct the specimens, the outcomes from the push-off tests, and a discussion of the effectiveness of each surface roughening. Also provided is a comparison of the results to those obtained by Scott (2010) and to predicted values from the AASHTO LRFD specifications. The second section reviews the Virginia Inverted T-Beam sub-assemblage specimen results, including the concrete strengths and readings from both the monotonic testing and ultimate failure load test. A discussion of the specimen performance compared to previously tested sub-assemblage adhesion-based connection specimens is included.

4.2 Horizontal Shear Push-off Specimens

4.2.1 Concrete Strengths

The horizontal shear push-off specimens were cast in three batches and each had a bottom section and top section that were placed at separate times, meaning that concrete was ordered six separate times to complete construction. Three of the deliveries were for 8000 psi concrete and the other three were 4000 psi concrete. The same mix design was used for all the concrete of each strength, but small variations in actual component values lead to variations in the concrete strengths.

Table 4.1 shows the compressive strength of the top and bottom sections in each batch at the time of testing. All three of the cast-in-place concrete mixes reached a compressive strength of over 4000 psi, but only one of the precast mixes achieved a compressive strength over 8000 psi. Further information about the mix proportions and graphs of the strength over time can be found in Appendix B.

Table 4.1: Horizontal shear push-off specimens concrete compressive strength for all batches

Batch	Included Specimens	Theoretical Strength	Strength at 28-days	Strength at Time of Testing
1	CH-3.5-TC-01 CH-3.5-TC-02 CH-3.5-TC-03	8000 psi (Precast)	8140 psi	8750 psi
	RK-1-01 RK-1-02 RK-1-03	4000 psi (Cast-in-place)	5530 psi	5950 psi
2	RG-1-01 RG-1-02 RG-1-03 TG-1.5-01 TG-1.5-02 TG-1.5-03	8000 psi (Precast)	6290 psi	6760 psi
	RK-2-01 RK-2-02 RK-2-03 RK-3-01 RK-3-02 RK-3-03	4000 psi (Cast-in-place)	4100 psi	4400 psi
3	TG-3-01 TG-3-02 TG-3-03 SK-2.5-01 SK-2.5-02 SK-2.5-03	8000 psi (Precast)	7220 psi	7800 psi
	CH-3.5-PL-01 CH-3.5-PL-02 CH-3.5-PL-03 EA-01 EA-02 EA-03	4000 psi (Cast-in-place)	4440 psi	4520 psi

4.2.2 Push-off Results

This section provides an analysis of typical data from one horizontal shear push-off test, summarize the results of all tests, compare the outcomes to those obtained by other researchers and expected values, and discuss the significance of the results. Complete results from the testing of each specimen can be found in Appendix D.

Analysis of Typical Results

Each test proceeded in the same manner, which produced results that appear very similar. An example of a load versus time plot is shown in Figure 4.1. This plot, created for specimen TG-1.5-02, contains data from both the horizontal applied load and the vertical clamping force in the harness. The horizontal applied load is just the direct output from the load cell included in the test set-up. The vertical clamping force is a sum of the readings from the strain gauges on all four rods used in the clamping harness. The plots show that the test initially proceeded with the applied load increasing at a steady rate and the clamping force remaining constant. As the load reached its peak and the interface failed in shear, the clamping force in the harness increased slightly. This was mainly due to dilation of the interface crack and not from the rods elongating due to skew, as the harness rods were designed to remain vertical even as the top and bottom sections deflected horizontally respective to one another.

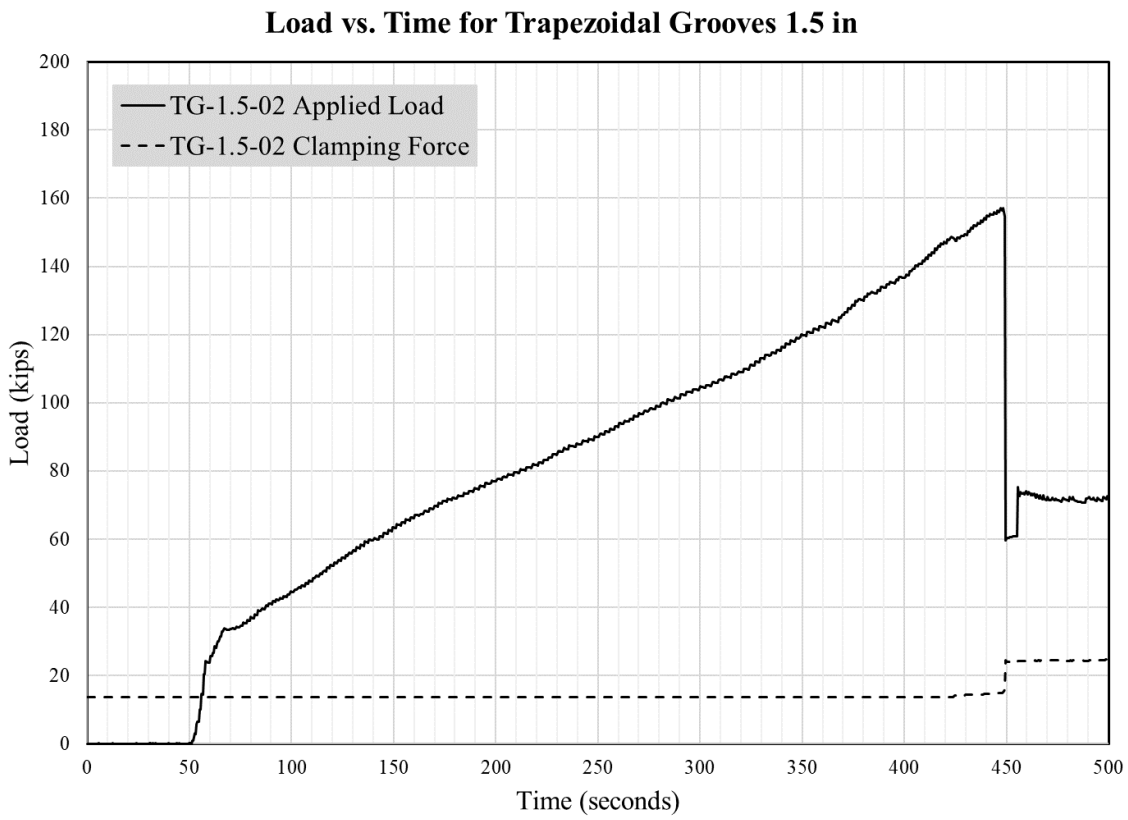

Figure 4.1: Plot of Load vs. Time for Horizontal Shear Push-off Specimen TG-1.5-02

Figure 4.2 shows a typical load versus slip plot, also from the test of TG-1.5-02. The slip is calculated by averaging all four of the LVDTs that were installed on each specimen. As the applied load initially increased, zero movement was induced across the shear interface, although a small amount of slip appears as the applied load neared its peak value. A corresponding slight increase in the clamping force was observed with the marginal amount of slip, caused by dilation of the interface. Once the peak load was surpassed, the load decreased by over 50% while the slip increased drastically. As the load was reengaged, the slip increased while the load remained constant, showing that the interface could not resist further load. The clamping force increased a slight amount when the interface fractured but did not increase further after the load reengaged and the slip increased, showing that the harness was designed correctly and only showed increase in force when the interface dilated.

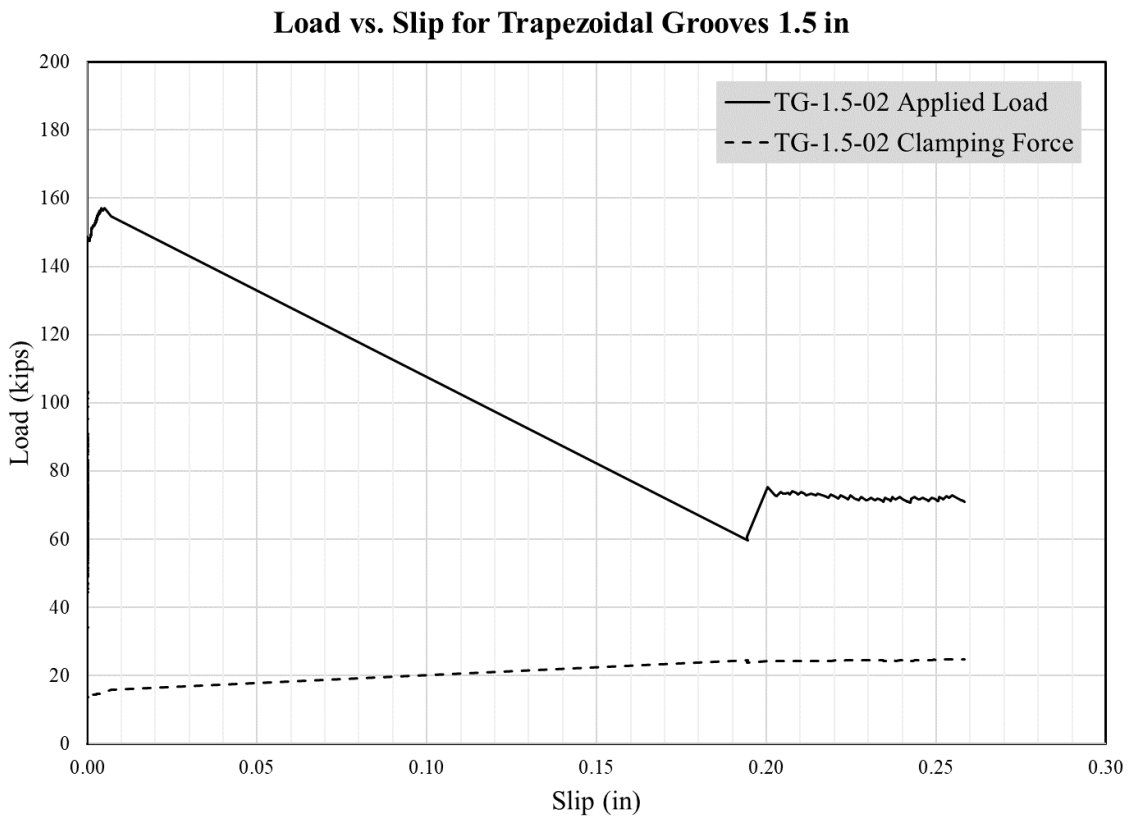

Figure 4.2: Plot of Load vs. Slip for Horizontal Shear Push-off Specimen TG-1.5-02

Summary of Results

As seen in both Figure 4.1 and Figure 4.2, the strength of the specimen drastically decreases once the interface fractures and the small residual strength is a function of the normal force applied to the specimen. This means that the interface only has a usable horizontal shear strength before fracture.

Table 4.2 shows the fracture stress for each specimen and averages for each type. Figure 4.3 is a set of box plots which show the mean and spread of the data for each texture type.

Table 4.2: Horizontal shear push-off specimen fracture loads

Texture Type	Specimen Names	Specimen Fracture Stress	Average Fracture Stress for Texture
Raked 1 in	RK-1-01	419 psi	373 psi
	RK-1-02	354 psi	
	RK-1-03	346 psi	
Raked 2 in	RK-2-01	275 psi	246 psi
	RK-2-02	258 psi	
	RK-2-03	204 psi	
Raked 3 in	RK-3-01	303 psi	321 psi
	RK-3-02	306 psi	
	RK-3-03	353 psi	
Rectangular Grooves	RG-1-01	328 psi	298 psi
	RG-1-02	287 psi	
	RG-1-03	279 psi	
Trapezoidal Grooves 1.5 in	TG-1.5-01	44 psi	393 psi
	TG-1.5-02	409 psi	
	TG-1.5-03	327 psi	
Trapezoidal Grooves 3 in	TG-3-01	341 psi	365 psi
	TG-3-02	385 psi	
	TG-3-03	370 psi	
Cross Hatch TuffCoat®	CH-3.5-TC-01	473 psi	414 psi
	CH-3.5-TC-02	383 psi	
	CH-3.5-TC-03	387 psi	
Cross Hatch Plastic	CH-3.5-PL-01	Data Not Available	261 psi
	CH-3.5-PL-02	276 psi	
	CH-3.5-PL-03	245 psi	
Square Knobs	SK-2.5-01	347 psi	321 psi
	SK-2.5-02	276 psi	
	SK-2.5-03	339 psi	
Exposed Aggregate	EA-01	272 psi	302 psi
	EA-02	282 psi	
	EA-03	353 psi	

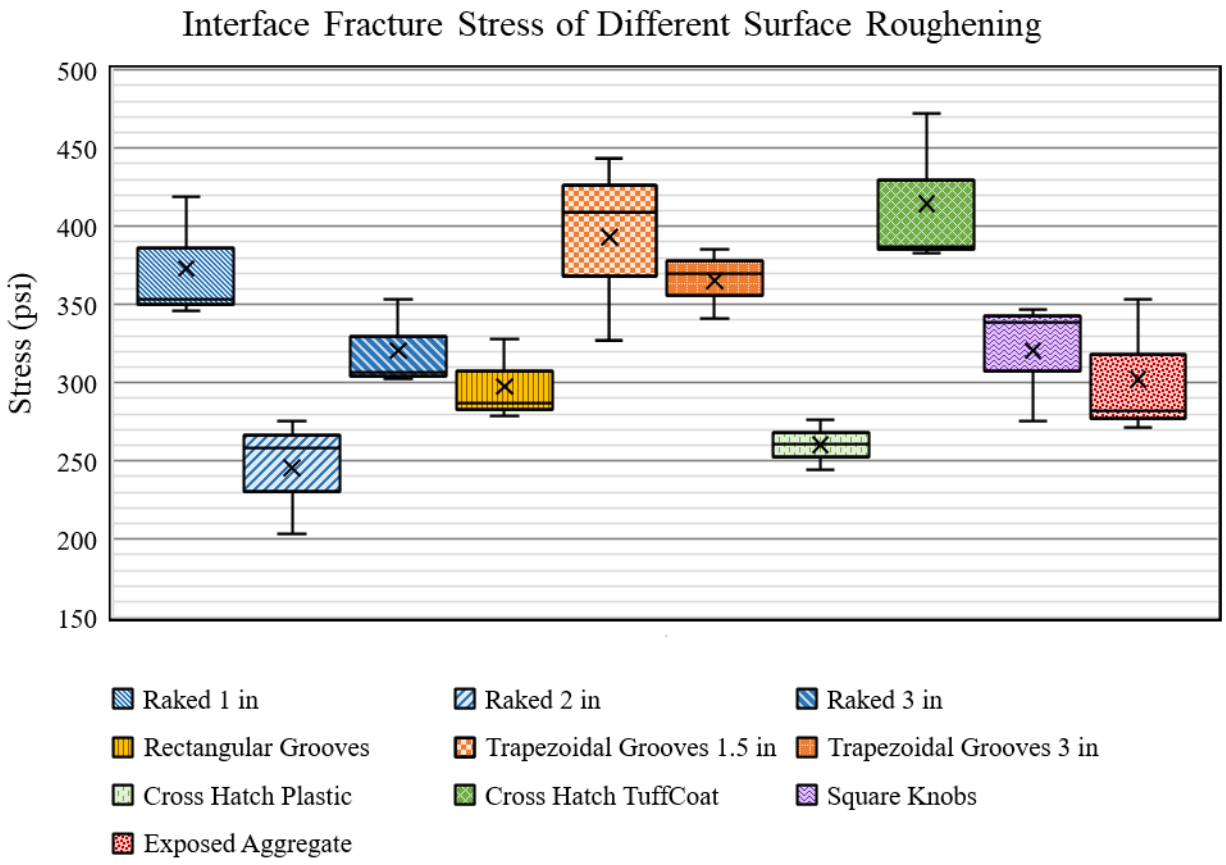

Figure 4.3: Interface fracture stress for surface roughening for horizontal shear push-off specimens

The highest average interface shear stresses were produced by the cross hatch that was de-bonded with TuffCoat®, 414 psi, and the trapezoidal grooves that were spaced 1.5 in., 393 psi. Both textures include sharp angles and were designed such that the surface area of the raised areas are equal to those of the lowered. TuffCoat® was utilized for de-bonding in both textures, which helped to preserve the sharp edges and keep the pore structure of the concrete more open, unlike a plastic coating.

The raked 1 in. texture and the trapezoidal grooves 3 in. both performed well, achieving fracture stresses over 350 psi. Closely spaced rakes, even though they do not feature sharp edges, are closer to achieving an equal surface area of raised and lowered areas. The trapezoidal grooves, although they did not feature equal surface areas of raised and lowered sections, did have sharp edges that helped to raise the fracture stress.

The rectangular grooves, square knobs, raked 3 in. and exposed aggregate all achieved adequate fracture stresses, around 300 psi. The rectangular grooves were damaged during construction, and so the fracture stress of the fully intact structure is likely well above the level it obtained during these tests. The square knobs featured two specimens that broke at nearly 350 psi with an outlier near 280 psi, which means that given further testing this texture might prove to be closer in stress to the trapezoidal grooves 3 in. The features of the square knobs, sharp edges but not equal in raised and lowered textures, is closer to that of the trapezoidal, so it is a possibility that it could display a higher average stress with further refinement of the pattern and testing. The raked 3 in. does not have close spacing or equal areas, although it does have defined 0.25 in. grooves which meant that it produced a fracture stress higher than that of the exposed aggregate, which does not have any regular ridges.

The cross hatch texture with the plastic used for de-bonding, which was used by Edwin (2017), produced one of the lowest interface shear stresses at fracture, with an average of only 261 psi. This value is very low, especially when compared to the 414 psi average that was achieved by the cross hatch texture with TuffCoat® used for de-bonding. Using plastic as a de-bonding agent decreased the shear strength of the texture by 150 psi. The effects can also be seen in the state of the interface after testing. Figure 4.4 shows the top and bottom sections for a specimen from both the plastic de-bonded cross hatch and the TuffCoat® de-bonded cross hatch. It is clearly shown that the interface of the TuffCoat® de-bonded cross hatch had much more interaction between the sections, whereas the plastic de-bonded cross hatch looks as though the sides merely slid apart.

Top Bottom Top Bottom

CH-3.5-TC-03 CH-3.5-PL-03

Figure 4.4: Interface of bottom and top sections of cross hatch specimens after testing

The results support the notion that an increase in spacing produces lower horizontal shear strength, especially when looking at the trapezoidal grooves textures. The trapezoidal grooves 1.5 in. achieved an average horizontal shear strength of 393 psi, but the trapezoidal grooves 3 in. only reached 365 psi.

The results from the raked textures do not fully support this relationship though. The raked 1 in. texture had an average shear stress at fracture of 373 psi, and the raked 3 in. texture had an average shear stress at fracture of 321 psi, meaning that the smaller spacing between 0.25 in. deep rakes produces a larger shear stress. The raked 2 in. unfortunately does not follow the pattern, as its average shear stress at fracture was 246 psi, much lower than that of the raked 3 in. All three sets of specimens were produced in the same manner, and the raked 2 in. and raked 3 in. were both part of Batch 2, so production method nor concrete composition can be to blame. It is evident in the pictures of the interfaces after testing for the raked 2 in. and the raked 3 in., shown in Figure 4.5, that there was more interaction between the sections in the raked 3 in. specimen. There aren't any features within the raked 2 in. specimen, such as large air bubbles, that would explain why it would have interacted less or why the raked 3 in. would have interacted more. More data is needed to determine if the discrepancy is a fluke or not.

Top Bottom Top Bottom
RK-2-03 RK-3-03

Figure 4.5: Interface of bottom and top sections of raked specimens after testing

Results Compared to Scott (2010)

Scott (2010) tested three specimens without reinforcement across the interface constructed from roughly 8000 psi concrete on the bottom and roughly 6000 psi concrete on the top. The size and shape of the specimens were identical to those tested in this research. The interface was described as "raked to an amplitude of 0.25 in." and, from inspections of the photographs, it appears as if the spacing was somewhere between 0.5 and 0.75 in. A normal force of 2.5 kips was applied during testing. The three specimens had interface fracture stresses of 398 psi (153 kips), 417 psi (160 kips), and 406 psi(156 kips), averaging at 407 psi [25]. The 407 psi average from Scott is very similar to the 373 psi average stress from the raked 1 in. in this research when the smaller spacing and larger normal force are taken into consideration. The results from both studies are consistent.

Results Compared to AASHTO LRFD Bridge Design Specifications

Two situations in AASHTO LRFD section 5.7.4.4 could apply to these specimens, if the minimum reinforcing has been provided, which it has not been. The first is for cast-in-place concrete slabs placed on intentionally roughened girders, which would mean the following predicted strength:

$$V_{ni} = cA_{cv} + \mu\left(A_{vf}f_y + P_c\right) = (0.28\text{ ksi})(384\text{ in}^2) + (1.0)(0\text{ kips} + 15\text{ kips}) = \mathbf{123\text{ kips}}$$
$$\leq \min\begin{Bmatrix} K_1 f'_c A_{cv} \\ K_2 A_{cv} \end{Bmatrix} = \min\begin{Bmatrix} (0.3)(4\text{ ksi})(384\text{ in}^2) \\ (1.8\text{ ksi})(384\text{ in}^2) \end{Bmatrix} = \min\begin{Bmatrix} 461\text{ kip} \\ 691\text{ kip} \end{Bmatrix} = 461\text{ kips}$$

$$\frac{123\text{ kips}}{384\text{ in}^2} = \mathbf{320\text{ psi}}$$

The second is for normal weight concrete placed on an intentionally roughened concrete surface and predicts the following strength:

$$V_{ni} = cA_{cv} + \mu\left(A_{vf}f_y + P_c\right) = (0.24\text{ ksi})(384\text{ in}^2) + (1.0)(0\text{ kips} + 15\text{ kips}) = \mathbf{107\text{ kips}}$$
$$\leq \min\begin{Bmatrix} K_1 f'_c A_{cv} \\ K_2 A_{cv} \end{Bmatrix} = \min\begin{Bmatrix} (0.25)(4\text{ ksi})(384\text{ in}^2) \\ (1.5\text{ ksi})(384\text{ in}^2) \end{Bmatrix} = \min\begin{Bmatrix} 384\text{ kip} \\ 691\text{ kip} \end{Bmatrix} = 384\text{ kips}$$

$$\frac{107\text{ kips}}{384\text{ in}^2} = \mathbf{279\text{ psi}}$$

The first prediction, for normal weight concrete on girders, is at about the average fracture stress for all specimens combined (330 psi). Only four textures reached an average fracture stress higher than the predicted 320 psi: raked 1 in., trapezoidal grooves 1.5 in. and 3 in., and cross hatch de-bonded with TuffCoat®. The second prediction, for normal weight concrete not on girders, is conservative for some of the better performing textures but is higher than those that underperformed, such at the cross hatch de-bonded with plastic and the raked 2 in.

Selected Texture for Virginia Inverted T-Beam Sub-Assemblage Specimen

Several factors were considered when selecting the texture to be utilized for the sub-assemblage specimen. Looking specifically at the two textures with the highest average shear stresses, the cross hatch with TuffCoat® and the trapezoidal grooves 1.5 in., a few differences in the textures helped to make the decision. First, two of the three cross hatch specimens failed at about 385 psi with an outlier at approximately 470 psi, whereas two out of the three trapezoidal groove specimens failed above 400 psi with the outlier at about 330 psi. More tests would need to be done to confirm this trend, but it is possible that the trapezoidal grooves texture could outperform

the cross hatch texture. Second, the trapezoidal grooves proved to be easier to construct. Lastly, trapezoidal grooves have been previously utilized on a constructed Virginia Inverted T-Beam bridge, and so the trapezoidal grooves 1.5 in. texture was chosen for use in the sub-assemblage specimen.

4.3 Virginia Inverted T-Beam Sub-Assemblage Specimen

4.3.1 Concrete Strengths

The bottom precast beams were constructed using an 8000 psi concrete mix, and the top cast-in-place slab was constructed using a 4000 psi concrete mix. The plots of the compressive strength over time for both mixes are shown in Figure 4.6 and Figure 4.7. The precast mix was just below 8000 psi when the cyclic tested was started but increased in strength to just above 8000 psi by the time of the monotonic test to failure. The cast-in-place mix never reached 4000 psi but was very close.

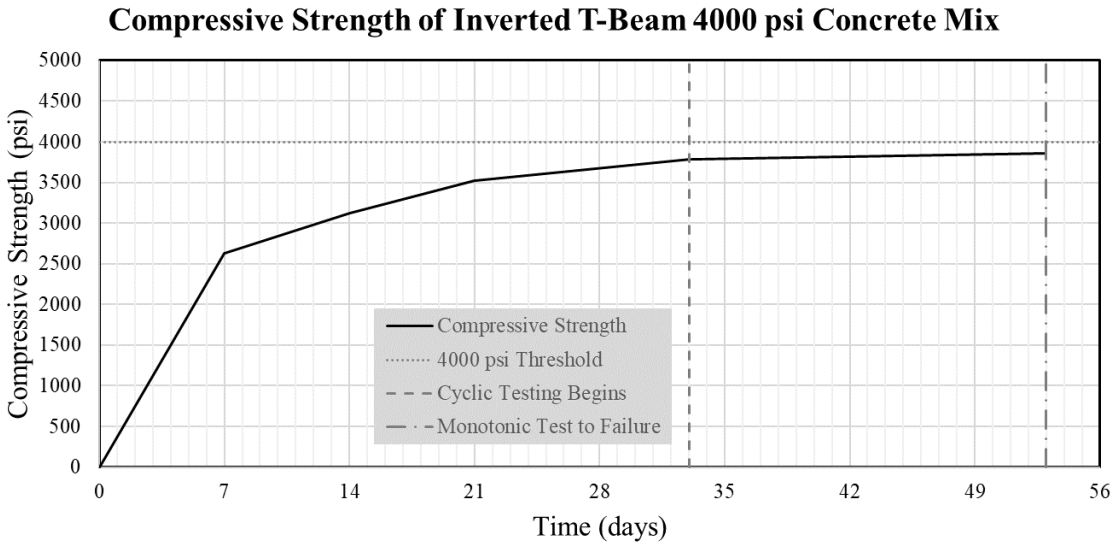

Figure 4.6: Compressive strength of Inverted T-Beam 4000 psi concrete mix

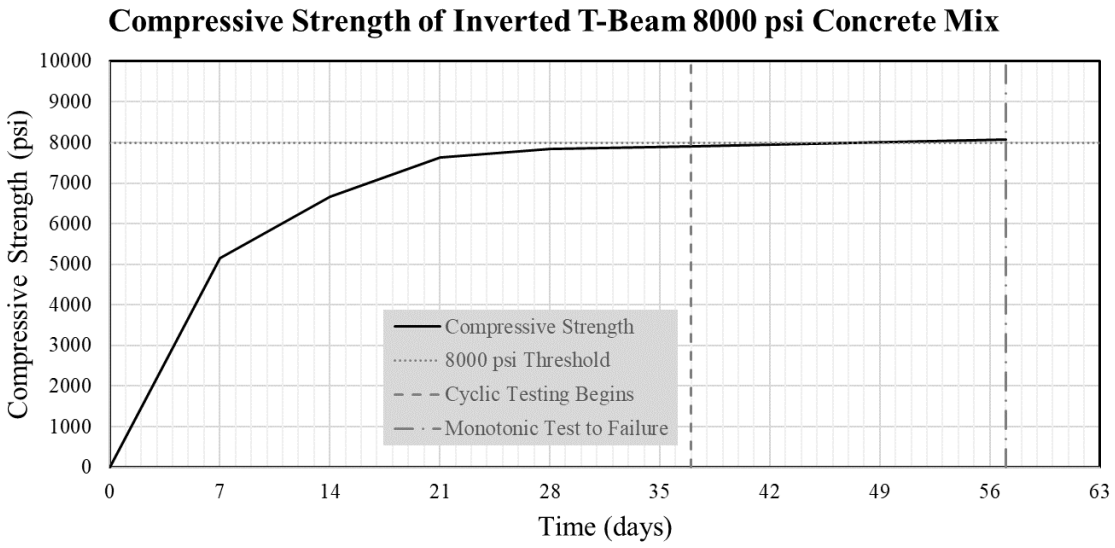

Figure 4.7: Compressive strength of Inverted T-Beam 8000 psi concrete mix

4.3.2 Monotonic Test Results

The cyclic testing was paused at different increments to perform monotonic tests to compare the response of the specimen at different times within the life-span in terms of deflection, strain in the reinforcement, and interface crack opening. Tests were done after the following number of cycles: 0, 10, 100, 1000, 10000, 100000, 300000, 500000… 3500000, 3650000. The monotonic tests were not always performed after the exact amount of cycles were performed, but the actual number is reported with the data from each individual test in Appendix E. To evaluate the changes in response of the specimen at different numbers of cycles, five monotonic tests were chosen to be compared: 10000, 500000, 1500000, 2500000, and 3650000.

Four LVDTs were installed on the specimen to track the dilating of the interface between the precast and cast-in-place sections of the specimen along the sloped sides. All throughout the cyclic tests, these instruments only recorded zero opening meaning that the interface remained fully bonded. The data from these is not discussed further in this section, but can be found in Appendix E.

After the monotonic test at 3300000 cycles, hairline cracks were observed along the centerline on both sides of the specimen, extending from the precast sections flange joint to the top of the cast-in-place slab.

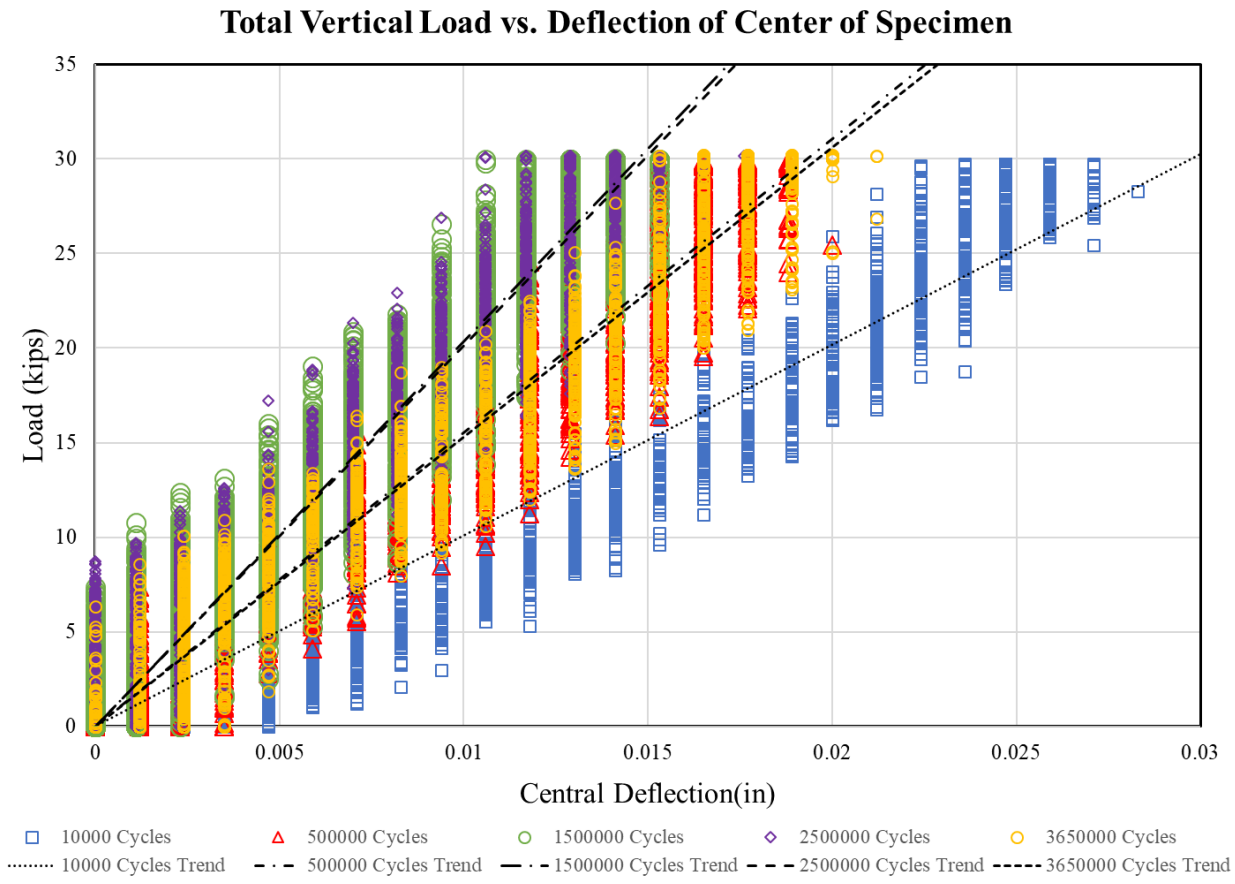

Figure 4.8: Inverted T-Beam cyclic testing – total vertical load vs. deflection of center of specimen

The applied load versus the deflection of the center of the specimen, as reported by the north middle wire pot, for each of the five cycles is shown in Figure 4.8. The data from all the cycles is very similar with most of the data overlapping, and so trend lines have been provided for each data set so that they can be more easily discernable. The trend lines vary slightly, with slopes ranging from 1000 kip/in to 2000 kip/in. The data with the shallowest slope, and therefore lowest stiffness, is from the earliest test which suggests that the small changes in slope are from instrument variability, not from stiffness decreasing over time. Essentially, there was no discernable change in the deflection response of the specimen between the beginning and end of the cyclic testing.

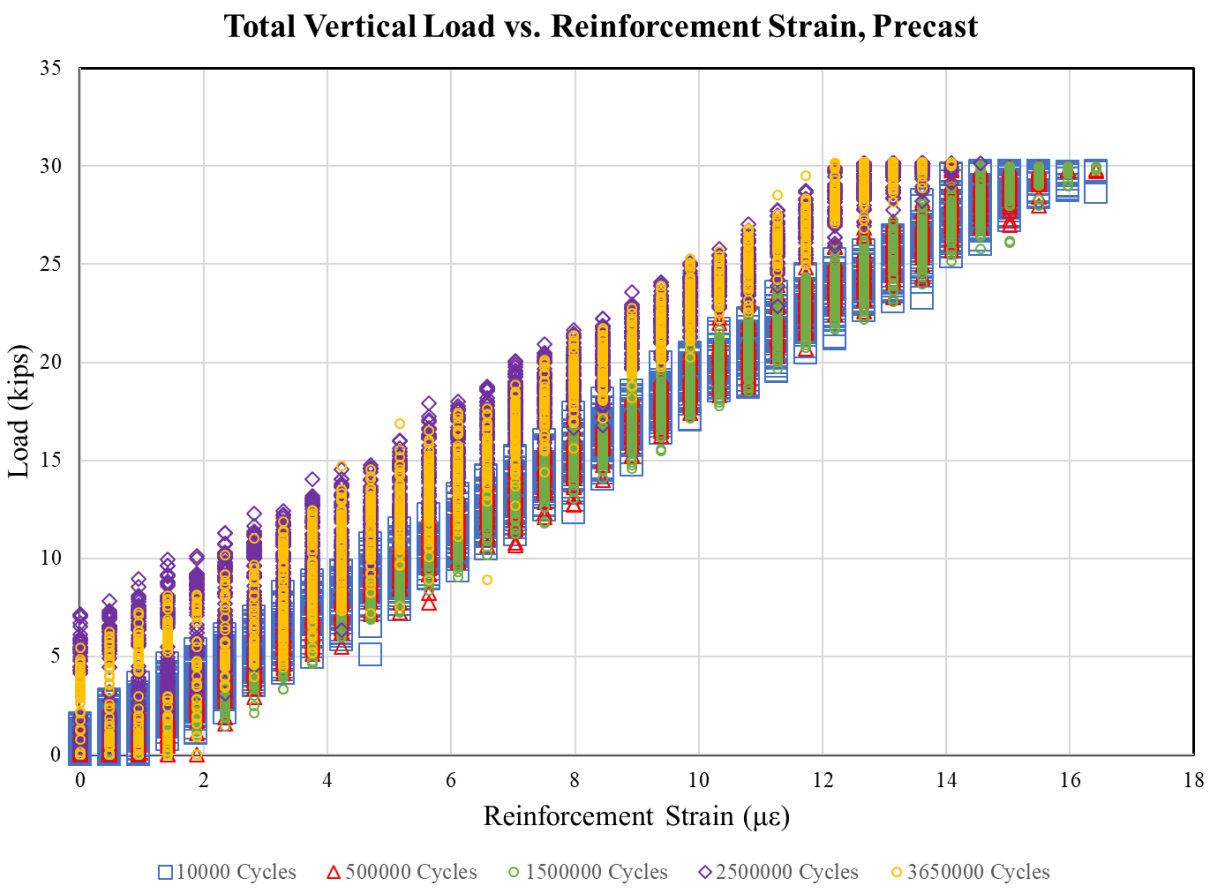

Figure 4.9: Inverted T-Beam cyclic testing – total vertical load vs. reinforcement strain, precast

The applied load versus the reinforcement strain in the precast sections, reported by the precast north-east strain gauge, is shown in Figure 4.9. The data is even more consistent across cycles than the deflection data, with the data points falling into a tighter band. The distribution has a slope of approximately 2 kip/με. This graph shows that the strain levels within the precast sections did not change throughout the cyclic testing.

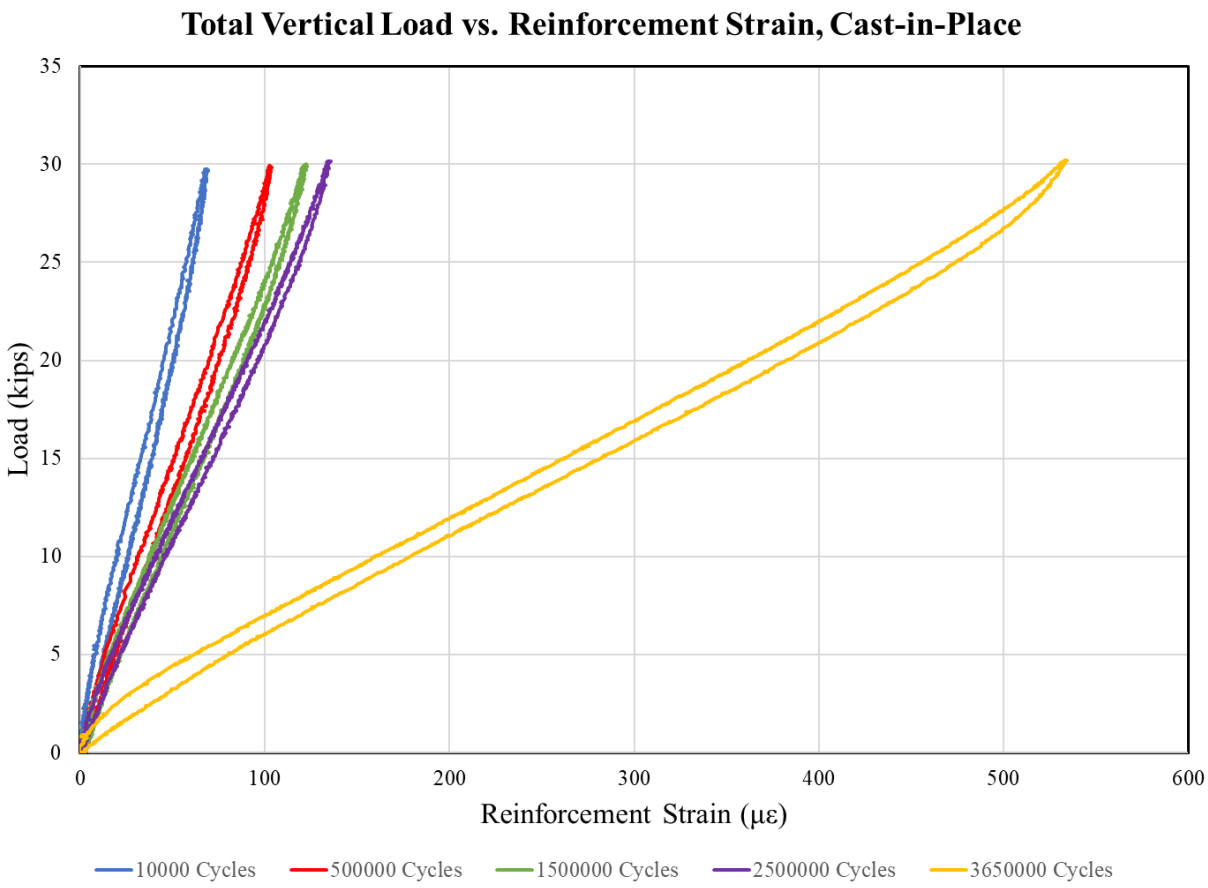

Figure 4.10: Inverted T-Beam cyclic testing – total vertical load vs. reinforcement strain, cast-in-place

The applied load vs. reinforcement strain in the cast-in-place slab, reported by the cast-in-place east strain gauge, is shown in Figure 4.10. The data from the first four monotonic tests is still very consistent, although each test showed a slight increase in the maximum strain in the reinforcement. The test at 10000 cycles has a slope of 0.5 kip/με, and the test at 2500000 cycles has a slope of 0.225 kip/με. The values for the test at 3650000 cycles are drastically different; the slope is approximately 0.056 kip/με, which is an order of magnitude different from the first four tests.

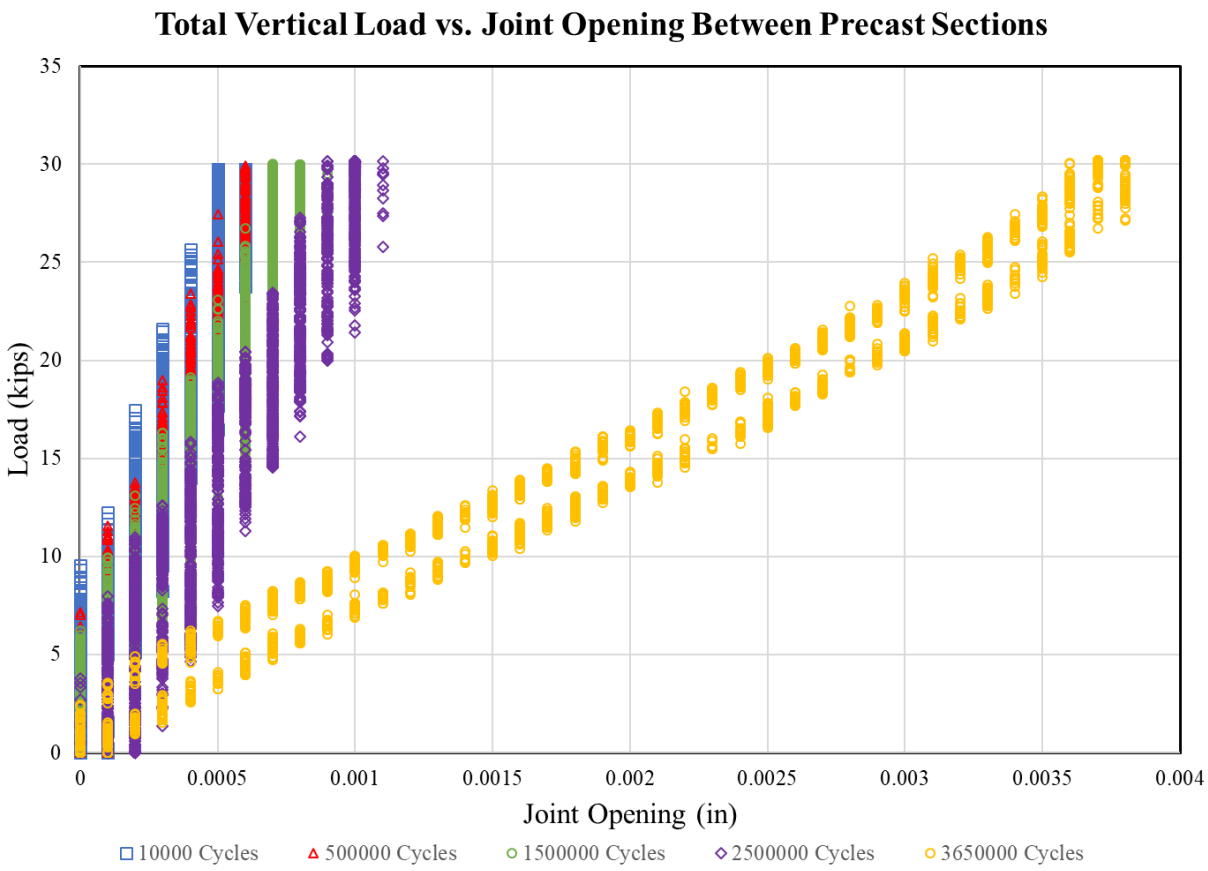

Figure 4.11: Inverted T-Beam cyclic testing – total vertical load vs. joint opening between precast sections

The applied load versus joint opening between the precast sections, reported by the east middle LVDT, is shown in Figure 4.11. This plot has the same trend as the previous, showing that the central joint between the precast beams began opening approximately five times more than during the first four tests. The first four tests have a slope of approximately 40000 kip/in, and the last has a slope of 8000 kip/in. The increase in the opening of the joint corresponds to the increase in reinforcement strain in the cast-in-place slab.

It is apparent from the data that something changed within the specimen that increased the reinforcement strain in the cast-in-place slab and the joint opening. Cracking around the joint between the precast beams could have caused the changes as small cracks would affect local behavior, such as reinforcing strain in the cast-in-place and crack widths, but would not affect global behaviors, like deflection. This is supported by the presence of the hairline cracks found along the centerline on both sides of the specimen.

4.3.3 Theoretical Cracking Calculations

To determine if cracking was to be expected in the specimen at service loading, a theoretical calculation of the cracking moment was performed. A split tensile test was performed for the 4000 psi cast-in-place concrete mix after the completion of testing and it was found that the tensile strength of the concrete was 320 psi. Using this value, as well as the known compressive strength and geometry of the specimen, the cracking moment was calculated using the software Response-2000. For the purposes of the analysis, it was assumed that the height of the section was from the top of the cast-in-place slab to the top of the precast flanges because the flanges were not connected in any manner and thus contributed no strength to the section. All inputs and results from Response-2000 can be found in Appendix F. The analysis resulted in a cracking moment of 97 kip-ft. By assuming the weight as an uniformly distributed load, (150 lb./ft.^{3})(4 ft.)(25.5 in) = 1.275 kip/ft., the moment was calculated as such:

$$M_{Self} = \frac{\left(1.275\ \frac{kip}{ft}\right)(6\ ft)^2}{2} = 23\ kip - ft$$

The corresponding cracking load can be solved for using the knowledge that, for this test set-up, the moment at the center of the specimen due to the applied load is equal to half of the total load, X, multiplied by the distance between the support and the load points. Therefore:

$$\frac{X_{Yield}}{2}(3\ ft) = 97 - 23\ kip - ft$$

$$X_{Yield} = 49\ kip$$

This cracking load is almost 20 kips larger than was applied to the specimen, so the beam would not have cracked during the cyclic loading if it had been in original condition. Since cracking did occur during service level loading, it is possible that the accumulation of damage throughout the cyclic loading allowed for cracks to appear at lower loads than expected. Microcracking at the center of the specimen most likely lead to a weakening of the tensile capacity of the concrete and the cracking of the specimen.

4.3.4 Ultimate Failure Test Results

After the 3.65 million cycles were completed, the test set-up was altered to include a 200 kip hydraulic cylinder and a monotonic test was performed until failure occurred. The ultimate total vertical load achieved by the specimen was 130 kips and the failure mode was flexural cracking and fracture of the central reinforcing bars in the cast-in-place slab. Figure 4.12 and Figure 4.13 show the cracking on the east and west sides of the specimen after failure.

Figure 4.12: Inverted T-Beam Failure – East Side

Figure 4.13: Inverted T-Beam Failure – West Side

The following observations were made during the test:

- The interface between the precast and cast-in-place sections on the south side of the specimen appeared to have cracks along the full surface (including the flange, sloped web, and level upper surface) at the 50 kip level.
- The interface between the precast and cast-in-place section on the north side of the specimen appeared to have cracks along the full surface at the 70 kip level.
- Small chunks of concrete were observed falling from along the centerline of the specimen at 113 kips and 126 kips.
- Several of the wire pots along the bottom of the specimen had failures of their epoxy glue towards the end of the test such that there was not a measurement of the deflection of the center of the specimen being recorded, so a manual recording was taken at 130 kips.
- The specimen failed by way of a large crack in the cast-in-place slab above the precast joint and the failure of center reinforcing within the cast-in-place slab at 130 kips, marked by an audible popping noise and a drop of the load to about 80 kips.

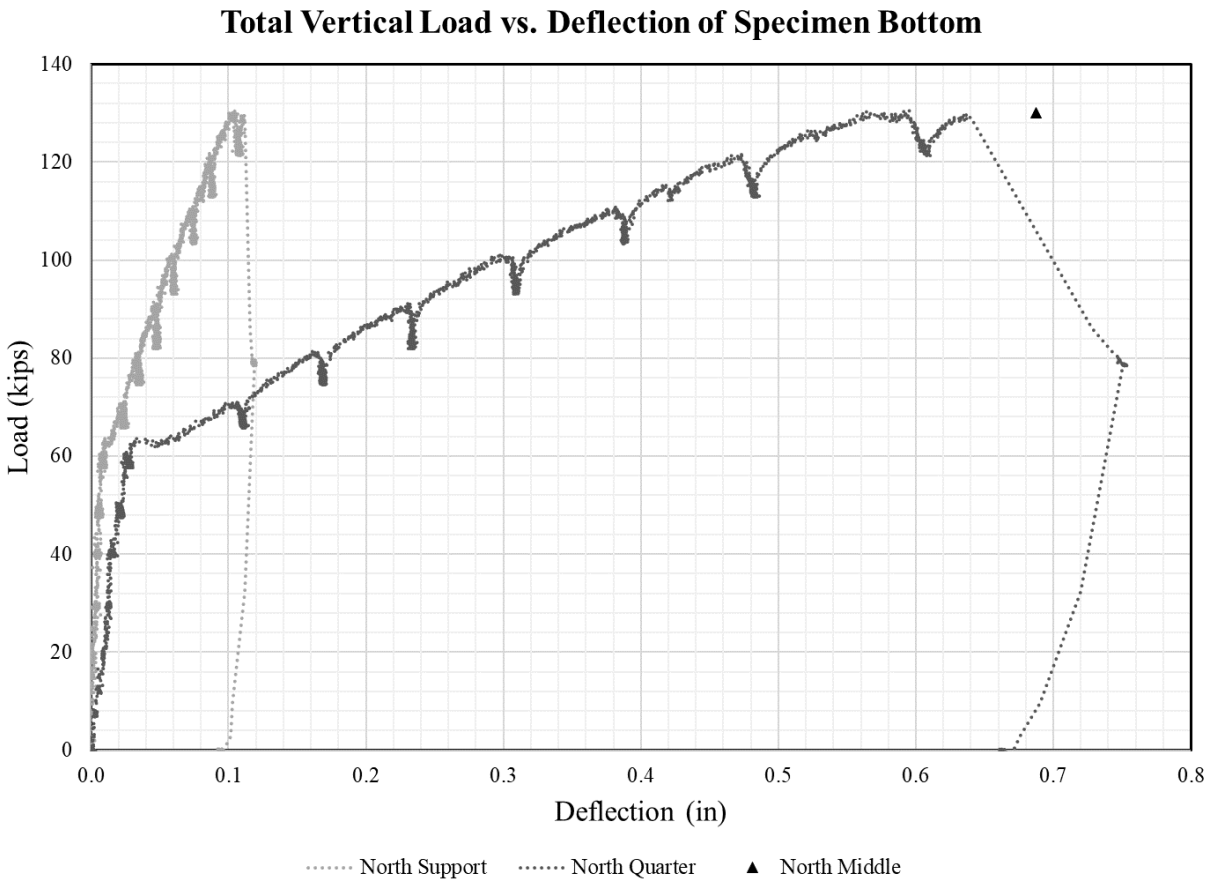

Figure 4.14: Inverted T-Beam failure – combined vertical load vs. deflection of specimen

The deflection of the bottom of the specimen during the failure testing is shown in Figure 4.14. Several of the wire pots fell during the early stages of the test and others were observed to have strings that became stuck while retracting, therefore only two wire pots gave viable data: the north support and the north quarter point. The manually recorded deflection taken of the center of the specimen, in line with the north middle wire pot, is also included on the plot. The final deflection of the specimen in the center is very similar to the final deflection of the quarter point, as was found to be true during the monotonic tests, so it can be assumed that the north quarter point reading had the same patterns as the mid span deflection. For the first 63 kips of the test, the trend was very linear elastic, following the same path even as the load dropped during the pauses at every 10 kips. This portion has a slope of 2000 kip/in, which is the same as the upper trend line found in the cyclic data. At 63 kips, the deflection increased 0.1 in. while the load remained steady then the load and deflection increased together again, but at a less-steep slope. The trend remained linear until about 125 kips of load and 0.5 in. of deflection, where the trend

rounded out and began to decline. The specimen failed as soon as the load returned to 130 kips after the pause for inspection.

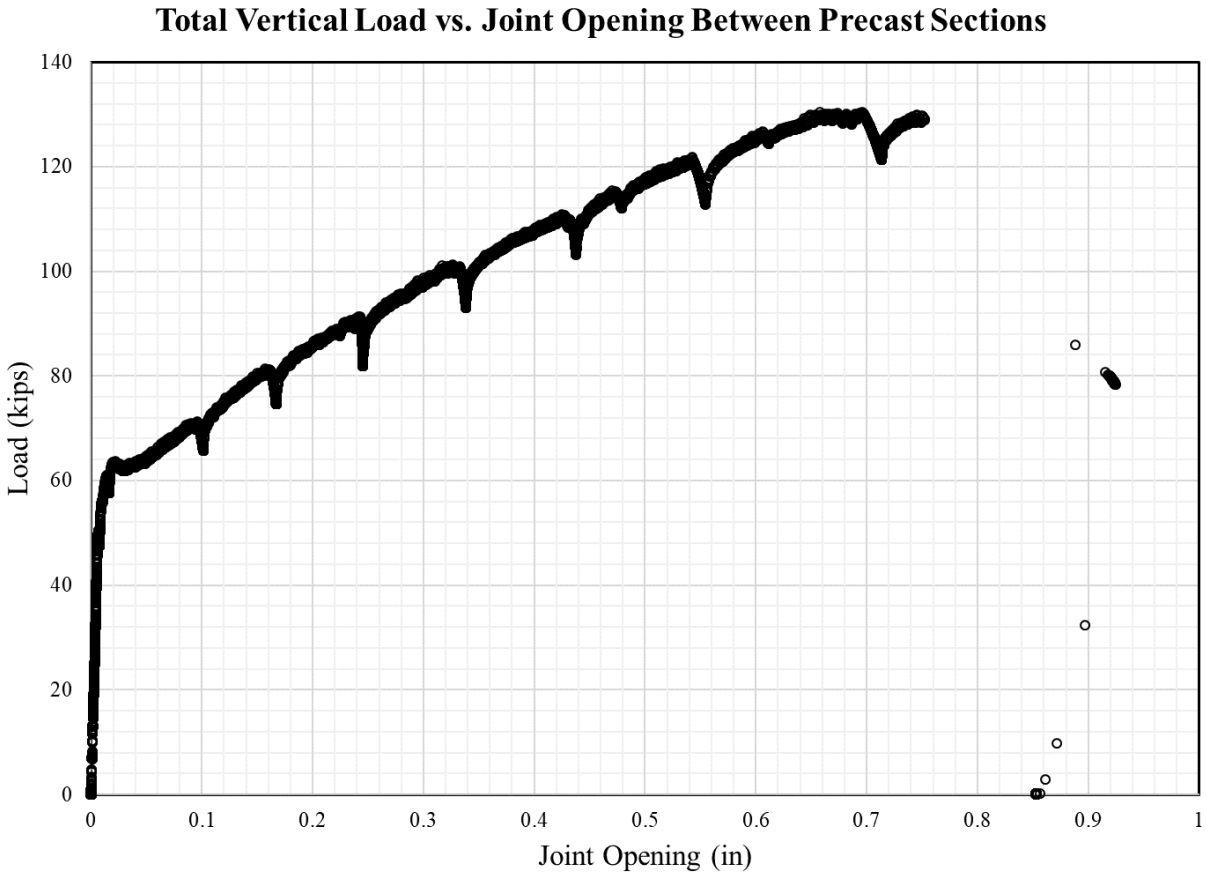

Figure 4.15: Inverted T-Beam failure – combined vertical load vs. joint opening between precast sections

The measured opening of the joint between the precast sections, as reported by the east middle LVDT, is shown in Figure 4.15. The trend of this graph mirrors that of the deflected shape graph, with an initial linear elastic section until 50 kips, a slight decrease in slope until 63 kips, and a much less steep section until flattening out and failing at 130 kips. The first slope is very similar to the 8000 kip/in that characterized the response during the 3650000-cycle monotonic test. The maximum joint opening was 0.75 in. before failure and 0.92 in. after failure.

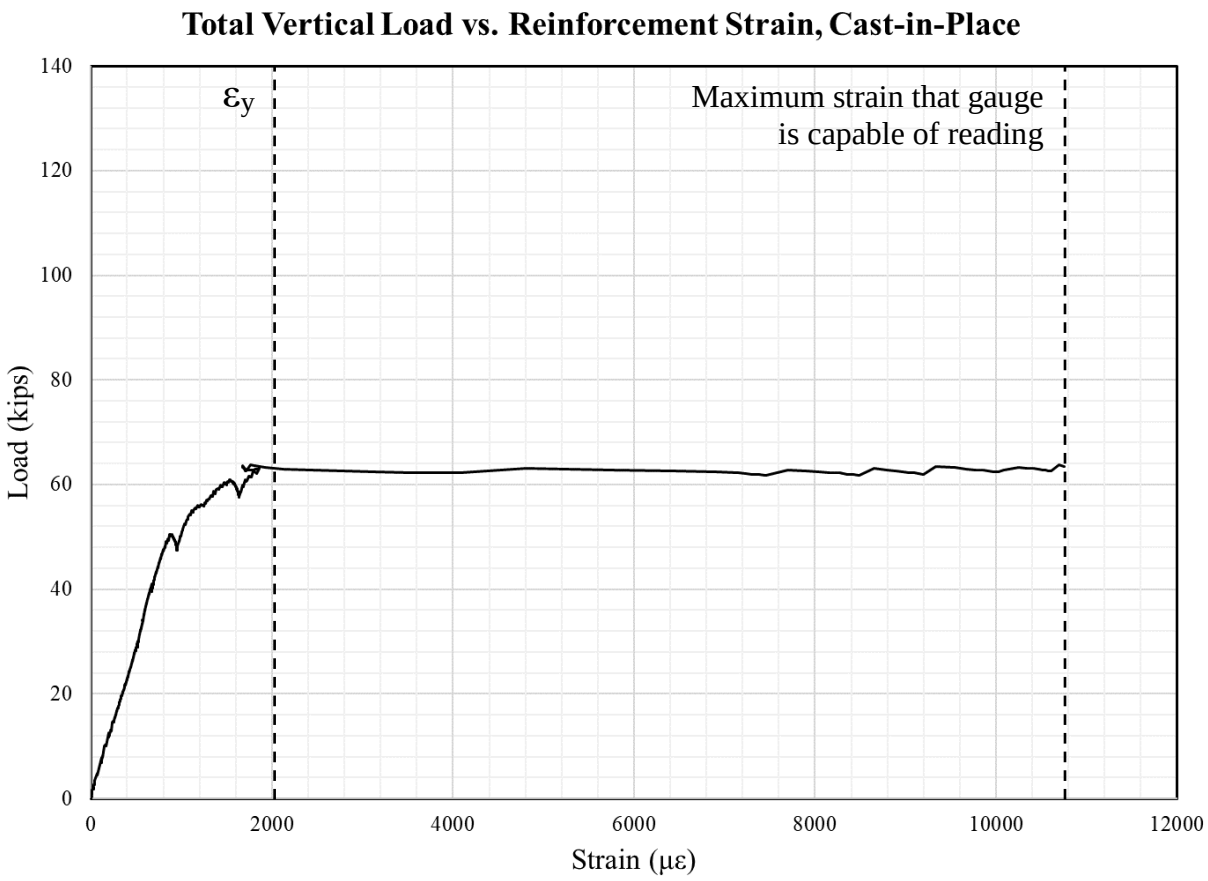

Figure 4.16: Inverted T-Beam failure – combined vertical load vs. reinforcement strain, cast-in-place

The reinforcement strain in the cast-in-place section, as reported by the cast-in-place east strain gauge, is shown in Figure 4.16. The strain shows that the reinforcement is linear elastic until about 50 kips when yielding begins. The linear section has a slope of 0.062 kip/με, which is very close to the 0.056 kip/με from the 3650000 test. The trend plateaus at about 63 kips and the strain increases without a load increase until the strain gauges break at approximately 10800-με.

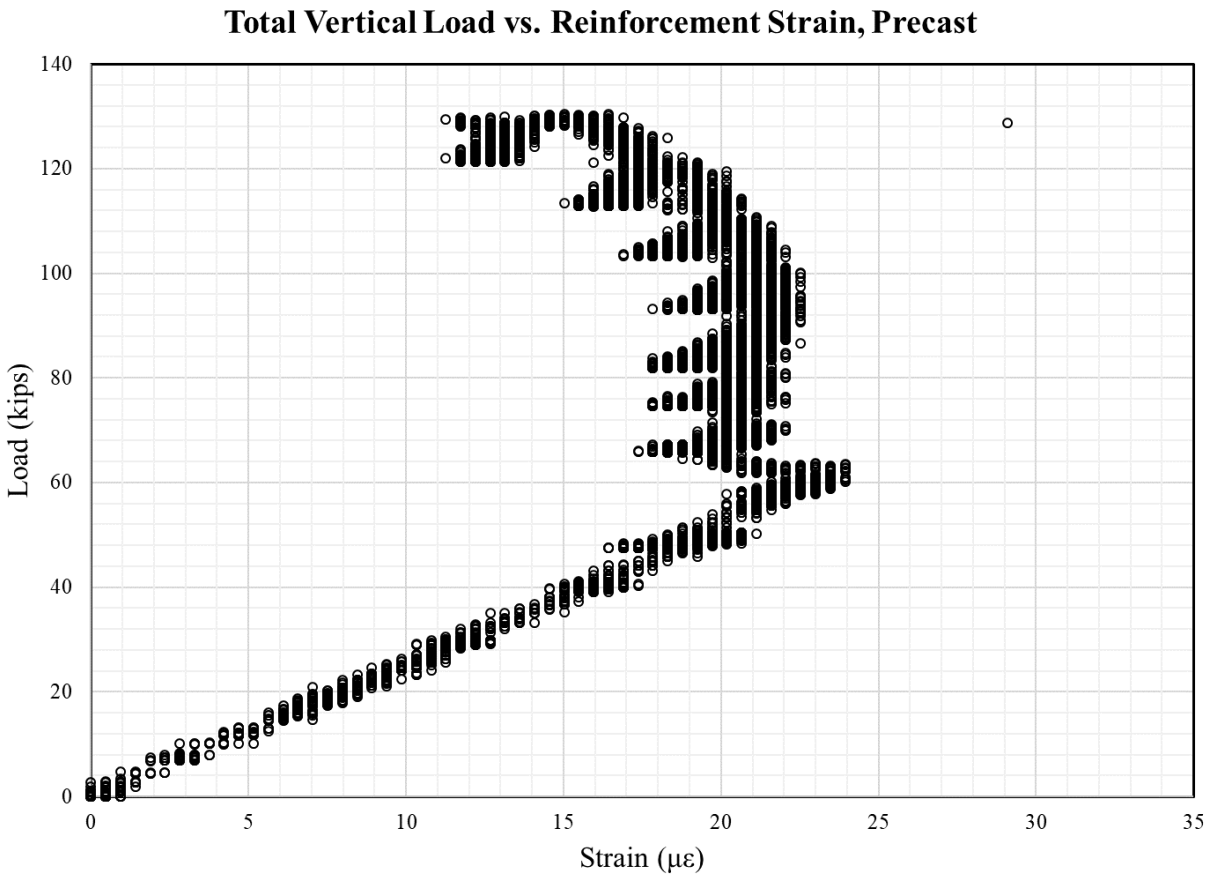

Figure 4.17: Inverted T-Beam failure – combined vertical load vs. reinforcement strain, precast

The reinforcement strain in the precast section, as reported by the precast north-east strain gauge, is shown in Figure 4.17. Up to about 63 kips, the strain linearly increases to about 24-με a slope of 2.5 kip/με. This is very similar to the slope of 2 kip/με that was found for the monotonic tests. After 63 kips, the strain decreases to around 22-με until it begins to fall off at around 100 kips. This decrease occurs much sooner than the deflection or joint opening begin to change, which shows that the load path within the specimen really started to change earlier than the deflection would suggest.

The data shows that the specimen behaved in a linear manner until 63 kips, although the reinforcement strain in the cast-in-place section and the joint opening data show that the reinforcing was beginning to yield at about 50 kips. The specimen began to displace more quickly after 120 kips and ultimately failed at 130 kips.

4.3.5 Comparison to Previous Adhesion-Based Connection Specimen Tests

Three adhesion-based connection sub-assemblage specimens with different reinforcing configurations were tested by Menkulasi (2014). Those specimens failed at loads that ranged from 90 to 240 kips, but the specimen most similar to that tested in this research is the one that failed at 240 kips. Both of the specimen tested by Menkulasi and that of this research failed by way of a large crack in the cast-in-place topping above the joint of the precast flanges [3]. The 110 kip difference between the strength of the specimens can be attributed to the effects from the cyclic testing.

An adhesion-based connection sub-assemblage specimen, identical to the one tested in this research other than the interface roughening, was tested by Edwin (2017) in the same manner as conducted in this research. Similar data was collected in this study as was by Edwin and Table 4.3 summarizes how the values compare. The slopes of the data from the beginning cycles and the end cycles, and slopes were estimated where they weren't given in Edwin (2017) [8].

Table 4.3: Inverted T-Beam data comparison with Edwin (2017)

	Edwin (2017)		**This Research**	
	Beginning	*End*	*Beginning*	*End*
Slope of Load vs. Deflection Curve (kip/in)	2797	1956	1000	2000
Slope of Load vs. Joint Opening (kip/in)	45000	30000	40000	8000
Slope of Load vs. Precast Strain (kip/με)	1.5	1.5	2	2
Slope of Load vs. Cast-in-Place Strain (kip/με)	0.7	0.7	0.5	0.056

The values in the table show many similarities between the specimens. The slopes of the Edwin specimen are all steeper than those in this research except for the precast strain. This means that the Edwin specimen experienced smaller displacements, joint openings, and reinforcement strains in the cast-in-place section, but higher reinforcement strain in the precast section. The Edwin specimen also did not have changes in the values between the beginning and end cycles as large as this research, showing that it did not suffer the same cracking that the specimen in this research did. The values for slope of the load vs. deflection curves the two specimens are

especially different at the beginning, but they are very close at the end. This is most likely due to a variation in the instrumentation readings.

The failure of the Edwin specimen happened at 63 kips and was due to a shear failure of the textured interface between the precast and cast-in-place sections. This value is less than half of the strength achieved by the specimen in this research. The shear failure is much less desirable than a flexural one as it is much more sudden and brittle. Both specimens featured yielding of the central reinforcing in the cast-in-place slab at approximately 63 kips, showing that the nominal construction of the specimens was the same and just the response to the yielding varied. As the reinforcement yielded, alternate pathways would need to be found for further load to be carried and the change in load path exposed the interface of the Edwin specimen as too weak to support those paths. The horizontal shear strength of the interface of the specimen in this research was enough to allow the alternate load paths which lead to an increase in the failure load over that of the Edwin specimen.

Table 5 compares the cracking and failure loads of the three Virginia Inverted T-Beam sub-assemblage specimens from Menkulasi, Edwin, and this research. The factor of safety for each load was calculated by dividing the load by the service load of 30 kip. It is easy to see that the only specimen that was not subjected to cyclic loading, Menkulasi (2014) Specimen 5, exhibited both a much higher cracking strength and a much higher ultimate strength. The factor of safety for the specimen in this research for ultimate is not as high as that of the Menkulasi specimen, but is still adequate at 4.3.

Table 4.4: Comparison of loads and factors of safety for Virginia Inverted T-Beam sub-assemblage tests

	Cracking		**Ultimate**	
	Load (kip)	*Factor of Safety*	*Load (kip)*	*Factor of Safety*
Menkulasi (2014) Specimen 5	70	2.3	240	8.0
Edwin (2017) "No Connection"	40	1.3	63	2.1
This Research	30	1.0	130	4.3

4.3.6 Theoretical Yield and Failure Calculations

To determine if the specimen failure was to be expected at 130 kips and the effects of the cyclic loading, a theoretical calculation of the yielding and failure loads was performed. The same software that was used for the theoretical cracking calculation, Response-2000, and the same inputs were used for these calculations. All inputs and results from Response-2000 can be found in Appendix F. The calculation of yield resulted in a value of 173 kip-ft. and the ultimate in a value of 253 kip-ft. The self-weight moment that was calculated in the theoretical cracking calculation section remains the same, and so the yield load and ultimate load were calculated as follows:

$$X_{Yield} = \frac{173 - 23\ kip - ft}{\frac{3\ ft}{2}} = 100\ kip$$

$$X_{Ultimate} = \frac{253 - 23\ kip - ft}{\frac{3\ ft}{2}} = 153\ kip$$

The actual failure load of 130 kip is directly between the theoretical yield load of 100 kip and ultimate load of 153 kip. The difference between the theoretical ultimate and actual failure loads is most likely due to the cyclic loading, although the use of an assumed reinforcement load vs. strain profile could have also contributed to the difference.

CHAPTER 5: SUMMARY, CONCLUSIONS, AND RECOMMENDATIONS

5.1 Summary

Accelerated Bridge Construction (ABC) is a method of bridge construction or repair that aims at decreasing the duration of time that existing traffic patterns are disrupted. One type of ABC is the Virginia Inverted T-Beam bridge system, the concept of which started out as a beam-slab system being used in France and was refined at the University of Minnesota and Virginia Tech. Two variations of the system are in use today, the welded flange connection and the adhesion-based connection, with the former approved for use in high traffic areas and the latter approved for low traffic areas. The adhesion-based connection is much easier and cheaper to construct, and so approval for its use in high traffic areas was desired. The approval hinged on the ability of tests to prove that the adhesion-based connection could maintain a high ultimate failure strength after the fatigue of a 50 year design life.

Cyclic tests were performed on the two different connection configurations. Each specimen underwent an equivalent 50 year design life of service loading and then was tested for an ultimate failure load. The welded connection specimen performed adequately, but issues with the selected surface roughening lead to a premature failure of the adhesion-based connection specimen at only 63 kips, roughly 30 kips less than desired. It was suspected that the failure was caused by a lack of shear strength across the interface between the precast and cast-in-place sections. It was recommended that an investigation be done into what surface roughening methods produced adequate shear strength and that the cyclic testing be redone on a new specimen with a better interface connection.

The first phase of this research consisted of testing 10 different surface roughening textures to determine the attributes that contribute to higher shear strength. A total of 30 horizontal shear push-off specimens with an interface area of 384 in^2 were constructed and tested. An average interface fracture stress was found for each texture type and the values compared. The texture utilized for the previous sub-assemblage specimens, a cross hatch pattern de-bonded from the

form with plastic, was found to have one of the lowest fracture stresses, and a trapezoidal grooves texture with 1.5 in. spacing was recommended for the new sub-assemblage specimen.

The second phase of this research began with the construction of an adhesion-based connection sub-assemblage specimen with the trapezoidal grooves texture. The specimen was then subjected to 3,650,000 loading cycles to simulate 50 years of design life, followed by an ultimate failure load test. The specimen failed by way of a flexural crack in the center of the specimen at 130.4 kips. The behavior of the specimen up to the previous level of failure is very similar except that the previous specimen did not gain strength after the reinforcement began to yield.

5.2 Conclusions

5.2.1 Horizontal Shear Push-off Specimens

The following conclusions were made using the data that was discussed in section 4.2 Horizontal Shear Push-off Specimens:

- The surface textures that produced the highest horizontal shear strengths featured sharp edges and equal amounts of surface area allotted at the high and low points of the texture.
- The horizontal shear strength is dependent upon the spacing of the grooves; the closer they are, the higher the strength.
- For applications where horizontal shear strength is desired in two perpendicular directions, a cross hatch type texture can be used without sacrificing the strength in the first direction.
- Raked textures are adequate if the spacing is small (1-in) but the nature of the production of the texture increases the variability in the quality of the texture and therefore the strength.
- Exposed aggregate texture strengths are highly dependent upon the aggregate type and size used within the concrete mix.
- The type of de-bonding method used to produce manufactured type textures matters; the application of a TuffCoat® spay worked much better than plastic sheeting for textures produced out of plywood sheeting, although care must also be taken when producing textures with other mediums to ensure that the edges of the texture remain sharp.

5.2.2 Virginia Inverted T-Beam Sub-Assemblage Specimen

The following conclusions were made using the data that was discussed in section 4.3 Virginia Inverted T-Beam Sub-Assemblage Specimen:

- The degradation of the interface over a 50 year design life will decrease the ultimate failure strength of the Virginia Inverted T-Beam bridge system featuring an adhesion-based connection as compared to the original strength.
- Flexural type failures occur at higher loads than shear type failures.
- A surface treatment that has an adequate horizontal shear strength is necessary to achieve a flexural type failure.
- When an adequate surface treatment is used on the interface between the precast and cast-in-place sections, the Virginia T-Beam bridge system does have enough strength at the end of a 50 year design life to warrant approval for high daily traffic bridges.

5.3 Recommendations

5.3.1 Interface Roughening Methods

Currently, very little guidance is given designers and constructors on how to produce sufficient shear strength besides requiring 0.25 in. amplitude of roughening. Suggestions about what shapes and spacing of the roughening are adequate for different situations are given below.

For situations where the bond between a precast section and a cast-in-place slab is critical to the performance of the system, such as in the adhesion-based connection version of the Virginia Inverted T-Beam bridge system, the use of the following interface roughening methods are recommended:

- For surfaces cast against formwork, such as sloped webs and flanges (provided that the integrity of the texture is preserved during form removal):
  - Trapezoidal grooves, spaced a maximum of 3 in.
  - Cross hatch, spaced 3.5 in.
  - Straight sided grooves, spaced 1 in.
- For the surfaces exposed during casting, such as the tops of the beams:
  - Raked grooves, spaced a maximum of 1 in.

For situations where the bond between a precast section and a cast-in-place slab is not critical to the performance of the system, such as in the welded connection version of the Virginia Inverted T-Beam bridge system, the use of the following interface roughening methods are recommended:

- For surfaces cast against formwork, such as sloped webs and flanges:
  - Square knobs, spaced 2.5 in.
  - Exposed aggregate
- For surfaces exposed during casting, such as the tops of beams:
  - Raked grooves, spaced a maximum of 3 in.

5.3.2 Virginia Inverted T-Beam Bridge System

The adhesion-based connection version of the Virginia Inverted T-Beam bridge system is recommended for use in high daily traffic areas.

5.3.3 Future Research

More data is needed to determine if the non-linear relationship between spacing and shear strength that appeared with the raked specimens was in fact a fluke. Testing more specimens with different spacing patterns would help reveal if an increase in spacing does cause a decrease in shear strength, or if unpredictability is simply an aspect of the texture type. Additional research should be conducted to ensure that formed surface textures produced at precast plants with metal forms produce the same shear strengths as those produced in the laboratory with plywood forms.

REFERENCES

[1] M. P. Culmo, "Accelerated Bridge Construction," USDOT FHWA, McLean VA, 2011.

[2] E. P. Steinberg and A. A. Semendary, "Evaluation of Transverse Tie Rods in a 50-Year-old Adjacent Prestressed Concrete Box Beam Bridge," *Journal of Bridge Engineering,* vol. 22, no. 3, 2017.

[3] F. Menkulasi, "The Development of a Concrete Bridge System for Short-to-Medium-Span Bridges," Virginia Polytechnic Institute & State University, Blacksburg, VA, 2014.

[4] Matiere, "Poutre Dalle," 2018. [Online]. Available: https://www.matiere-tp.fr/poutre-dalle/. [Accessed 18 April 2018].

[5] C. M. Bell II, C. E. French and C. K. Shield, "Application of Precast Decks and Other Elements to Bridge Structures," MnDOT, Minneapolis, MN, 2006.

[6] F. Menkulasi, T. Cousins and C. L. Roberts-Wollmann, *IMPLEMENTATION OF A PRECAST INVERTED T-BEAM SYSTEM,* Charlottesville VA: Virgninia Center for Transportation Innovation and Research, 2017.

[7] C. L. Roberts-Wollmann, T. Cousins and F. Menkulasi, "Virginia's Development of an Inverted-tee Beam Bridge System," *ASPIRE - The Concrete Bridge Magazine,* 2016.

[8] E. B. A. Edwin, "Refinement of the Inverted T-Beam Bridge System for Virginia," Virginia Polytechnic Institute & State University, Blacksburg, VA, 2017.

[9] M. Lang, "Analysis of the AASHTO LRFD Horizontal Shear Strength Equation," Virginia Polytechnic Institute & State University, Blacksburg VA, 2011.

[10] N. W. Hanson, "Precast-Prestressed Concrete Bridges 2. Horizontal Shear Connections," *Journal of the PCA Research and Development Laboratores,* vol. 2, no. 2, pp. 38-60, 1960.

[11] J. C. Saemann and G. W. Washa, "Horizontal Shear Connections Between Precast Beams and Cast-in-Place Slabs," *Journal of the American Concrete Institute,* vol. 11, no. 61, pp. 1383-1408, 1964.

[12] J. A. Hofbeck, I. O. Ibrahim and et al., "Shear Transfer in Reinforced Concrete," *Journal of American Concrete Institute,* vol. 1, no. 66, pp. 119-128, 1969.

[13] A. H. Mattock, L. Johal and et al., "Shear Transfer in Reinforced Concrete with Moment or Tension Acting Across the Shear Plane," *PCI Journal,* vol. 4, no. 20, pp. 76-93, 1975.

[14] A. H. Mattock, W. K. Li and et al., "Shear Transfer in Lightweight Reinforced Concrete," *PCI Journal,* vol. 1, no. 21, pp. 20-39, 1976.

[15] J. C. Walraven and H. W. Reinhardt, "Theory and Experiments on the Mechanical Behaviour of Cracks in Plain and Reinforced Concrete Subjected to Shear Loading," *Heron,* vol. 1a, no. 26, p. 68, 1981.

[16] R. A. Bass, R. L. Carrasquillo and et al., "Shear Transfer across New and Existing Concrete Interfaces," *ACI Structural Journal,* vol. 4, no. 86, pp. 383-393, 1989.

[17] R. E. Loov and A. K. Patnaik, "Horizontal Shear Strength of Composite Concrete Beams With a Rough Interface," *PCI Journal,* vol. 1, no. 39, pp. 48-69, 1994.

[18] D. Choi, "An Experimental Investigation of Interface Bond Strength of Concrete Using Large Powder-Driven Nails.," The University of Texas at Austin, Austin, Tx, 1996.

[19] M. R. Kamel, "Innovative Precast Concrete Composite Bridge Systems," University of Nebraska, Lincoln, Ne, 1996.

[20] R. Valluvan, M. E. Kreger and et al., "Evaluation of ACI 318-95 Shear-Friction Provisions," *ACI Structural Journal,* vol. 4, no. 96, pp. 473-481, 1999.

[21] A. K. Patnaik, "Behavior of Composite Concrete Beams with Smooth Interface," *Journal of Structural Engineering,* vol. 4, no. 127, pp. 359-366, 2001.

[22] L. F. Kahn and A. D. Mitchell, "Shear Friction Tests with High-Strength Concrete," *ACI Structural Journal,* vol. 1, no. 99, pp. 98-103, 2002.

[23] L. F. Kahn and A. Slapkus, "Interface Shear in High Strength Composite T-Beams," *PCI Journal,* vol. 4, no. 49, pp. 102-110, 2004.

[24] T. E. Banta, "Horizontal Shear Transfer Between Ultra High Performance Concrete and Ligheweight Concrete," Virginia Polytechnic Institute & State University, Blacksburg VA, 2005.

[25] J. Scott, "Interface Shear Strength in Lightweight Concrete Bridge Girders," Virginia Polytechnic Institute & State University, Blacksburg VA, 2010.

[26] E. B. Sells, "Self-Consolidating Concrete for Infrastructure Elements Shear Characteristics," Missouri University of Science and Technology, Rolla, MO, 2012.

[27] D. M. Shaw, "Direct Shear Transfer of Lightweight Aggregate Concretes With Non-Monolithic Interface Conditions," Missouri University of Science and Technology, Rolla, MO, 2013.

[28] K. Krc, "An Investigation of Shear-Friction of Lightweight Aggregate Concrete," Missouri University of Science and Technology, Rolla, MO, 2015.

[29] M. Soltani, "Interface Shear Transfer in Reinforced Concrete Members: Code Evaluation, Modeling, and Testing," Clemson University, Clemson, SC, 2016.

[30] American Association of State Highway and Transportation Officials, "AASHTO LRFD Bridge Design Specifications," AASHTO, Washington, DC, 2017.

[31] American Concrete Institute, "Building Code Requirements for Structural Concrete (ACI 318-14)," American Concrete Institute, Farmington Hills, MI, 2015.

[32] International Federation for Structural Concrete, "fib Model Code for Concrete Structures 2010," fib, Lausanne, Switzerland, 2013.

[33] Rhino Linings Corportation, *TuffCoat Data Sheet.*

APPENDIX A: REINFORCEMENT DETAILS

Horizontal Shear Push-off Specimens Reinforcing Cage Specifications

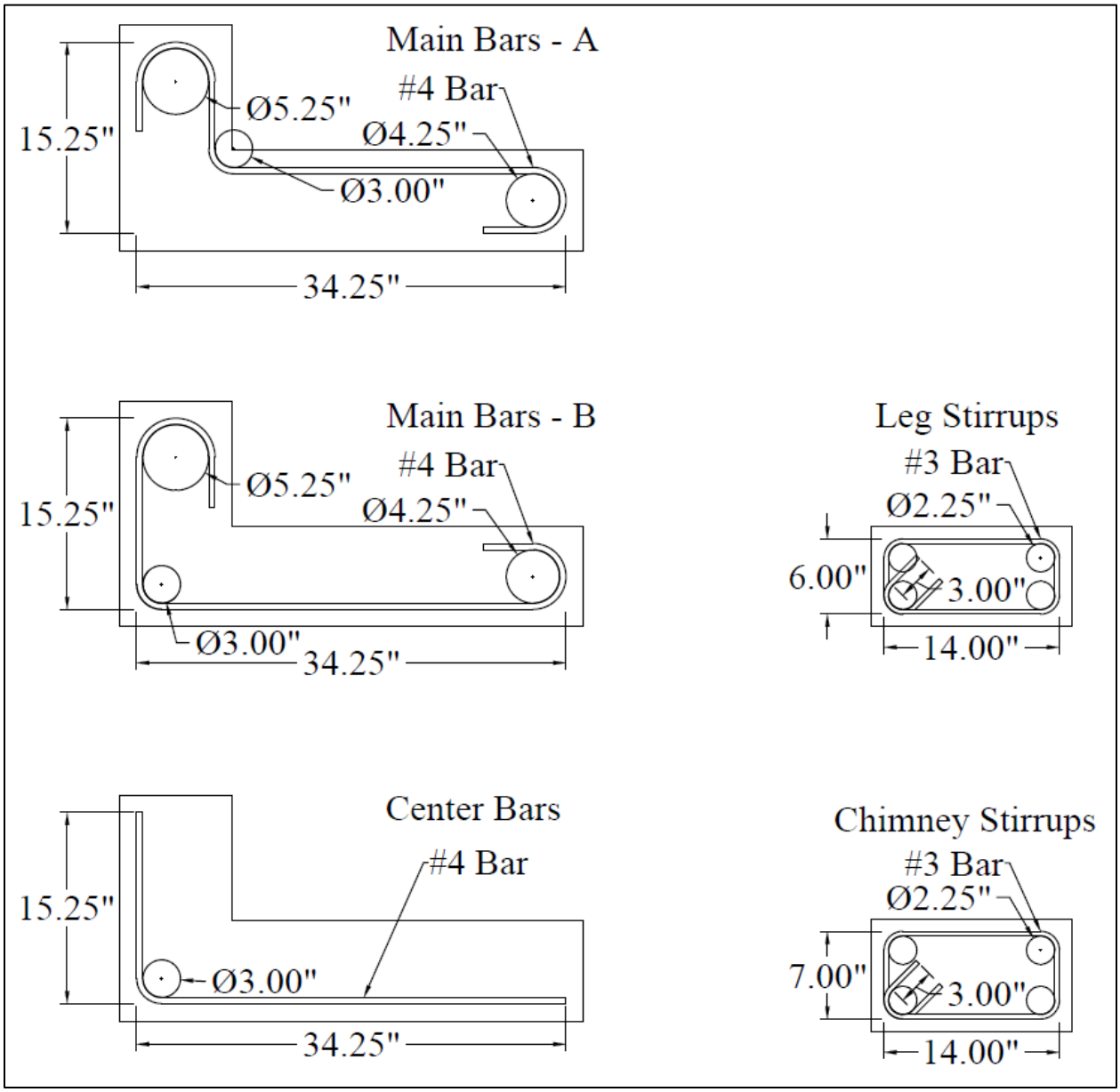

Each cage (two cages per specimen) requires two of each Main Bars – A, Main Bars – B, and Center Bars, and three of each Leg Stirrups and Chimney Stirrups.

Virginia Inverted T-Beam Sub-Assemblage Specimen Reinforcing Cage Specifications

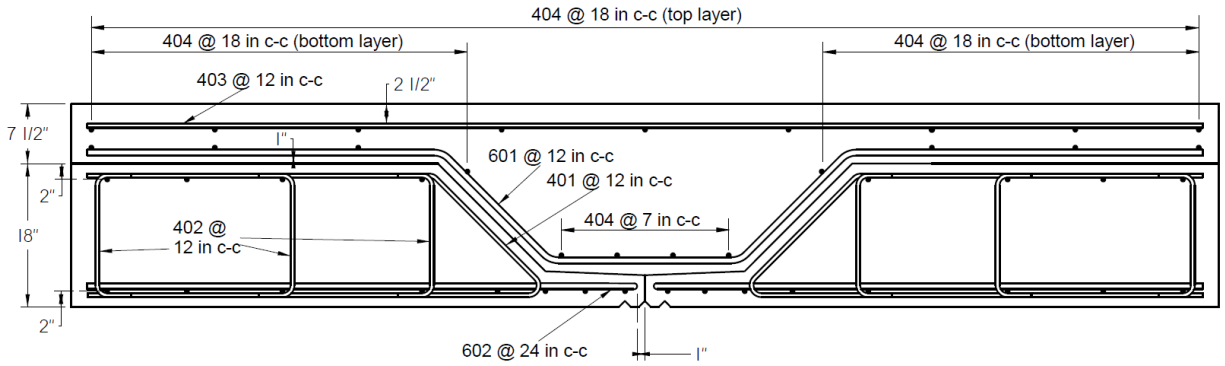

No Connection Connection

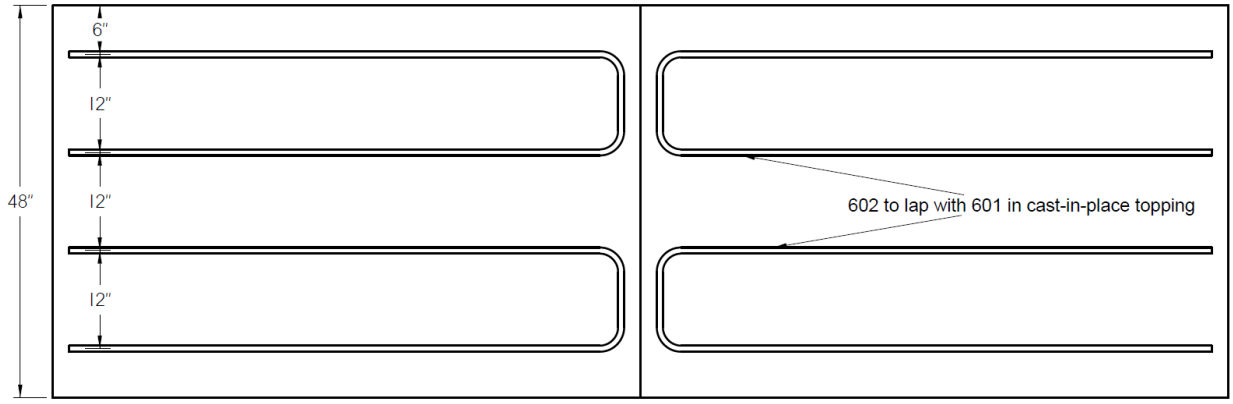

Plan View of Layout of Bottom Reinforcement for No Connection Connection

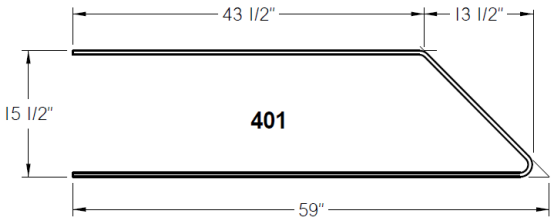

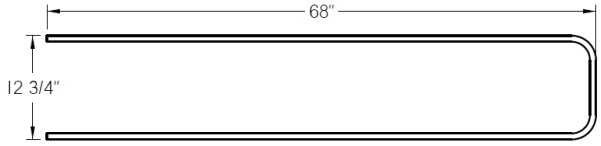

602

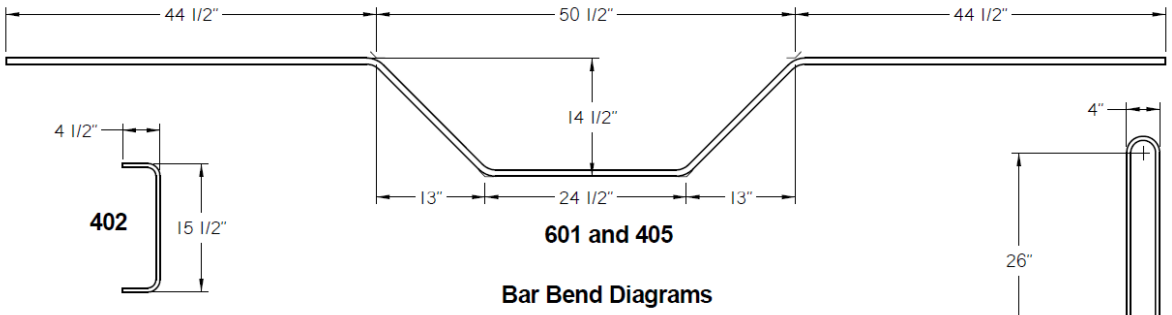

601 and 405

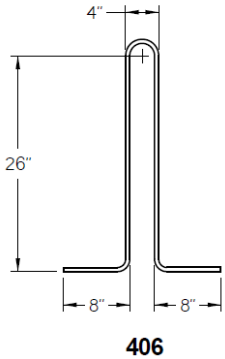

406

Bar Bend Diagrams

Mark	Size	Bend	Length	Wt. each, lbs	No. Required	Total Wt., lbs	Type
601	#6	601	12’-10.5”	19.34	4	77.4	A615 Gr60
602	#6	602	12”-5”	18.65	5	93.2	A615 Gr60
401	#4	401	9’-8”	6.46	8	51.7	A615 Gr60
402	#4	402	2’-0.5”	1.36	25	34.1	A615 Gr60
403	#4	STR	11’-8”	7.79	4	31.2	A615 Gr60
404	#4	STR	3’-8”	2.45	50	122.5	A615 Gr60
406	#4	406	6’-8.5”	4.48	6	26.9	A615 Gr60

APPENDIX B: CONCRETE MIXES AND STRENGTHS

Horizontal Shear Push-off Specimens Concrete Mix Designs

4000 psi (Conrock Mix No. 2010-02-10)

W/C Ratio – 0.44
Theoretical Unit Weight – 144.84 lbs./ft^3
Air Content – 6.5%
Slump – 2 to 4 in

Cement – (Type I/II) 536 lbs.
Fly Ash – 134 lbs.
Sand – 1177 lbs.
No. 57 Aggregate – 1773 lbs.
Water – (35 gal.) 291.5 lbs.
Air Entrainment – varies
Retarder – varies
Water Reducer - varies

8000 psi (Conrock Mix No. 80003)

W/C Ratio – 0.35
Theoretical Unit Weight – 147.18 lbs./ft^3
Air Content – 5.5%
Slump – 5 to 7 in.

Cement – (Type I/II) 675 lbs.
Microsilica – 53 lbs.
Sand – 1444 lbs.
#8 Aggregate – 1544 lbs.
Water – (31 gal.) 259 lbs.
Air Entrainment – varies
Retarder – varies
Water Reducer – varies

Horizontal Shear Push-off Specimens Concrete Mix Proportions

6/20/2017 8000 psi mix (3 yd^3)

Unit Weight – 144 lbs./ft^3
Air Content – 5.5%
Slump – 2.5 in (3.5 in after added water)

Note: mix was very stiff due to high temperature, so extra water was added

#8 Aggregate – 4640 lbs.
Sand – 4560 lbs.
Cement – 1955 lbs.
Water – 50 gal. (12 gal. wash, 4 gal. added)
Air Entrainment – 3 fl. oz.
Retarder – 68 fl. oz.
Medium Range Water Reducer – 78 fl. oz.

6/20/2017 4000 psi mix (3 yd^3) – Not Available

8/2/2017 8000 psi mix (3 yd^3)

Unit Weight – NA
Air Content – 5.2%
Slump – 6.5 in

#8 Aggregate – 4640 lbs.
Sand – 4560 lbs.
Cement – 1955 lbs.
Water – 68 gal. (5 gal. wash)
Air Entrainment – 6 fl. oz.
Retarder – 68 fl. oz.
Medium Range Water Reducer – 20 fl. oz.

8/17/2017 4000 psi mix (3 yd^3)

Unit Weight – 148.4 lbs./ft^3
Air Content – 5%
Slump – 3 in (4 in after added water)

#8 Aggregate – 5320 lbs.
Sand – 3580 lbs.
Cement – 1610 lbs.
Fly Ash – 400 lbs.
Water – 103 gal. (7 gal. wash, added 5 gal.))
Air Entrainment – 7 fl. oz.
Retarder – 101 fl. oz.
Medium Range Water Reducer – 20 fl. oz.

9/12/2017 8000 psi mix (3 yd^3)

Unit Weight – NA
Air Content – 6%
Slump – 6 in

#8 Aggregate – 4640 lbs.
Sand – 4600 lbs.
Cement – 1955 lbs.
Water – 50 gal. (5 gal. wash, 10 gal. added)
Air Entrainment – 3 fl. oz.
Retarder – 68 fl. oz.
Medium Range Water Reducer – 20 fl. oz.

10/3/2017 4000 psi mix (3 yd^3)

Unit Weight – NA

Air Content – 5.9%

Slump – 6.5 in

#8 Aggregate – 5320 lbs.

Sand – 3580 lbs.

Cement – 1610 lbs.

Fly Ash – 400 lbs.

Water – 103 gal. (5 gal. wash)

Air Entrainment – 7 fl. oz.

Retarder – 101 fl. oz.

Medium Range Water Reducer – 20 fl. oz.

Horizontal Shear Push-off Specimens Concrete Compressive Strengths

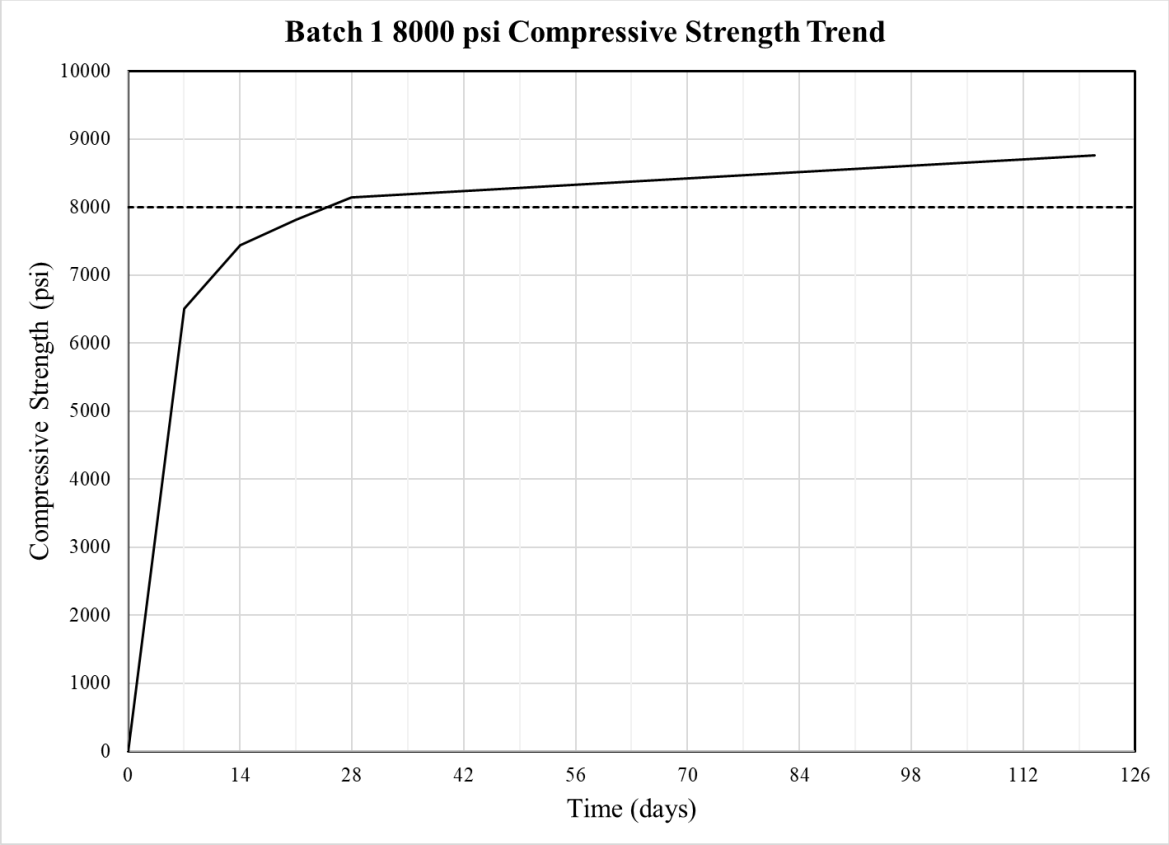

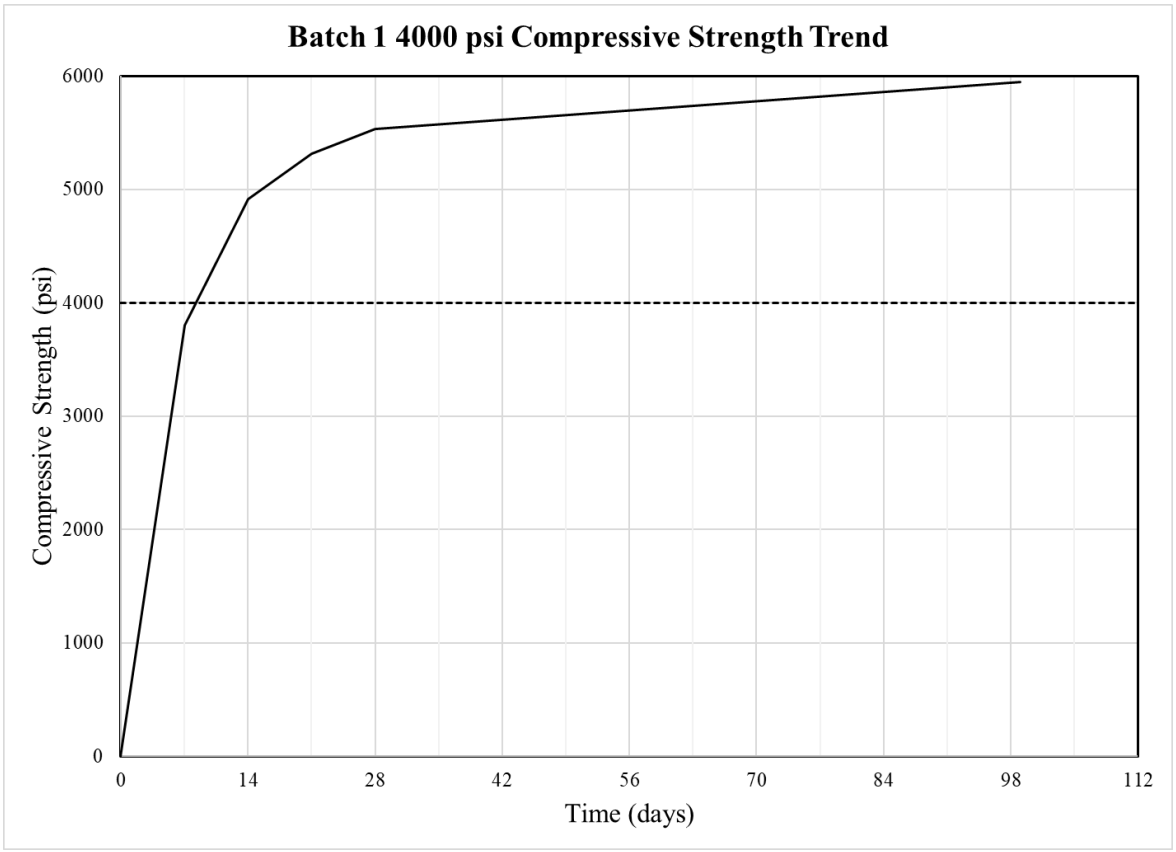
Batch 1 4000 psi Compressive Strength Trend
Compressive Strength (psi)
6000
5000
4000
3000
2000
1000
0
0
14
28
42
56
70
84
98
112
Time (days)

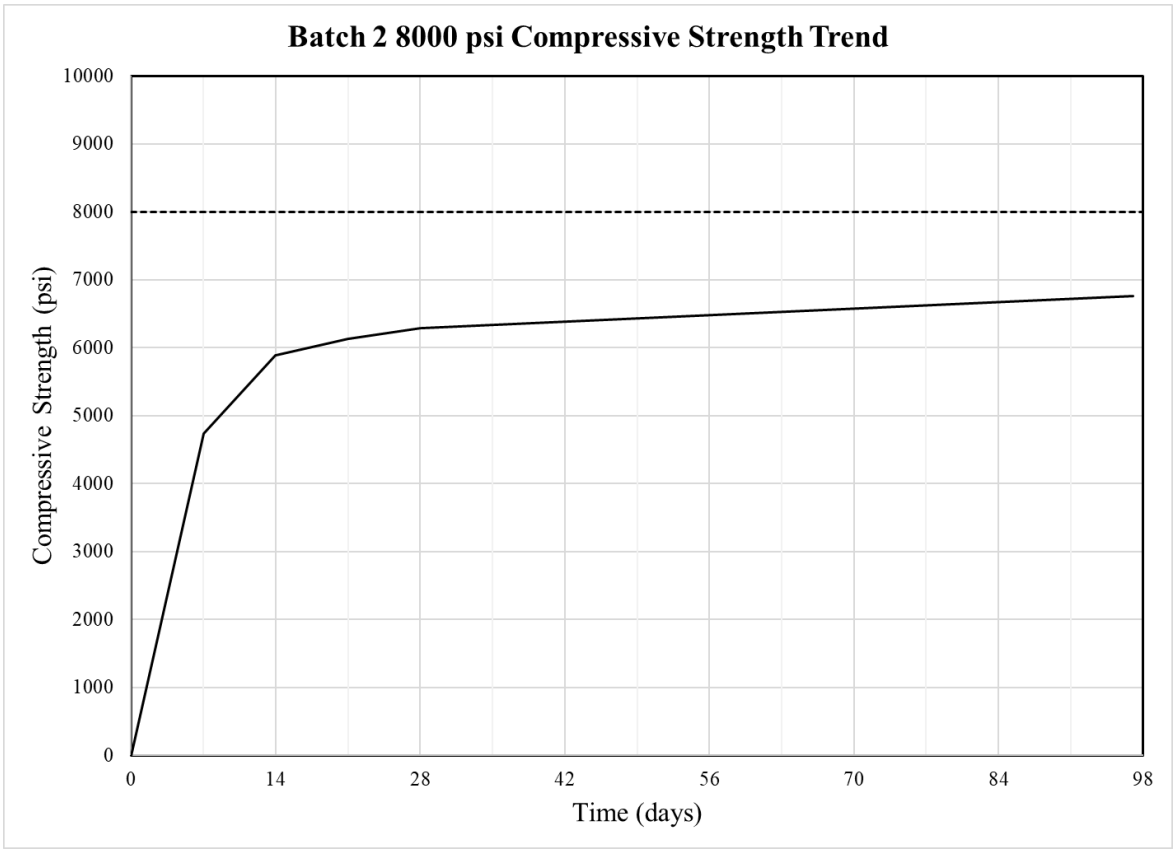
Batch 2 8000 psi Compressive Strength Trend
Compressive Strength (psi)
10000
9000
8000
7000
6000
5000
4000
3000
2000
1000
0
0
14
28
42
56
70
84
98
Time (days)

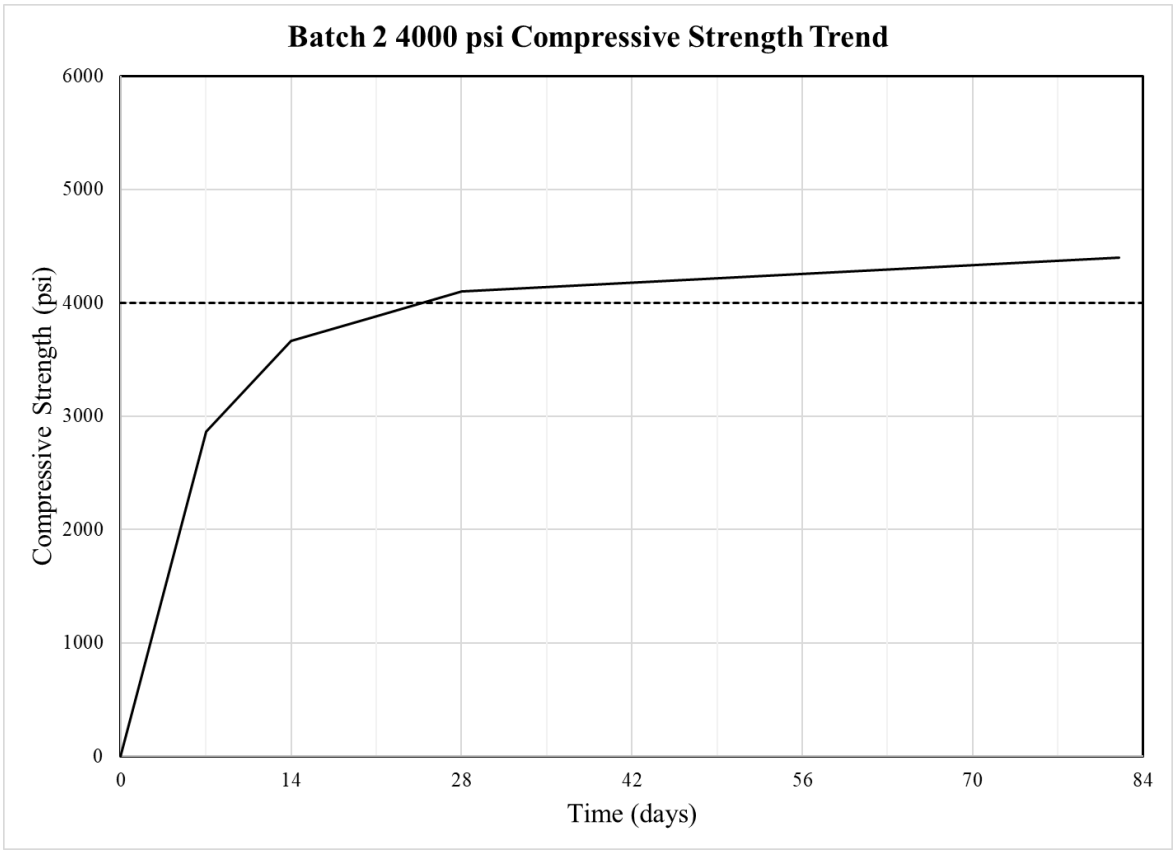
Batch 2 4000 psi Compressive Strength Trend
Compressive Strength (psi)
6000
5000
4000
3000
2000
1000
0
0
14
28
42
56
70
84
Time (days)

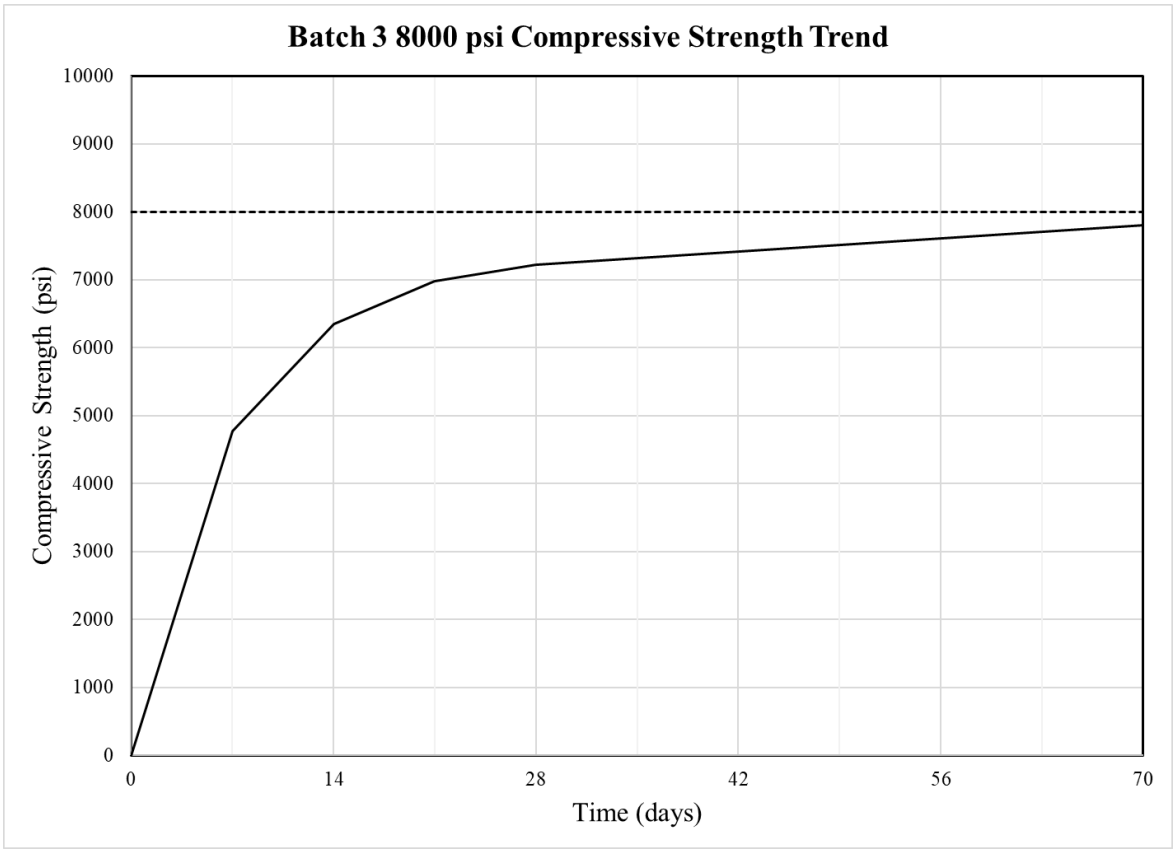
Batch 3 8000 psi Compressive Strength Trend
Compressive Strength (psi)
10000
9000
8000
7000
6000
5000
4000
3000
2000
1000
0
0
14
28
42
56
70
Time (days)

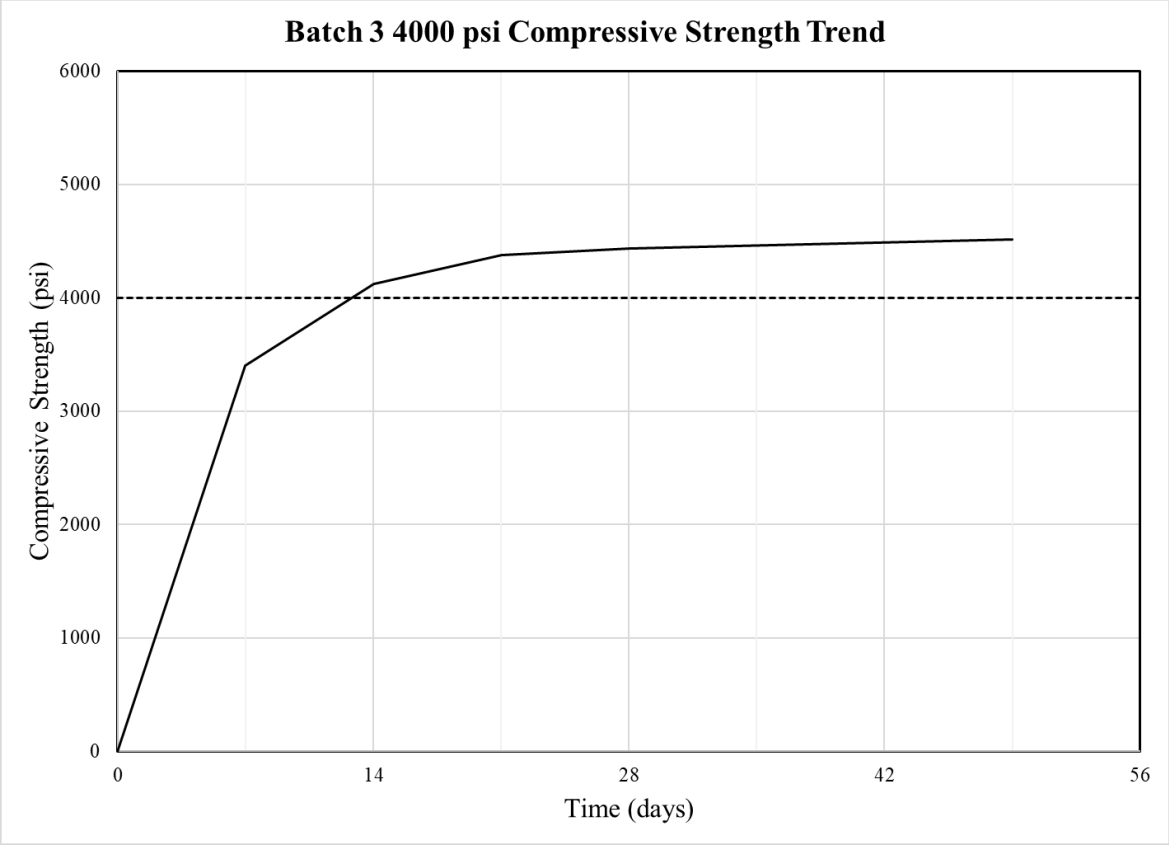
Batch 3 4000 psi Compressive Strength Trend
6000
5000
4000
3000
2000
1000
0
Compressive Strength (psi)
0
14
28
42
56
Time (days)

Inverted T-Beam Sub-Assemblage Specimen Concrete Mix Designs

4000 psi (Chandler Mix V40F)

W/C Ratio – 0.42
Theoretical Unit Weight – 145.7 lbs./ft^3
Air Content – 5%
Slump – 2 to 4 in

Cement – (Type I/II) 540 lbs.
Fly Ash – 135 lbs.
Sand – 1240 lbs.
No. 57 Aggregate – 1736 lbs.
Water –283 lbs.
Air Entrainment – 1.10/C
Retarder – 4.00/C

8000 psi (Chandler Mix V80G)

W/C Ratio – 0.33
Theoretical Unit Weight – 148.9 lbs./ft^3
Air Content – 5.5%
Slump – 5 to 7 in.

Cement – (Type I/II) 475 lbs.
Slag Cement – 317 lbs.
Sand – 11347 lbs.
No. 68 Aggregate – 1620 lbs.
Water –262 lbs.
Air Entrainment – 0.10/C
Retarder – 2.00/C
Water Reducer – 5.00/C

Inverted T-Beam Sub-Assemblage Specimen Concrete Mix Proportions

2/5/2018 8000 psi mix (3 yd^3)

Unit Weight – 150.7 lbs./ft^3
Air Content – 5.5%
Slump – 6 in

No. 68 Aggregate – 4840 lbs.
Sand – 4180 lbs.
Cement – 1430 lbs.
Slag Cement – 1050 lbs.
Water – 555 lbs. (141.9 lbs. wash)
Air Entrainment – 2 fl. oz.
Retarder – 47 fl. oz.
Medium Range Water Reducer – 116 fl. oz.

2/9/2017 4000 psi mix (3 yd^3)

Unit Weight – 145.7 lbs.

Air Content – 5.2%

Slump – 2 in (4.5 in after added water)

No. 57 Aggregate – 5260 lbs.

Sand – 3780 lbs.

Cement – 1610 lbs.

Fly Ash – 410 lbs.

Water – 570 lbs. (166.9 lbs. wash)

Air Entrainment – 22 fl. oz.

Retarder – 81 fl. oz.

Inverted T-Beam Sub-Assemblage Specimen Concrete Compressive Strengths

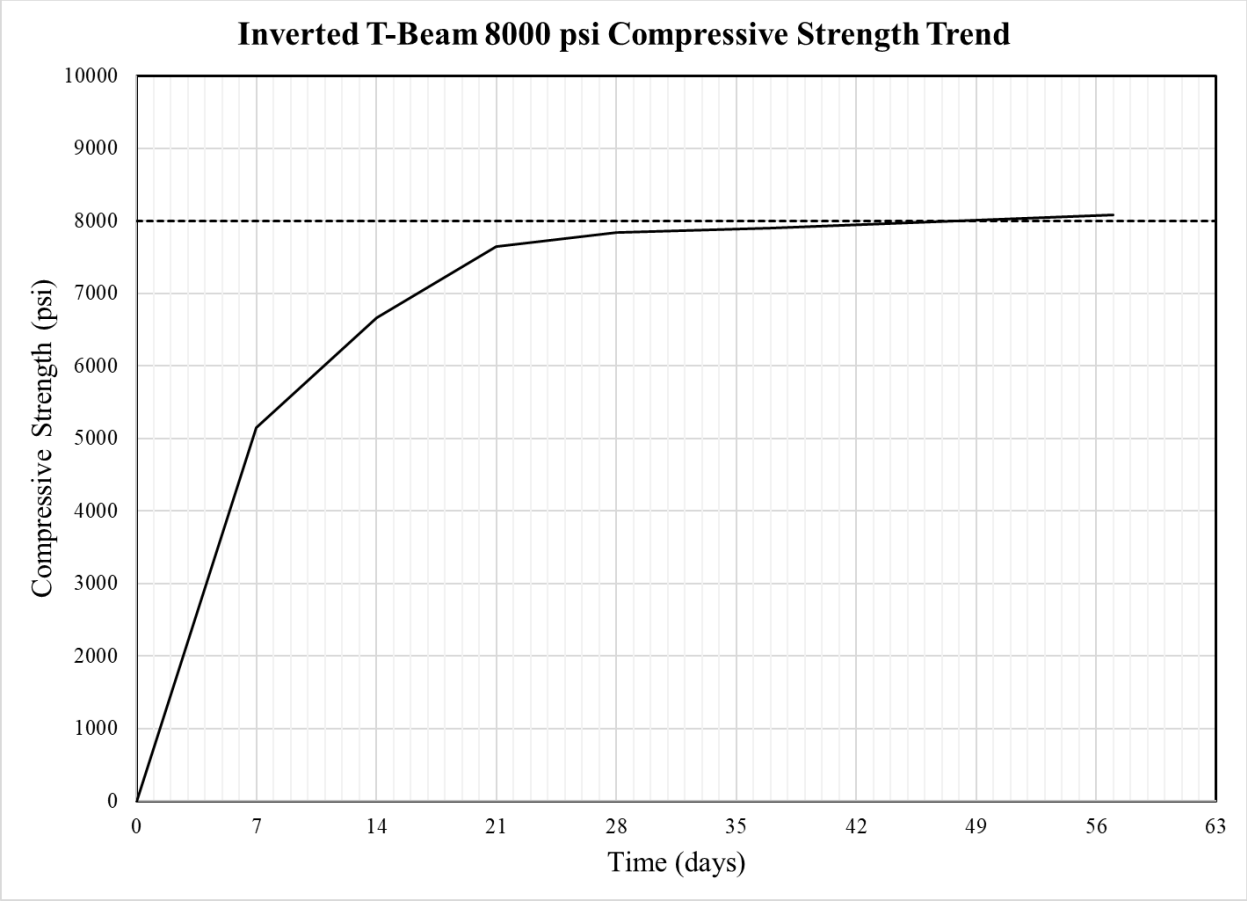

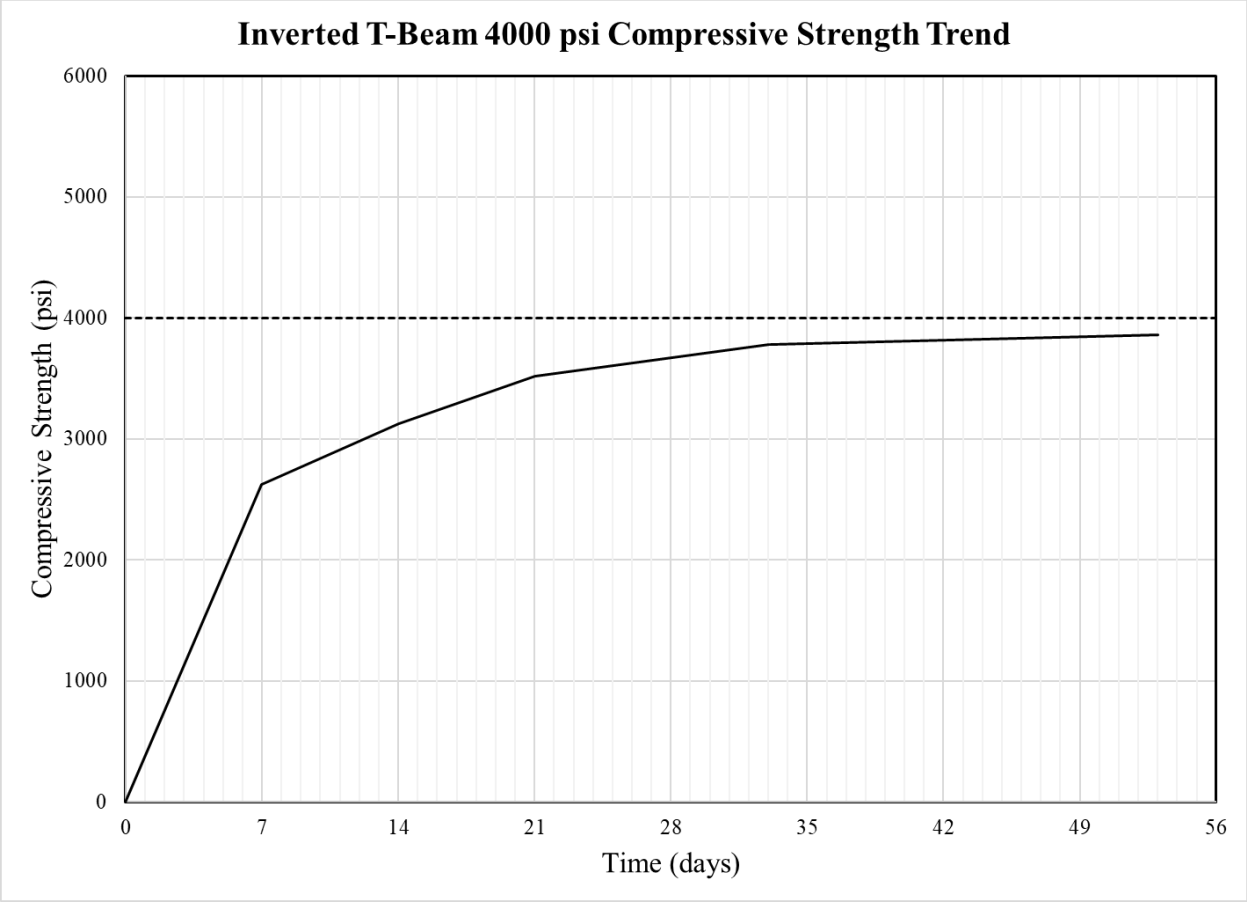
Inverted T-Beam 4000 psi Compressive Strength Trend
Compressive Strength (psi)
6000
5000
4000
3000
2000
1000
0
0
7
14
21
28
35
42
49
56
Time (days)

APPENDIX C: PRODUCT SPECIFICATIONS

TML STRAIN GAUGE TEST DATA

GAUGE TYPE	: WFLA-6-11	TESTED ON	: SS 400
LOT NO.	: A514712	COEFFICIENT OF THERMAL EXPANSION	: 11.8 $\times 10^{-6}$/℃
GAUGE FACTOR	: 2.11 ±1%	TEMPERATURE COEFFICIENT OF G.F.	: +0.1±0.05 %/10℃
ADHESIVE	: P-2	DATA NO.	: B0222

THERMAL OUTPUT (ε app : APPARENT STRAIN)

$\varepsilon app = -2.68\times10^{1}+2.42\times T^{1}-6.16\times10^{-2}\times T^{2}+3.93\times10^{-4}\times T^{3}-8.68\times10^{-7}\times T^{4}$ (μm/m)

TOLERANCE : ±0.85 [(μm/m)/℃] , T : TEMPERATURE

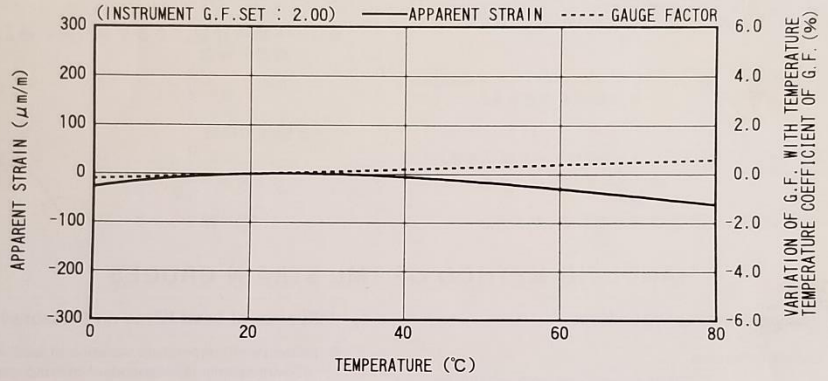

ひずみゲージ取扱いの注意事項

- ●上記の特性データは、リード線の取付けによる影響を含んでおりません。裏面記載のリード線の測定値への影響に従って補正してください。
- ●ゲージの使用温度は、接着剤の耐熱温度などにより変わります。
- ●絶縁抵抗などの点検は、印加電圧を５０V以下にしてください。
- ●ゲージリード線に無理な力を加えないでください。
- ●ゲージ裏面に接着剤を塗布して接着してください。
- ●ひずみゲージの裏面は脱脂洗浄してありますので、汚さないように取扱いしてください。
- ●ゲージの包装を開封後は、乾燥した場所で保管してください。
- ●ご使用に際してご不明な点などがございましたら、当社までお問い合わせください。

CAUTIONS ON HANDLING STRAIN GAUGES

- ● The above characteristic data do not include influence due to lead wires. Correct the data in accordance with the influence of lead wires on measured values described overleaf.
- ● The service temperature of strain gauge depends on the operating temperature of adhesive, etc.
- ● Check of insulation resistance, etc. should be made at a voltage of less than 50V.
- ● Do not apply an excessive force to the gauge leads.
- ● Apply an adhesive to the back of a strain gauge and stick the gauge to a specimen.
- ● As the back of strain gauge has been degreased and washed, do not contaminate it.
- ● After unpacking, store strain gauges in a dry place.
- ● If you have any questions on strain gauges or installation, contact TML or your local agent.

Made in Japan

TML 株式會社 東京測器研究所

〒140-8560 東京都品川区南大井 6-8-2
TEL 03-3763-5611
FAX 03-3763-6128

Tokyo Sokki Kenkyujo Co., Ltd.

8-2, Minami-Ohi 6-Chome
Shinagawa-ku, Tokyo 140-8560

TMLひずみゲージの取扱い方法

基本的な接着手順

1. 接着剤の選択 — 使用する条件に合った、ひずみゲージ用の接着剤を選びます。
2. 表面処理 — 被接着面のさび・塗料などを除去し、120～180番（ｱﾙﾐﾆｳﾑ:240～320番）のサンドペーパーで軽く磨きアセトンなどで清浄して、ゲージ接着位置をけがいてください。
3. ゲージ接着 — 接着剤の取扱説明書を参照してください。
4. キュアリング — 接着剤の取扱説明書を参照してください。
5. 点検 — ひずみゲージのゲージ抵抗値・絶縁抵抗値の点検を行ってください。
6. 結線 — リード線はゲージ端子を使用して、はんだ付けで接続してください。

・必要に応じて防湿処理を施してください。

リード線の測定値への影響

●リード線の温度変化による影響。
（３線式結線法では、温度影響はありません。）

$$\varepsilon l = \frac{r \cdot L \cdot \alpha \cdot \Delta T}{K\,(R + r \cdot L)} \qquad <式１>$$

εl ＝リード線の熱出力
r ＝リード線１m当たりの往復の抵抗値（Ω／m）
L ＝リード線の長さ（m）
α ＝リード線の抵抗温度係数
（銅線＝3.9×10^{-3}／℃）
ΔT ＝温度変化量
K ＝ゲージ率
R ＝ゲージ抵抗

●リード線の結線によるゲージ率の補正。
・２線式の場合

$$Ko = \frac{R}{R + r \cdot L} \cdot K \qquad <式２>$$

・３線式の場合

$$Ko = \frac{R}{R + \frac{r \cdot L}{2}} \cdot K \qquad <式３>$$

Ko＝補正したゲージ率

HANDLING METHOD OF TML STRAIN GAUGES

Basic Bonding Procedures

1. Select adhesive — Select an adhesive most suitable for test conditions.
2. Surface treatment — Remove grease, rust, paint, etc. from the bonding surface of a specimen, lightly polish with an abrasive paper of #120 ~ 180 (#240 ~ 320 for aluminium), wipe with acetone, etc. and mark gauge installation position.
3. Gauge installation — Refer to the operation manual of adhesive.
4. Adhesive curing — Refer to the operation manual of adhesive.
5. Gauge installation check — Check gauge resistance and insulation resistance.
6. Lead wire attachment — Solder lead wires to the strain gauges through connecting terminals.

・If necessary, apply waterproof coating.

Influence of Lead Wires on Measured Values

● Influence of temperature variation of lead wires
(3-wire system is independent of temperature.)

$$\varepsilon l = \frac{r \cdot L \cdot \alpha \cdot \Delta T}{K\,(R + r \cdot L)} \qquad <Equation1>$$

where
εl = *thermal output of lead wires*
r = *total resistance per meter of lead wires (Ω/m)*
L = *length of lead wires (m)*
α = *temperature coefficient of resistance of lead wires (copper wire = 3.9×10^{-3}/℃)*
ΔT = *temperature variation*
K = *gauge factor*
R = *gauge resistance*

● Gauge Factor Correction due to Lead Wire Attachment

・ In case of 2-wire system

$$Ko = \frac{R}{R + r \cdot L} \cdot K \qquad <Equation2>$$

・ In case of 3-wire system

$$Ko = \frac{R}{R + \frac{r \cdot L}{2}} \cdot K \qquad <Equation3>$$

where Ko = *corrected gauge factor*

リード線１m当たりの往復の抵抗値
Total Resistance per Meter of Lead Wires

構成（心数／直径） Lead wires(number of cores / diameter)	ポリイミド線 polyimide	ポリイミド線 polyimide	7/0.12	10/0.12	12/0.18	20/0.18
リード線の直径または断面積 Diameter or cross sectional area of lead wires	φ 0.14mm	φ 0.18mm	0.08 mm²	0.11 mm²	0.3 mm²	0.5 mm²
1m当たりの往復の抵抗値 Total resistance per meter	2.5 Ω/m	1.5 Ω/m	0.44 Ω/m	0.32 Ω/m	0.12 Ω/m	0.07 Ω/m

RhinoPro™ TuffCoat

Data Sheet

ISO 9001:2000
FM62236

DESCRIPTION:

RhinoPro™ TuffCoat™ is a two-component, 100% solids (no VOCs, no solvents), rapid curing, elastomeric polyurea hybrid lining. The protective lining system is packaged in a dual 750 ml cartridge for use with the lightweight, portable RhinoPro™ Cartridge Gun. The disposable, quick-load cartridges are great for truck bedliners, small jobs, hard to reach places and repairs.

FEATURES & BENEFITS:

- High tensile strength and tear strength properties.
- Very good abrasion and impact resistance.
- Good chemical resistance.
- Excellent corrosion resistance.
- Bonds to virtually all substrates, including metals, woods, concrete and fiberglass, with proper surface preparation.
- Stable from -40°F (-40°C) to 175°F (80°C).

APPLICATIONS:

- Spray-on application creates a monolithic, seamless lining which conforms to any shape and size.
- Casting of small parts, void filling.
- Elastomeric properties allow for application to surfaces subject to: vibration, expansion, contraction, movement, flexing, abrasion and impact.

TYPICAL PHYSICAL PROPERTIES:

Hardness (Shore D)	55±5	ASTM D-2240
Tensile Strength (psi)*	2000 – 2100	ASTM D-412
Elongation (%)*	100 – 125	ASTM D-412
Tear Resistance (pli)*; Die C	200 – 250	ASTM D-624
Specific Gravity (grams/cc)	1.06 – 1.08	ASTM D-792
Water Absorption (%)	≤1.5	ASTM D-570

*Properties were checked of RhinoPro™ TuffCoat™ lining, 1/8" (125 mils), (3.18 mm) thick stock.

PROCESSING:

Reactivity:	Gel Time = 15 sec ±5 at 80°F. Tack Free Time = 1 – 5 minutes, based on ambient temperature.
Cure Time:	RhinoPro™ TuffCoat™ will set in 5 – 10 minutes at 70°F depending on substrate temperature and thickness. Full cure should be complete within 24 hours at 70°F.
Application:	Please refer to the RhinoPro™ Cartridge Gun manual for complete instructions on using these cartridges.
Coverage:	Dual 750 ml cartridges cover 8 sq ft at 1/16" (62 mils or 1.5 mm) thickness.
Surface Prep:	Before applying RhinoPro™ TuffCoat™, the surface should be prepared properly following recommended RhinoPro™ procedures. The substrate should be clean, dry and free of oil, dirt or other contaminant's. It is ideal to roughen the surface to create a profile to bond to. Depending on the application, the use of the appropriate RhinoPro™ primer may be required for best results.

CHEMICAL RESISTANCE:

Good resistance to many commercial and industrial chemicals such as acids, alkalies, oils and cleaning chemicals. For specific applications and information, please call us to speak to a RhinoPro™ representative.

SUBSTRATES:

The RhinoPro™ TuffCoat™ can be applied to metals, wood, concrete, fiberglass, geotextiles and other RhinoPro™ products as a patch material. If using as a repair or patch material, it is best to match the hardness rating of 55D with the lining being repaired. Please consult with RhinoPro™ for further technical support.

VOLATILE ORGANIC CONTENT:

None. 100% solids. No solvents.

RhinoPro™ TuffCoat

RhinoPro™ TuffCoat

STORAGE & SHELF LIFE:

RhinoPro™ TuffCoat™ Cartridges should be stored at 60 – 90°F in a dry condition in their original packaging. Shelf life is 6 months in unopened cartridges stored under proper conditions. If RhinoPro™ TuffCoat™ cartridge has been stored longer than 1 week, shake cartridge to insure proper distribution of chemicals and pigment.

COLOR OPTIONS:

Standard color - black, graphite, industrial tan, industrial gray.
Custom colors available by special order.

SAFETY PRECAUTIONS:

Health Considerations: Consult the RhinoPro™ Material Safety Data Sheets.
The uncured components of RhinoPro™ TuffCoat™ can cause irritation to the eyes, skin, mucous membranes and are harmful if swallowed. When handling, avoid contact with eyes and skin (especially open cuts). In case of contact, immediately wash off with plenty of water for at least fifteen (15) minutes. For eyes, obtain medical attention. Always wash hands before eating. Obtain immediate medical attention in case of ingestion.

RhinoPro™ TuffCoat™ contains isocyanates and may cause allergic skin or respiratory reactions. Do not use if you have chronic breathing problems (asthma) or if you have ever had reactions to isocyanates. When applying RhinoPro™ TuffCoat™, avoid breathing harmful vapors. Fresh air-supplied standard painter's hood and full face respirator must be worn by all personnel entering the area where RhinoPro™ TuffCoat™ is being spray applied until all vapors have been exhausted. In case of extreme exposure or adverse reaction, remove affected personnel to fresh air immediately and obtain medical help.

RhinoPro™ TuffCoat™ components are combustible liquids Class IIIB. Store and transport according to regulation.

Important: Consult the RhinoPro™ Material Safety Data Sheets.
Read and follow warning labels on all components. For professional use only. The information herein is believed to be reliable, but unknown risks may be present. All warranties of any kind, express or implied, including warranties of fitness for a particular purpose, are specifically disclaimed.

For Your Protection:
The information and recommendations in this publication are, to the best of our knowledge, reliable. Suggestions made concerning the products and their uses, applications, storage and handling are only the opinion of Uberwurx an authorized reseller of Rhino Linings® products. Users should conduct their own tests to determine the suitability of these products for their own particular purposes and of the storage and handling methods herein suggested. The toxicity and risk characteristics of products made by Uberwurx will necessarily differ from the toxicity and risk characteristics developed when such products are used with other materials during a manufacturing process. The resulting risk characteristics should be determined and made known to ultimate end-users and processors. Because of numerous factors affecting results, Uberwurx makes no warranty of any kind, express or implied, other than that the material conforms to its applicable current Standard Specifications. Uberwurx hereby disclaims any and all other warranties, including but not limited to those of merchantability or fitness for a particular purpose. No statements made herein may be construed as a representation or warranty. The liability of Uberwurx for any claims arising from or sounding in breach of warranty, negligence, strict liability, or otherwise shall be limited to the purchase price of the material.

RhinoPro™ CARTRIDGE SYSTEM

Contact our Corporate Office for additional information.

Phone: 855-41RHINO (1-855-417-4466)
Fax: 281-492-7907
Web: www.rhinoprocs.com

APPENDIX D: HORIZONTAL SHEAR PUSH-OFF RESULTS

RK-1-01

Summary Table

Specimen Name	RK-1-01
Texture Type	Raked 1 in
Amplitude	0.25 in
Spacing	1 in
De-bonding	---
Concrete Compressive Strengths	Bottom: 8754 psi
	Top: 5948 psi
Interface Fracture Stress	419 psi

Theoretical Surface Treatment

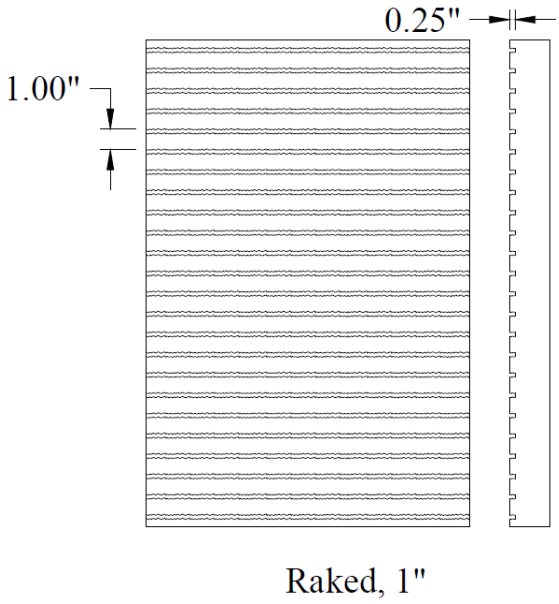

Actual Surface Treatment

Photo Not Available

Bottom Section After Test

Top Section After Test

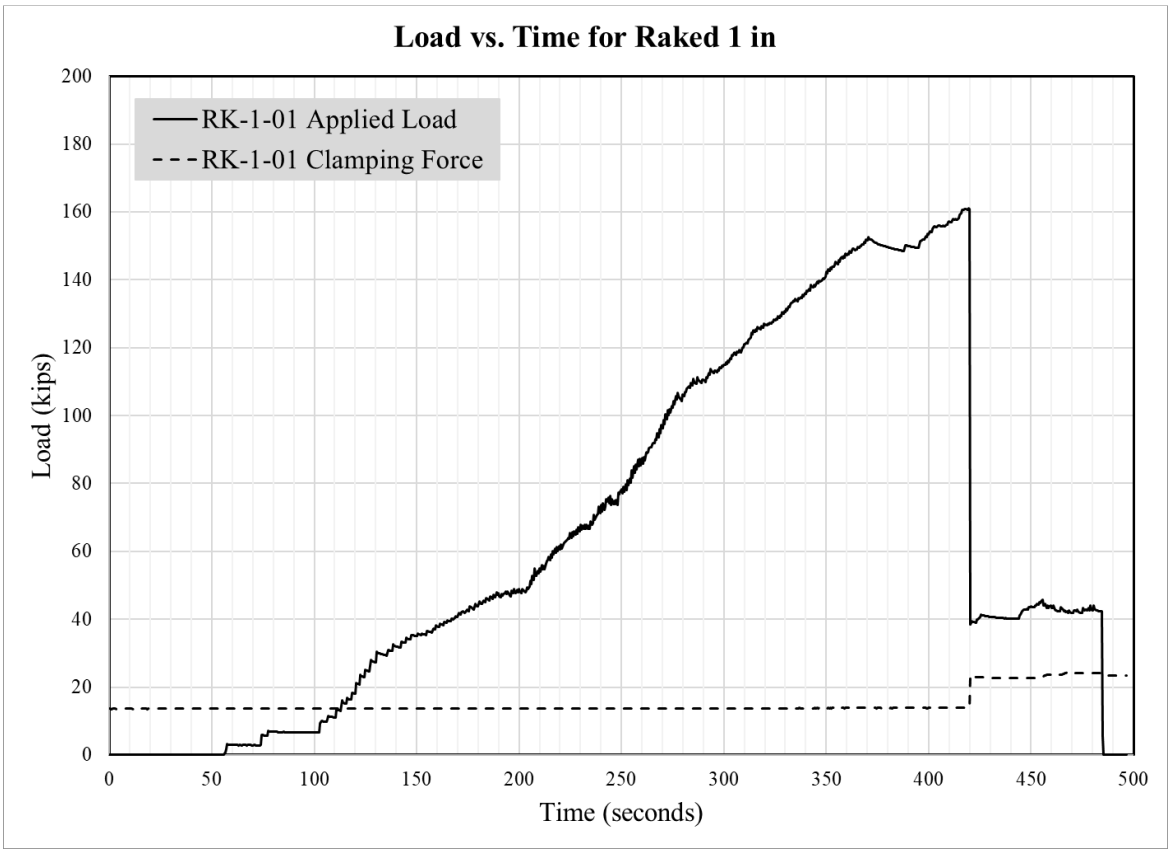
Load vs. Time for Raked 1 in
RK-1-01 Applied Load
RK-1-01 Clamping Force
Load (kips)
Time (seconds)
0
20
40
60
80
100
120
140
160
180
200
0
50
100
150
200
250
300
350
400
450
500

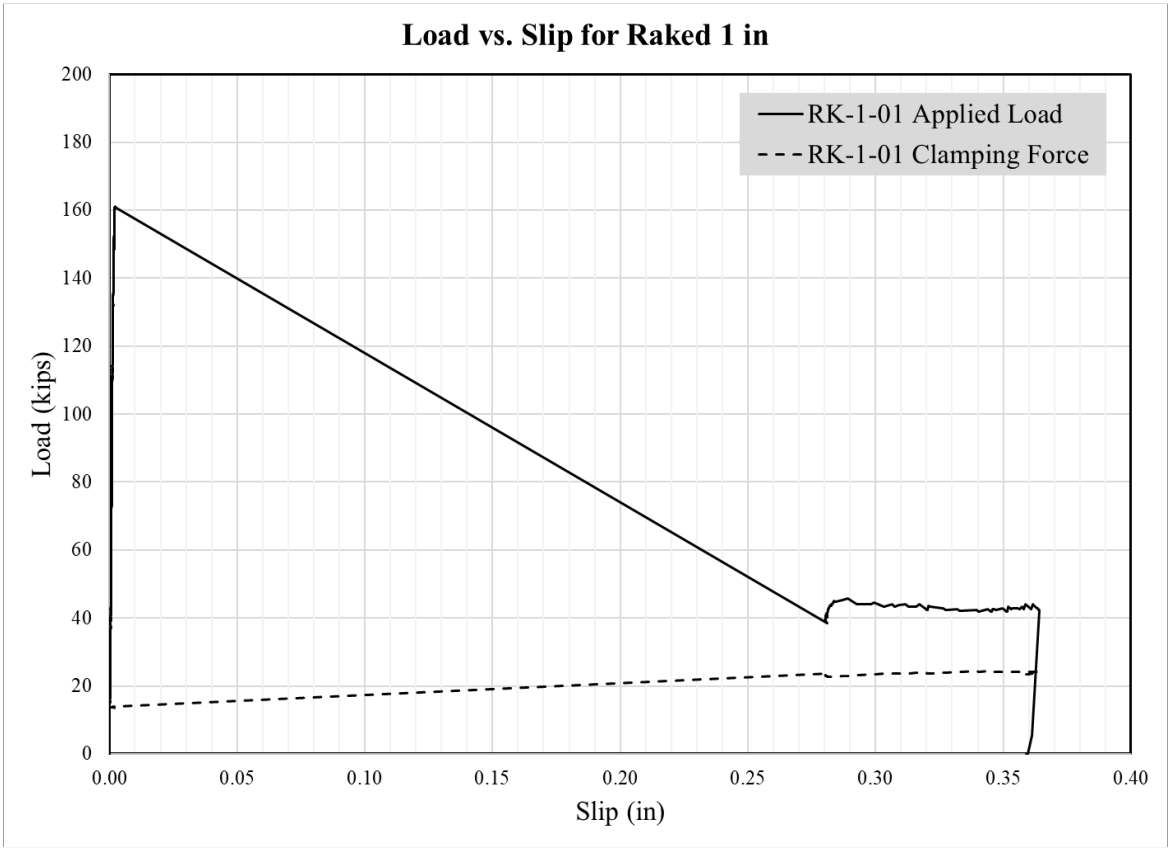
Load vs. Slip for Raked 1 in
RK-1-01 Applied Load
RK-1-01 Clamping Force
Load (kips)
Slip (in)
0
20
40
60
80
100
120
140
160
180
200
0.00
0.05
0.10
0.15
0.20
0.25
0.30
0.35
0.40

RK-1-02

Summary Table

Specimen Name	RK-1-02
Texture Type	Raked 1 in
Amplitude	0.25 in
Spacing	1 in
De-bonding	---
Concrete Compressive Strengths	Bottom: 8754 psi
	Top: 5948 psi
Interface Fracture Stress	353 psi

Theoretical Surface Treatment

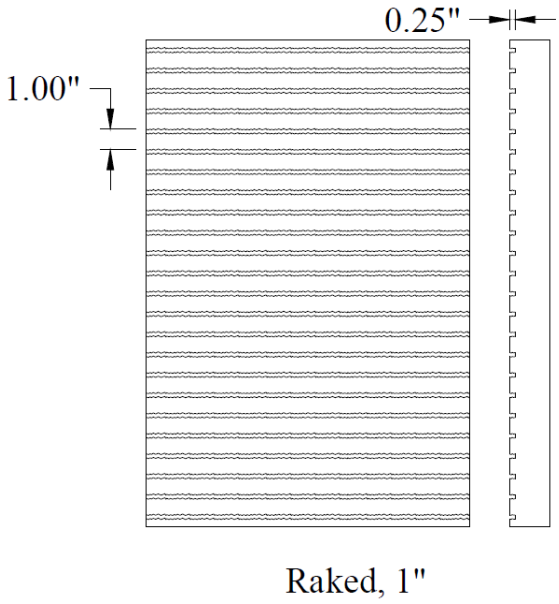

Actual Surface Treatment

Photo Not Available

Bottom Section After Test

Top Section After Test

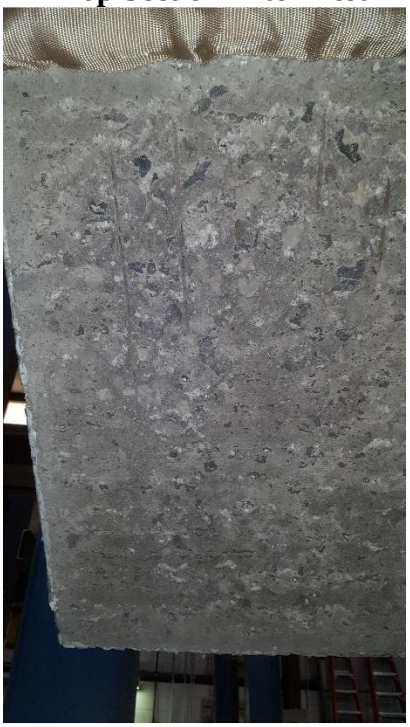

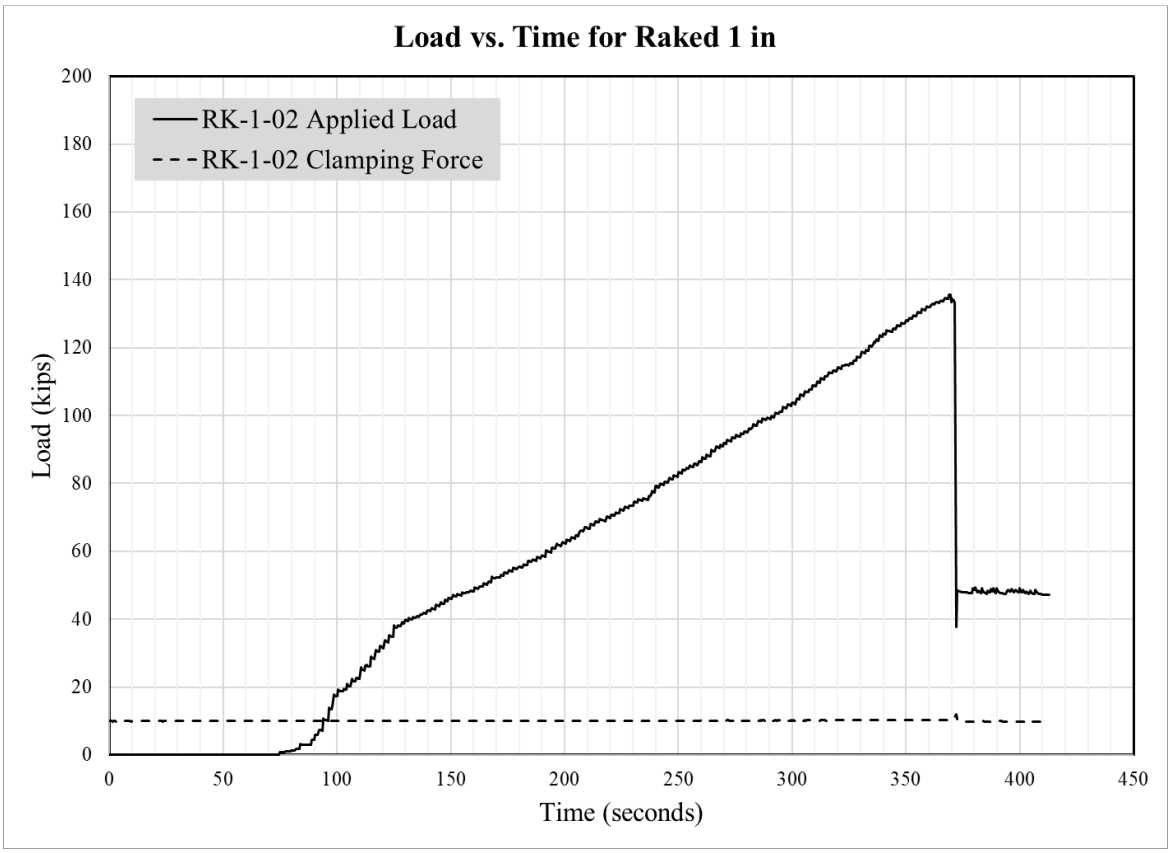
Load vs. Time for Raked 1 in
RK-1-02 Applied Load
RK-1-02 Clamping Force
Load (kips)
Time (seconds)
0
20
40
60
80
100
120
140
160
180
200
0
50
100
150
200
250
300
350
400
450

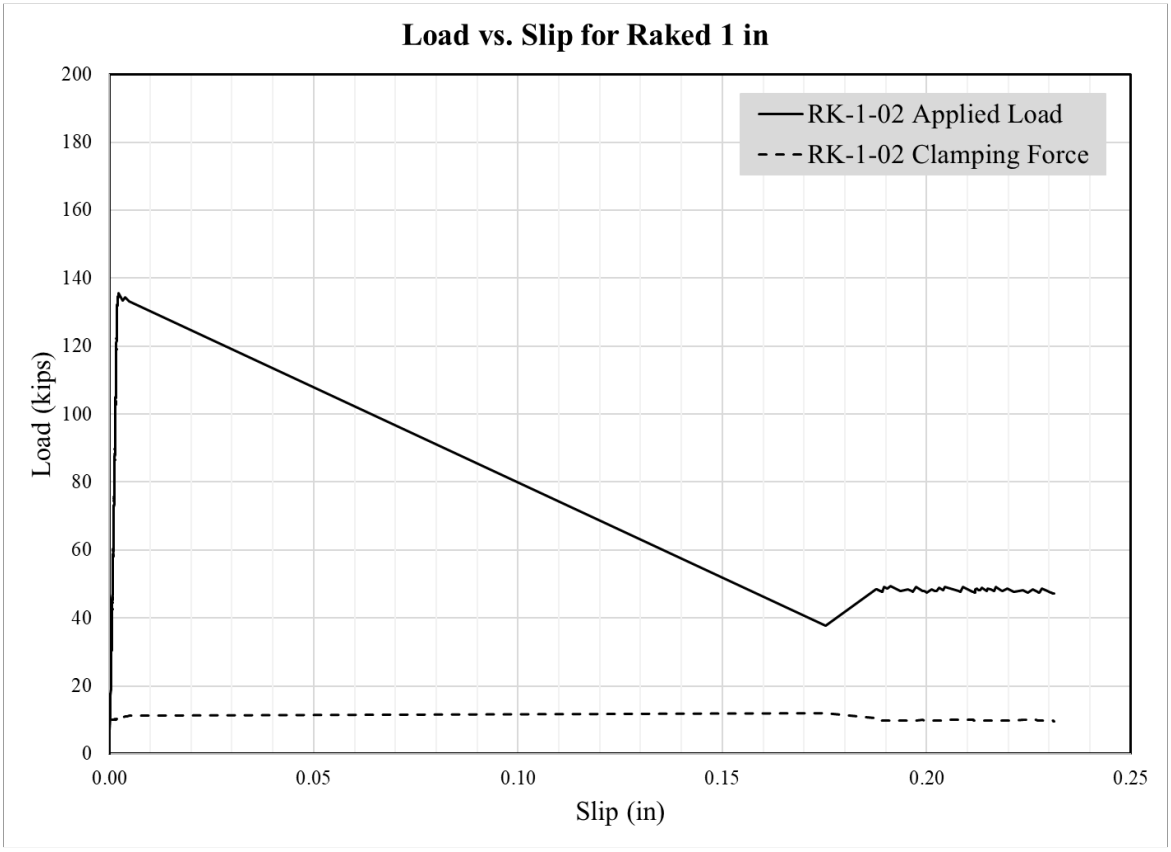
Load vs. Slip for Raked 1 in
RK-1-02 Applied Load
RK-1-02 Clamping Force
Load (kips)
Slip (in)
0
20
40
60
80
100
120
140
160
180
200
0.00
0.05
0.10
0.15
0.20
0.25

RK-1-03

Summary Table

Specimen Name	RK-1-03
Texture Type	Raked 1 in
Amplitude	0.25 in
Spacing	1 in
De-bonding	---
Concrete Compressive Strengths	Bottom: 8754 psi
	Top: 5948 psi
Interface Fracture Stress	346 psi

Theoretical Surface Treatment

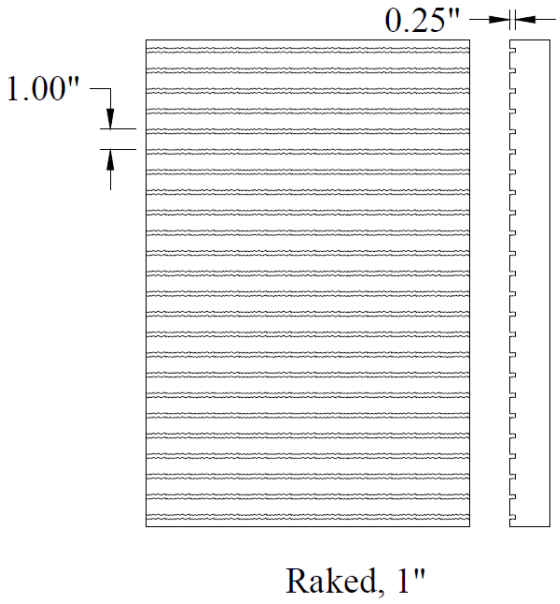

Actual Surface Treatment

Photo Not Available

Bottom Section After Test

Top Section After Test

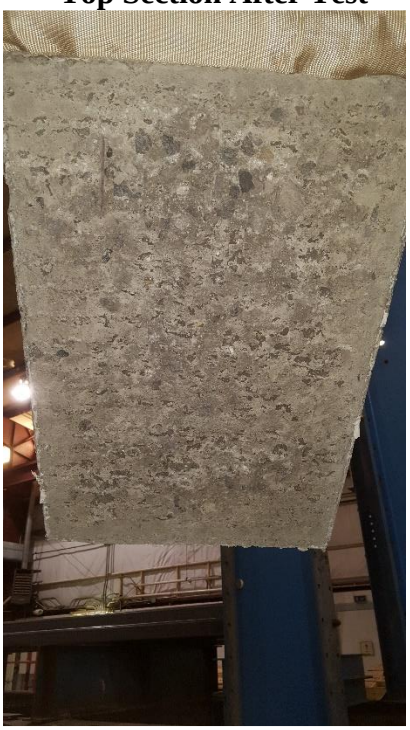

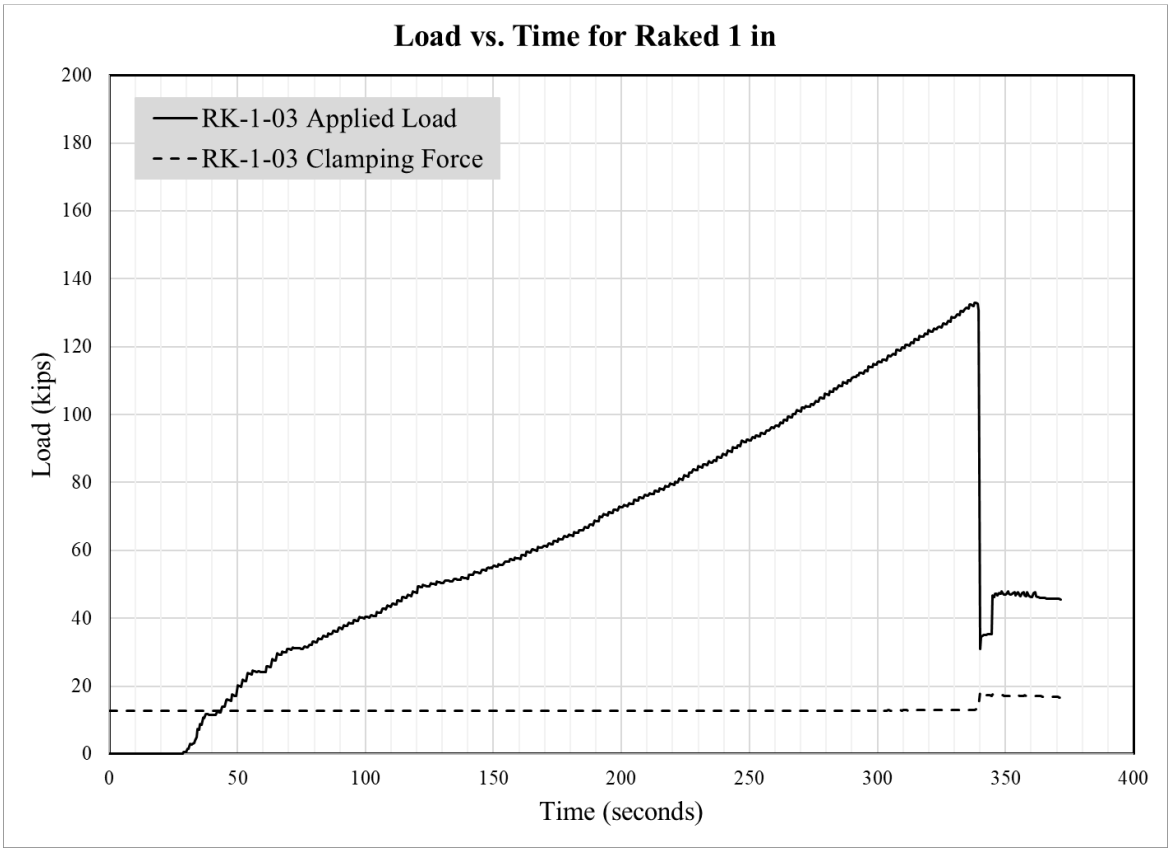
Load vs. Time for Raked 1 in
RK-1-03 Applied Load
RK-1-03 Clamping Force
Load (kips)
Time (seconds)
0
20
40
60
80
100
120
140
160
180
200
0
50
100
150
200
250
300
350
400

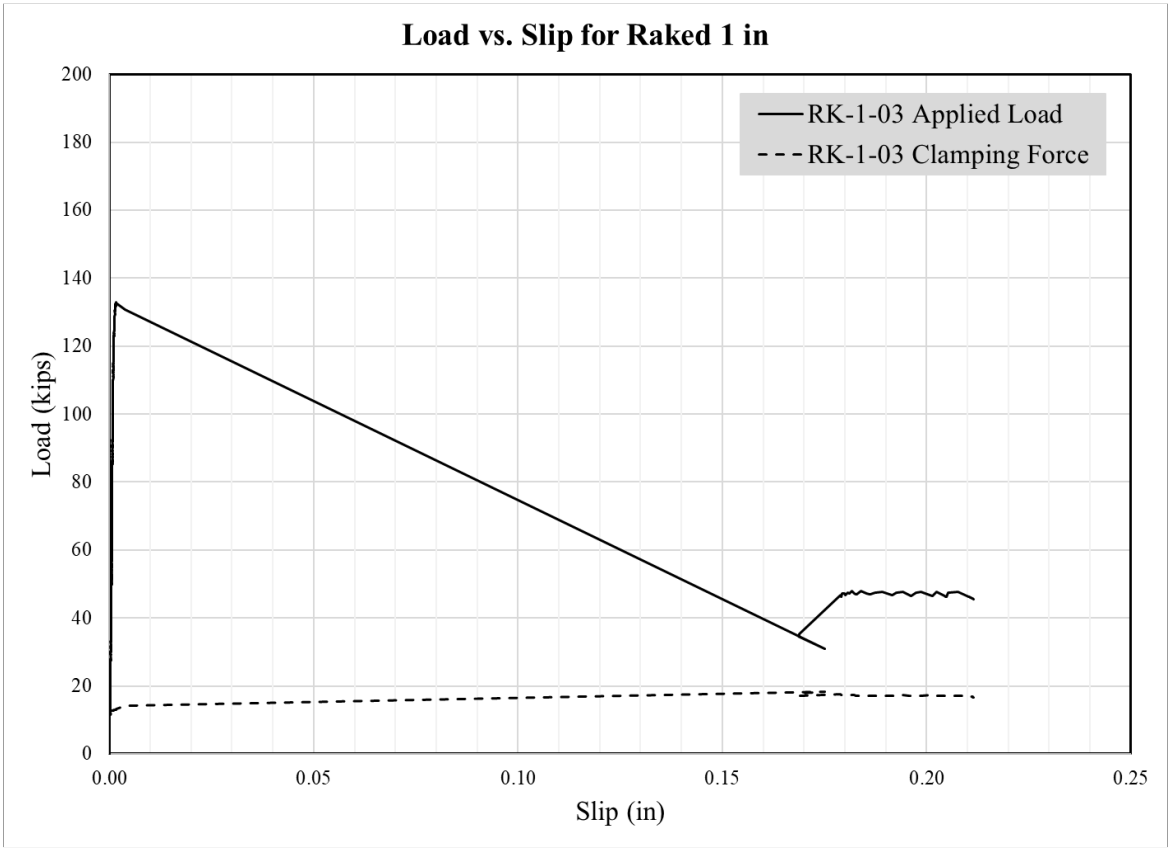
Load vs. Slip for Raked 1 in
RK-1-03 Applied Load
RK-1-03 Clamping Force
Load (kips)
Slip (in)
0
20
40
60
80
100
120
140
160
180
200
0.00
0.05
0.10
0.15
0.20
0.25

RK-2-01

Summary Table

Specimen Name	RK-2-01
Texture Type	Raked 2 in
Amplitude	0.25 in
Spacing	2 in
De-bonding	---
Concrete Compressive Strengths	Bottom: 6764 psi
	Top: 4397 psi
Interface Fracture Stress	275 psi

Theoretical Surface Treatment

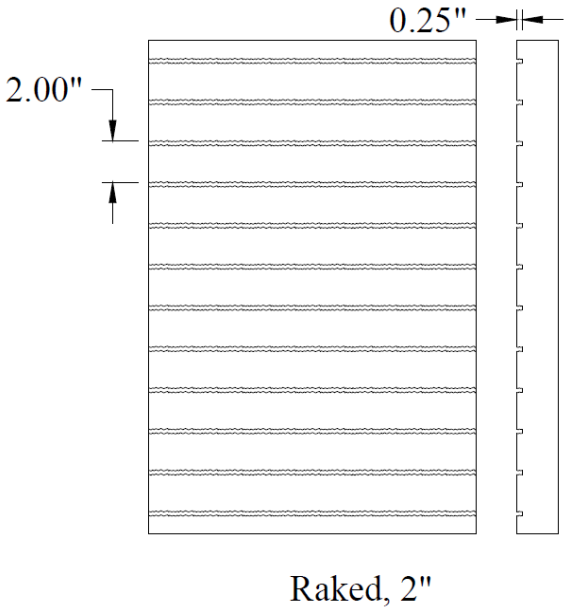

Actual Surface Treatment

Bottom Section After Test

Top Section After Test

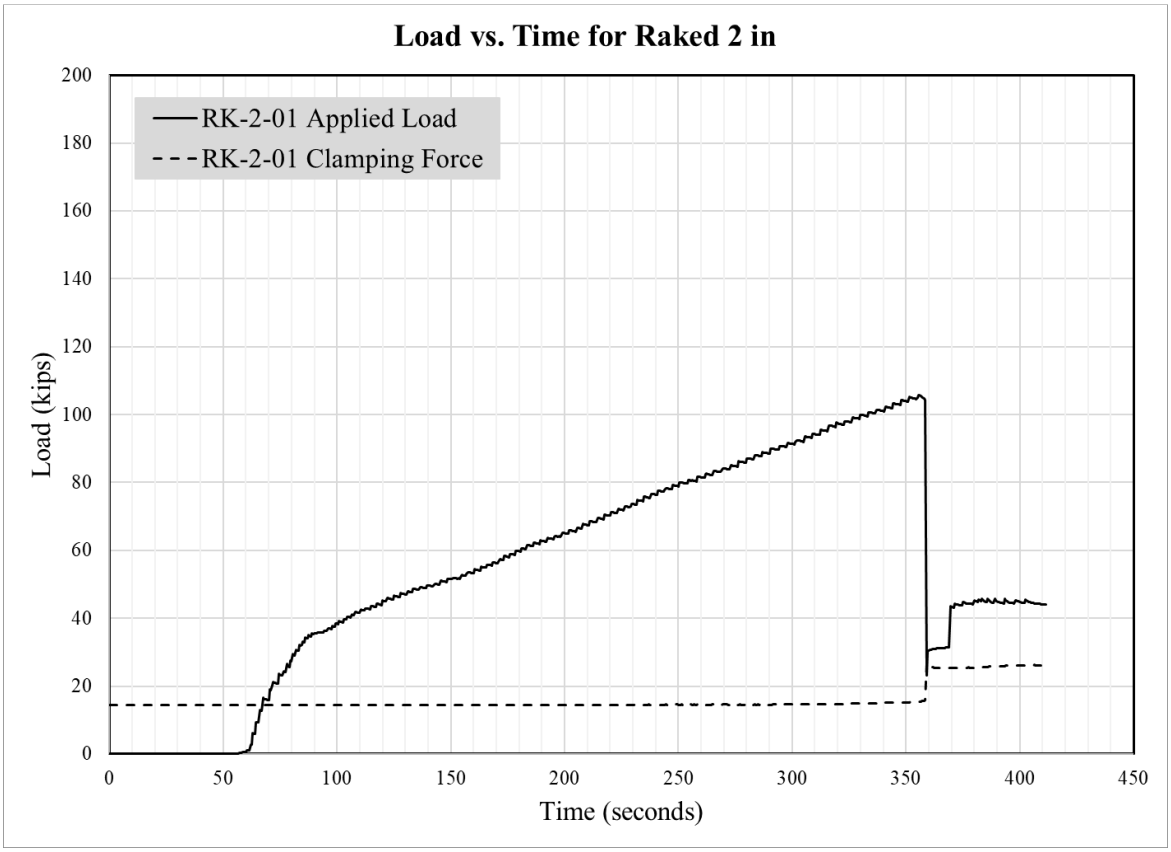
Load vs. Time for Raked 2 in
RK-2-01 Applied Load
RK-2-01 Clamping Force
Load (kips)
Time (seconds)
0
20
40
60
80
100
120
140
160
180
200
0
50
100
150
200
250
300
350
400
450

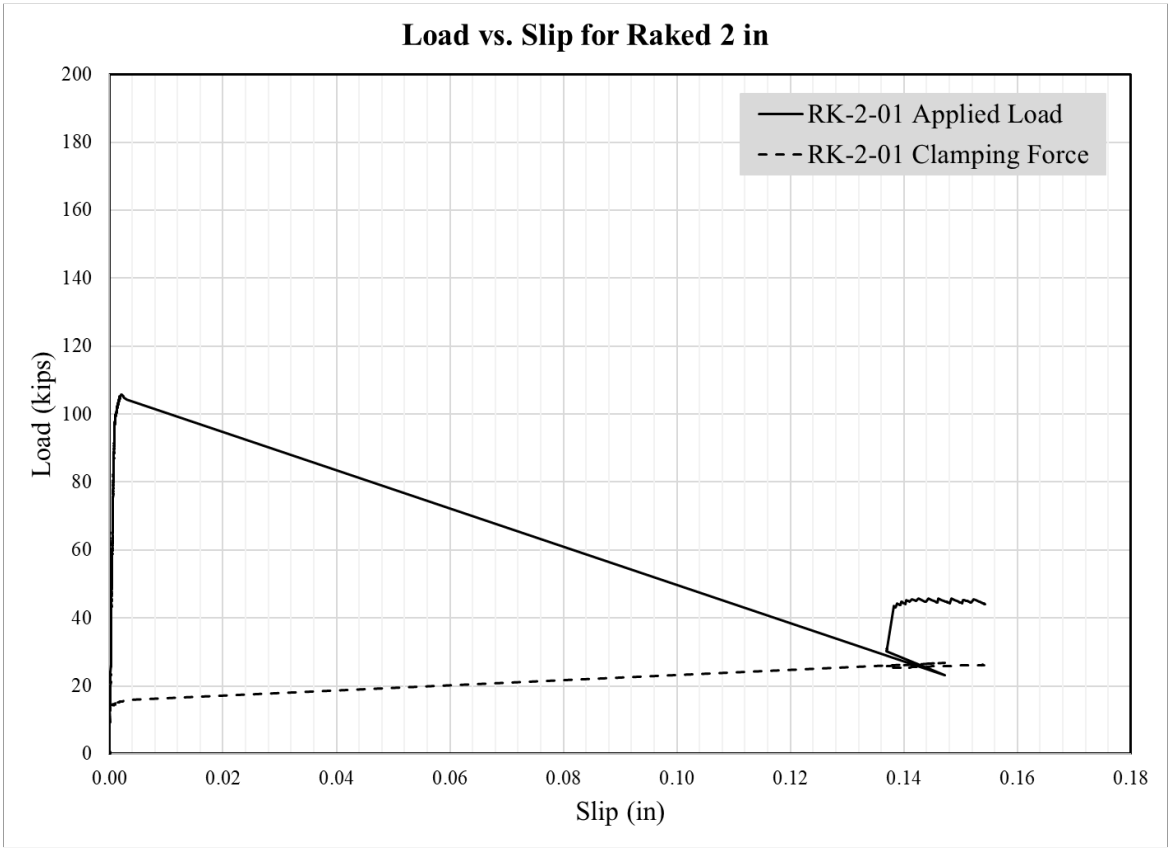
Load vs. Slip for Raked 2 in
RK-2-01 Applied Load
RK-2-01 Clamping Force
Load (kips)
Slip (in)
0
20
40
60
80
100
120
140
160
180
200
0.00
0.02
0.04
0.06
0.08
0.10
0.12
0.14
0.16
0.18

RK-2-02

Summary Table

Specimen Name	RK-2-02
Texture Type	Raked 2 in
Amplitude	0.25 in
Spacing	2 in
De-bonding	---
Concrete Compressive Strengths	Bottom: 6764 psi
	Top: 4397 psi
Interface Fracture Stress	258 psi

Theoretical Surface Treatment

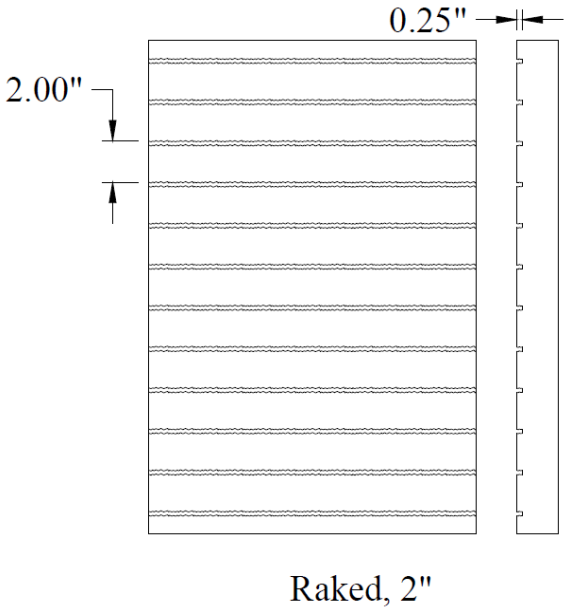

Actual Surface Treatment

Bottom Section After Test

Top Section After Test

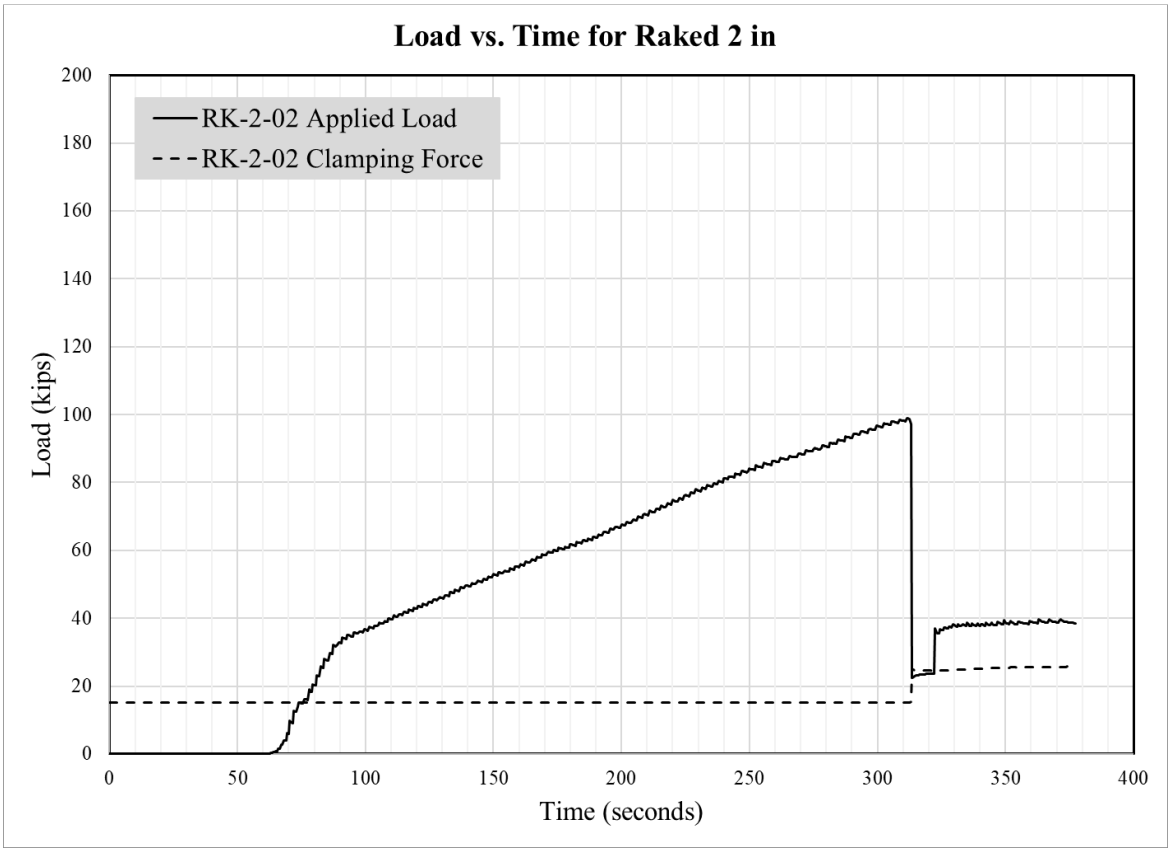
Load vs. Time for Raked 2 in
RK-2-02 Applied Load
RK-2-02 Clamping Force
Load (kips)
Time (seconds)
0
20
40
60
80
100
120
140
160
180
200
0
50
100
150
200
250
300
350
400

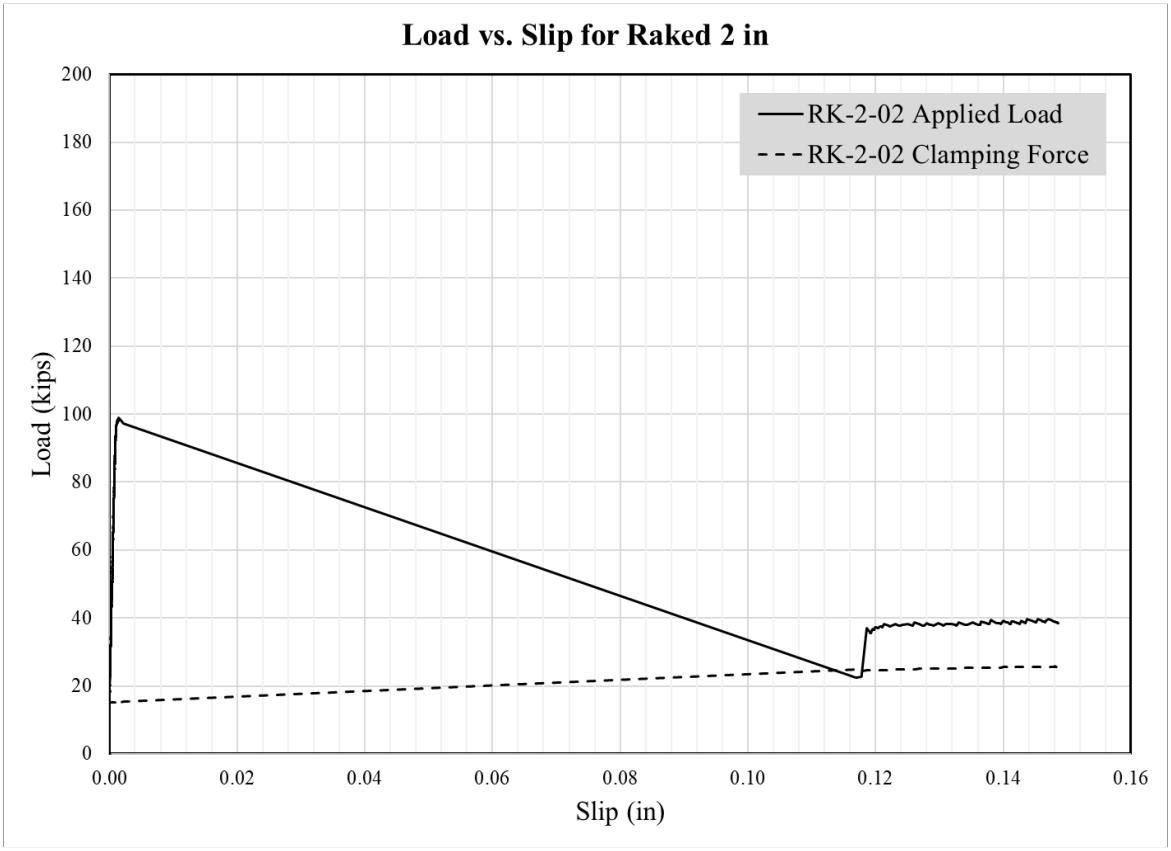
Load vs. Slip for Raked 2 in
RK-2-02 Applied Load
RK-2-02 Clamping Force
Load (kips)
Slip (in)
0
20
40
60
80
100
120
140
160
180
200
0.00
0.02
0.04
0.06
0.08
0.10
0.12
0.14
0.16

RK-2-03

Summary Table

Specimen Name	RK-2-03
Texture Type	Raked 2 in
Amplitude	0.25 in
Spacing	2 in
De-bonding	---
Concrete Compressive Strengths	Bottom: 6764 psi
	Top: 4397 psi
Interface Fracture Stress	203 psi

Theoretical Surface Treatment

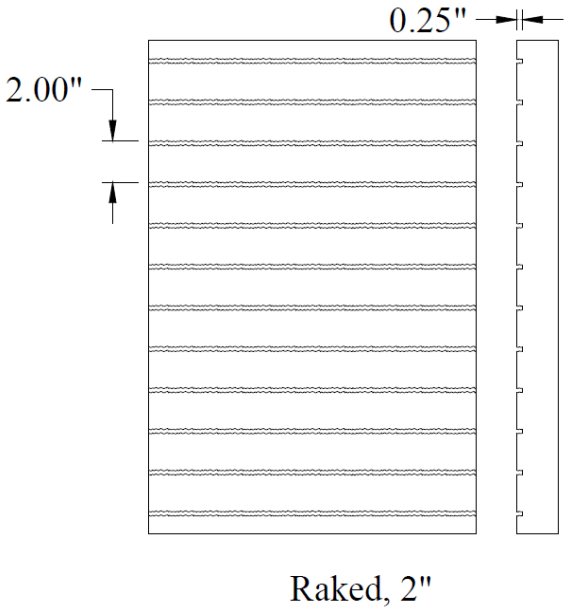

Actual Surface Treatment

Bottom Section After Test

Top Section After Test

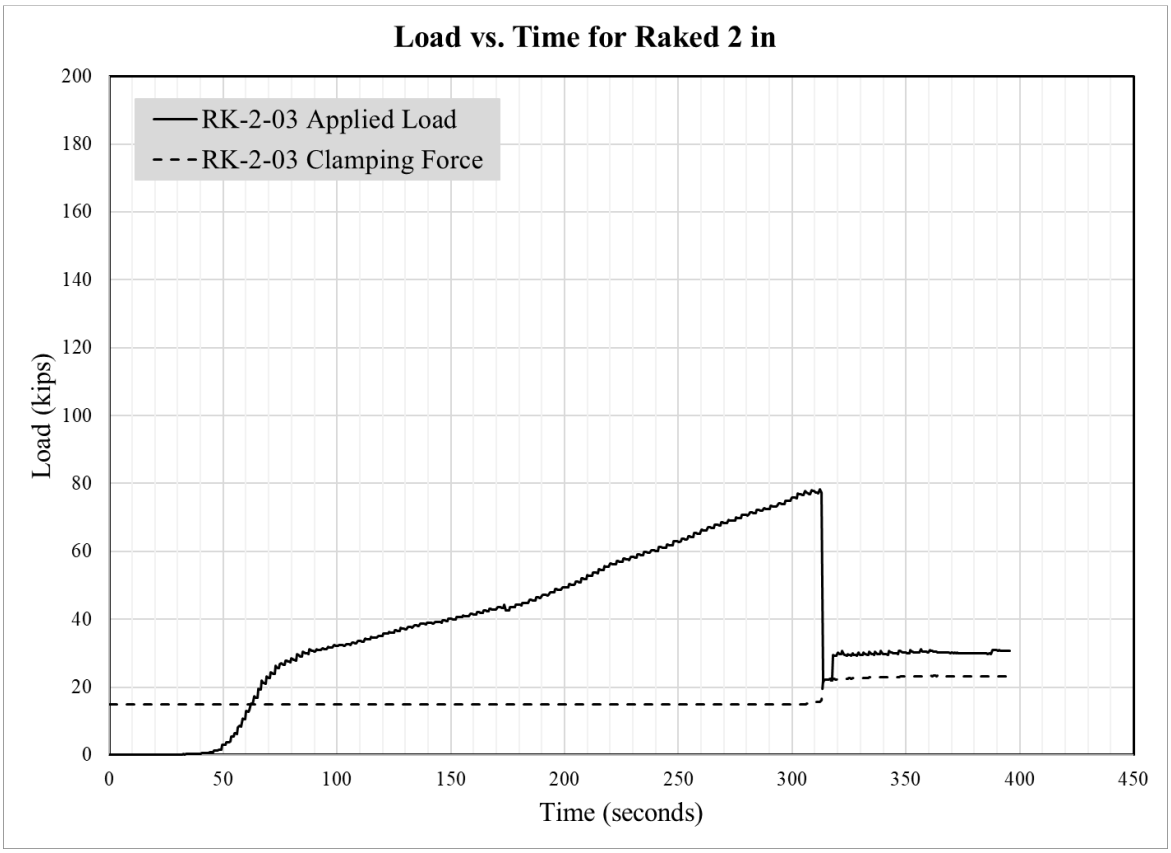
Load vs. Time for Raked 2 in
RK-2-03 Applied Load
RK-2-03 Clamping Force
Load (kips)
Time (seconds)
0
20
40
60
80
100
120
140
160
180
200
0
50
100
150
200
250
300
350
400
450

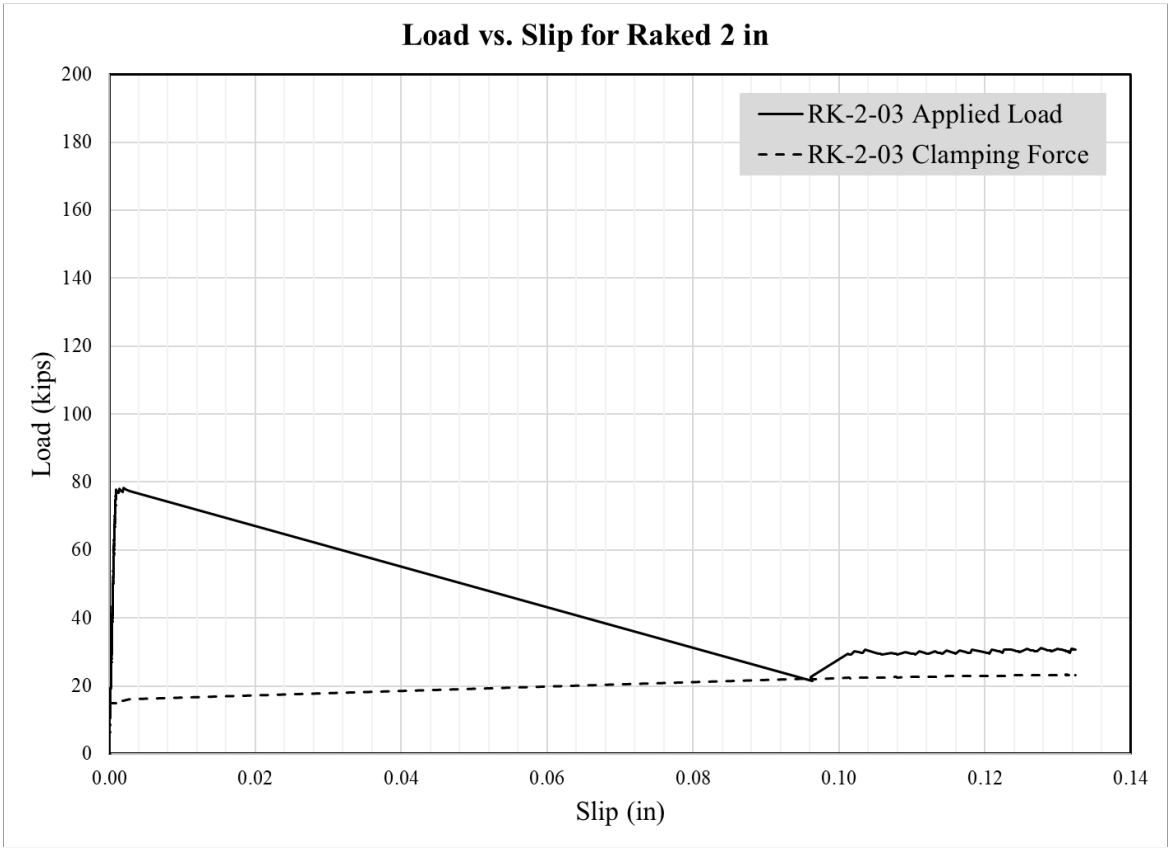
Load vs. Slip for Raked 2 in
RK-2-03 Applied Load
RK-2-03 Clamping Force
Load (kips)
Slip (in)
0
20
40
60
80
100
120
140
160
180
200
0.00
0.02
0.04
0.06
0.08
0.10
0.12
0.14

RK-3-01

Summary Table

Specimen Name	RK-3-01
Texture Type	Raked 3 in
Amplitude	0.25 in
Spacing	3 in
De-bonding	---
Concrete Compressive Strengths	Bottom: 6764 psi
	Top: 4397 psi
Interface Fracture Stress	303 psi

Theoretical Surface Treatment

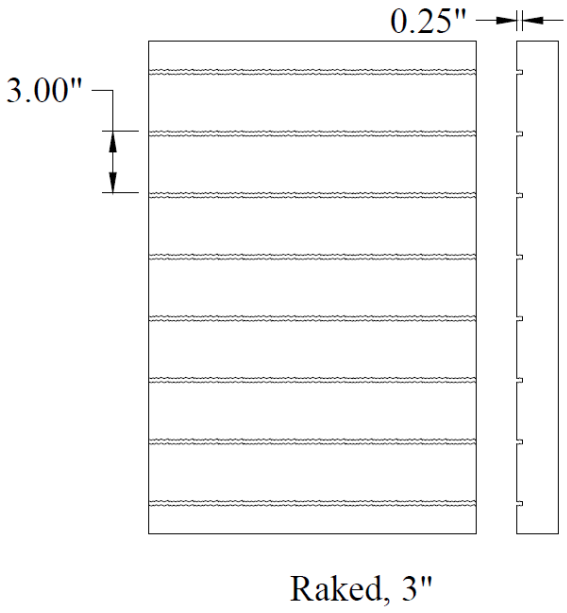

Actual Surface Treatment

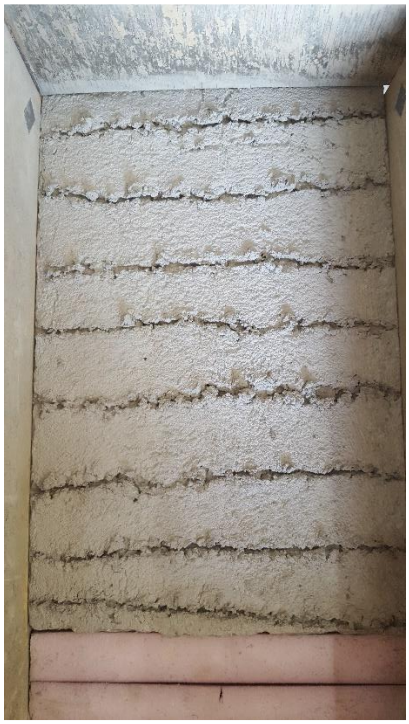

Bottom Section After Test

Top Section After Test

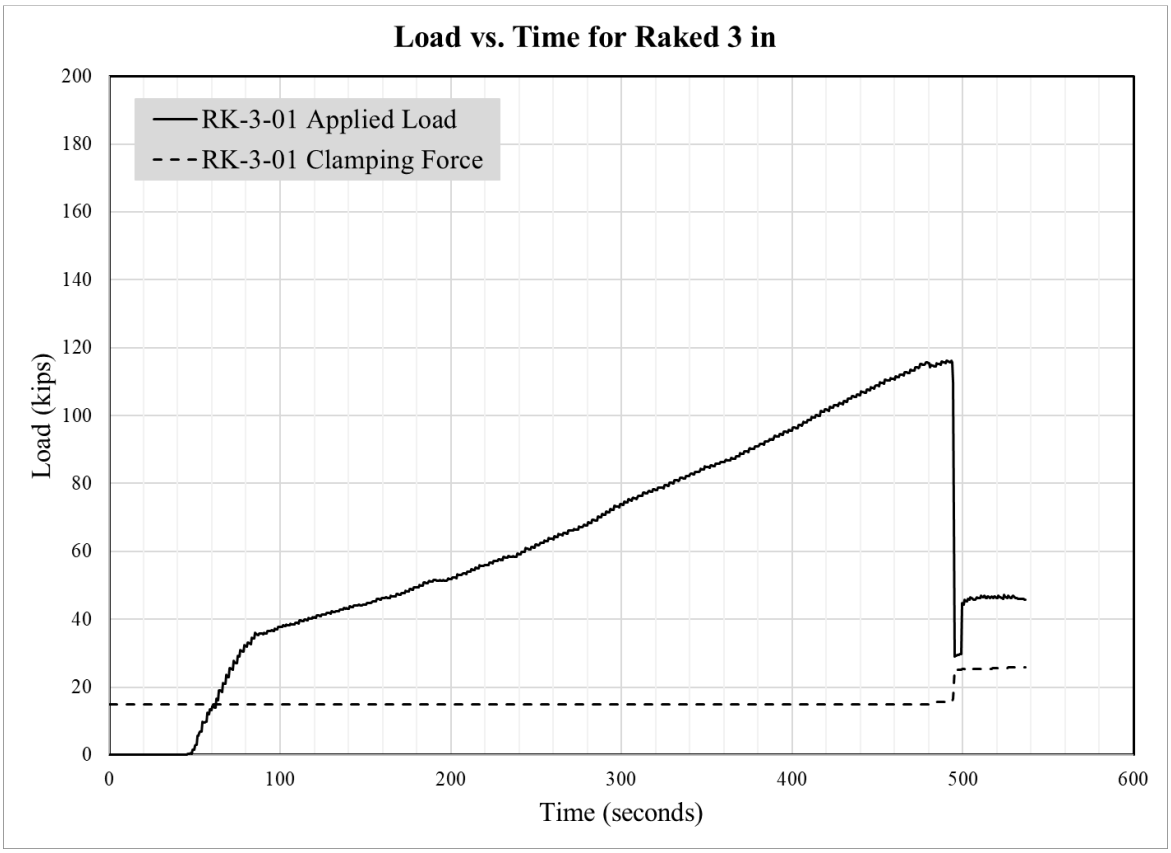
Load vs. Time for Raked 3 in
RK-3-01 Applied Load
RK-3-01 Clamping Force
Load (kips)
Time (seconds)
0
20
40
60
80
100
120
140
160
180
200
0
100
200
300
400
500
600

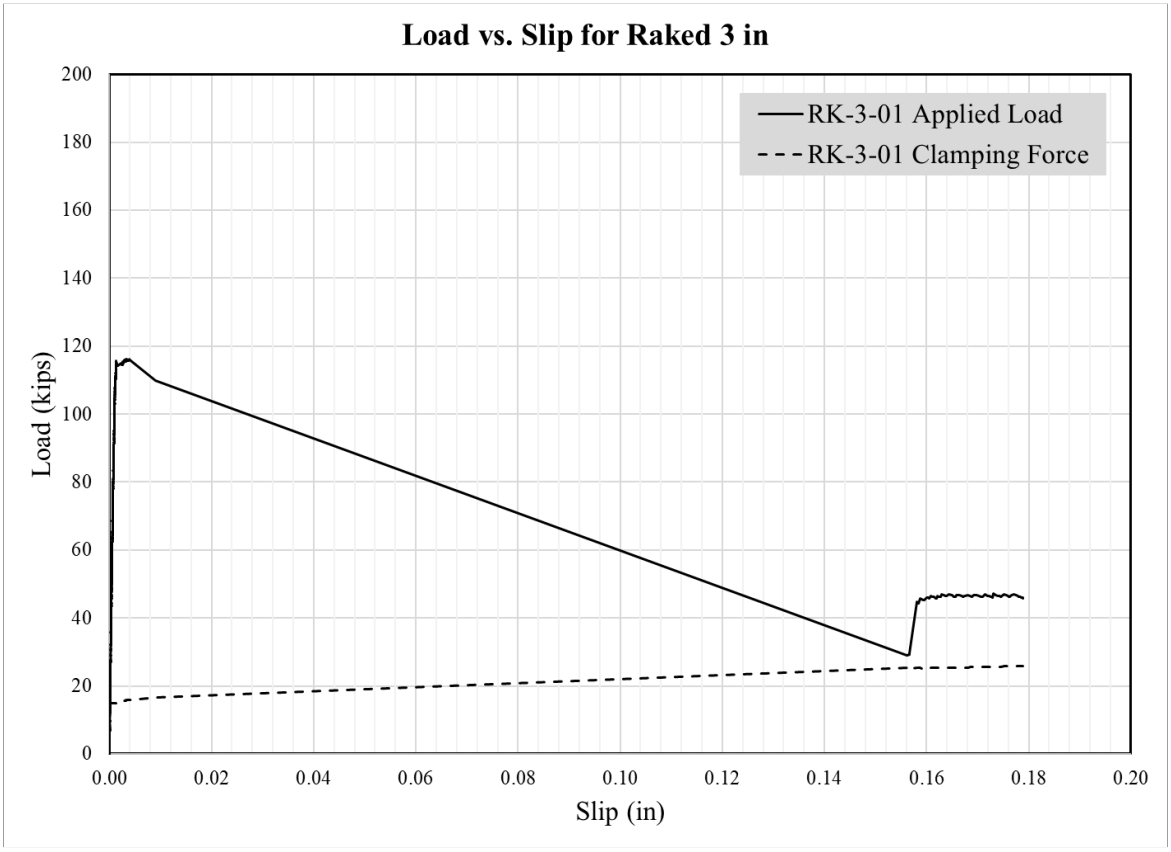
Load vs. Slip for Raked 3 in
RK-3-01 Applied Load
RK-3-01 Clamping Force
Load (kips)
Slip (in)
0
20
40
60
80
100
120
140
160
180
200
0.00
0.02
0.04
0.06
0.08
0.10
0.12
0.14
0.16
0.18
0.20

RK-3-02

Summary Table

Specimen Name	RK-3-02
Texture Type	Raked 3 in
Amplitude	0.25 in
Spacing	3 in
De-bonding	---
Concrete Compressive Strengths	Bottom: 6764 psi
	Top: 4397 psi
Interface Fracture Stress	306 psi

Theoretical Surface Treatment

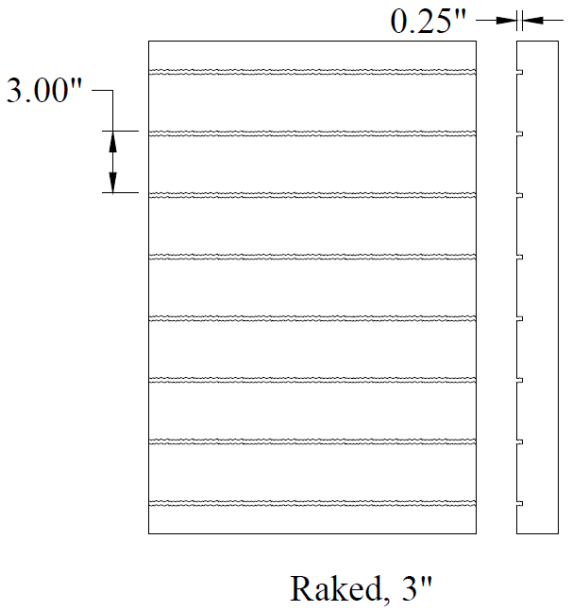

Actual Surface Treatment

Bottom Section After Test

Top Section After Test

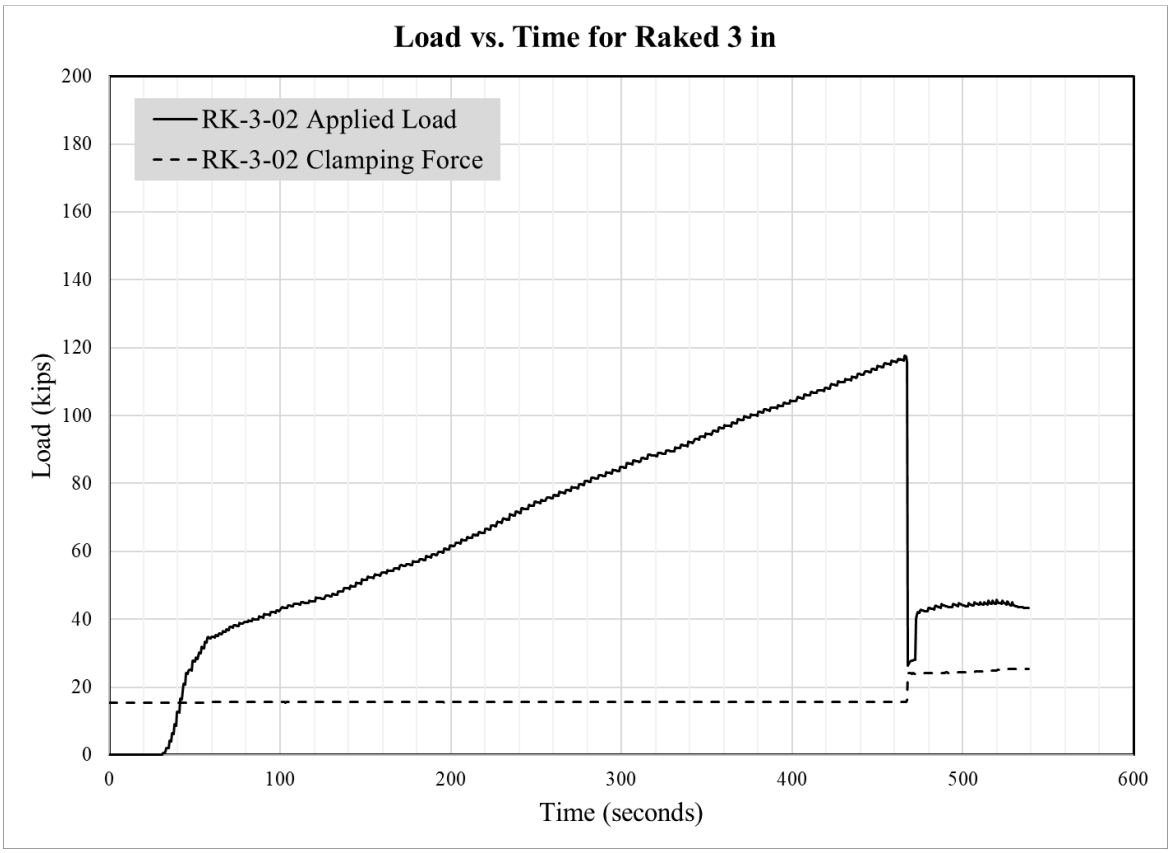
Load vs. Time for Raked 3 in
RK-3-02 Applied Load
RK-3-02 Clamping Force
Load (kips)
Time (seconds)
0
20
40
60
80
100
120
140
160
180
200
0
100
200
300
400
500
600

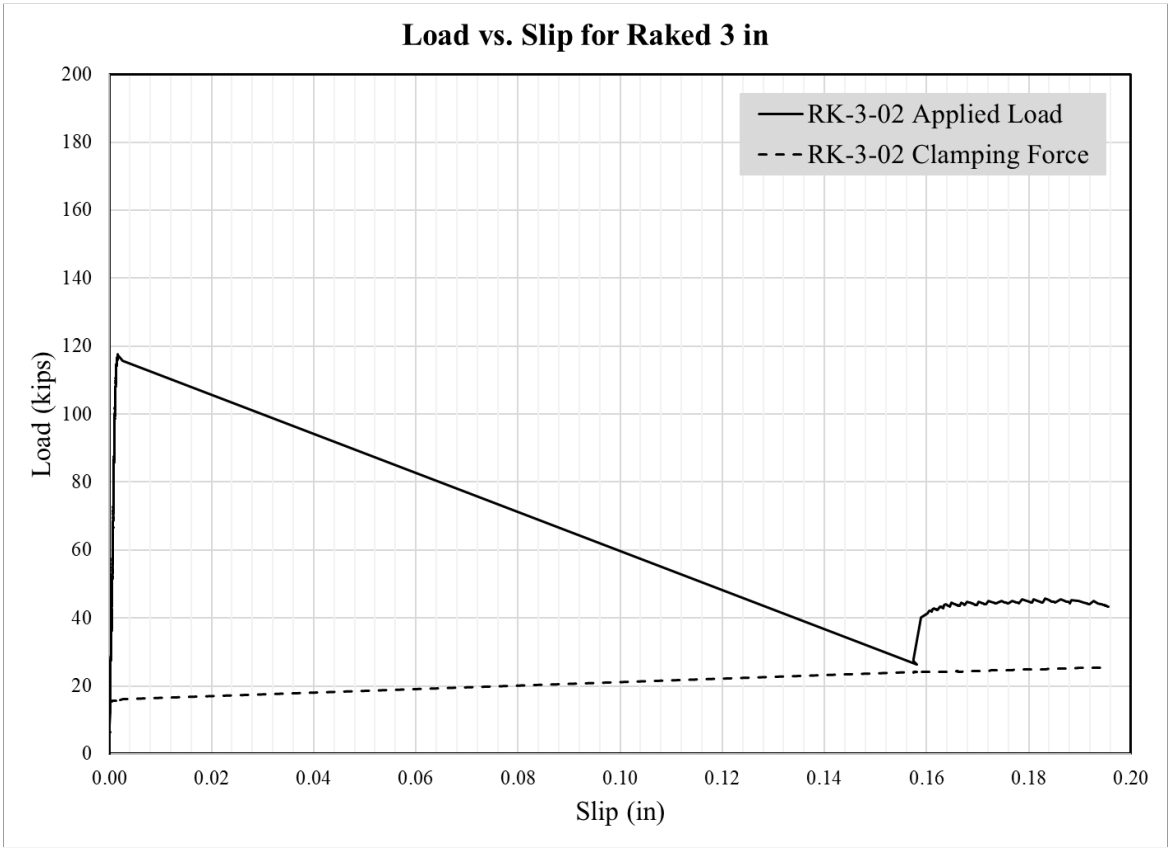
Load vs. Slip for Raked 3 in
RK-3-02 Applied Load
RK-3-02 Clamping Force
Load (kips)
Slip (in)
0
20
40
60
80
100
120
140
160
180
200
0.00
0.02
0.04
0.06
0.08
0.10
0.12
0.14
0.16
0.18
0.20

RK-3-03

Summary Table

Specimen Name	RK-3-03
Texture Type	Raked 3 in
Amplitude	0.25 in
Spacing	3 in
De-bonding	---
Concrete Compressive Strengths	Bottom: 6764 psi
	Top: 4397 psi
Interface Fracture Stress	353 psi

Theoretical Surface Treatment

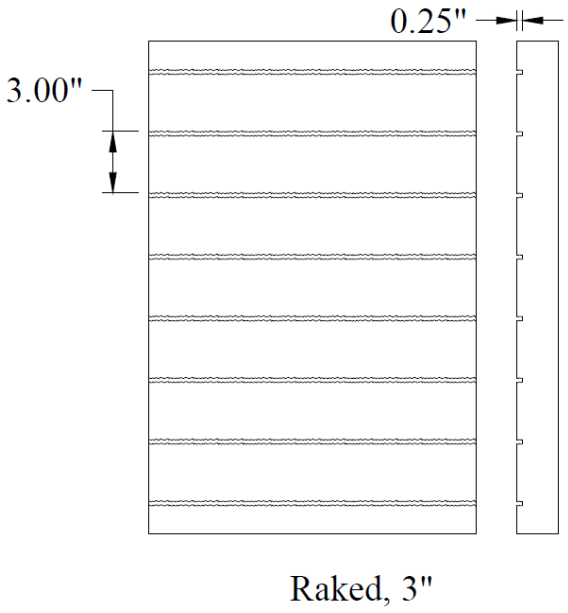

Actual Surface Treatment

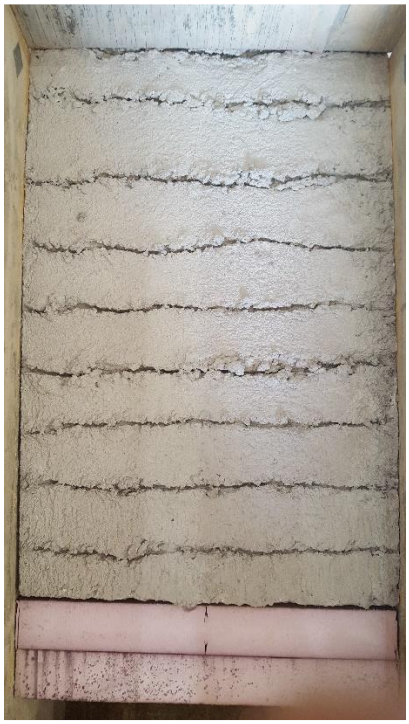

Bottom Section After Test

Top Section After Test

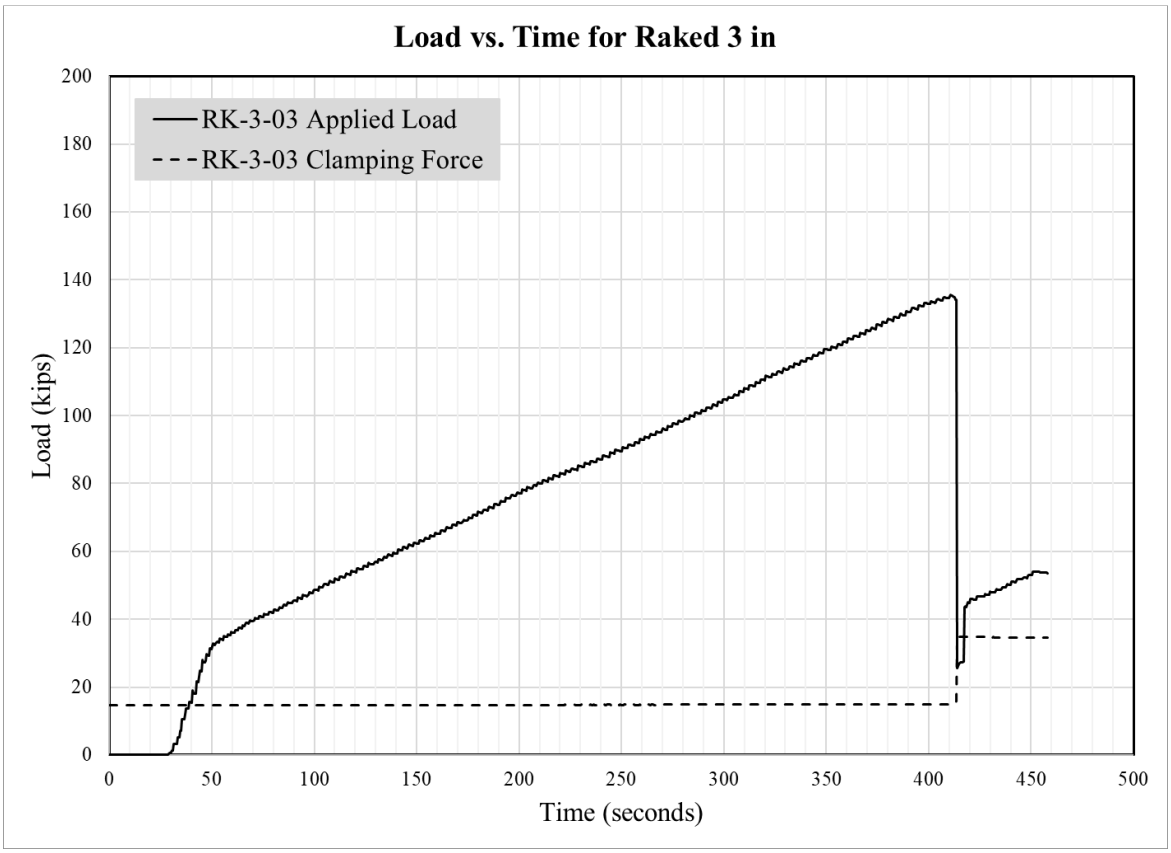
Load vs. Time for Raked 3 in
RK-3-03 Applied Load
RK-3-03 Clamping Force
Load (kips)
Time (seconds)
0
20
40
60
80
100
120
140
160
180
200
0
50
100
150
200
250
300
350
400
450
500

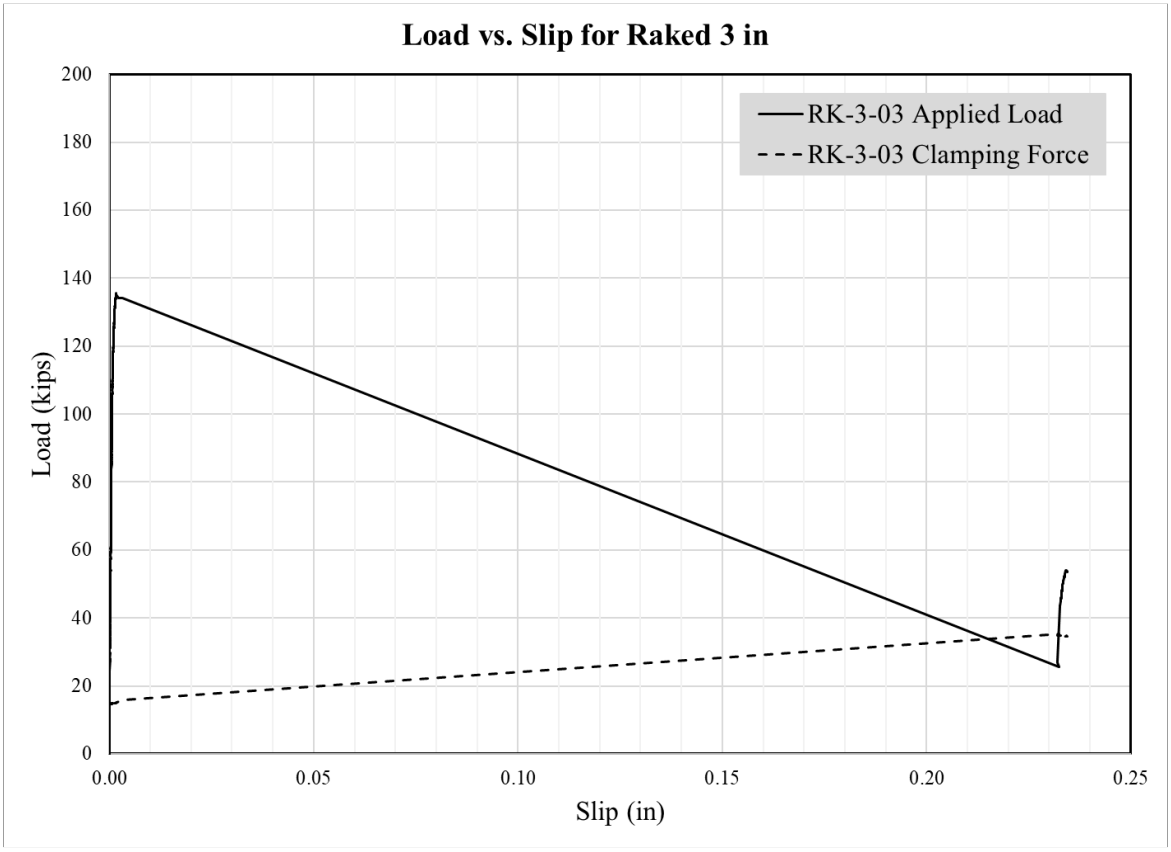
Load vs. Slip for Raked 3 in
RK-3-03 Applied Load
RK-3-03 Clamping Force
Load (kips)
Slip (in)
0
20
40
60
80
100
120
140
160
180
200
0.00
0.05
0.10
0.15
0.20
0.25

RG-1-01

Summary Table

Specimen Name	RG-1-01
Texture Type	Rectangular Grooves
Amplitude	0.25 in
Spacing	1 in
De-bonding	TuffCoat®
Concrete Compressive Strengths	Bottom: 6764 psi
	Top: 4397 psi
Interface Fracture Stress	328 psi

Theoretical Surface Treatment

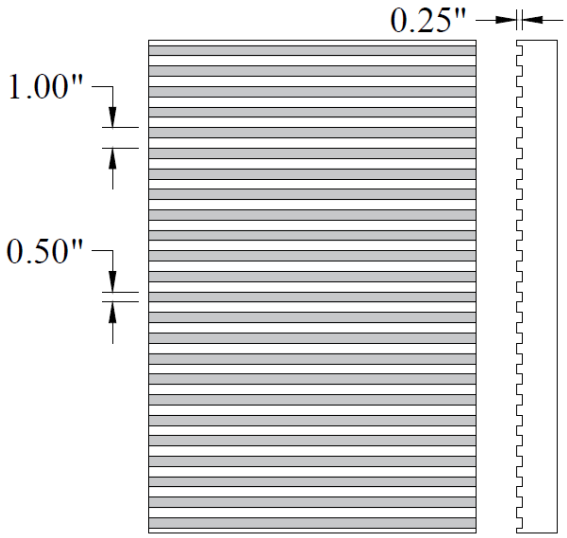

Rectangular Grooves

Actual Surface Treatment

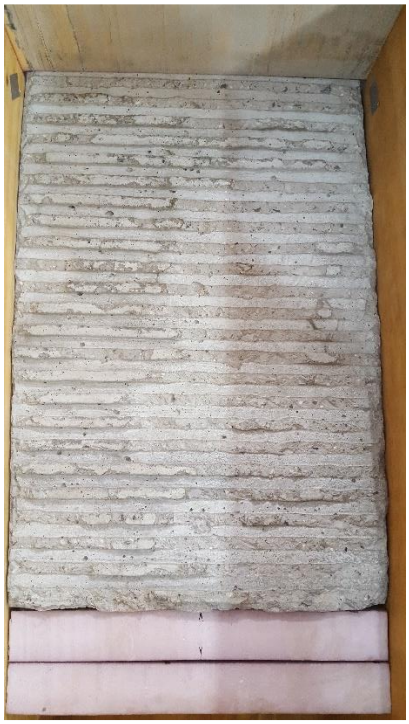

Bottom Section After Test

Top Section After Test

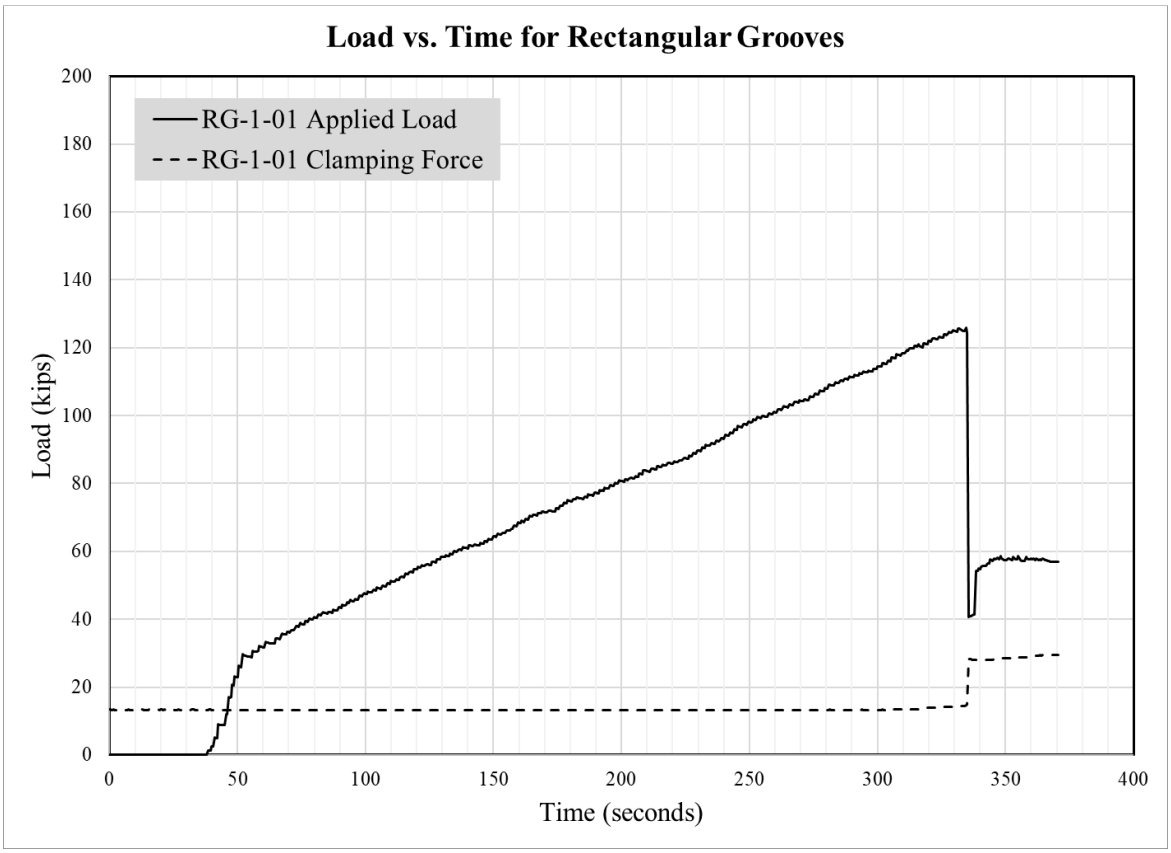
Load vs. Time for Rectangular Grooves
RG-1-01 Applied Load
RG-1-01 Clamping Force
Load (kips)
Time (seconds)
0
20
40
60
80
100
120
140
160
180
200
0
50
100
150
200
250
300
350
400

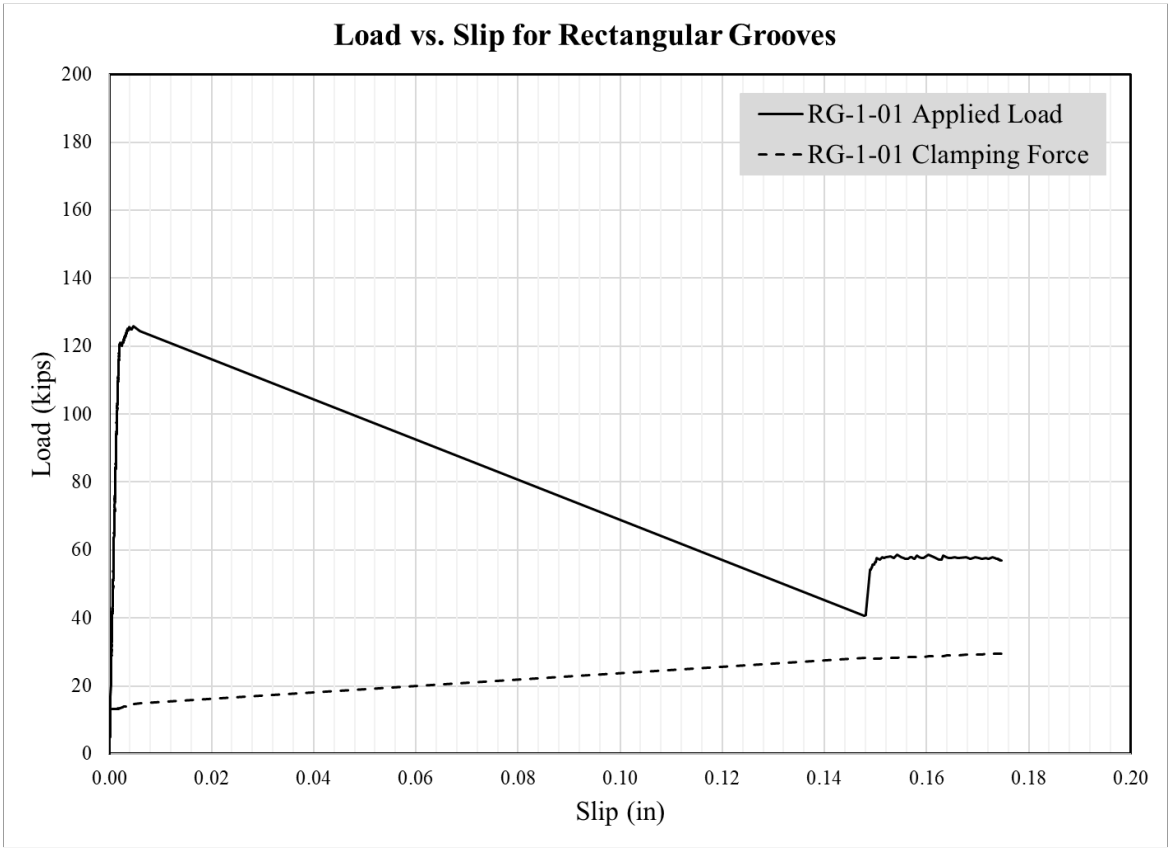
Load vs. Slip for Rectangular Grooves
RG-1-01 Applied Load
RG-1-01 Clamping Force
Load (kips)
Slip (in)
0
20
40
60
80
100
120
140
160
180
200
0.00
0.02
0.04
0.06
0.08
0.10
0.12
0.14
0.16
0.18
0.20

RG-1-02

Summary Table

Specimen Name	RG-1-02
Texture Type	Rectangular Grooves
Amplitude	0.25 in
Spacing	1 in
De-bonding	TuffCoat®
Concrete Compressive Strengths	Bottom: 6764 psi
	Top: 4397 psi
Interface Fracture Stress	287 psi

Theoretical Surface Treatment

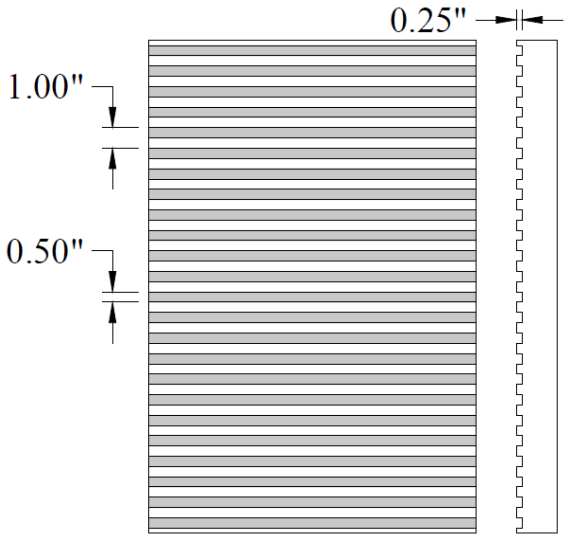

Rectangular Grooves

Actual Surface Treatment

Bottom Section After Test

Top Section After Test

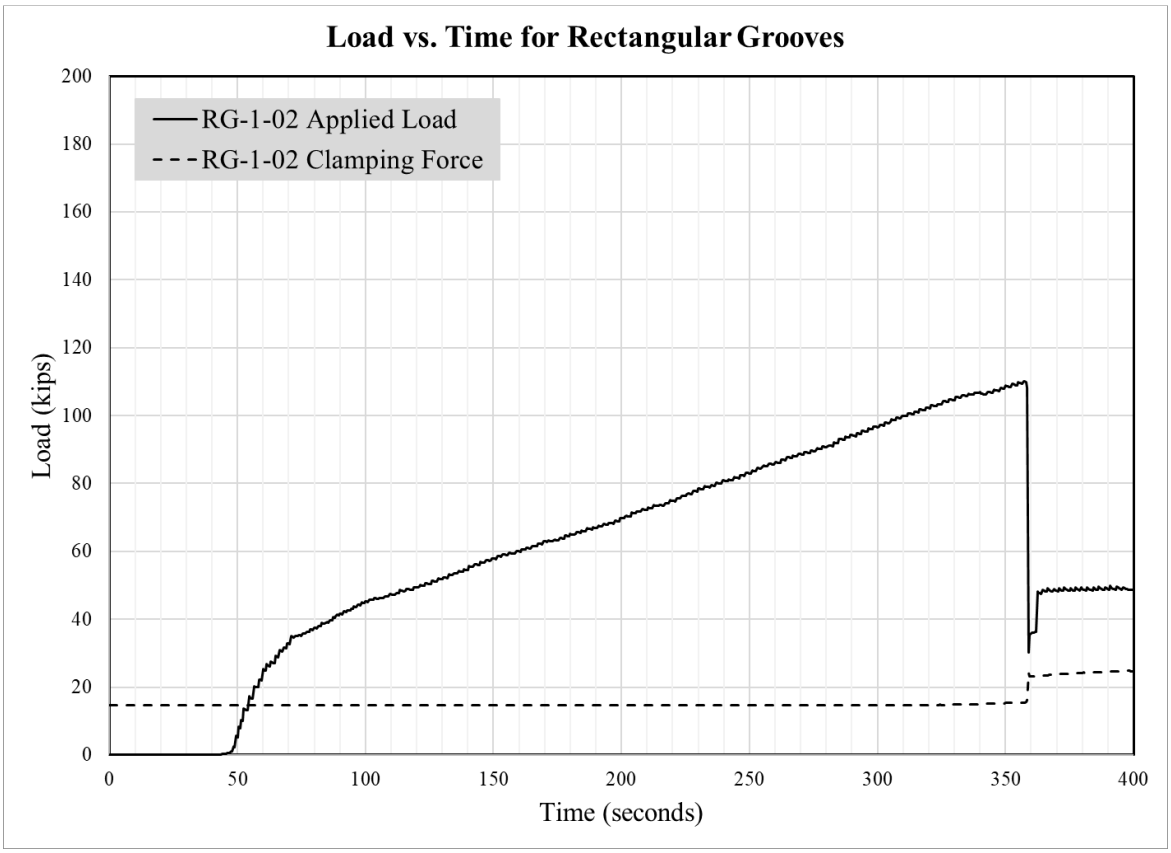
Load vs. Time for Rectangular Grooves
RG-1-02 Applied Load
RG-1-02 Clamping Force
Load (kips)
Time (seconds)
0
20
40
60
80
100
120
140
160
180
200
0
50
100
150
200
250
300
350
400

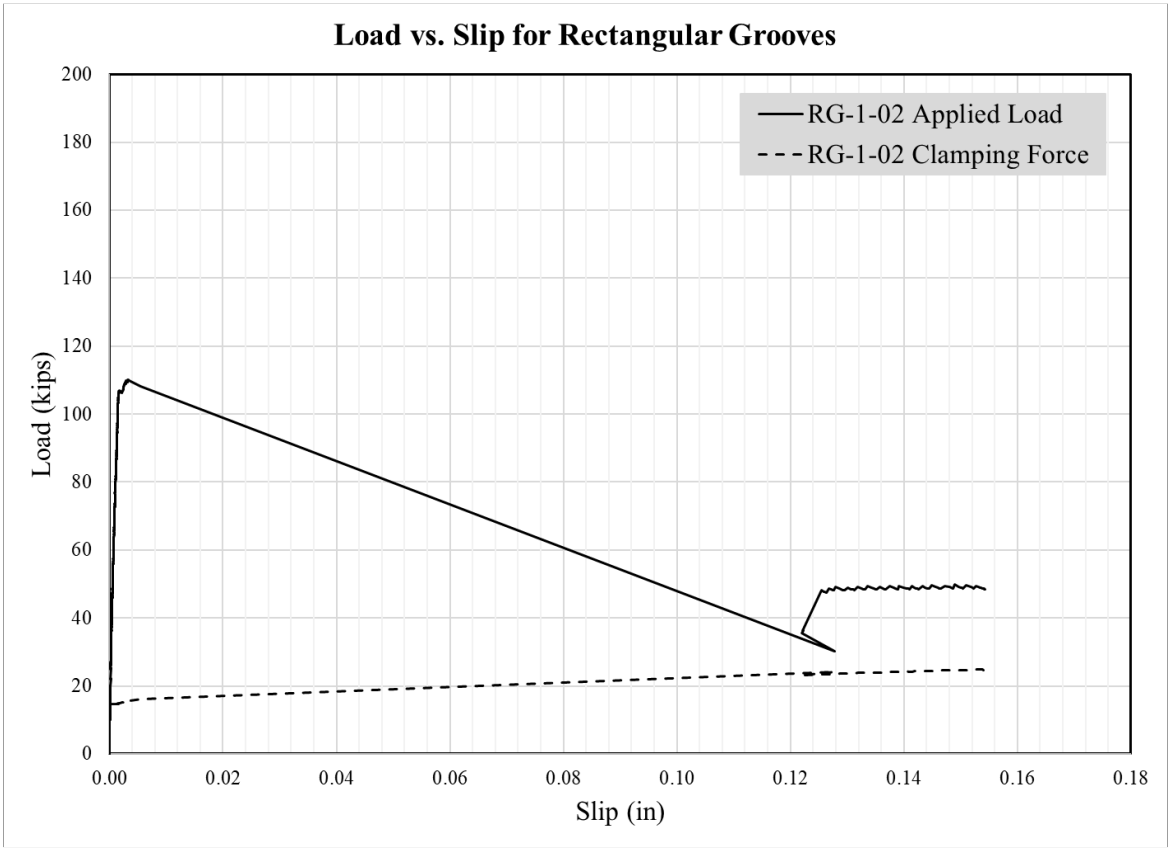
Load vs. Slip for Rectangular Grooves
RG-1-02 Applied Load
RG-1-02 Clamping Force
Load (kips)
Slip (in)
0
20
40
60
80
100
120
140
160
180
200
0.00
0.02
0.04
0.06
0.08
0.10
0.12
0.14
0.16
0.18

RG-1-03

Summary Table

Specimen Name	RG-1-03
Texture Type	Rectangular Grooves
Amplitude	0.25 in
Spacing	1 in
De-bonding	TuffCoat®
Concrete Compressive Strengths	Bottom: 6764 psi
	Top: 4397 psi
Interface Fracture Stress	279 psi

Theoretical Surface Treatment

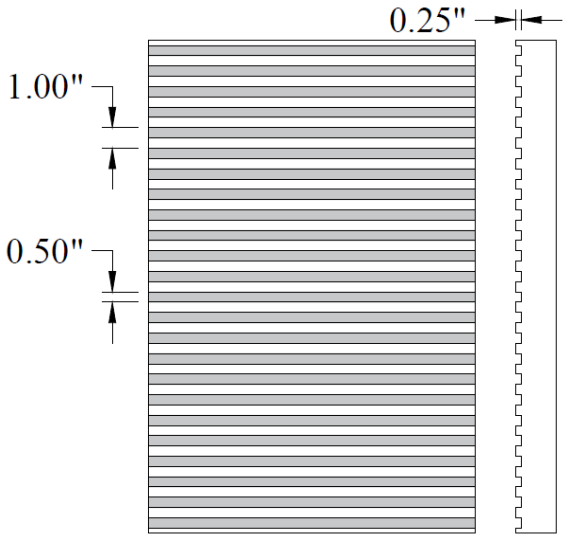

Rectangular Grooves

Actual Surface Treatment

Bottom Section After Test

Top Section After Test

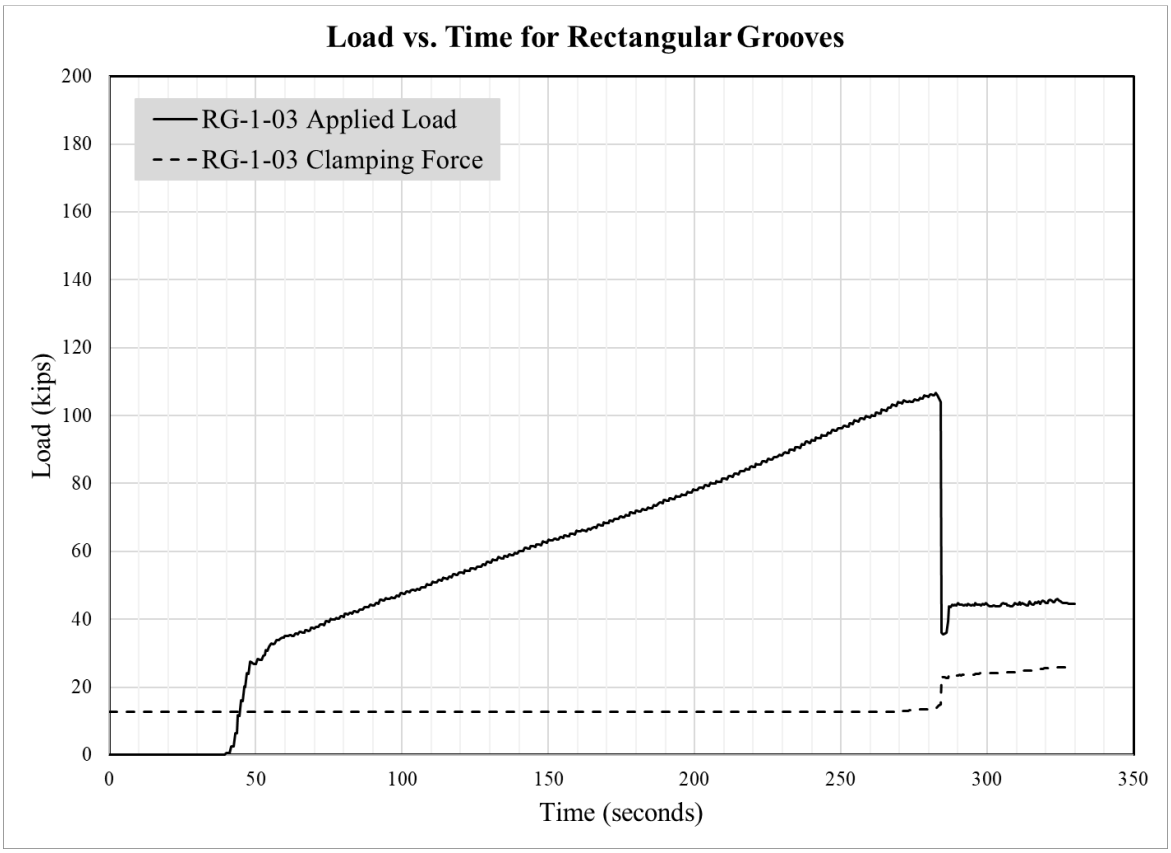
Load vs. Time for Rectangular Grooves
RG-1-03 Applied Load
RG-1-03 Clamping Force
Load (kips)
Time (seconds)
0
20
40
60
80
100
120
140
160
180
200
0
50
100
150
200
250
300
350

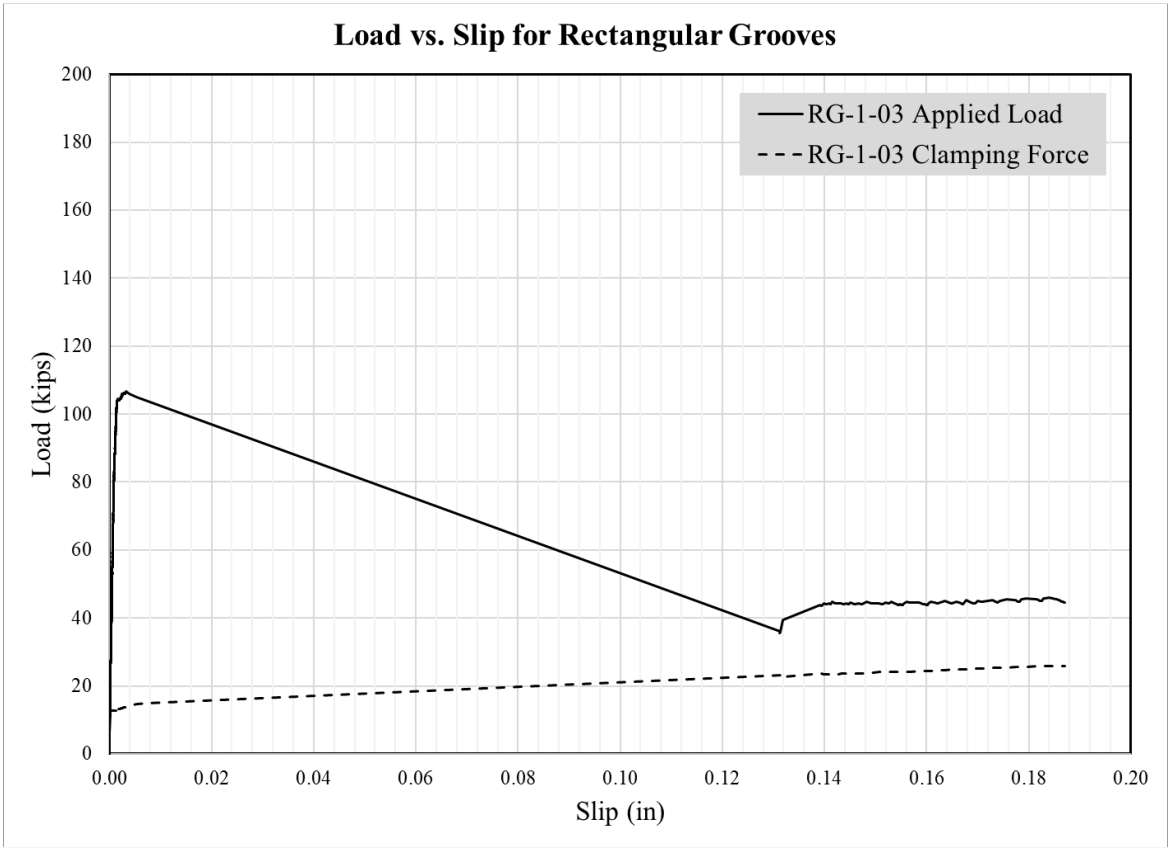
Load vs. Slip for Rectangular Grooves
RG-1-03 Applied Load
RG-1-03 Clamping Force
Load (kips)
Slip (in)
0
20
40
60
80
100
120
140
160
180
200
0.00
0.02
0.04
0.06
0.08
0.10
0.12
0.14
0.16
0.18
0.20

TG-1.5-01

Summary Table

Specimen Name	TG-1.5-01
Texture Type	Trapezoidal Grooves 1.5 in
Amplitude	0.25 in
Spacing	1.5 in
De-bonding	TuffCoat®
Concrete Compressive Strengths	Bottom: 6764 psi
	Top: 4397 psi
Interface Fracture Stress	443 psi

Theoretical Surface Treatment

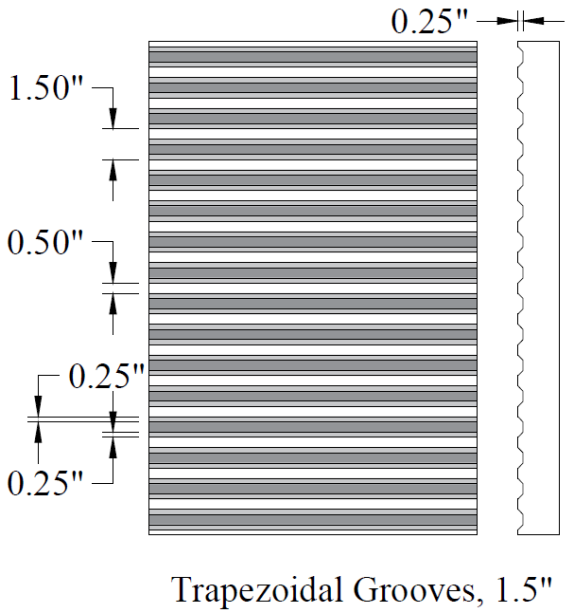

Trapezoidal Grooves, 1.5"

Actual Surface Treatment

Bottom Section After Test

Top Section After Test

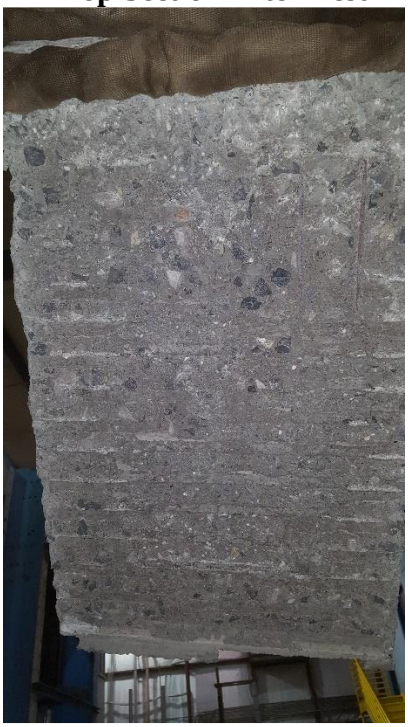

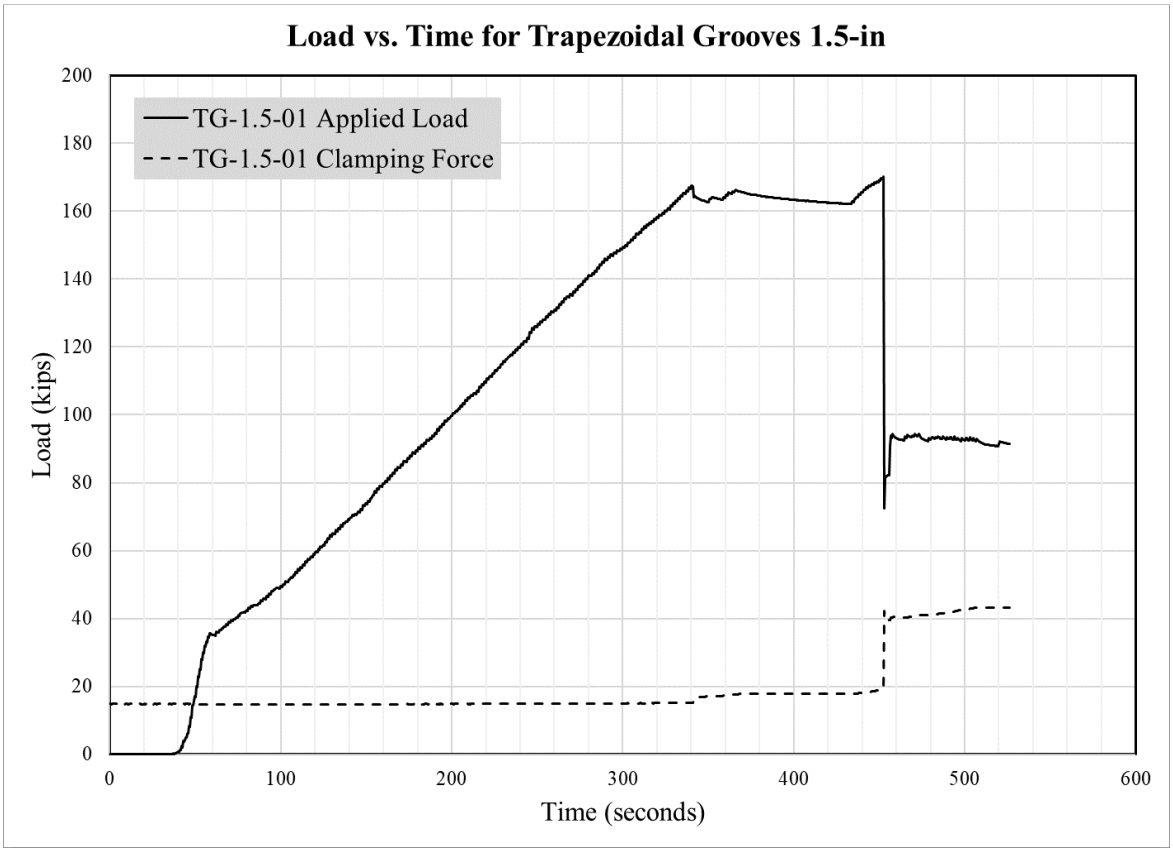
Load vs. Time for Trapezoidal Grooves 1.5-in
TG-1.5-01 Applied Load
TG-1.5-01 Clamping Force
Load (kips)
Time (seconds)
0
20
40
60
80
100
120
140
160
180
200
0
100
200
300
400
500
600

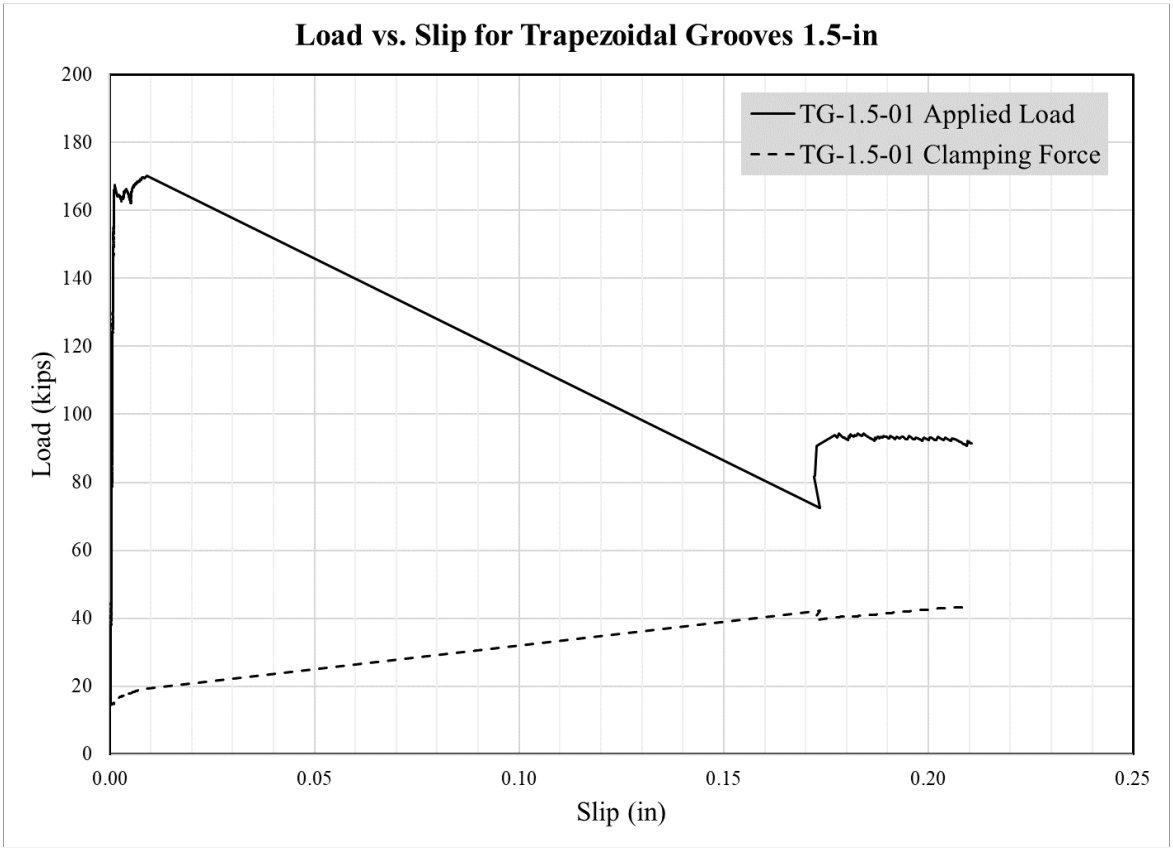
Load vs. Slip for Trapezoidal Grooves 1.5-in
TG-1.5-01 Applied Load
TG-1.5-01 Clamping Force
Load (kips)
Slip (in)
0
20
40
60
80
100
120
140
160
180
200
0.00
0.05
0.10
0.15
0.20
0.25

TG-1.5-02

Summary Table

Specimen Name	TG-1.5-02
Texture Type	Trapezoidal Grooves 1.5 in
Amplitude	0.25 in
Spacing	1.5 in
De-bonding	TuffCoat®
Concrete Compressive Strengths	Bottom: 6764 psi
	Top: 4397 psi
Interface Fracture Stress	409 psi

Theoretical Surface Treatment

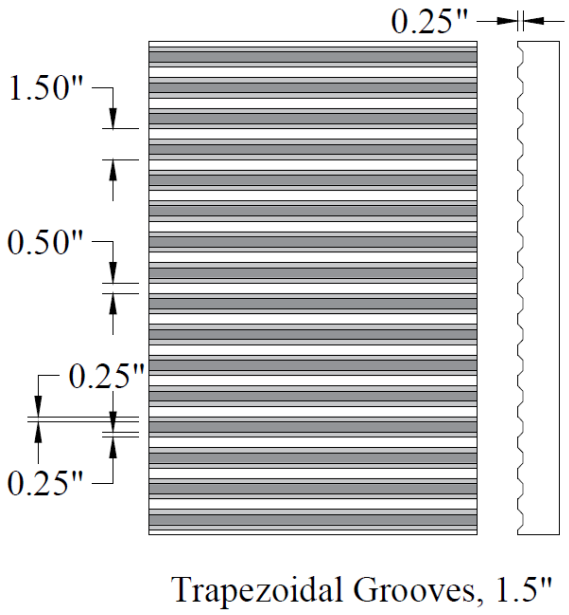

Trapezoidal Grooves, 1.5"

Actual Surface Treatment

Bottom Section After Test

Top Section After Test

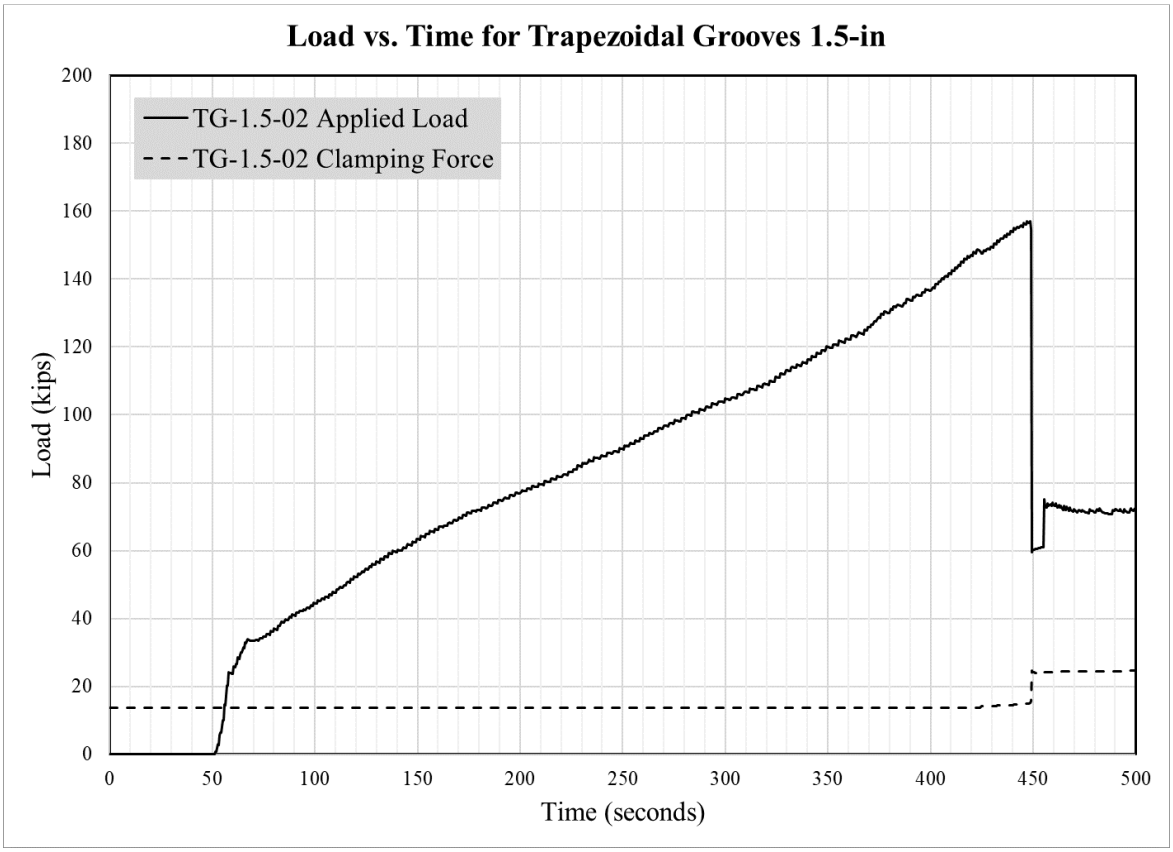
Load vs. Time for Trapezoidal Grooves 1.5-in
TG-1.5-02 Applied Load
TG-1.5-02 Clamping Force
Load (kips)
Time (seconds)
0
20
40
60
80
100
120
140
160
180
200
0
50
100
150
200
250
300
350
400
450
500

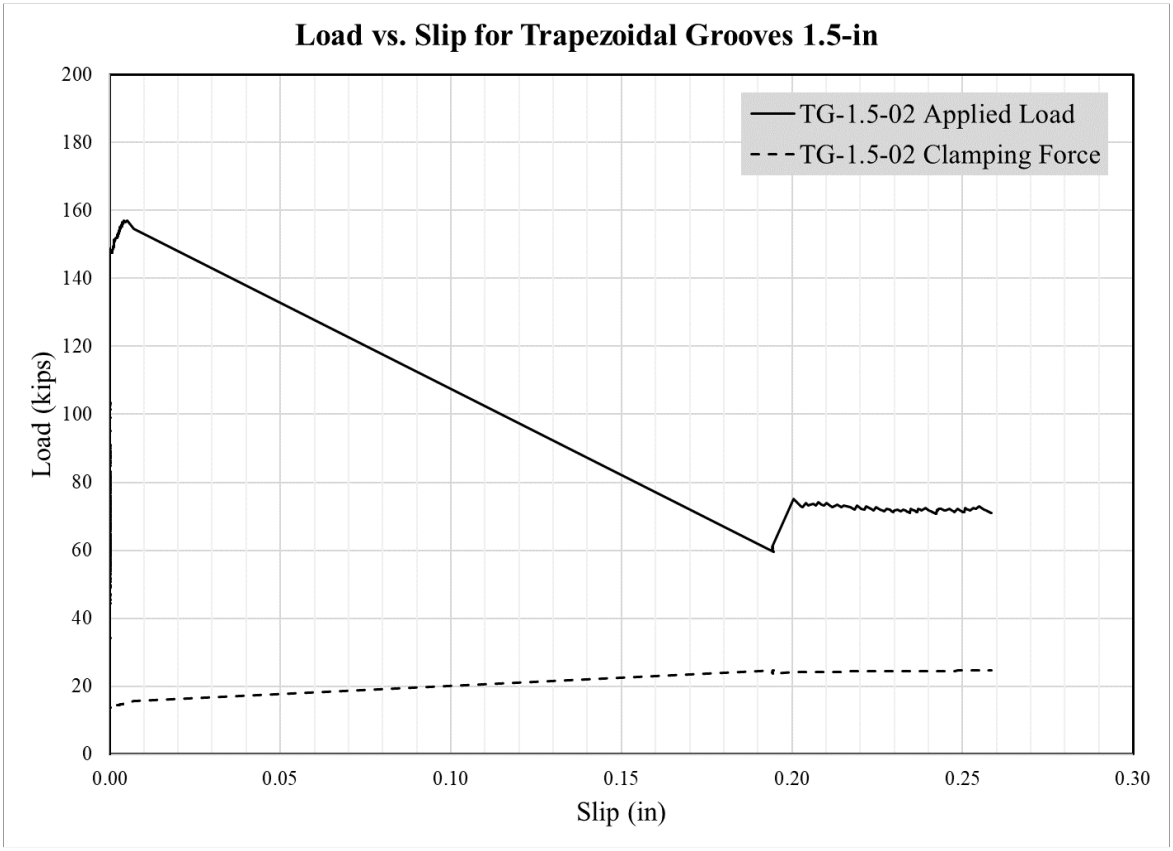
Load vs. Slip for Trapezoidal Grooves 1.5-in
TG-1.5-02 Applied Load
TG-1.5-02 Clamping Force
Load (kips)
Slip (in)
0
20
40
60
80
100
120
140
160
180
200
0.00
0.05
0.10
0.15
0.20
0.25
0.30

TG-1.5-03

Summary Table

Specimen Name	TG-1.5-03
Texture Type	Trapezoidal Grooves 1.5 in
Amplitude	0.25 in
Spacing	1.5 in
De-bonding	TuffCoat®
Concrete Compressive Strengths	Bottom: 6764 psi
	Top: 4397 psi
Interface Fracture Stress	327 psi

Theoretical Surface Treatment

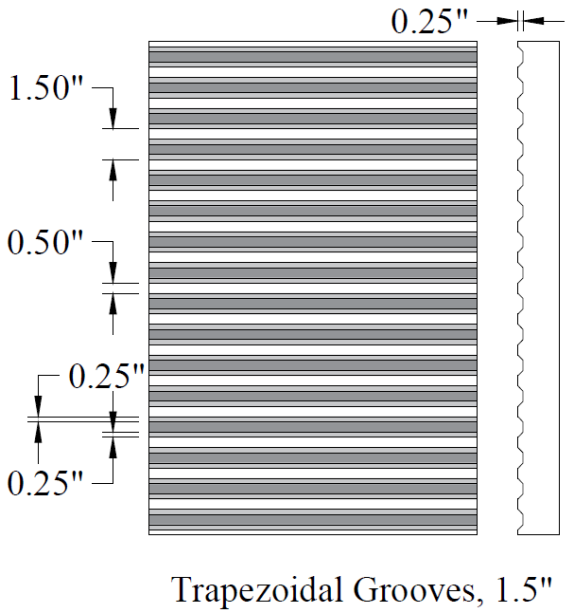

Trapezoidal Grooves, 1.5"

Actual Surface Treatment

Bottom Section After Test

Top Section After Test

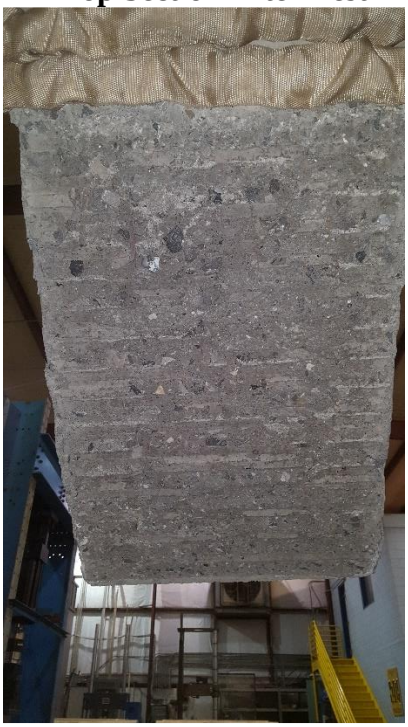

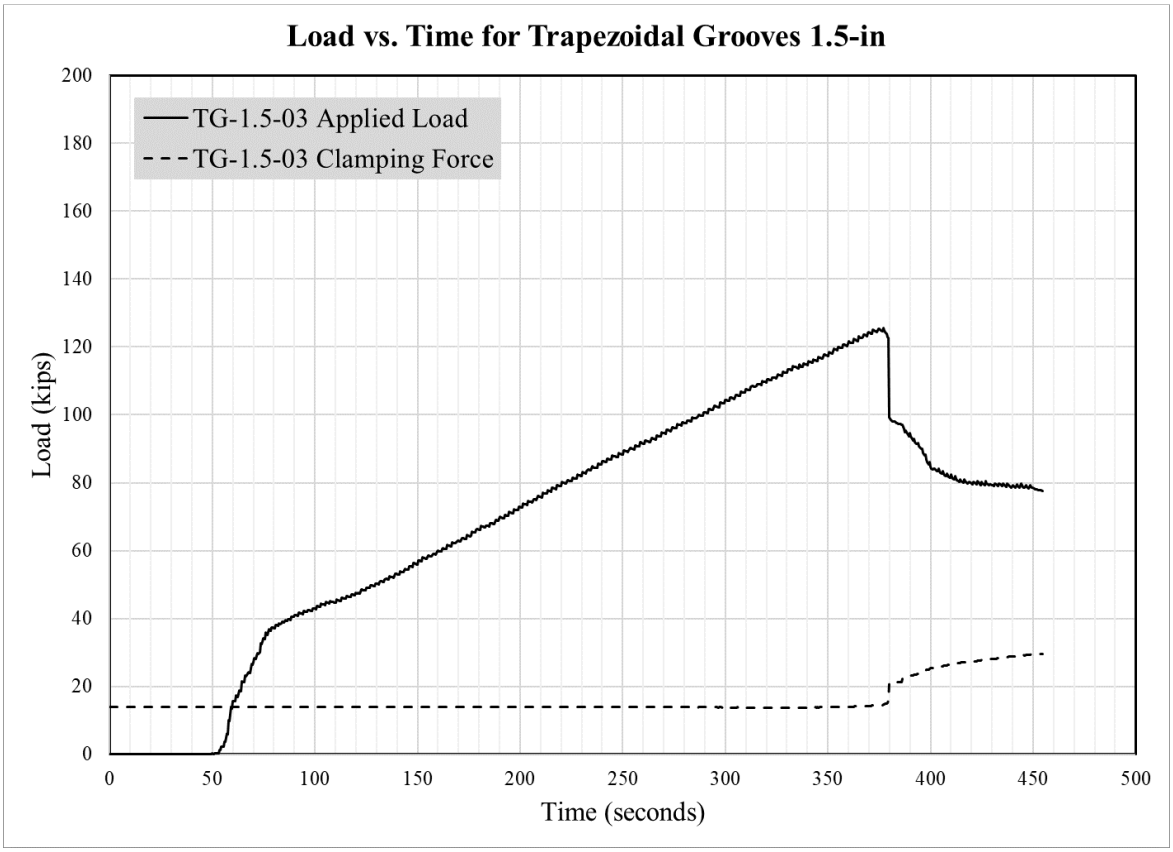
Load vs. Time for Trapezoidal Grooves 1.5-in
TG-1.5-03 Applied Load
TG-1.5-03 Clamping Force
Load (kips)
Time (seconds)
0
20
40
60
80
100
120
140
160
180
200
0
50
100
150
200
250
300
350
400
450
500

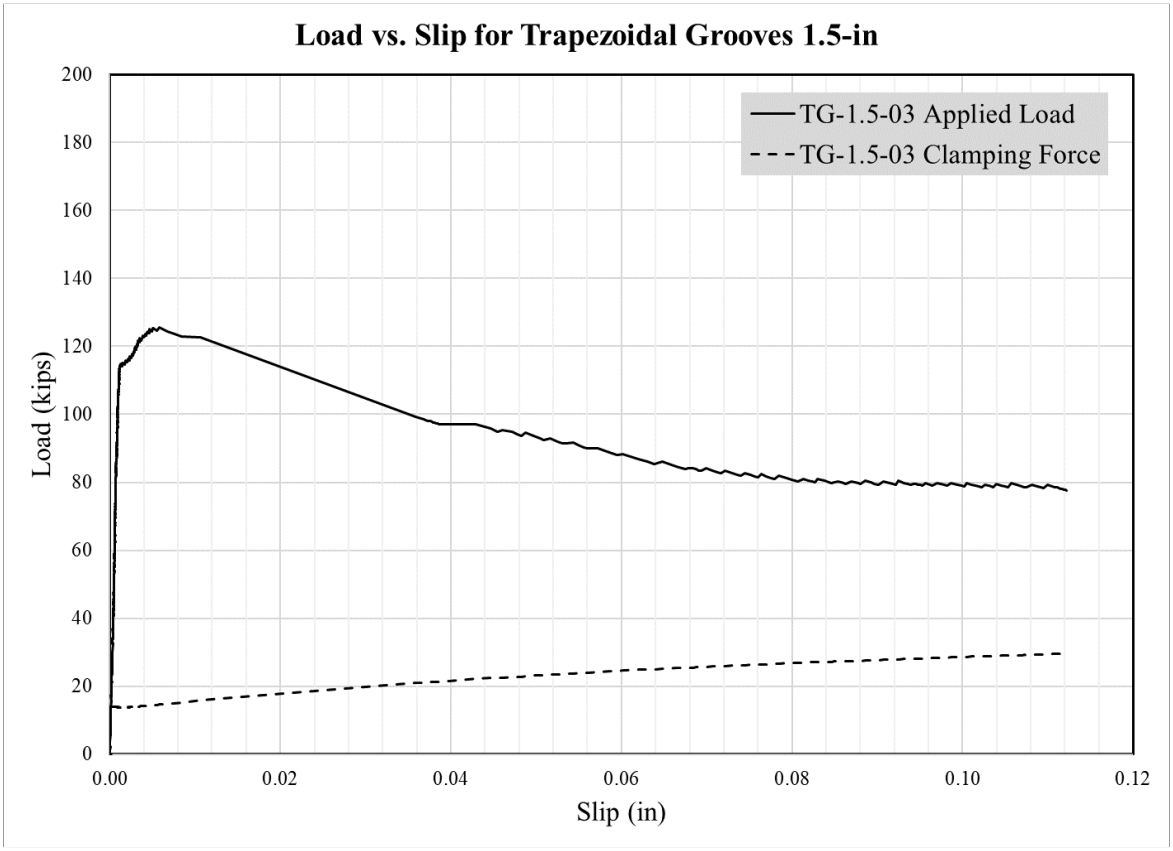
Load vs. Slip for Trapezoidal Grooves 1.5-in
TG-1.5-03 Applied Load
TG-1.5-03 Clamping Force
Load (kips)
Slip (in)
0
20
40
60
80
100
120
140
160
180
200
0.00
0.02
0.04
0.06
0.08
0.10
0.12

TG-3-01

Summary Table

Specimen Name	TG-3-01
Texture Type	Trapezoidal Grooves 3 in
Amplitude	0.25 in
Spacing	3 in
De-bonding	TuffCoat®
Concrete Compressive Strengths	Bottom: 7799 psi
	Top: 4516 psi
Interface Fracture Stress	341 psi

Theoretical Surface Treatment

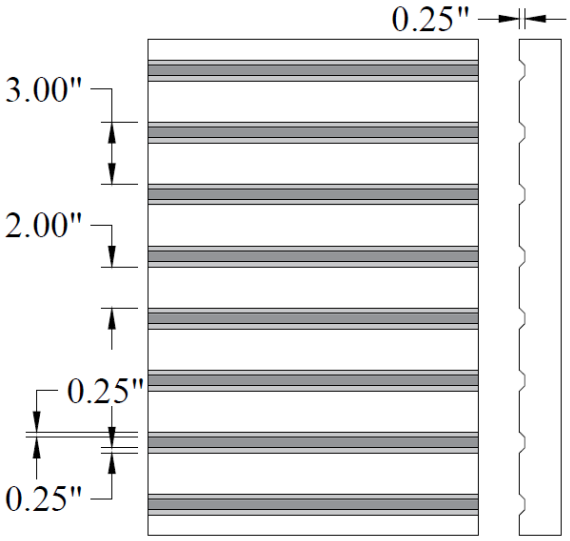

Trapezoidal Grooves, 3"

Actual Surface Treatment

Bottom Section After Test

Top Section After Test


Load vs. Time for Trapezoidal Grooves 3-in
TG-3-01 Applied Load
TG-3-01 Clamping Force
Load (kips)
Time (seconds)
0
20
40
60
80
100
120
140
160
180
200
0
50
100
150
200
250
300
350
400
450
500

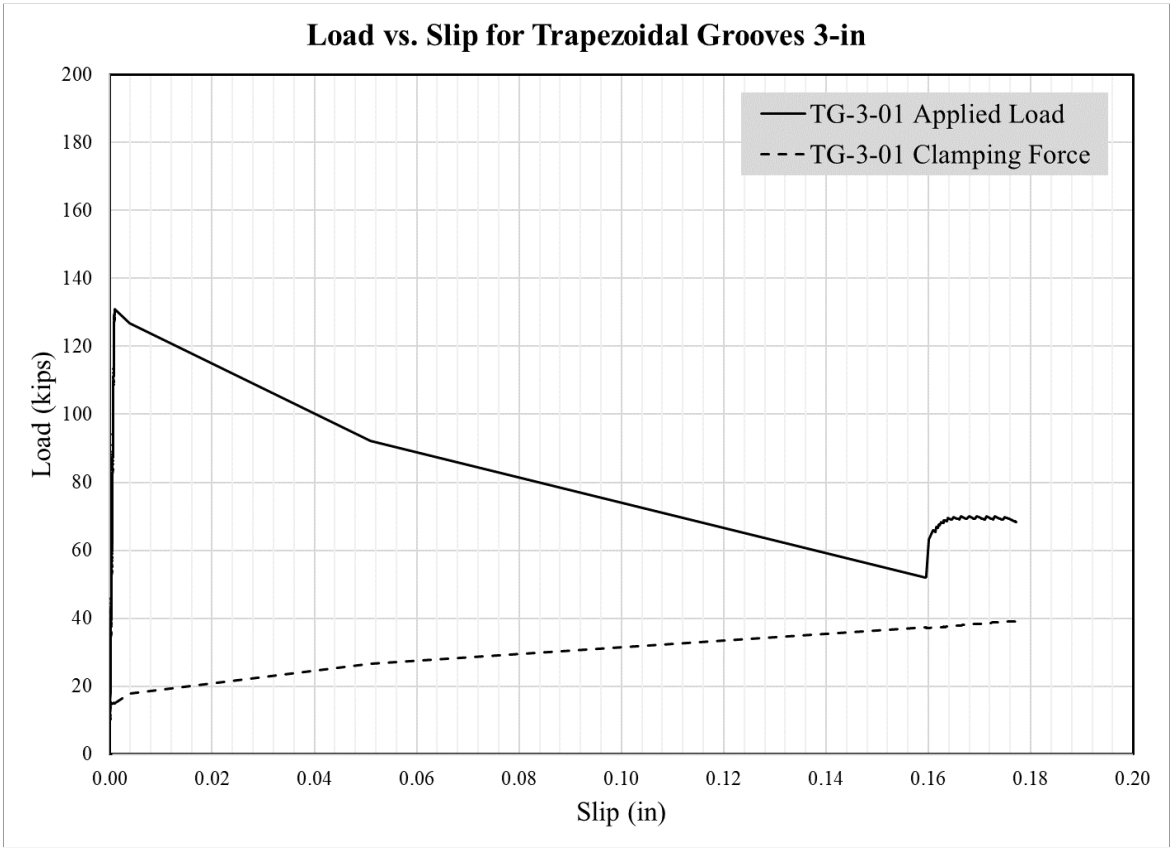
Load vs. Slip for Trapezoidal Grooves 3-in
TG-3-01 Applied Load
TG-3-01 Clamping Force
Load (kips)
Slip (in)
0
20
40
60
80
100
120
140
160
180
200
0.00
0.02
0.04
0.06
0.08
0.10
0.12
0.14
0.16
0.18
0.20

TG-3-02

Summary Table

Specimen Name	TG-3-02
Texture Type	Trapezoidal Grooves 3 in
Amplitude	0.25 in
Spacing	3 in
De-bonding	TuffCoat®
Concrete Compressive Strengths	Bottom: 7799 psi
	Top: 4516 psi
Interface Fracture Stress	385 psi

Theoretical Surface Treatment

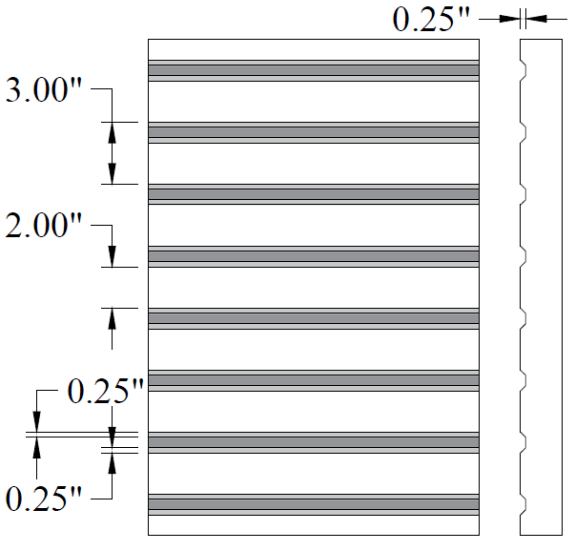

Trapezoidal Grooves, 3"

Actual Surface Treatment

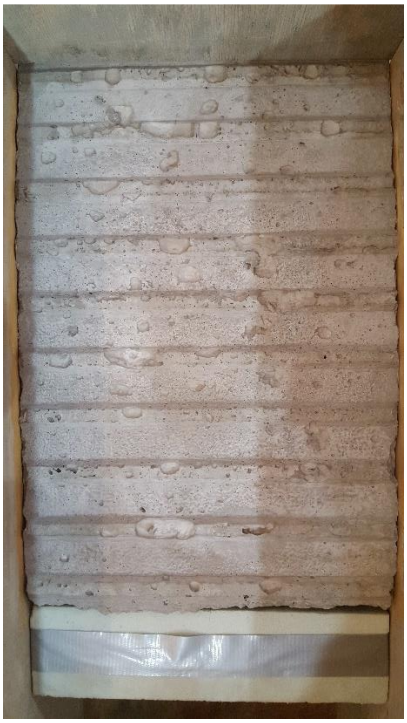

Bottom Section After Test

Top Section After Test

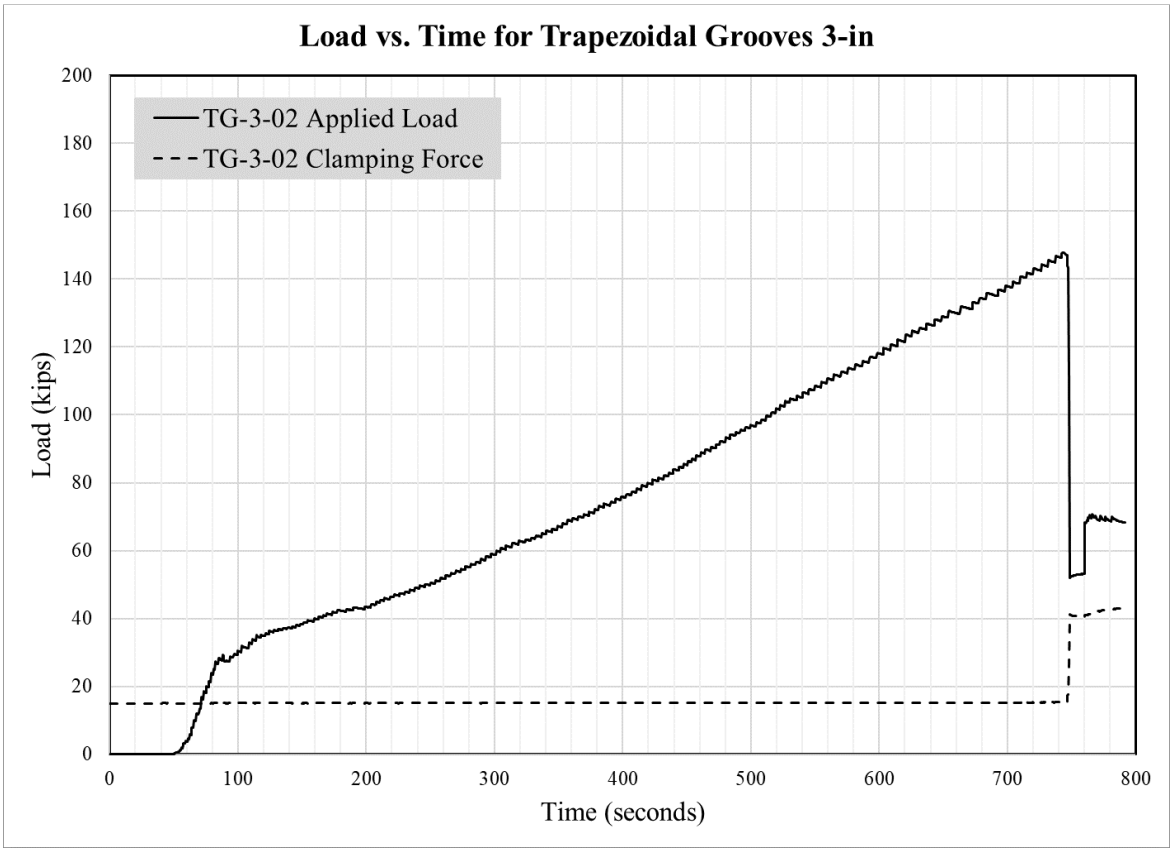
Load vs. Time for Trapezoidal Grooves 3-in
TG-3-02 Applied Load
TG-3-02 Clamping Force
Load (kips)
Time (seconds)
0
20
40
60
80
100
120
140
160
180
200
0
100
200
300
400
500
600
700
800

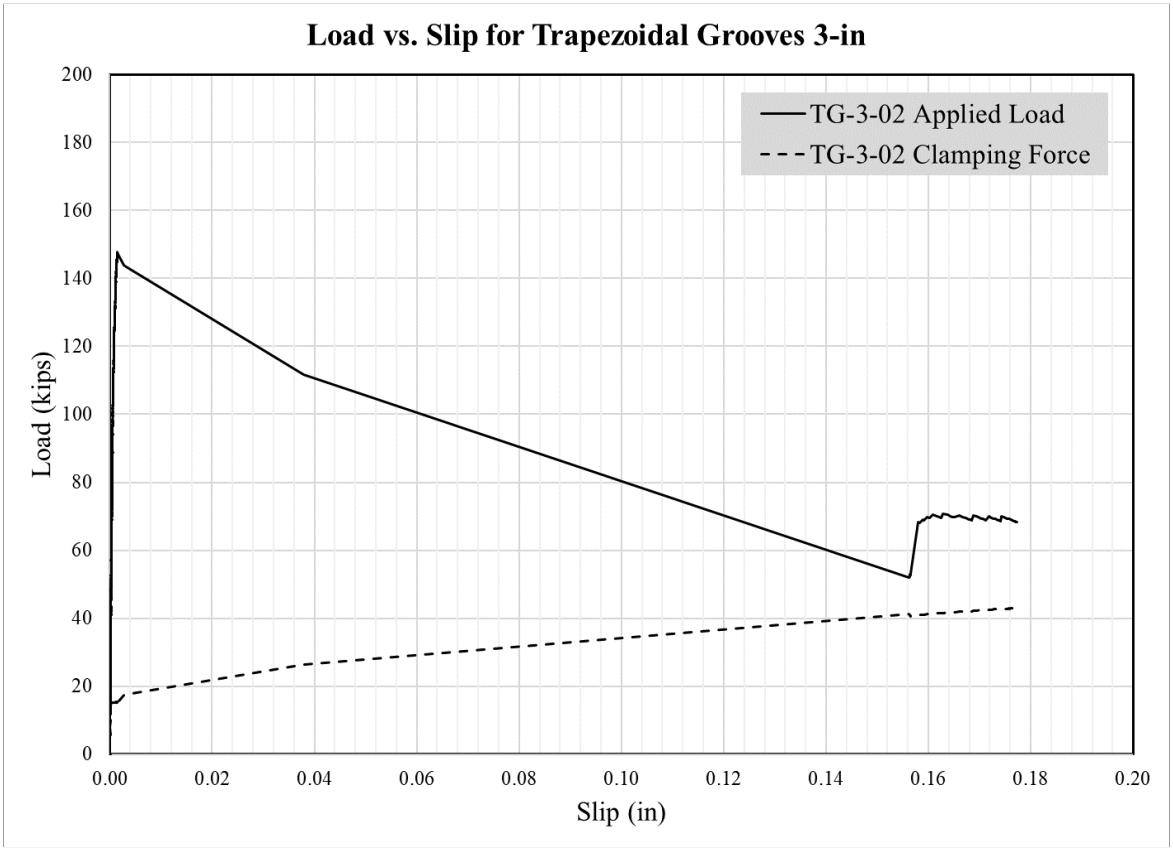
Load vs. Slip for Trapezoidal Grooves 3-in
TG-3-02 Applied Load
TG-3-02 Clamping Force
Load (kips)
Slip (in)
0
20
40
60
80
100
120
140
160
180
200
0.00
0.02
0.04
0.06
0.08
0.10
0.12
0.14
0.16
0.18
0.20

TG-3-03

Summary Table

Specimen Name	TG-3-03
Texture Type	Trapezoidal Grooves 3 in
Amplitude	0.25 in
Spacing	3 in
De-bonding	TuffCoat®
Concrete Compressive Strengths	Bottom: 7799 psi
	Top: 4516 psi
Interface Fracture Stress	370 psi

Theoretical Surface Treatment

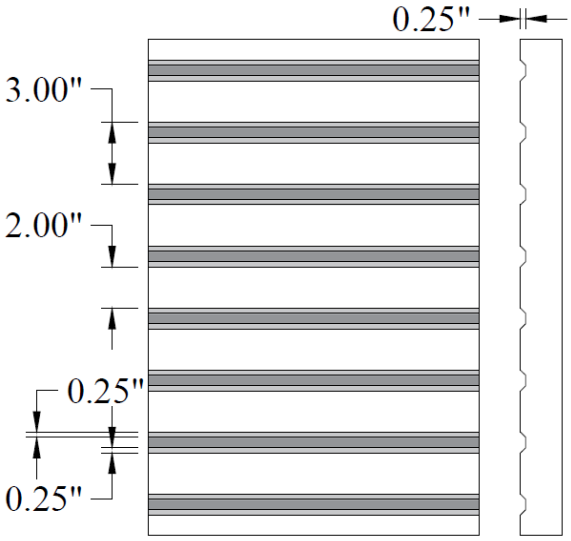

Trapezoidal Grooves, 3"

Actual Surface Treatment

Bottom Section After Test

Top Section After Test

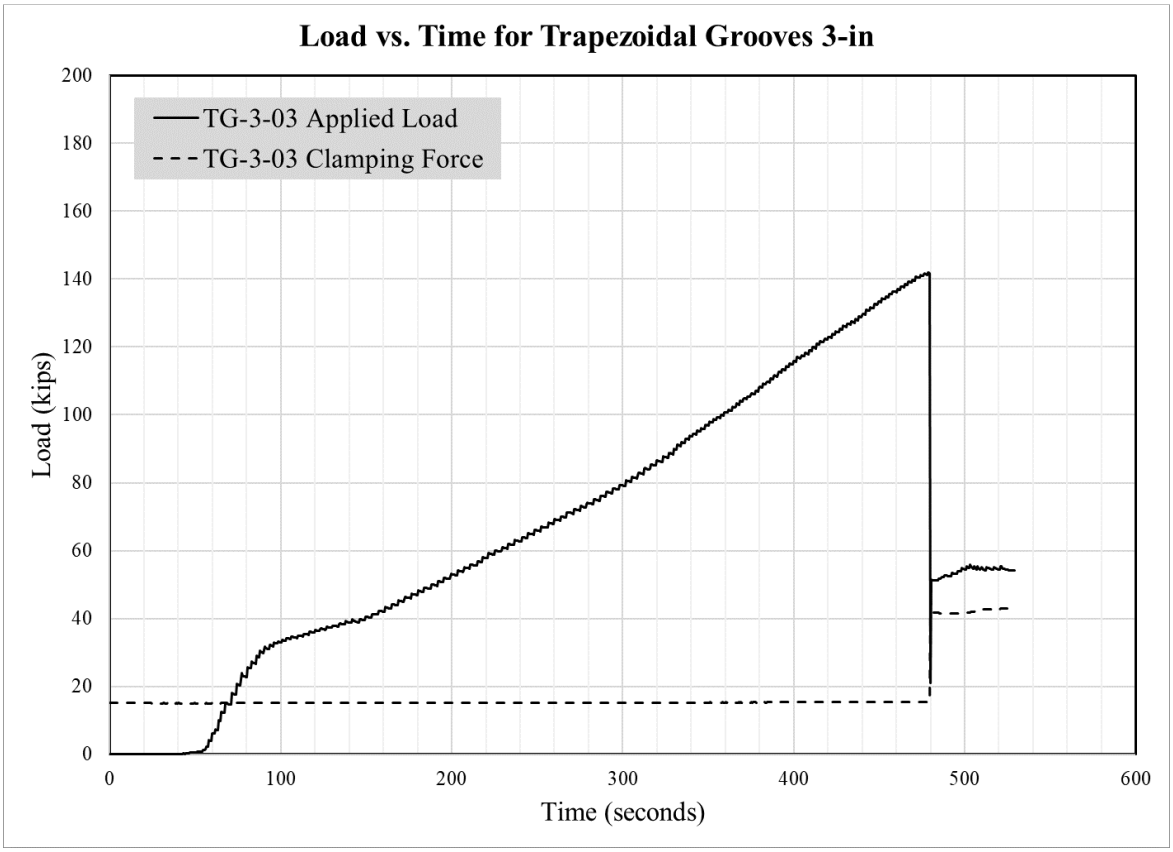
Load vs. Time for Trapezoidal Grooves 3-in
TG-3-03 Applied Load
TG-3-03 Clamping Force
Load (kips)
Time (seconds)
0
20
40
60
80
100
120
140
160
180
200
0
100
200
300
400
500
600

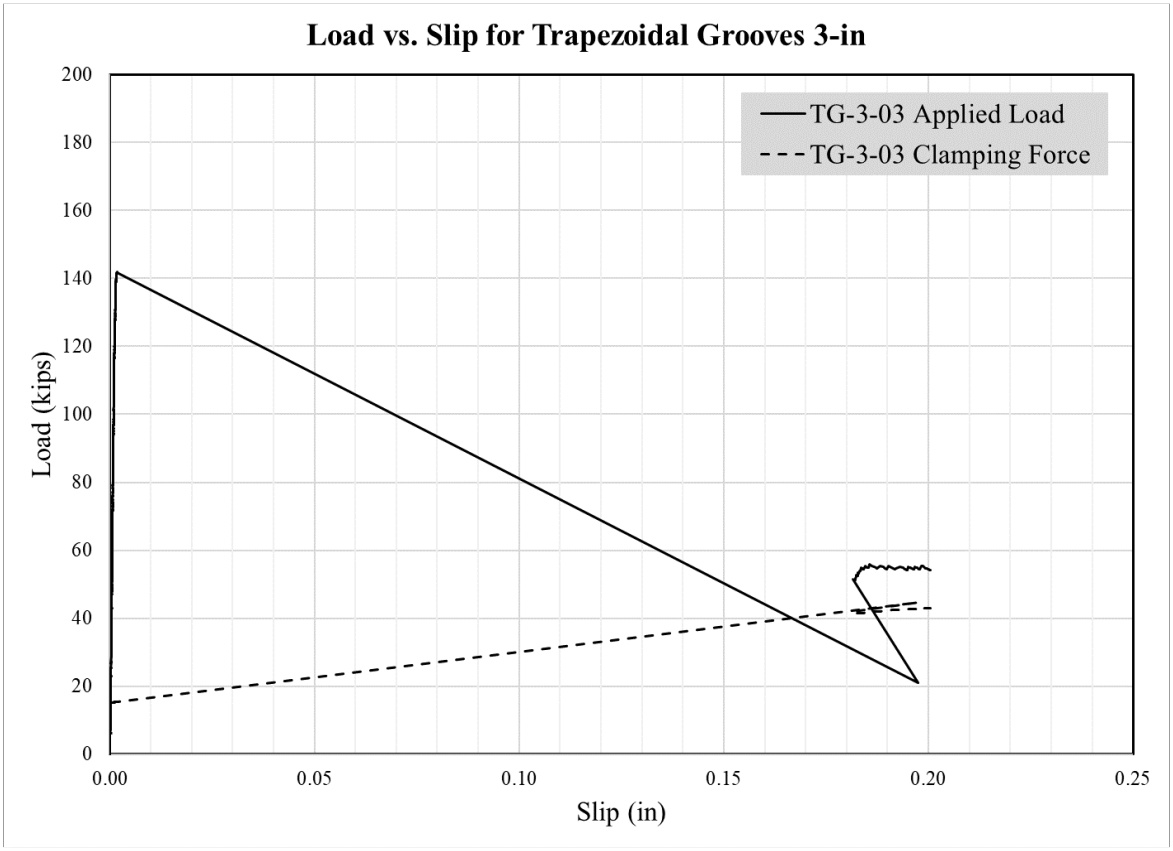
Load vs. Slip for Trapezoidal Grooves 3-in
TG-3-03 Applied Load
TG-3-03 Clamping Force
Load (kips)
Slip (in)
0
20
40
60
80
100
120
140
160
180
200
0.00
0.05
0.10
0.15
0.20
0.25

CH-3.5-TC-01

Summary Table

Specimen Name	CH-3.5-TC-01
Texture Type	Cross Hatch Plastic
Amplitude	0.25 in
Spacing	3.5 in
De-bonding	TuffCoat®
Concrete Compressive Strengths	Bottom: 8754 psi
	Top: 5948 psi
Interface Fracture Stress	473 psi

Theoretical Surface Treatment

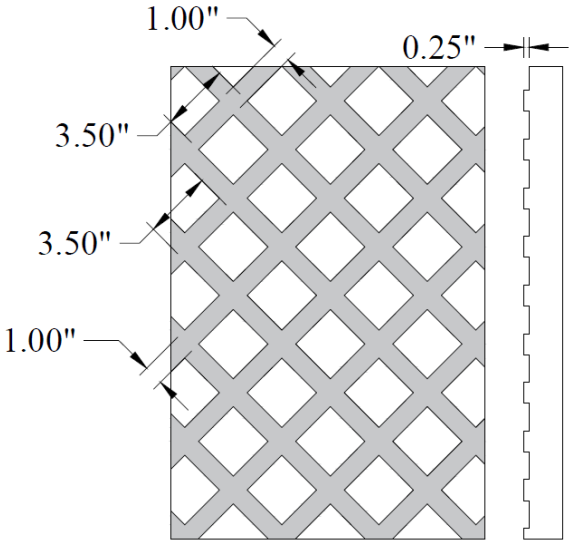

Cross Hatch

Actual Surface Treatment

Photo Not Available

Bottom Section After Test

Top Section After Test

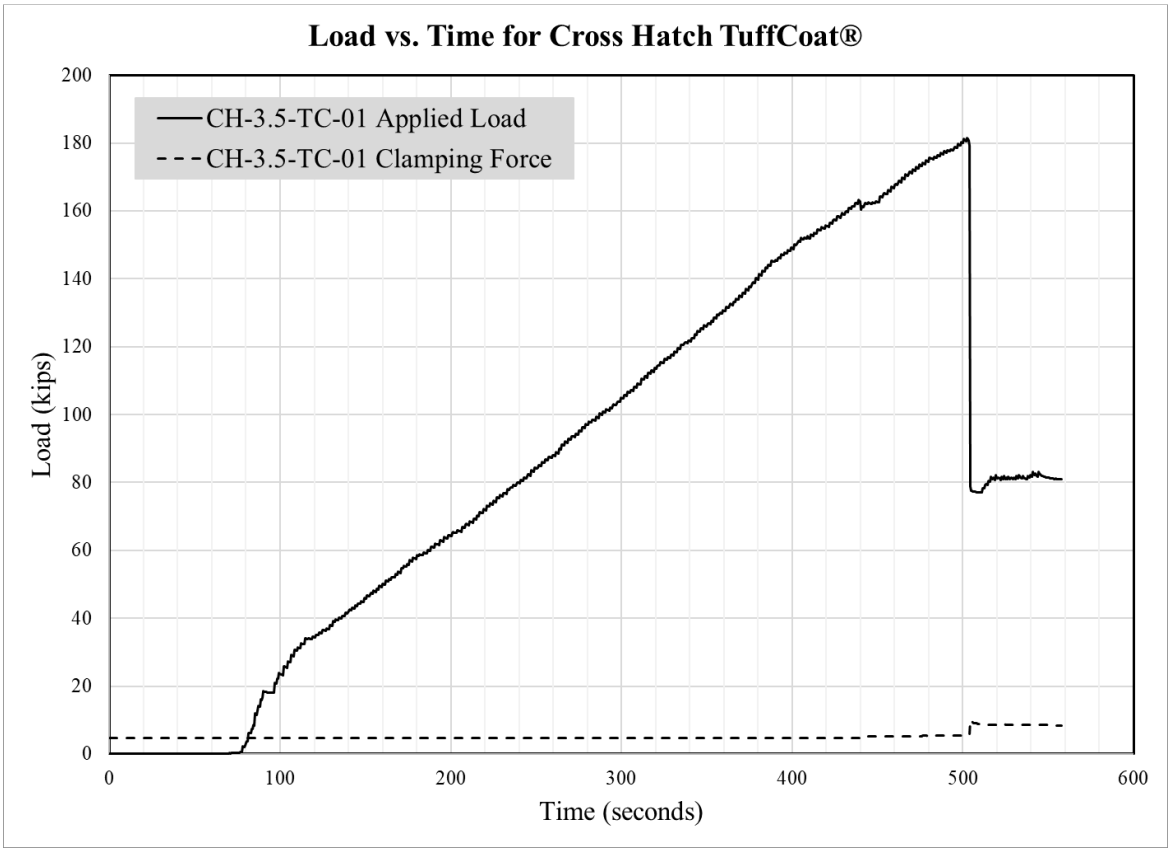
Load vs. Time for Cross Hatch TuffCoat®
CH-3.5-TC-01 Applied Load
CH-3.5-TC-01 Clamping Force
Load (kips)
Time (seconds)
0
20
40
60
80
100
120
140
160
180
200
0
100
200
300
400
500
600

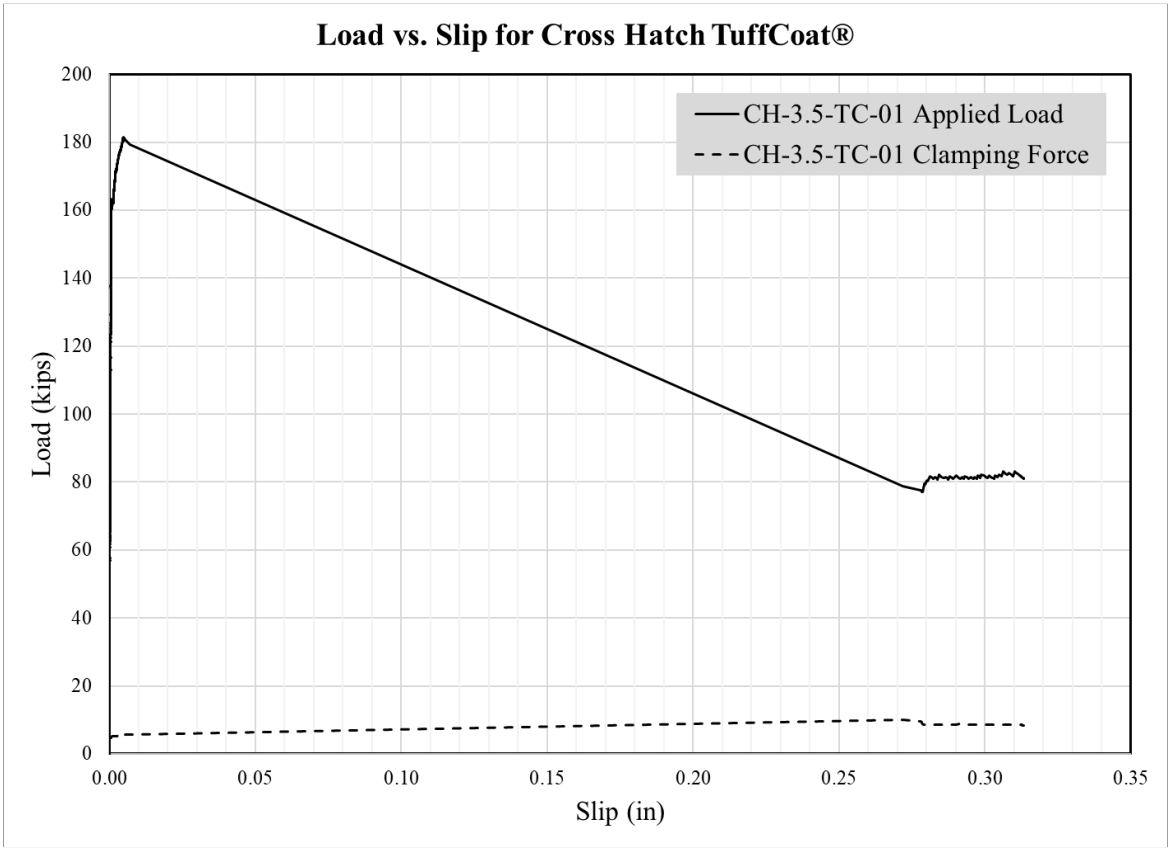
Load vs. Slip for Cross Hatch TuffCoat®
CH-3.5-TC-01 Applied Load
CH-3.5-TC-01 Clamping Force
Load (kips)
Slip (in)
0
20
40
60
80
100
120
140
160
180
200
0.00
0.05
0.10
0.15
0.20
0.25
0.30
0.35

CH-3.5-TC-02

Summary Table

Specimen Name	CH-3.5-TC-02
Texture Type	Cross Hatch Plastic
Amplitude	0.25 in
Spacing	3.5 in
De-bonding	TuffCoat®
Concrete Compressive Strengths	Bottom: 8754 psi
	Top: 5948 psi
Interface Fracture Stress	383 psi

Theoretical Surface Treatment

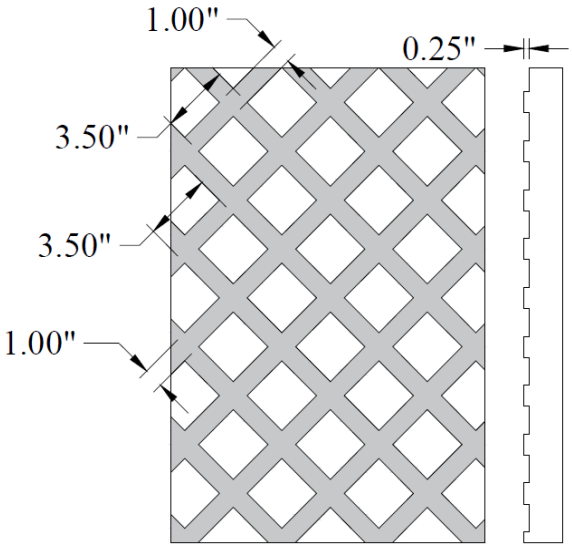

Cross Hatch

Actual Surface Treatment

Photo Not Available

Bottom Section After Test

Top Section After Test

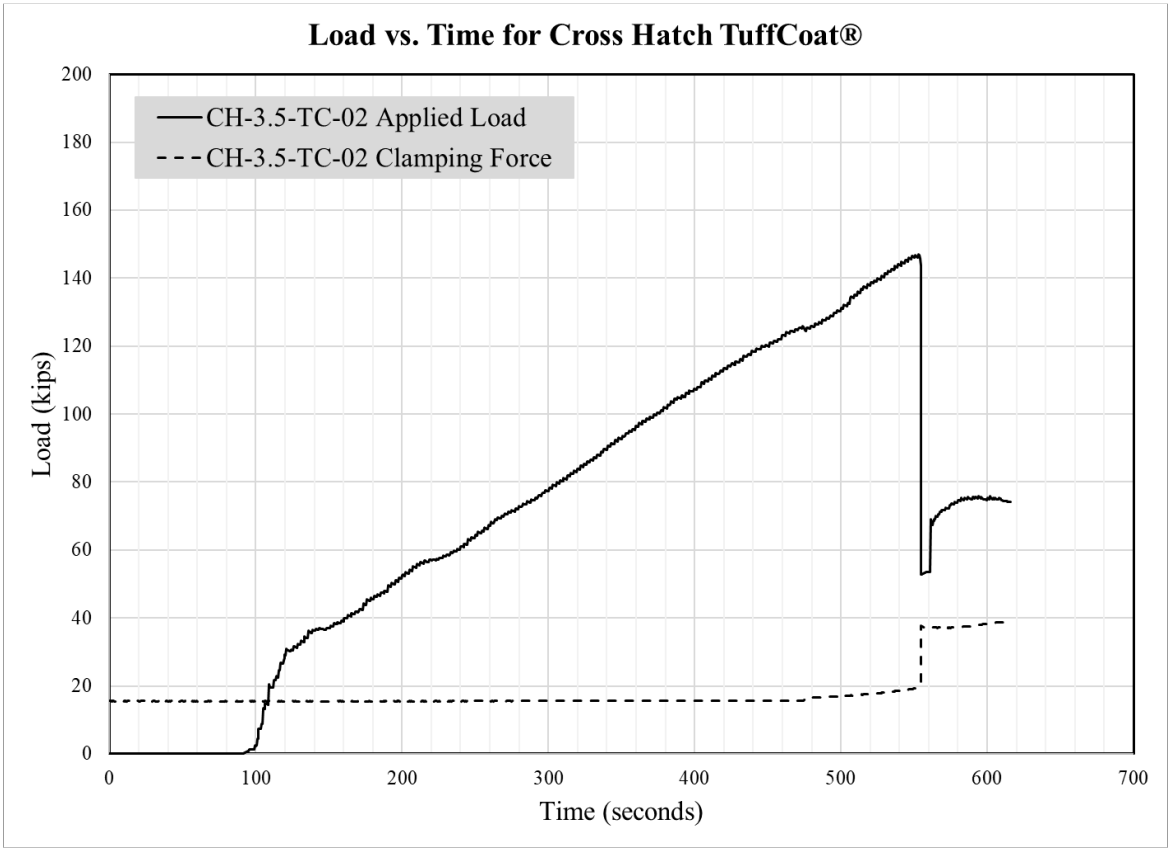
Load vs. Time for Cross Hatch TuffCoat®
CH-3.5-TC-02 Applied Load
CH-3.5-TC-02 Clamping Force
Load (kips)
Time (seconds)
0
20
40
60
80
100
120
140
160
180
200
0
100
200
300
400
500
600
700

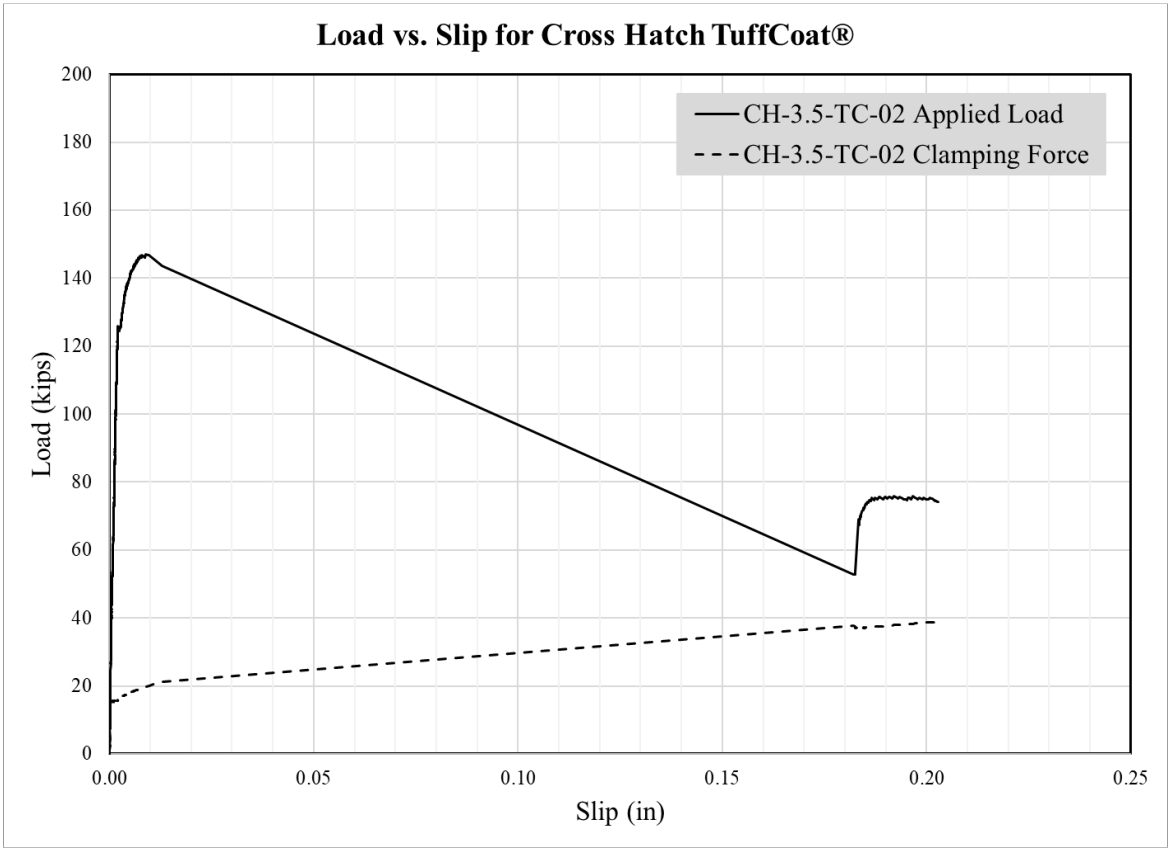
Load vs. Slip for Cross Hatch TuffCoat®
CH-3.5-TC-02 Applied Load
CH-3.5-TC-02 Clamping Force
Load (kips)
Slip (in)
0
20
40
60
80
100
120
140
160
180
200
0.00
0.05
0.10
0.15
0.20
0.25

CH-3.5-TC-03

Summary Table

Specimen Name	CH-3.5-TC-03
Texture Type	Cross Hatch Plastic
Amplitude	0.25 in
Spacing	3.5 in
De-bonding	TuffCoat®
Concrete Compressive Strengths	Bottom: 8754 psi
	Top: 5948 psi
Interface Fracture Stress	387 psi

Theoretical Surface Treatment

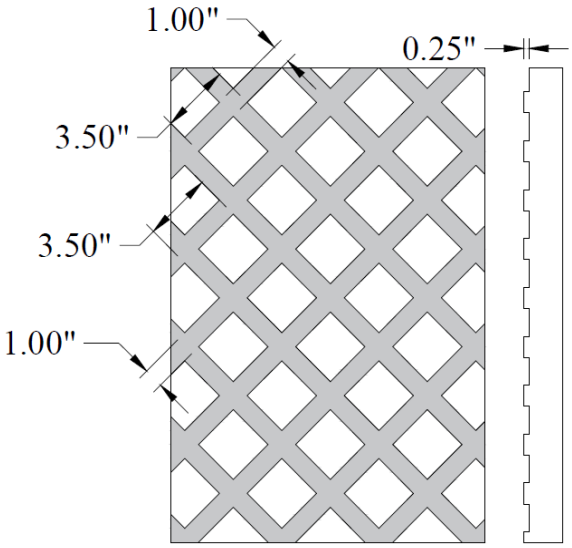

Cross Hatch

Actual Surface Treatment

Photo Not Available

Bottom Section After Test

Top Section After Test

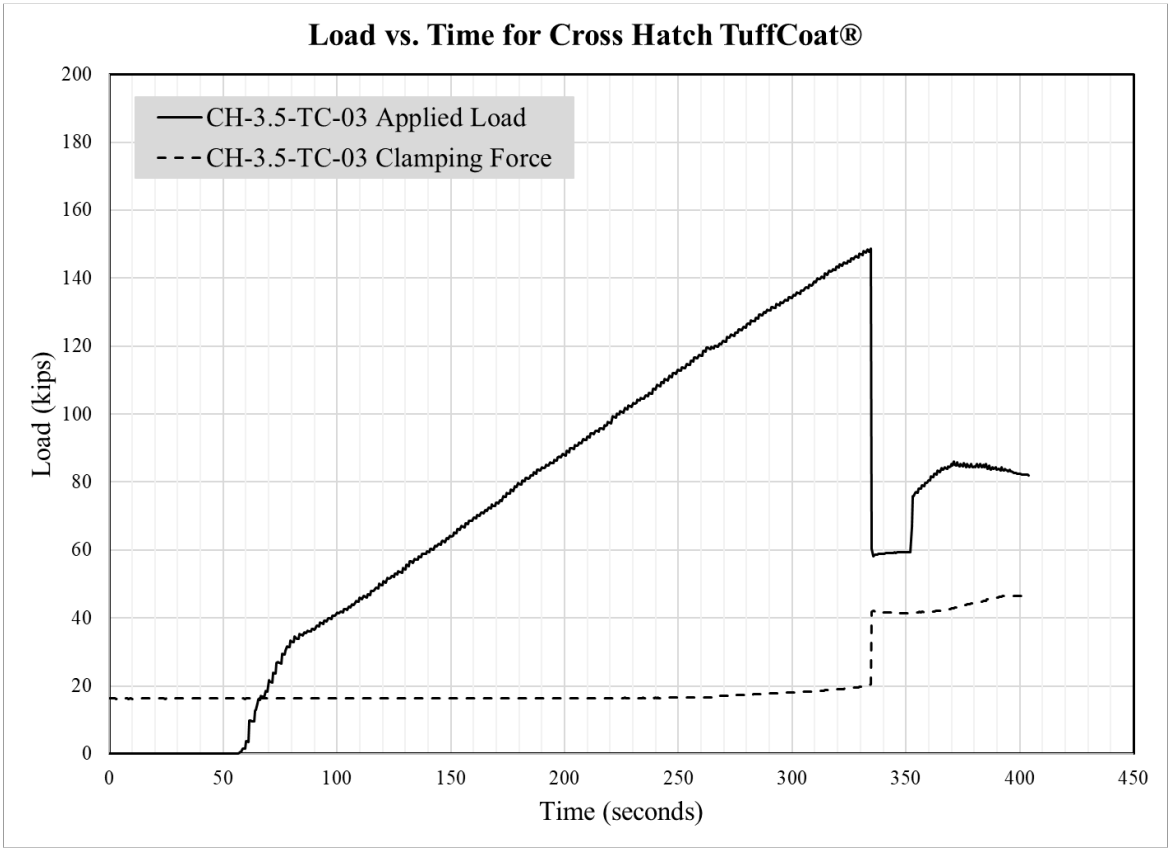
Load vs. Time for Cross Hatch TuffCoat®
CH-3.5-TC-03 Applied Load
CH-3.5-TC-03 Clamping Force
Load (kips)
Time (seconds)
0
20
40
60
80
100
120
140
160
180
200
0
50
100
150
200
250
300
350
400
450

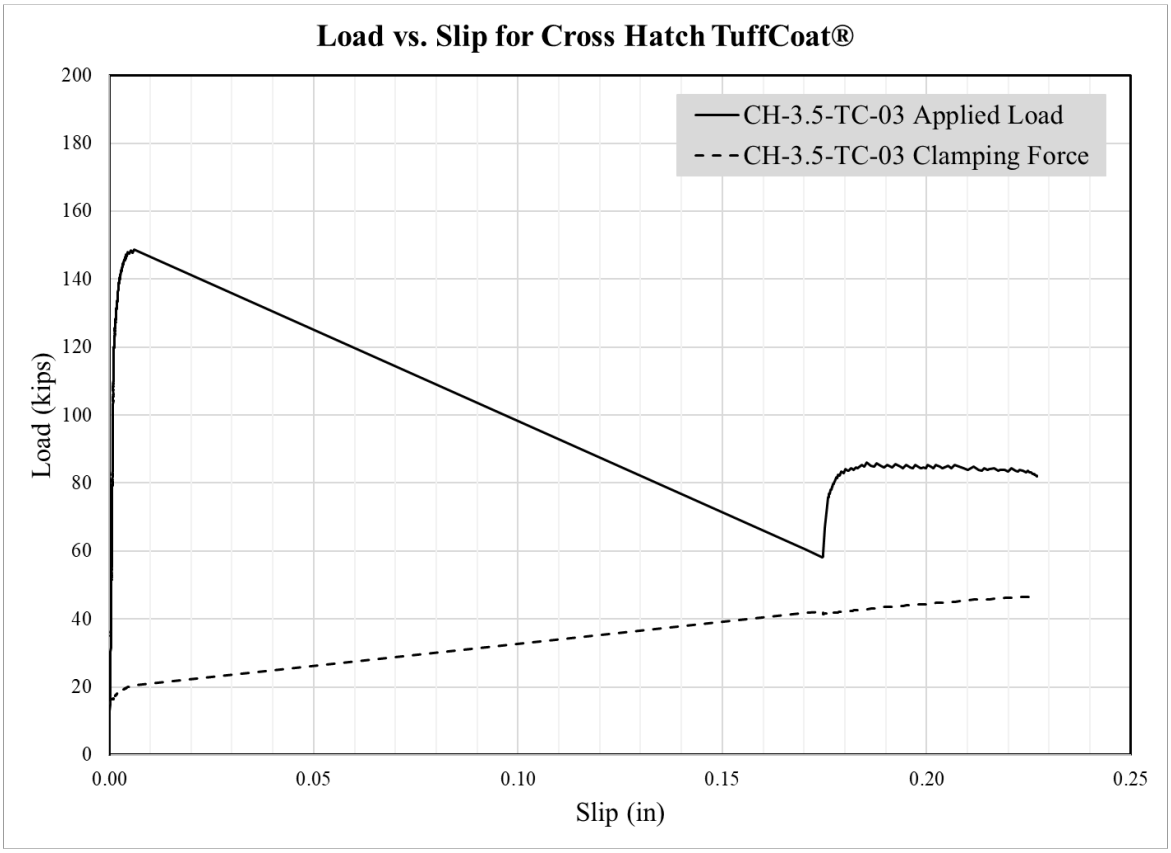
Load vs. Slip for Cross Hatch TuffCoat®
CH-3.5-TC-03 Applied Load
CH-3.5-TC-03 Clamping Force
Load (kips)
Slip (in)
0
20
40
60
80
100
120
140
160
180
200
0.00
0.05
0.10
0.15
0.20
0.25

CH-3.5-PL-01

Summary Table

Specimen Name	CH-3.5-PL-01
Texture Type	Cross Hatch Plastic
Amplitude	0.25 in
Spacing	3.5 in
De-bonding	Plastic
Concrete Compressive Strengths	Bottom: 7799 psi
	Top: 4516 psi
Interface Fracture Stress	NA

Theoretical Surface Treatment

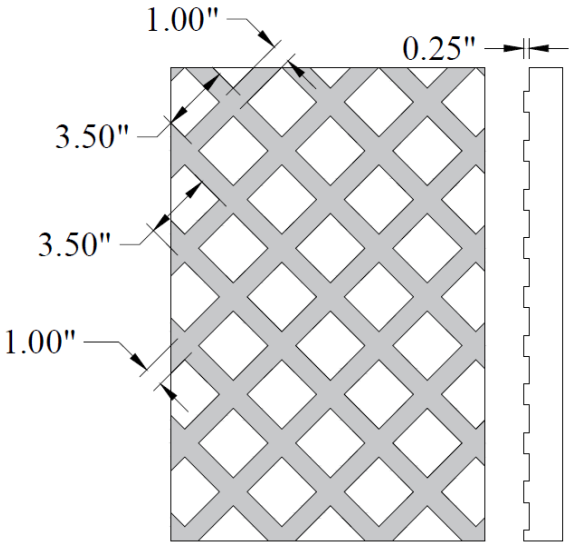

Cross Hatch

Actual Surface Treatment

Bottom Section After Test

Top Section After Test

Data Not Available

Data Not Available

CH-3.5-PL-02

Summary Table

Specimen Name	CH-3.5-PL-02
Texture Type	Cross Hatch Plastic
Amplitude	0.25 in
Spacing	3.5 in
De-bonding	Plastic
Concrete Compressive Strengths	Bottom: 7799 psi
	Top: 4516 psi
Interface Fracture Stress	276 psi

Theoretical Surface Treatment

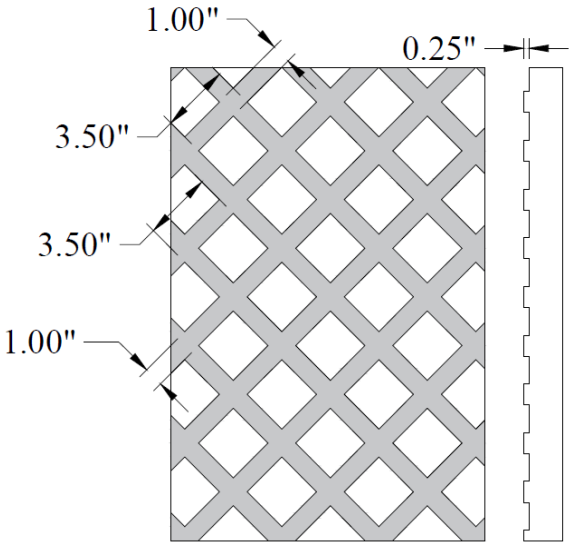

Cross Hatch

Actual Surface Treatment

Bottom Section After Test

Top Section After Test

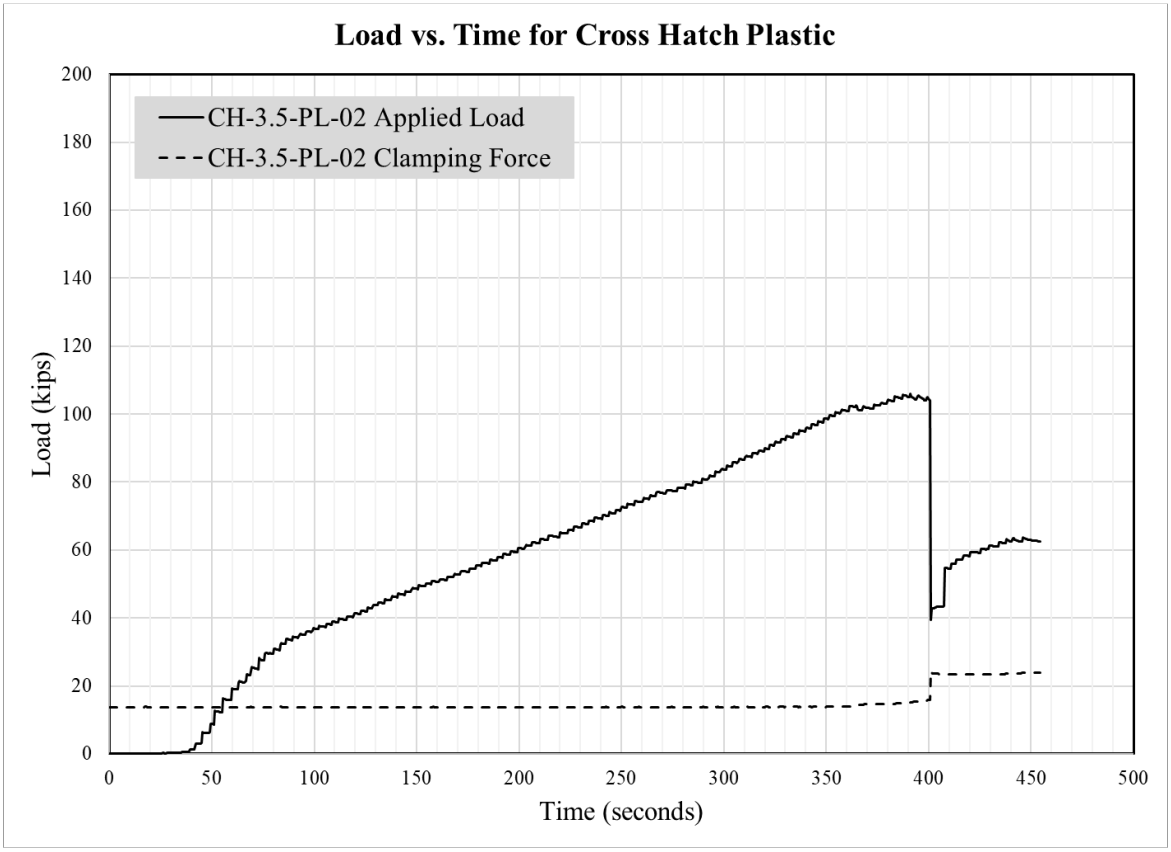
Load vs. Time for Cross Hatch Plastic
CH-3.5-PL-02 Applied Load
CH-3.5-PL-02 Clamping Force
Load (kips)
Time (seconds)
0
20
40
60
80
100
120
140
160
180
200
0
50
100
150
200
250
300
350
400
450
500

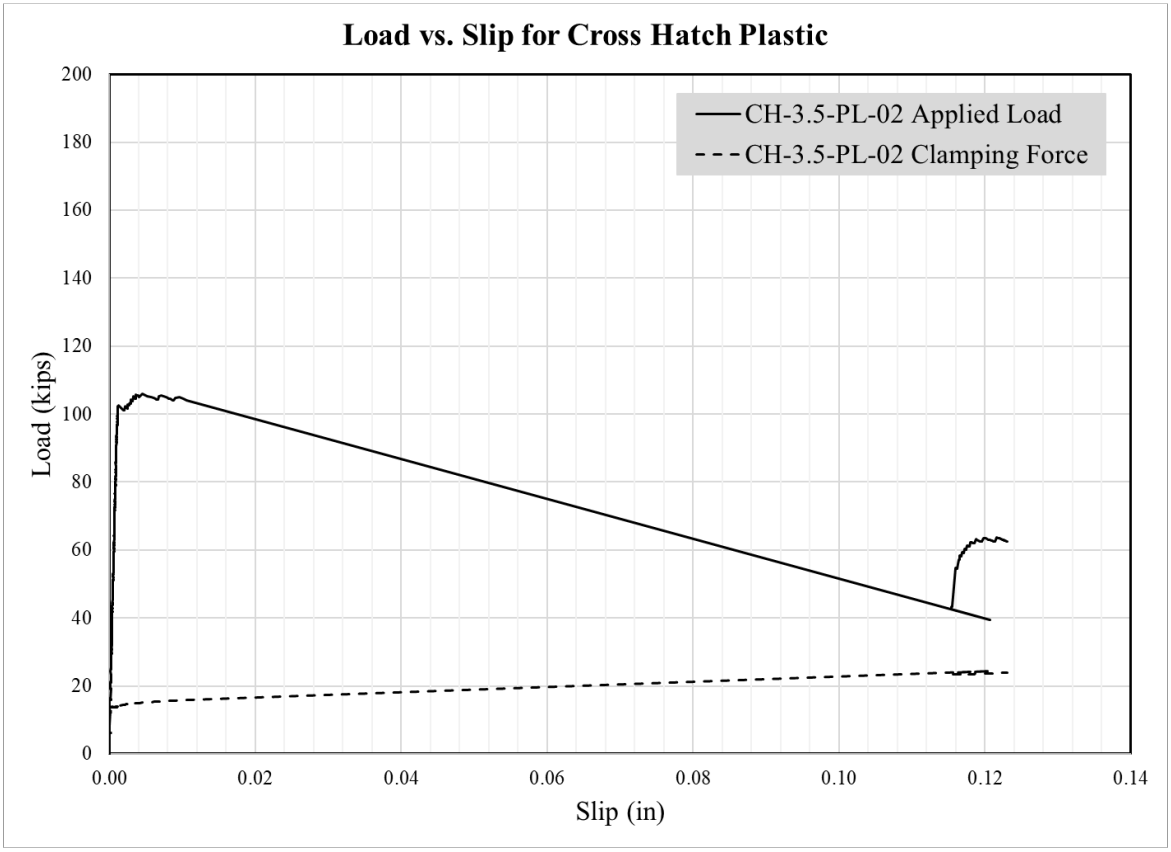
Load vs. Slip for Cross Hatch Plastic
CH-3.5-PL-02 Applied Load
CH-3.5-PL-02 Clamping Force
Load (kips)
Slip (in)
0
20
40
60
80
100
120
140
160
180
200
0.00
0.02
0.04
0.06
0.08
0.10
0.12
0.14

CH-3.5-PL-03

Summary Table

Specimen Name	CH-3.5-PL-03
Texture Type	Cross Hatch Plastic
Amplitude	0.25 in
Spacing	3.5 in
De-bonding	Plastic
Concrete Compressive Strengths	Bottom: 7799 psi
	Top: 4516 psi
Interface Fracture Stress	245 psi

Theoretical Surface Treatment

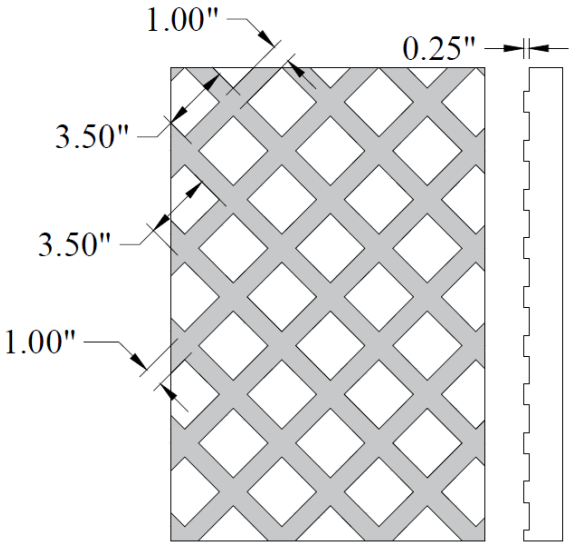

Cross Hatch

Actual Surface Treatment

Bottom Section After Test

Top Section After Test

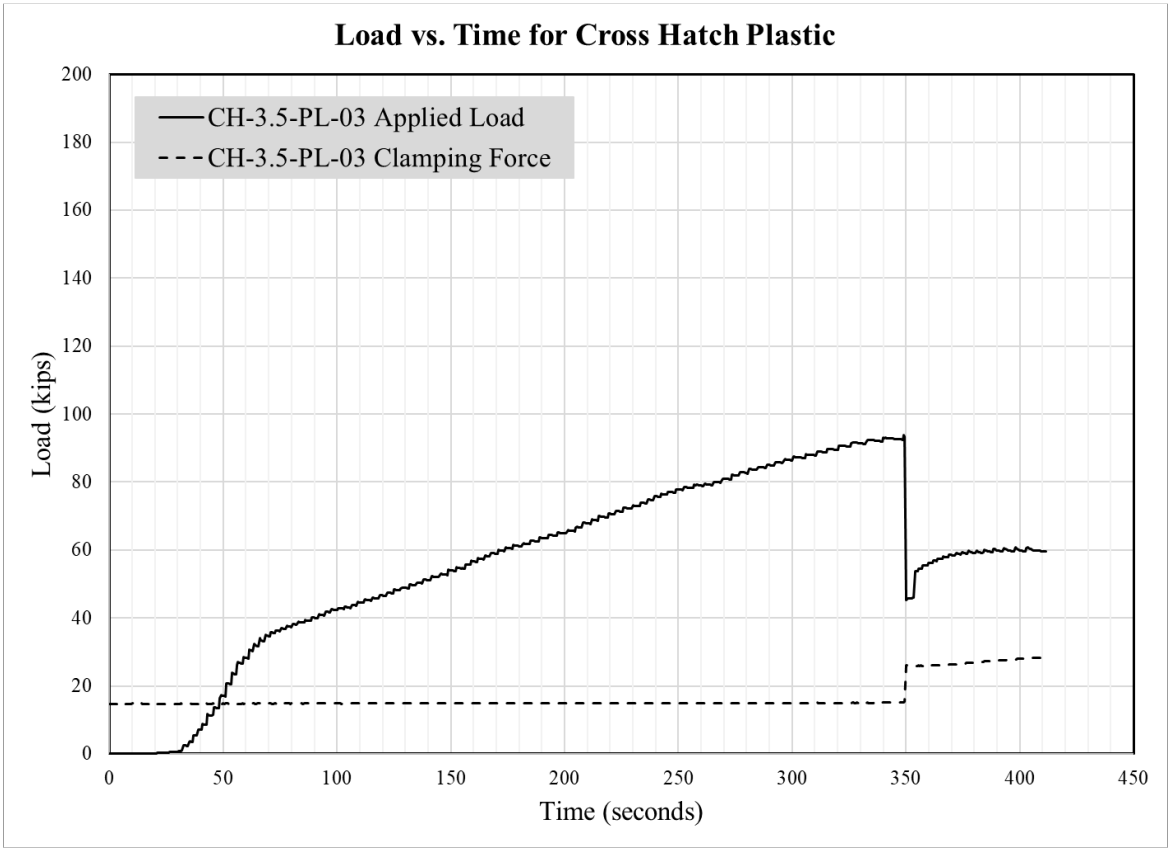
Load vs. Time for Cross Hatch Plastic
CH-3.5-PL-03 Applied Load
CH-3.5-PL-03 Clamping Force
Load (kips)
Time (seconds)
0
20
40
60
80
100
120
140
160
180
200
0
50
100
150
200
250
300
350
400
450

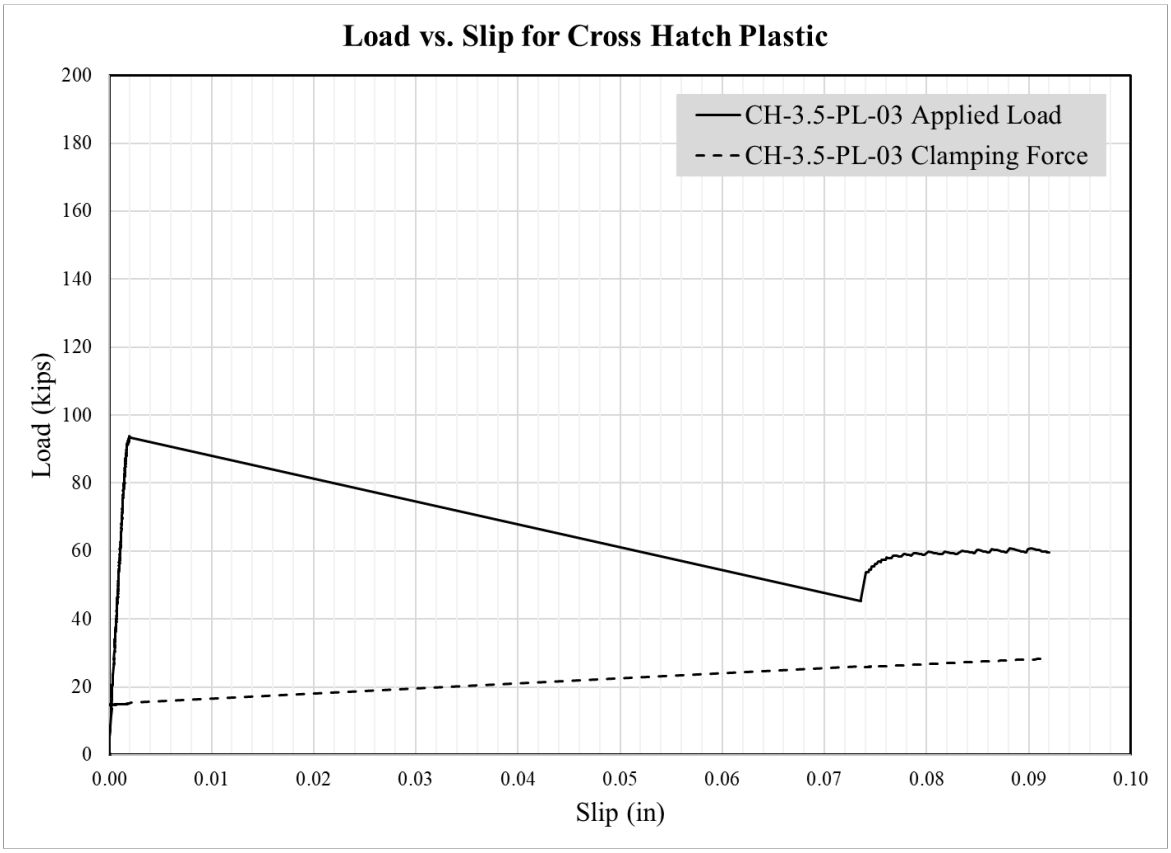
Load vs. Slip for Cross Hatch Plastic
CH-3.5-PL-03 Applied Load
CH-3.5-PL-03 Clamping Force
Load (kips)
Slip (in)
0
20
40
60
80
100
120
140
160
180
200
0.00
0.01
0.02
0.03
0.04
0.05
0.06
0.07
0.08
0.09
0.10

SK-2.5-01

Summary Table

Specimen Name	SK-2.5-01
Texture Type	Square Knobs
Amplitude	0.25 in
Spacing	2.5 in
De-bonding	TuffCoat®
Concrete Compressive Strengths	Bottom: 7799 psi
	Top: 4516 psi
Interface Fracture Stress	347 psi

Theoretical Surface Treatment

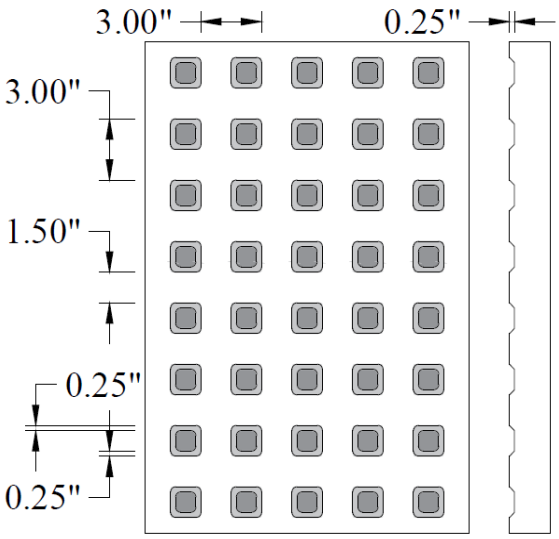

Square Knobs

Actual Surface Treatment

Bottom Section After Test

Top Section After Test

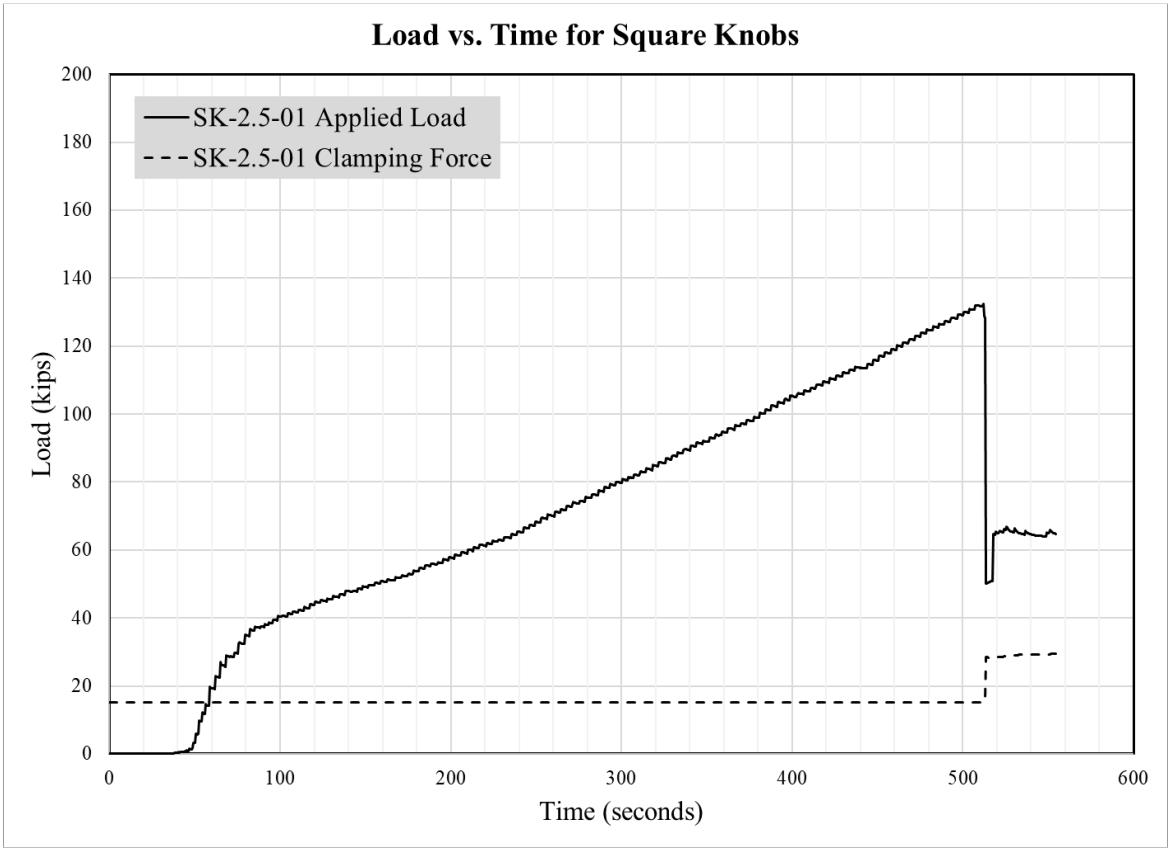
Load vs. Time for Square Knobs
SK-2.5-01 Applied Load
SK-2.5-01 Clamping Force
Load (kips)
Time (seconds)
0
20
40
60
80
100
120
140
160
180
200
0
100
200
300
400
500
600

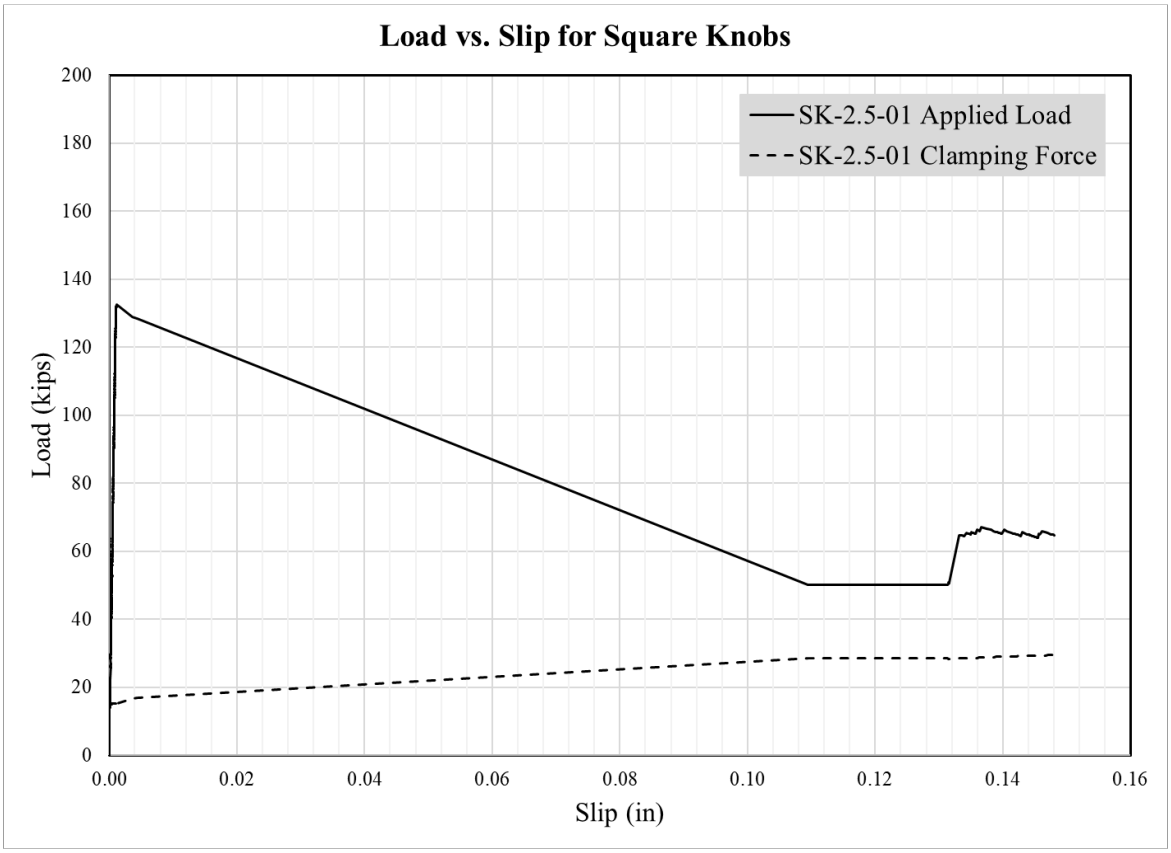
Load vs. Slip for Square Knobs
SK-2.5-01 Applied Load
SK-2.5-01 Clamping Force
Load (kips)
Slip (in)
0
20
40
60
80
100
120
140
160
180
200
0.00
0.02
0.04
0.06
0.08
0.10
0.12
0.14
0.16

SK-2.5-02

Summary Table

Specimen Name	SK-2.5-02
Texture Type	Square Knobs
Amplitude	0.25 in
Spacing	2.5 in
De-bonding	TuffCoat®
Concrete Compressive Strengths	Bottom: 7799 psi
	Top: 4516 psi
Interface Fracture Stress	276 psi

Theoretical Surface Treatment

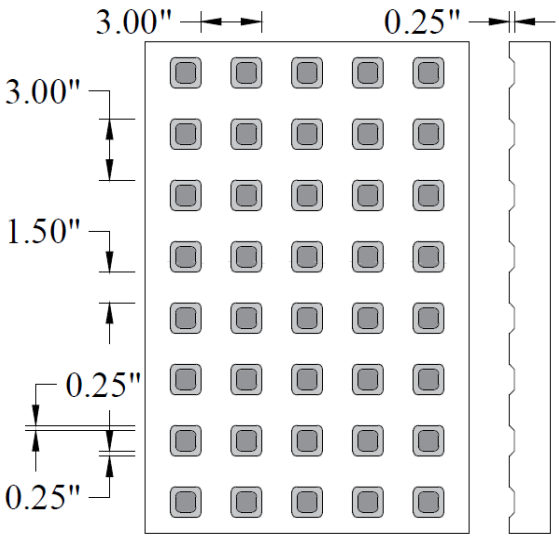

Square Knobs

Actual Surface Treatment

Bottom Section After Test

Top Section After Test

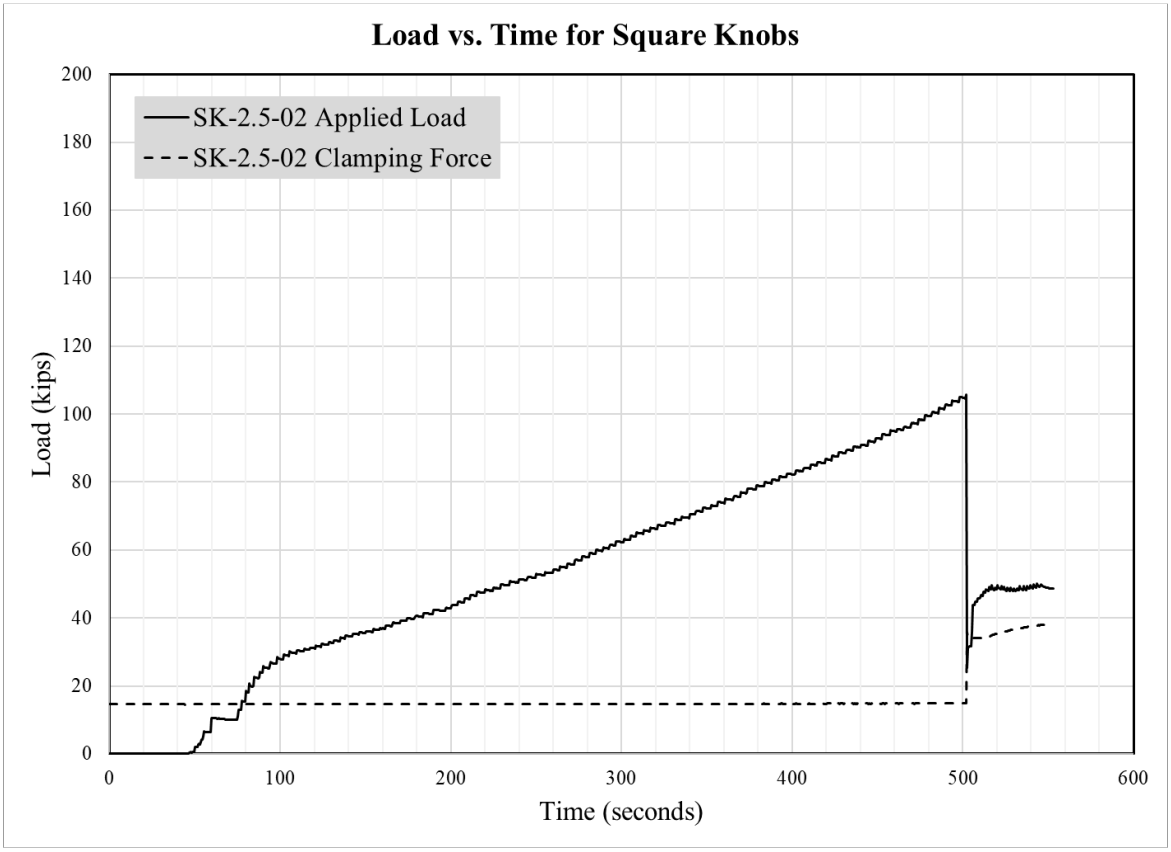
Load vs. Time for Square Knobs
SK-2.5-02 Applied Load
SK-2.5-02 Clamping Force
Load (kips)
Time (seconds)
0
20
40
60
80
100
120
140
160
180
200
0
100
200
300
400
500
600

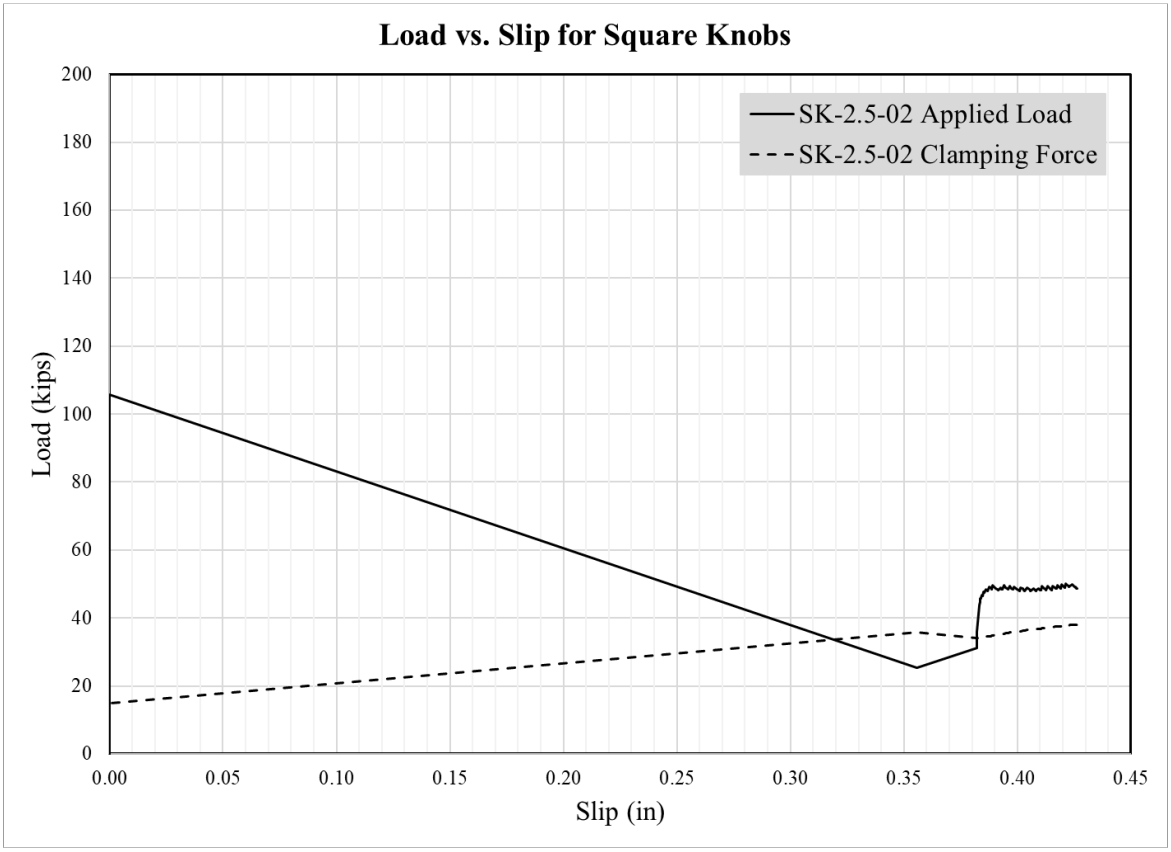
Load vs. Slip for Square Knobs
SK-2.5-02 Applied Load
SK-2.5-02 Clamping Force
Load (kips)
Slip (in)
0
20
40
60
80
100
120
140
160
180
200
0.00
0.05
0.10
0.15
0.20
0.25
0.30
0.35
0.40
0.45

SK-2.5-03

Summary Table

Specimen Name	SK-2.5-03
Texture Type	Square Knobs
Amplitude	0.25 in
Spacing	2.5 in
De-bonding	TuffCoat®
Concrete Compressive Strengths	Bottom: 7799 psi
	Top: 4516 psi
Interface Fracture Stress	339 psi

Theoretical Surface Treatment

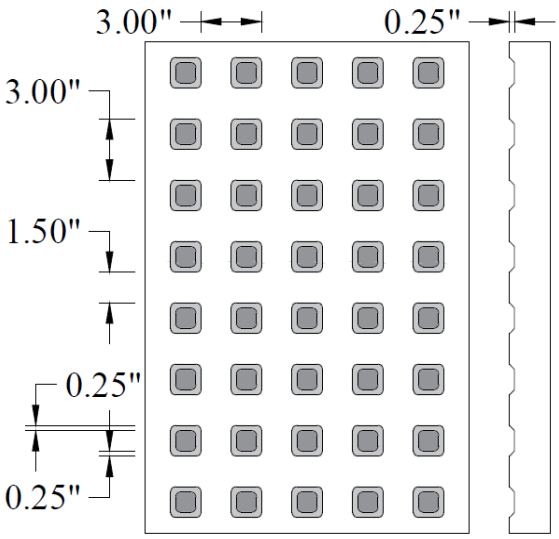

Square Knobs

Actual Surface Treatment

Bottom Section After Test

Top Section After Test

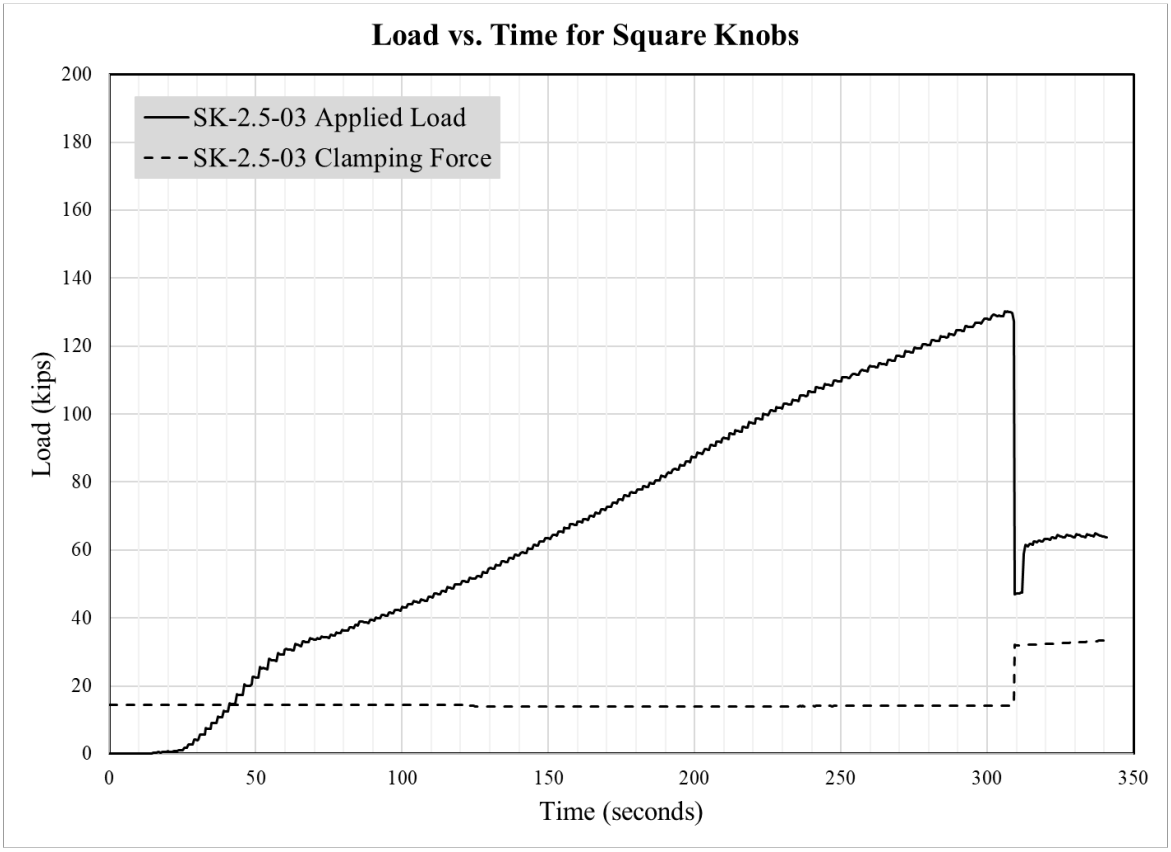
Load vs. Time for Square Knobs
SK-2.5-03 Applied Load
SK-2.5-03 Clamping Force
Load (kips)
Time (seconds)
0
20
40
60
80
100
120
140
160
180
200
0
50
100
150
200
250
300
350

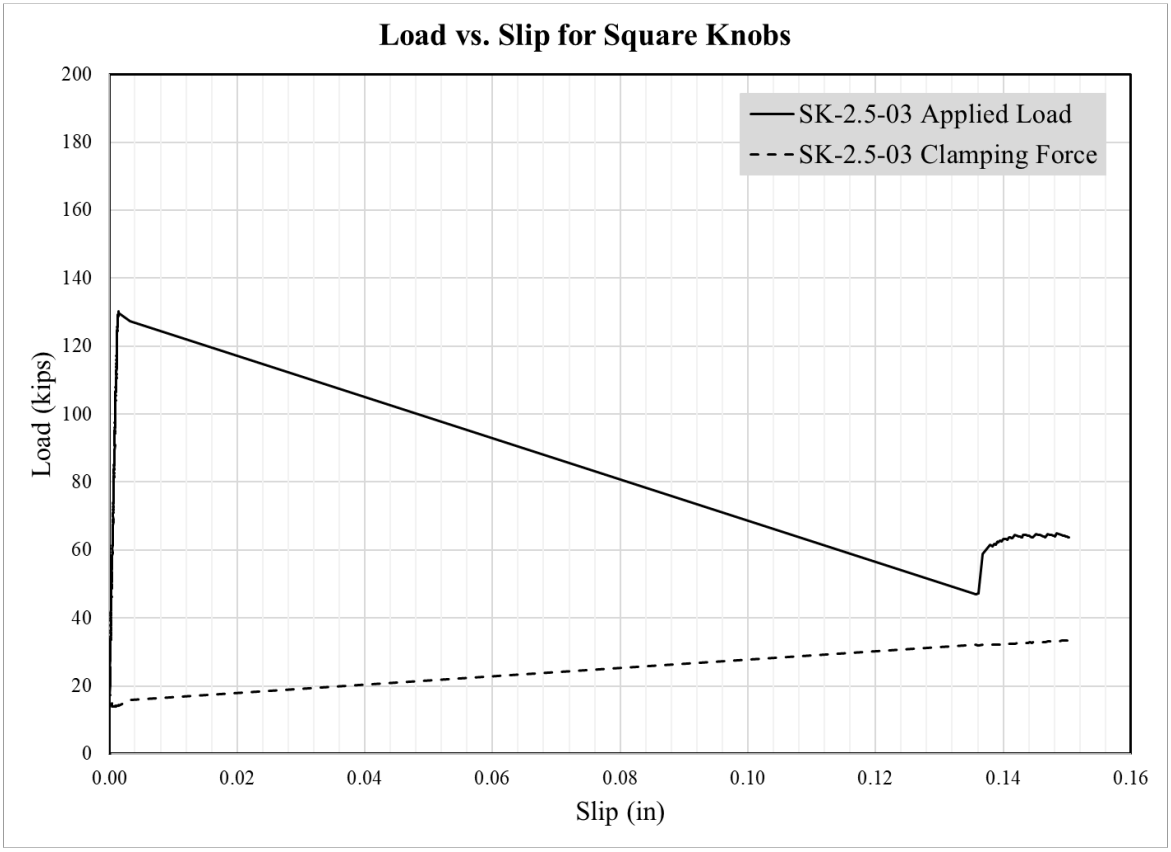
Load vs. Slip for Square Knobs
SK-2.5-03 Applied Load
SK-2.5-03 Clamping Force
Load (kips)
Slip (in)
0
20
40
60
80
100
120
140
160
180
200
0.00
0.02
0.04
0.06
0.08
0.10
0.12
0.14
0.16

EA-01

Summary Table

Specimen Name	EA-01
Texture Type	Exposed Aggregate
Amplitude	0.1875 in
Spacing	---
De-bonding	---
Concrete Compressive Strengths	Bottom: 7799 psi
	Top: 4516 psi
Interface Fracture Stress	272 psi

Theoretical Surface Treatment

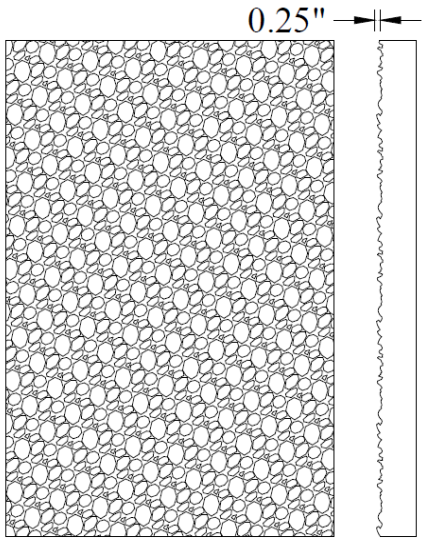

Exposed Aggregate

Actual Surface Treatment

Bottom Section After Test

Top Section After Test

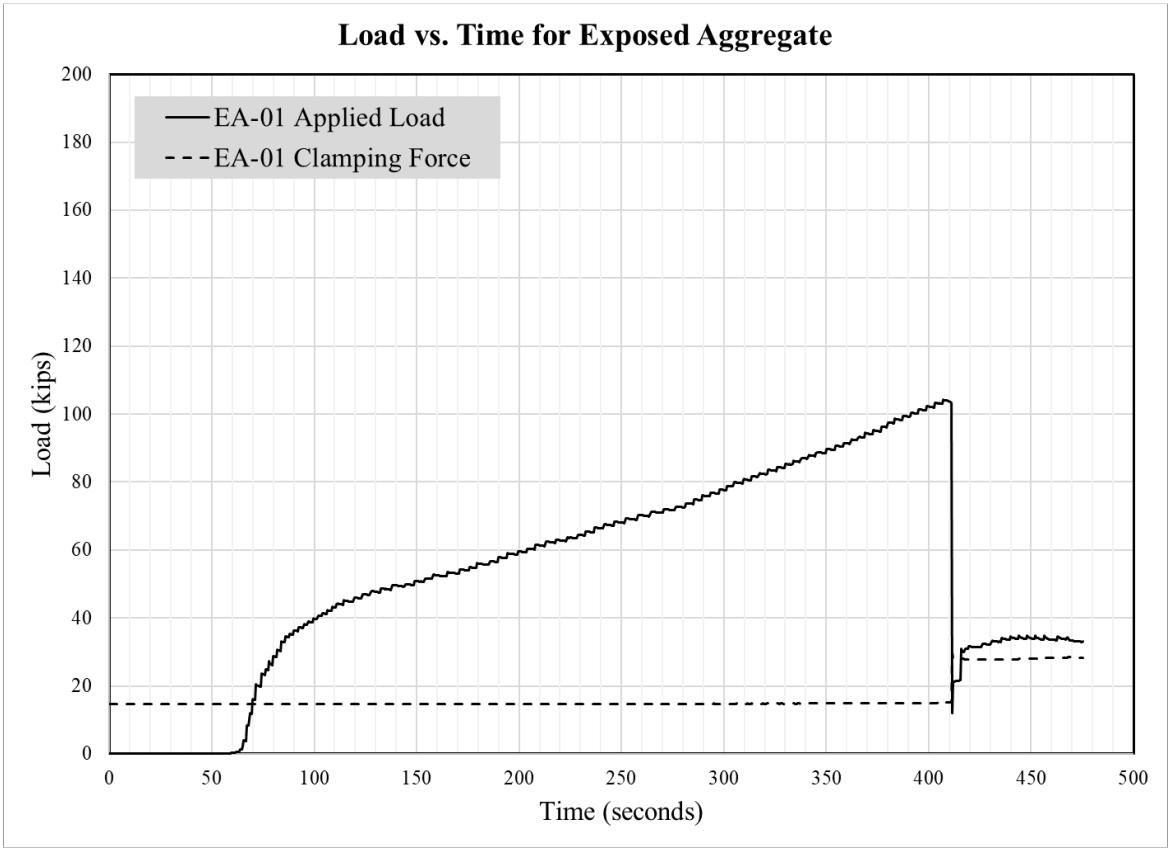
Load vs. Time for Exposed Aggregate
EA-01 Applied Load
EA-01 Clamping Force
Load (kips)
Time (seconds)
0
20
40
60
80
100
120
140
160
180
200
0
50
100
150
200
250
300
350
400
450
500

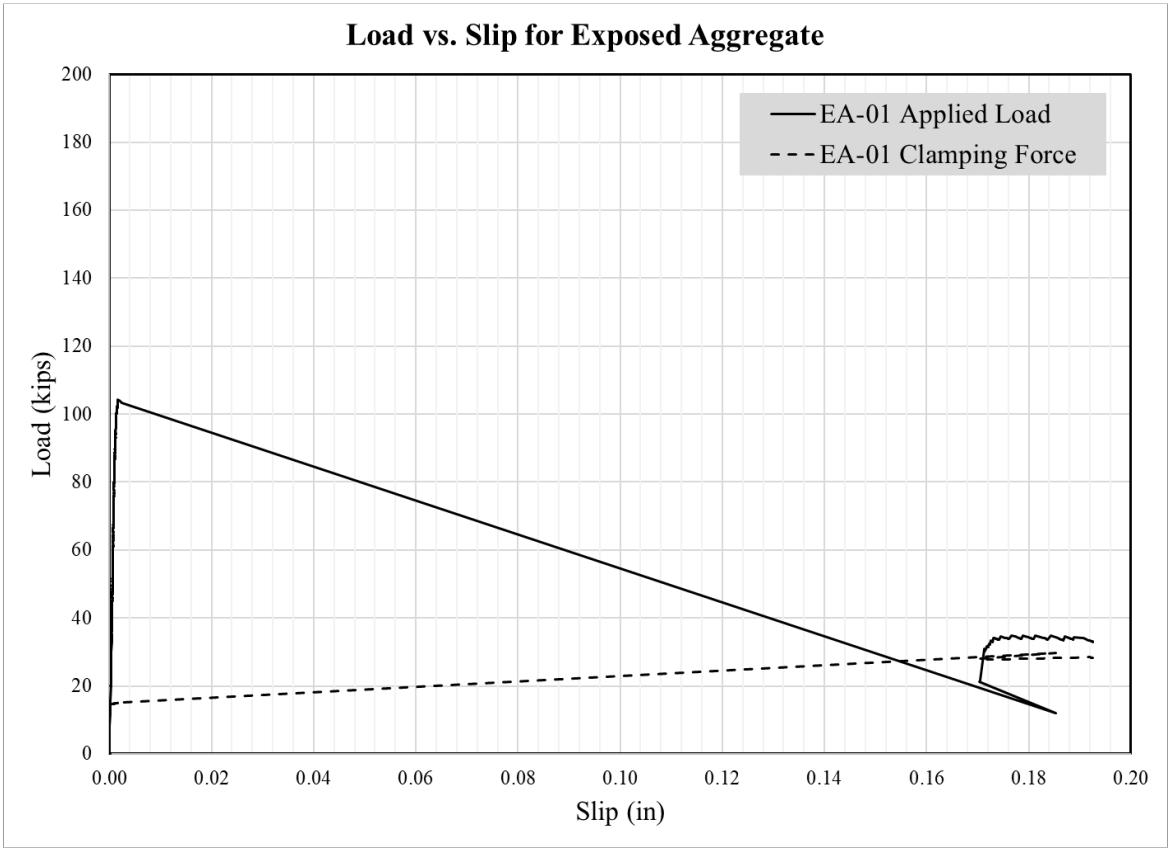
Load vs. Slip for Exposed Aggregate
EA-01 Applied Load
EA-01 Clamping Force
Load (kips)
Slip (in)
0
20
40
60
80
100
120
140
160
180
200
0.00
0.02
0.04
0.06
0.08
0.10
0.12
0.14
0.16
0.18
0.20

EA-02

Summary Table

Specimen Name	EA-02
Texture Type	Exposed Aggregate
Amplitude	0.1875 in
Spacing	---
De-bonding	---
Concrete Compressive Strengths	Bottom: 7799 psi
	Top: 4516 psi
Interface Fracture Stress	282 psi

Theoretical Surface Treatment

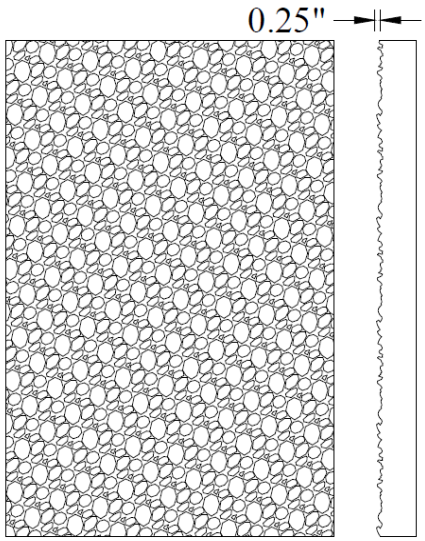

Exposed Aggregate

Actual Surface Treatment

Bottom Section After Test

Top Section After Test

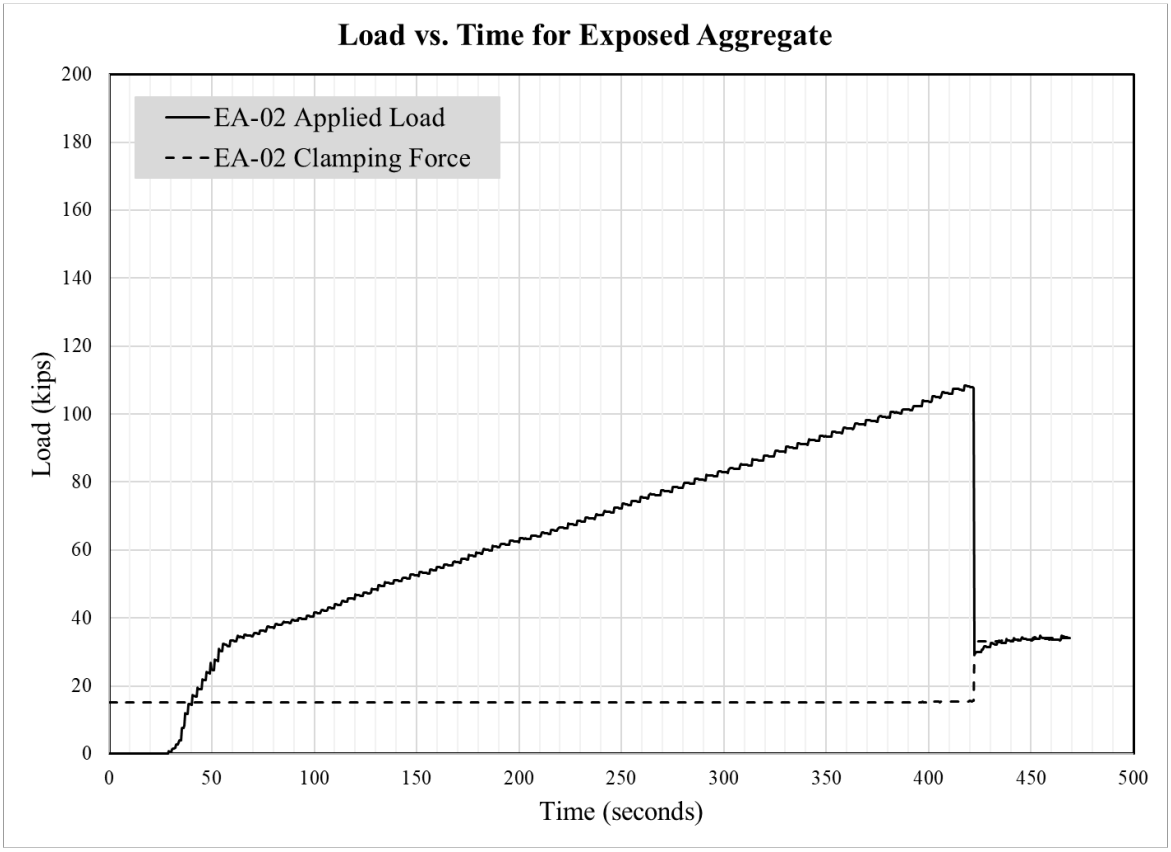
Load vs. Time for Exposed Aggregate
EA-02 Applied Load
EA-02 Clamping Force
Load (kips)
Time (seconds)
0
20
40
60
80
100
120
140
160
180
200
0
50
100
150
200
250
300
350
400
450
500

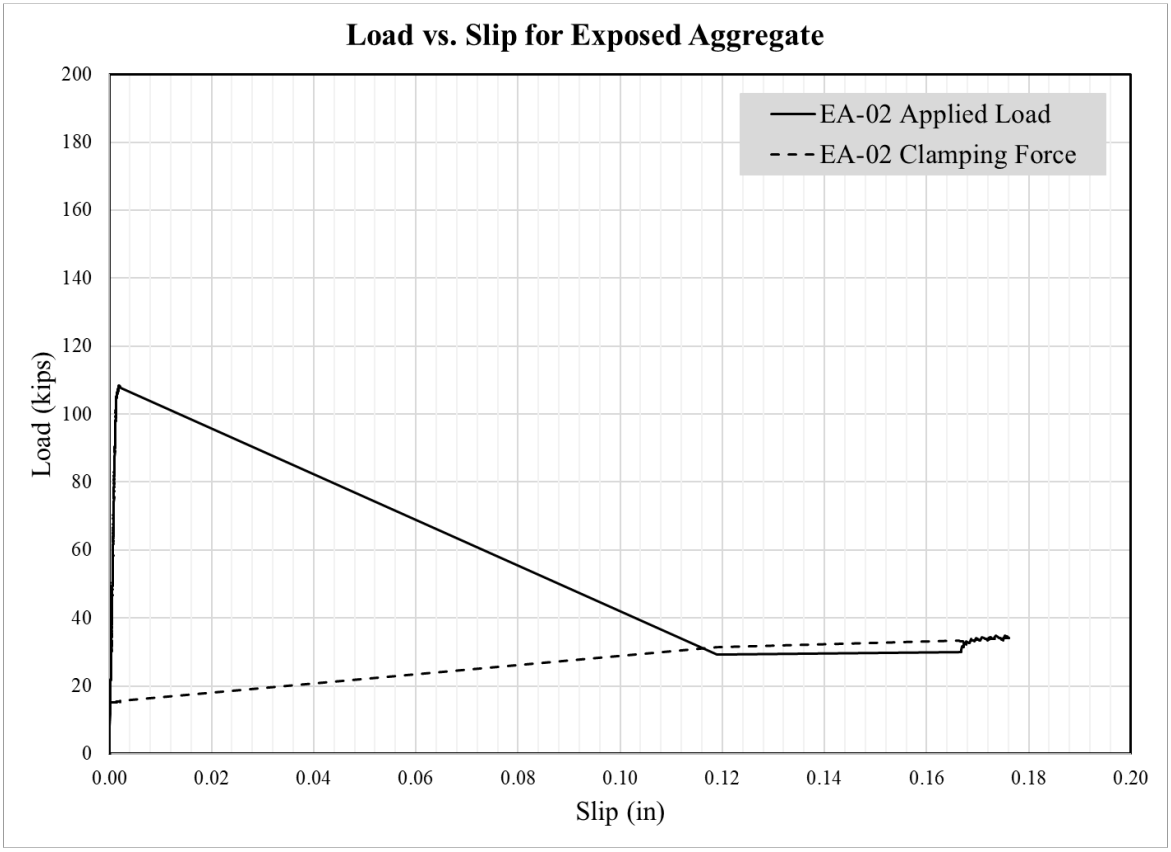
Load vs. Slip for Exposed Aggregate
EA-02 Applied Load
EA-02 Clamping Force
Load (kips)
Slip (in)
0
20
40
60
80
100
120
140
160
180
200
0.00
0.02
0.04
0.06
0.08
0.10
0.12
0.14
0.16
0.18
0.20

EA-03

Summary Table

Specimen Name	EA-03
Texture Type	Exposed Aggregate
Amplitude	0.1875 in
Spacing	---
De-bonding	---
Concrete Compressive Strengths	Bottom: 7799 psi
	Top: 4516 psi
Interface Fracture Stress	353 psi

Theoretical Surface Treatment

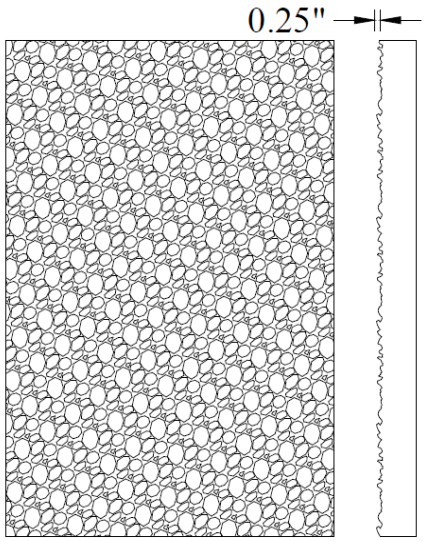

Exposed Aggregate

Actual Surface Treatment

Bottom Section After Test

Top Section After Test

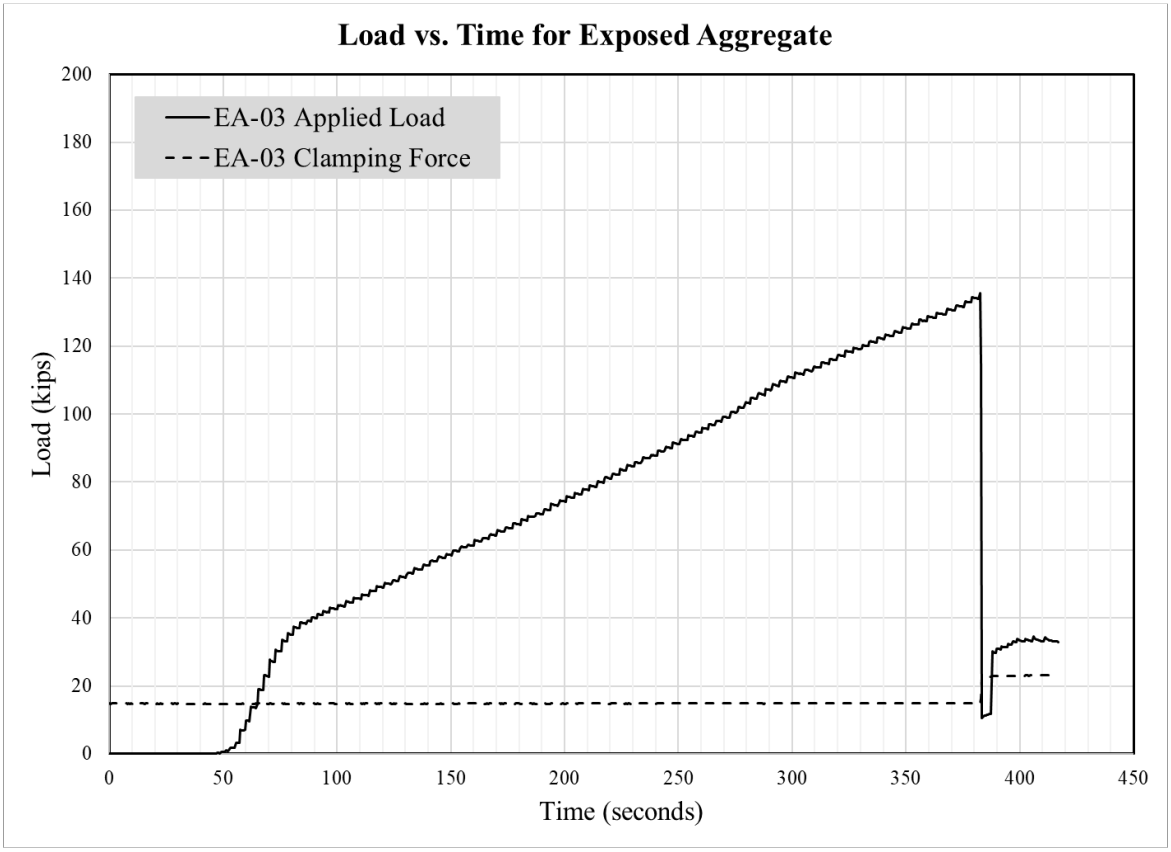
Load vs. Time for Exposed Aggregate
EA-03 Applied Load
EA-03 Clamping Force
Load (kips)
Time (seconds)
0
20
40
60
80
100
120
140
160
180
200
0
50
100
150
200
250
300
350
400
450

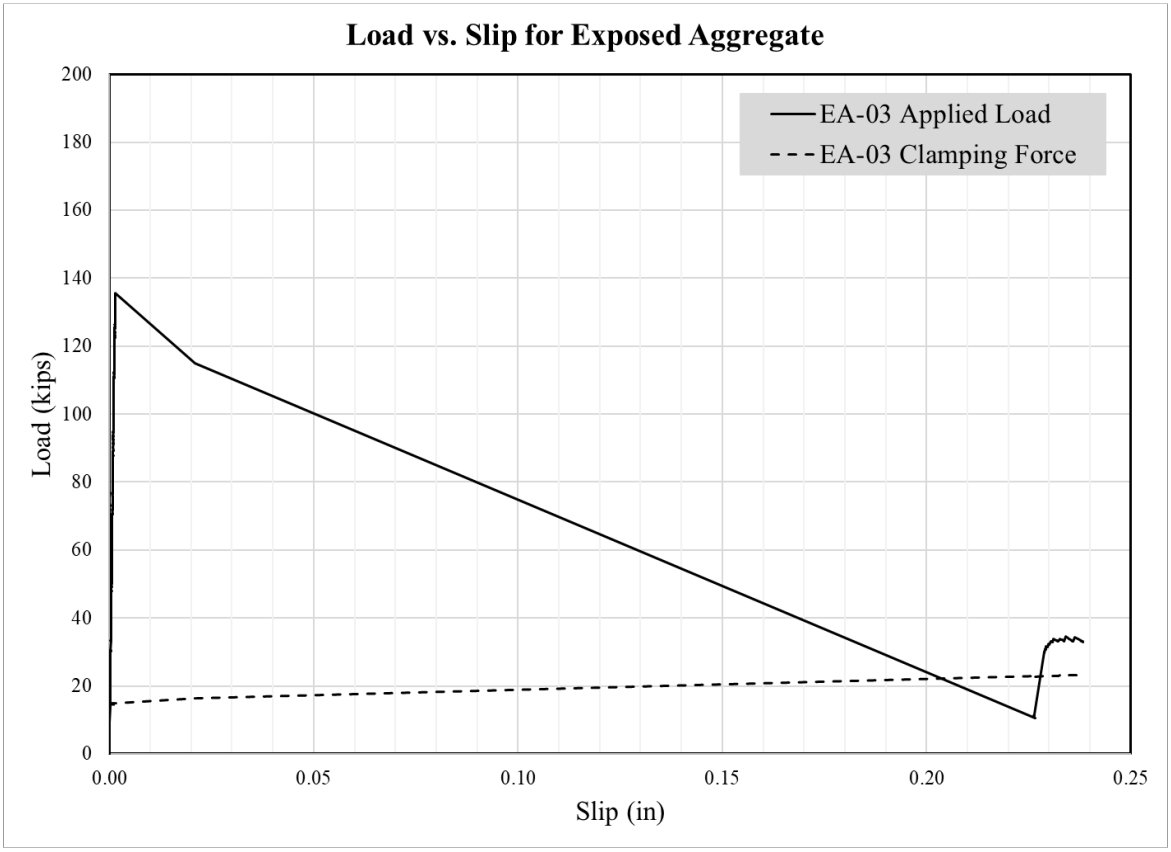
Load vs. Slip for Exposed Aggregate
EA-03 Applied Load
EA-03 Clamping Force
Load (kips)
Slip (in)
0
20
40
60
80
100
120
140
160
180
200
0.00
0.05
0.10
0.15
0.20
0.25

APPENDIX E: INVERTED T-BEAM CYCLIC TEST RESULTS

Monotonic Test at 0 Cycles

Summary	
Number of Cycles Performed Before Test	0 cycles
Central Deflection of Specimen at 30-kips	0.025 in
Maximum Opening of Joint Between Beams	0.001 in
Maximum Reinforcement Strain in Precast	18 με
Maximum Reinforcement Strain in Cast-in-Place	68 με

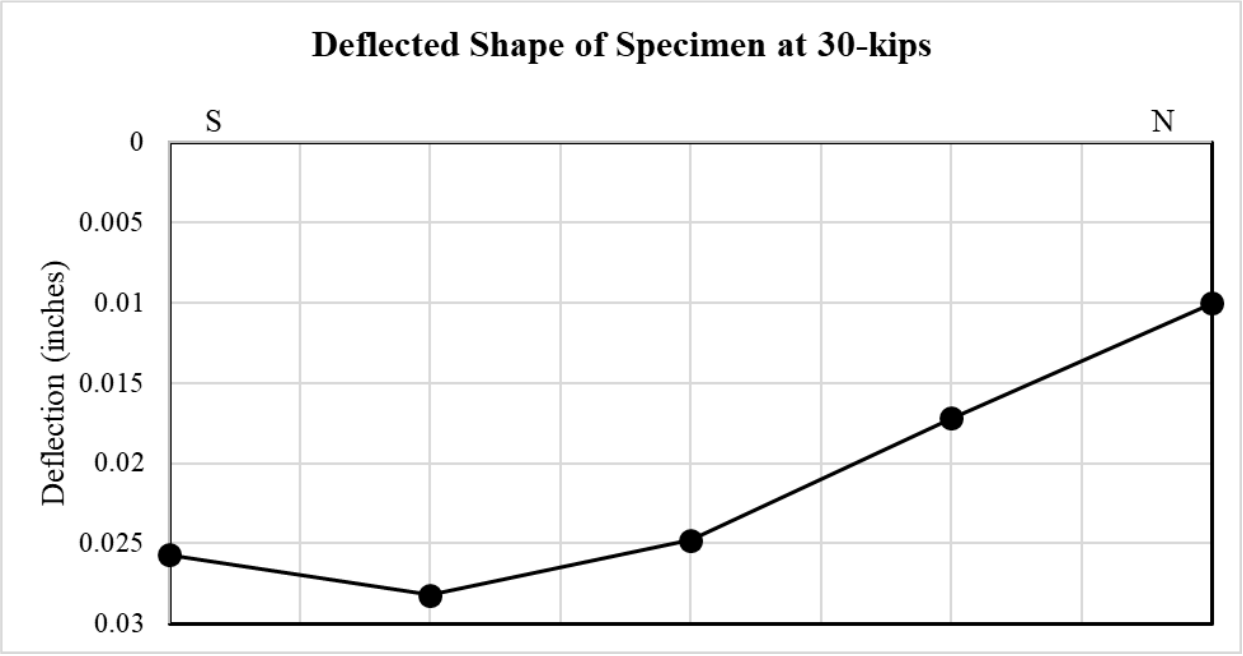

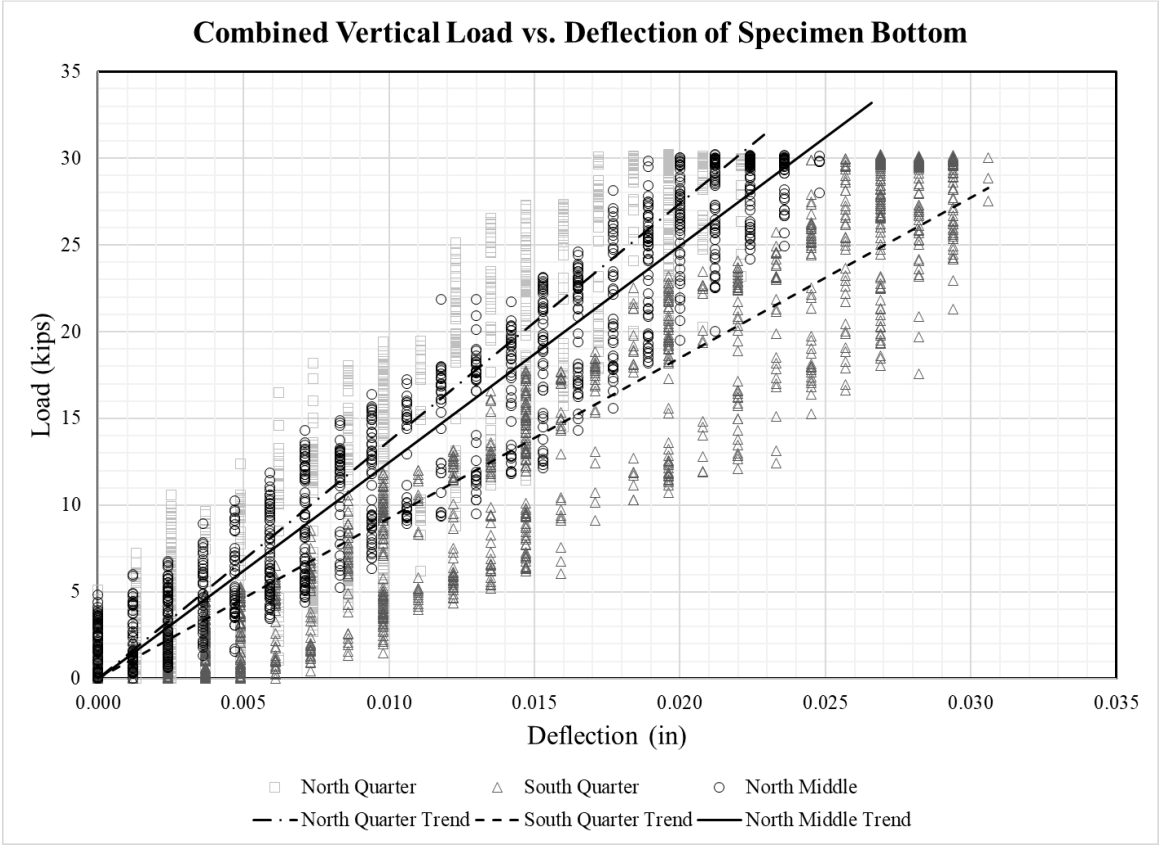
Combined Vertical Load vs. Deflection of Specimen Bottom
Load (kips)
Deflection (in)
0
5
10
15
20
25
30
35
0.000
0.005
0.010
0.015
0.020
0.025
0.030
0.035
North Quarter
South Quarter
North Middle
North Quarter Trend
South Quarter Trend
North Middle Trend


Combined Vertical Load vs. Strain in Reinforcement
Load (kips)
Strain (με)
0
5
10
15
20
25
30
35
0
10
20
30
40
50
60
70
80
Precast South-West
Precast North-West
Cast-in-Place West
Precast South-East
Precast North-East
Cast-in-Place East

Monotonic Test at 10 Cycles

Summary	
Number of Cycles Performed Before Test	10 cycles
Central Deflection of Specimen at 30-kips	0.026 in
Maximum Opening of Joint Between Beams	0.001 in
Maximum Reinforcement Strain in Precast	19 με
Maximum Reinforcement Strain in Cast-in-Place	40 με

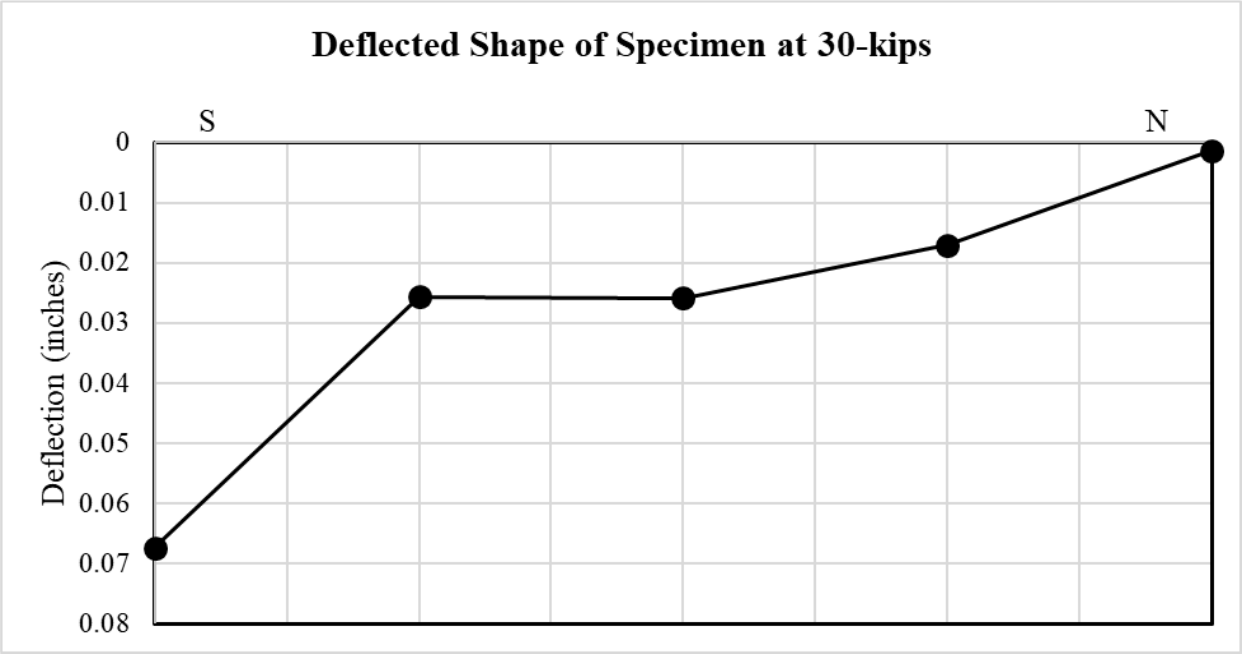

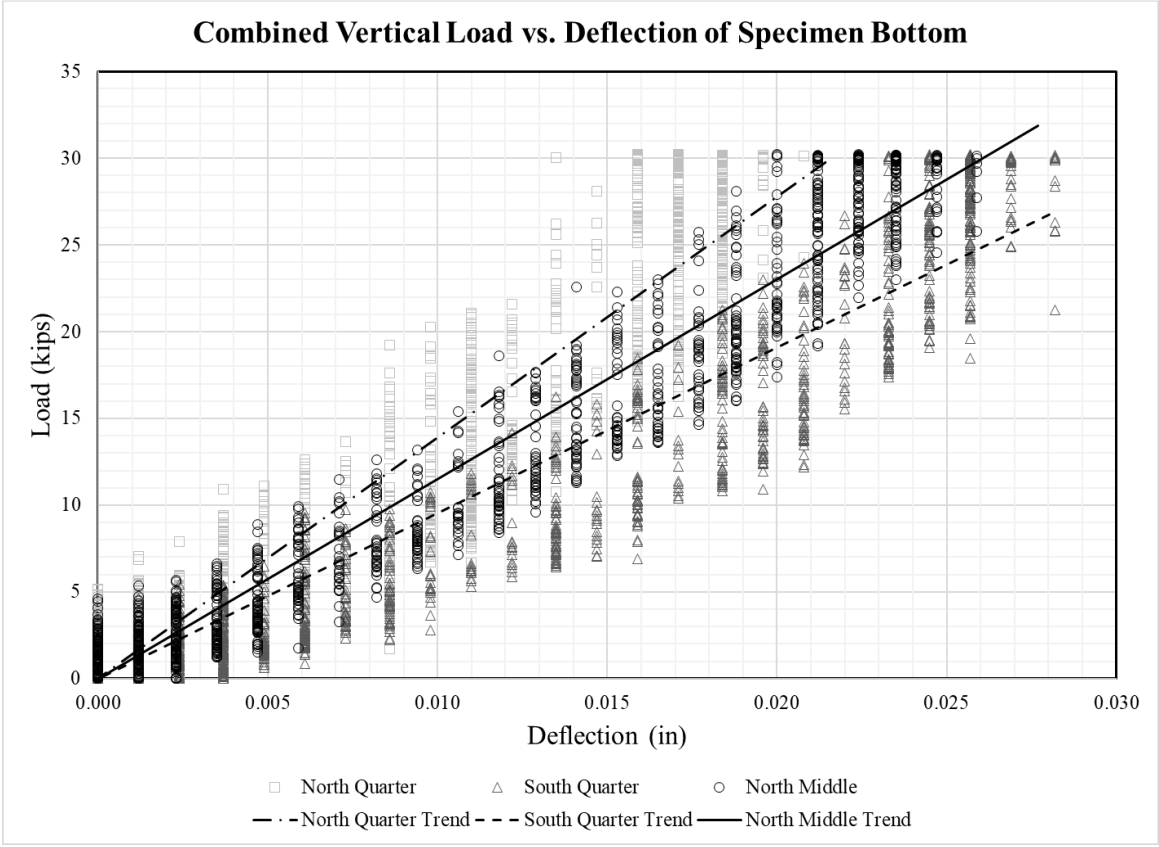
Combined Vertical Load vs. Deflection of Specimen Bottom
Load (kips)
Deflection (in)
0
5
10
15
20
25
30
35
0.000
0.005
0.010
0.015
0.020
0.025
0.030
North Quarter
South Quarter
North Middle
North Quarter Trend
South Quarter Trend
North Middle Trend


Combined Vertical Load vs. Strain in Reinforcement
Load (kips)
Strain (με)
0
5
10
15
20
25
30
35
0
5
10
15
20
25
30
35
40
45
Precast South-West
Precast North-West
Cast-in-Place West
Precast South-East
Precast North-East
Cast-in-Place East

Monotonic Test at 100 Cycles

Summary	
Number of Cycles Performed Before Test	100 cycles
Central Deflection of Specimen at 30-kips	0.027 in
Maximum Opening of Joint Between Beams	0.001 in
Maximum Reinforcement Strain in Precast	20 με
Maximum Reinforcement Strain in Cast-in-Place	41 με

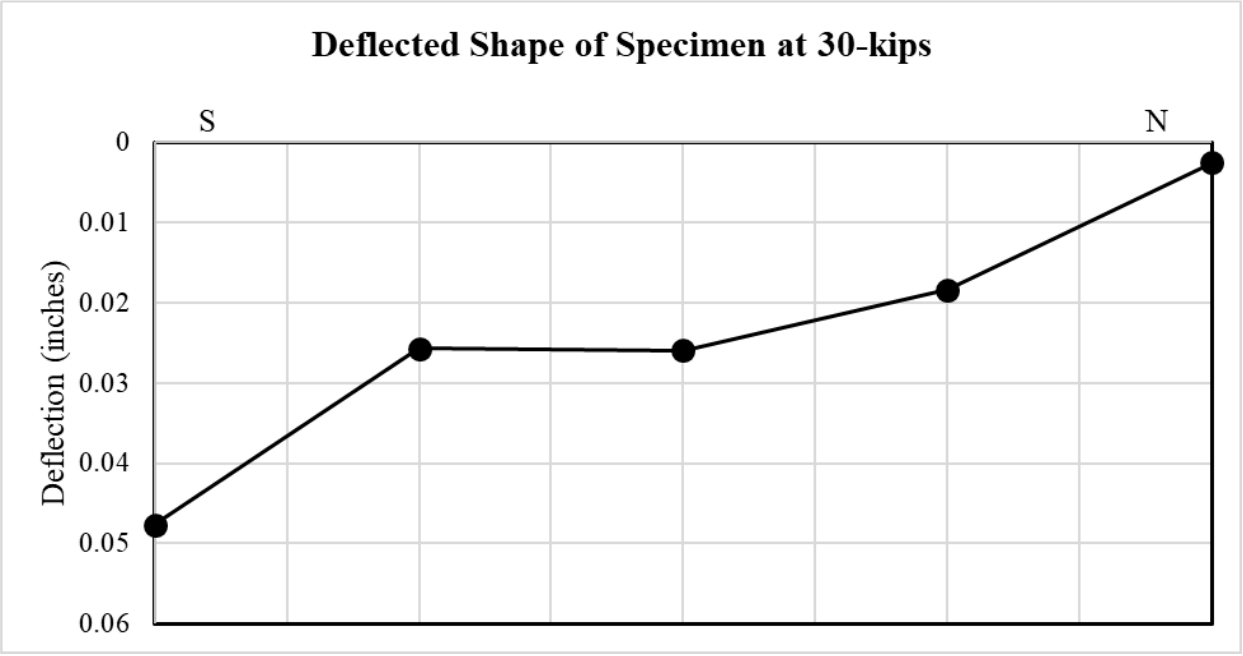

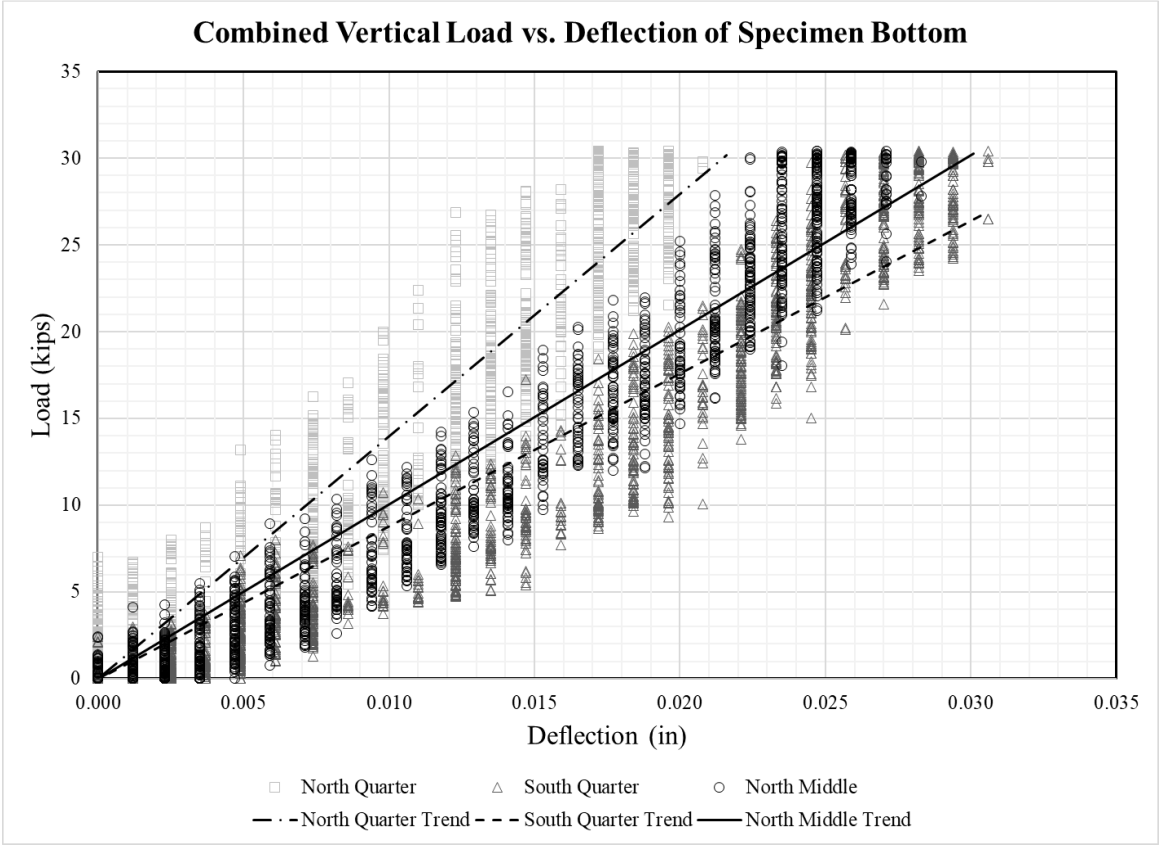
Combined Vertical Load vs. Deflection of Specimen Bottom
Load (kips)
Deflection (in)
0
5
10
15
20
25
30
35
0.000
0.005
0.010
0.015
0.020
0.025
0.030
0.035
North Quarter
South Quarter
North Middle
North Quarter Trend
South Quarter Trend
North Middle Trend

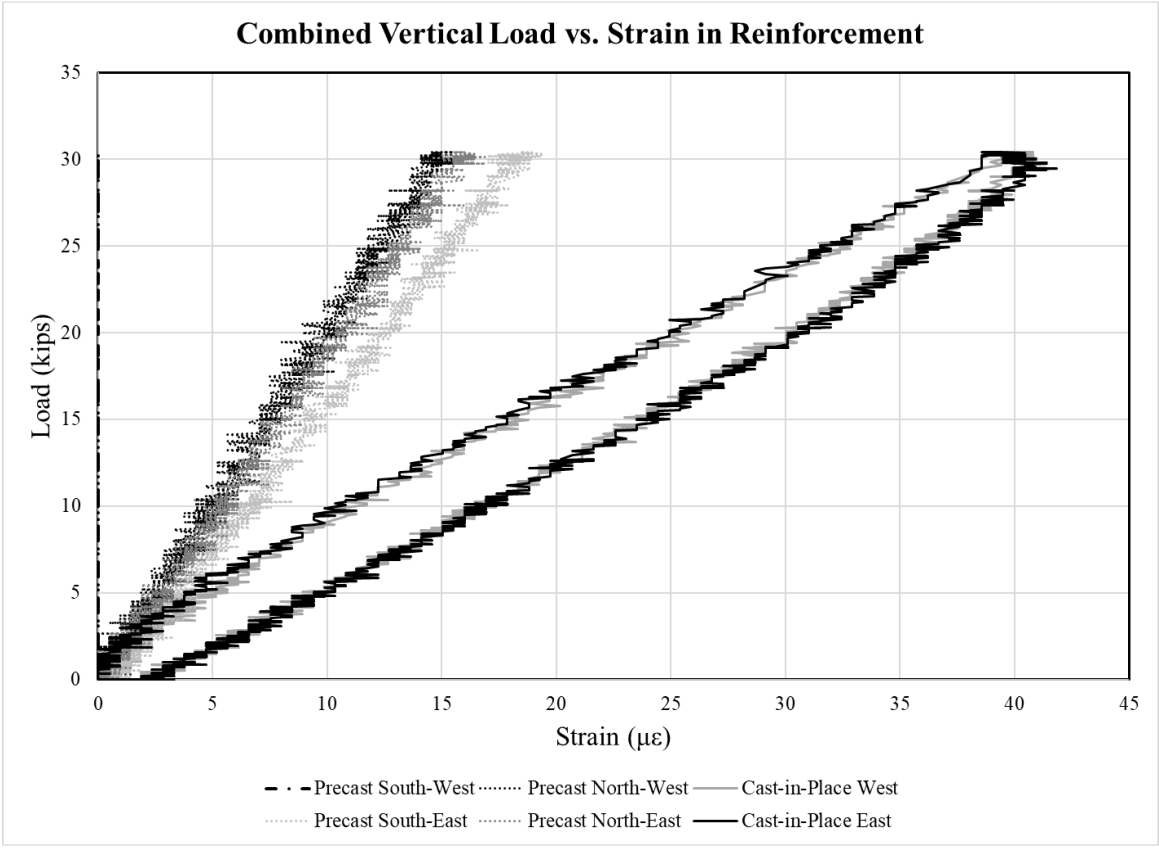
Combined Vertical Load vs. Strain in Reinforcement
Load (kips)
Strain (με)
0
5
10
15
20
25
30
35
40
45
Precast South-West
Precast North-West
Cast-in-Place West
Precast South-East
Precast North-East
Cast-in-Place East

Monotonic Test at 1000 Cycles

Summary	
Number of Cycles Performed Before Test	1000 cycles
Central Deflection of Specimen at 30-kips	0.027 in
Maximum Opening of Joint Between Beams	0.001 in
Maximum Reinforcement Strain in Precast	19 με
Maximum Reinforcement Strain in Cast-in-Place	51 με

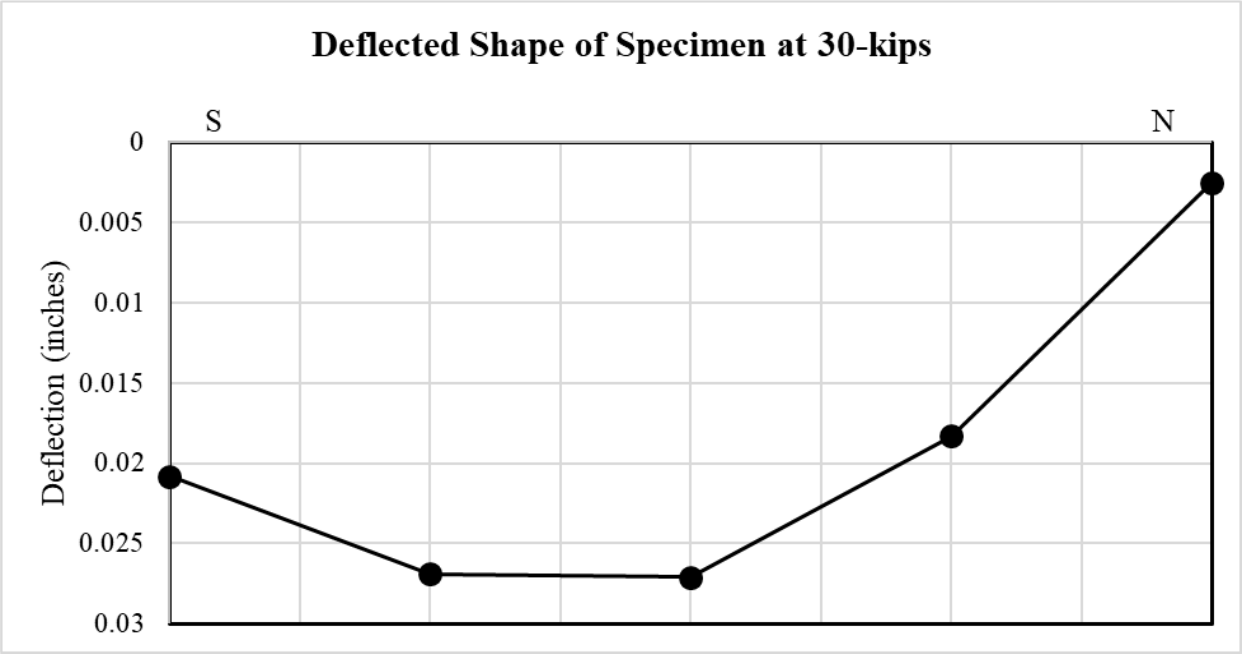

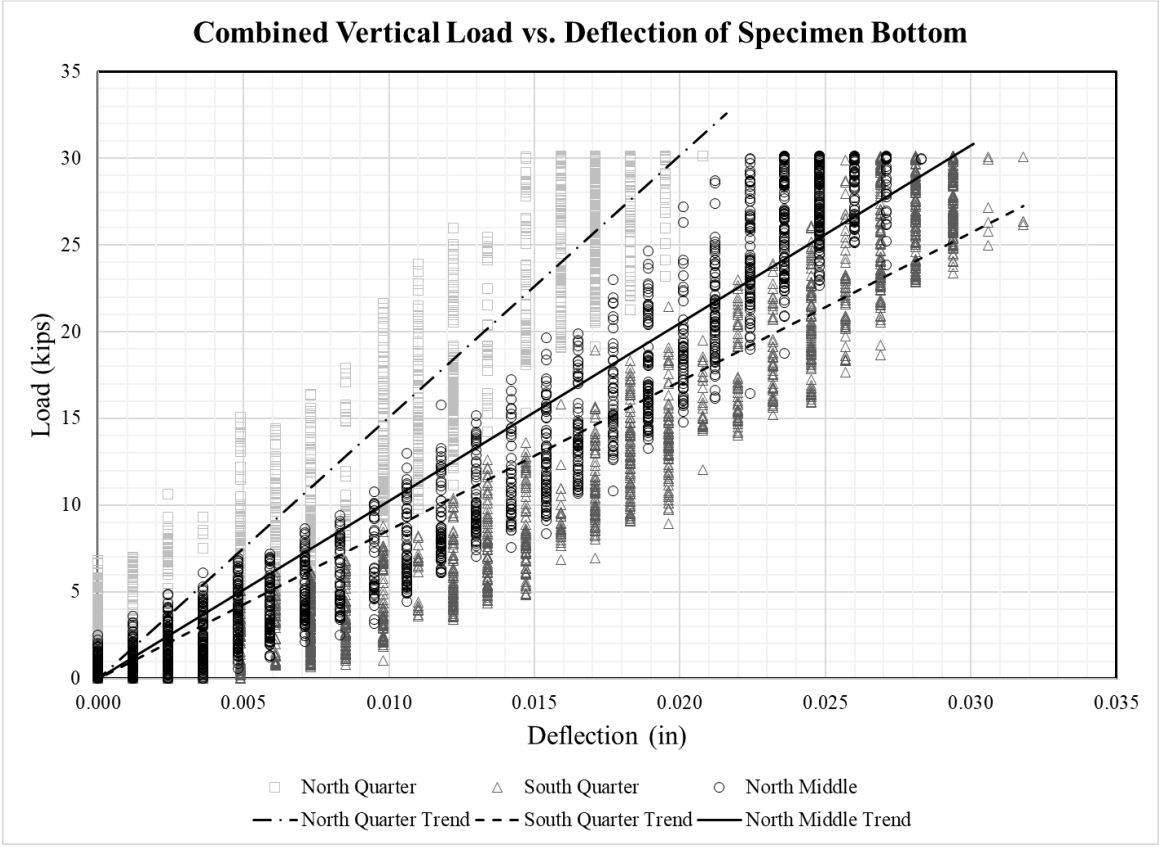
Combined Vertical Load vs. Deflection of Specimen Bottom
Load (kips)
Deflection (in)
0
5
10
15
20
25
30
35
0.000
0.005
0.010
0.015
0.020
0.025
0.030
0.035
North Quarter
South Quarter
North Middle
North Quarter Trend
South Quarter Trend
North Middle Trend

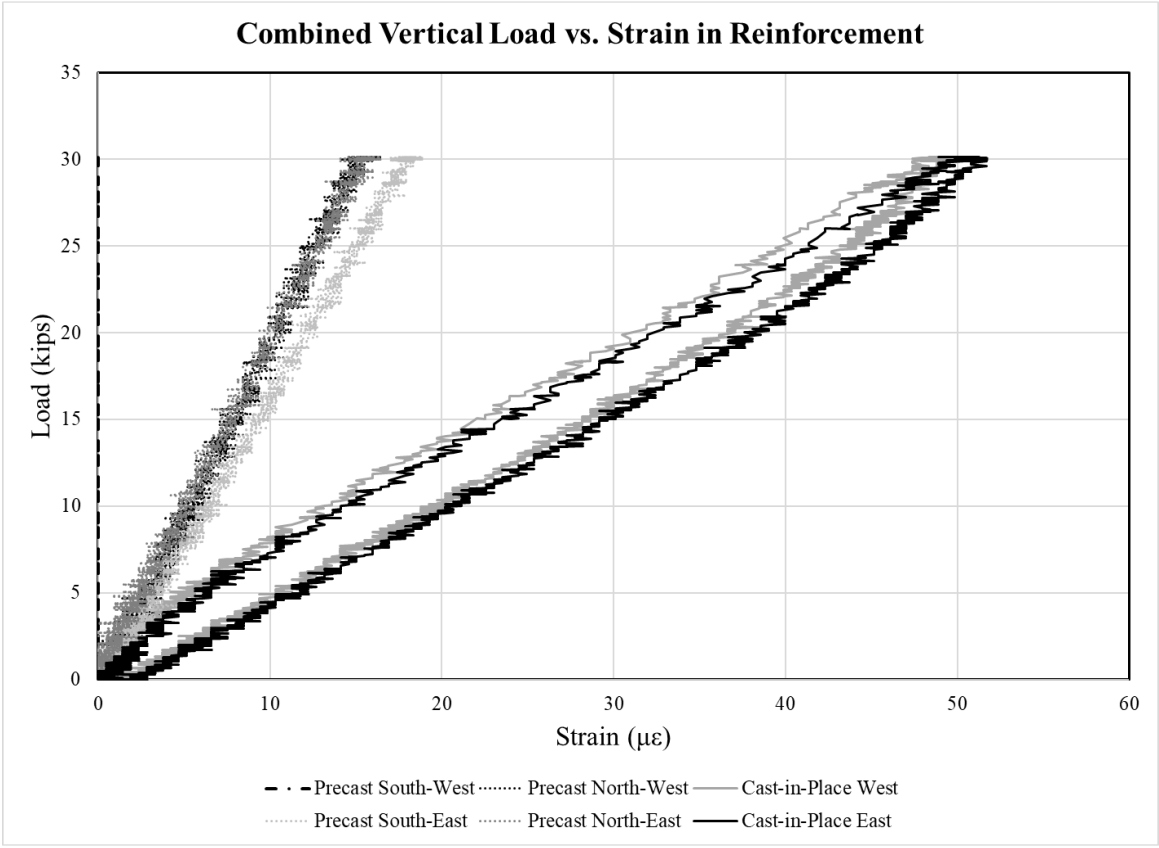
Combined Vertical Load vs. Strain in Reinforcement
Load (kips)
Strain (με)
0
5
10
15
20
25
30
35
0
10
20
30
40
50
60
Precast South-West
Precast North-West
Cast-in-Place West
Precast South-East
Precast North-East
Cast-in-Place East

Monotonic Test at 10,000 Cycles

Summary	
Number of Cycles Performed Before Test	10000 cycles
Central Deflection of Specimen at 30-kips	0.027 in
Maximum Opening of Joint Between Beams	0.001 in
Maximum Reinforcement Strain in Precast	19 με
Maximum Reinforcement Strain in Cast-in-Place	69 με

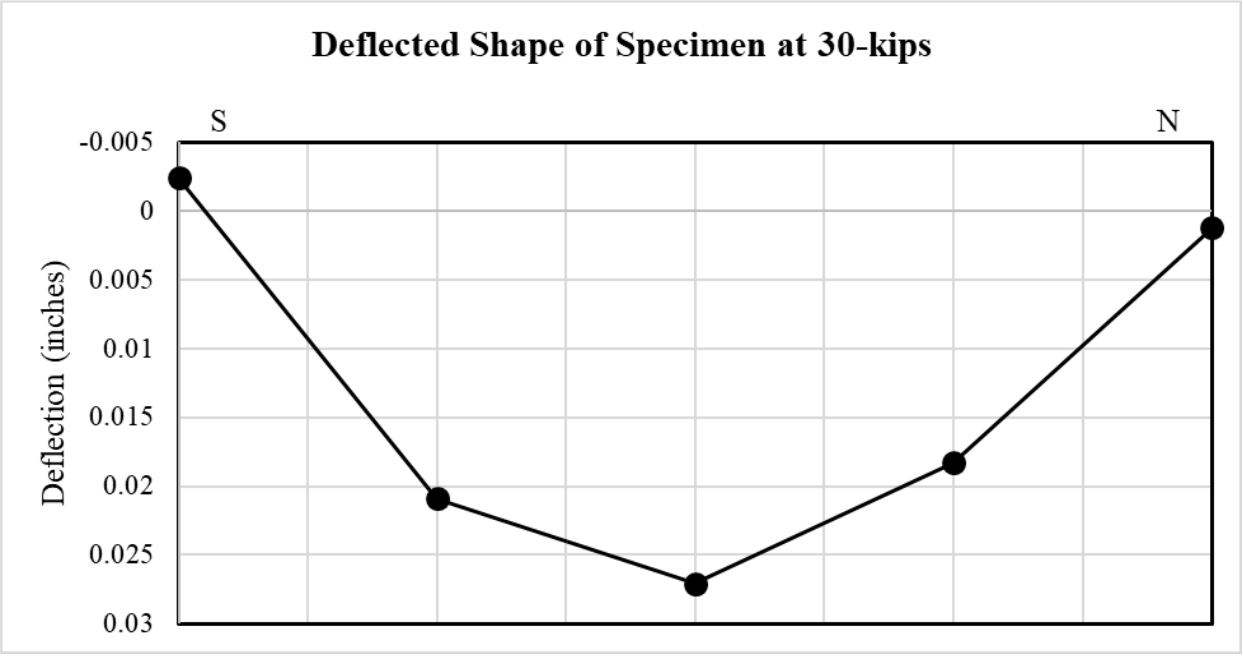

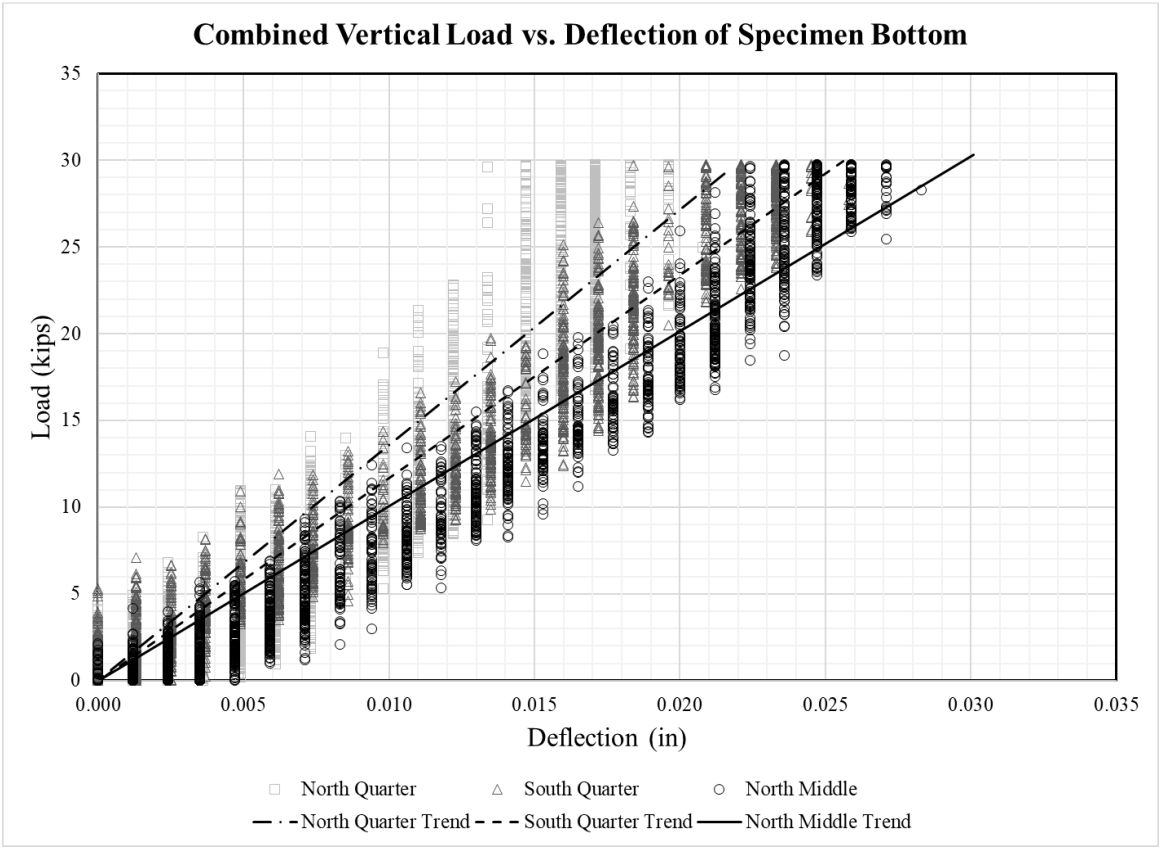
Combined Vertical Load vs. Deflection of Specimen Bottom
Load (kips)
Deflection (in)
0
5
10
15
20
25
30
35
0.000
0.005
0.010
0.015
0.020
0.025
0.030
0.035
North Quarter
South Quarter
North Middle
North Quarter Trend
South Quarter Trend
North Middle Trend

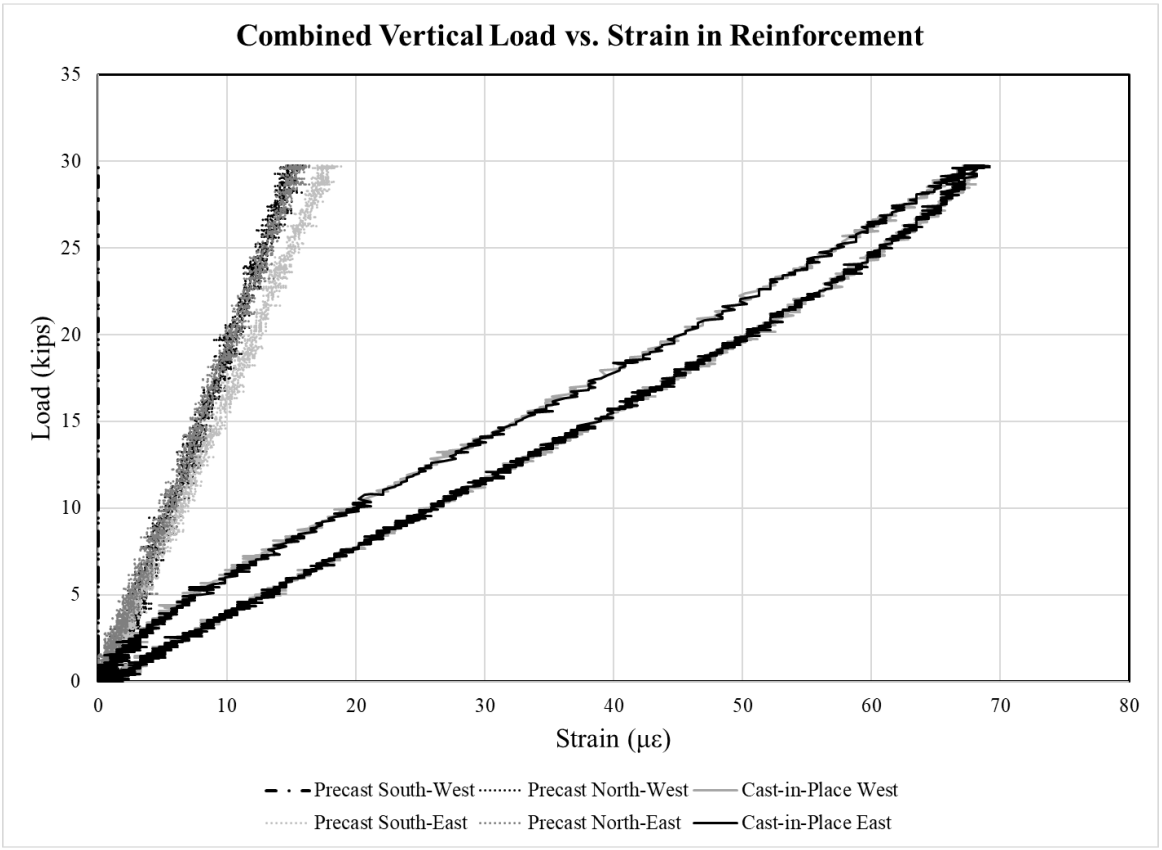
Combined Vertical Load vs. Strain in Reinforcement
Load (kips)
Strain (με)
0
5
10
15
20
25
30
35
0
10
20
30
40
50
60
70
80
Precast South-West
Precast North-West
Cast-in-Place West
Precast South-East
Precast North-East
Cast-in-Place East

Monotonic Test at 100,000 Cycles

Summary	
Number of Cycles Performed Before Test	100620 cycles
Central Deflection of Specimen at 30-kips	0.024 in
Maximum Opening of Joint Between Beams	0.001 in
Maximum Reinforcement Strain in Precast	19 με
Maximum Reinforcement Strain in Cast-in-Place	91 με

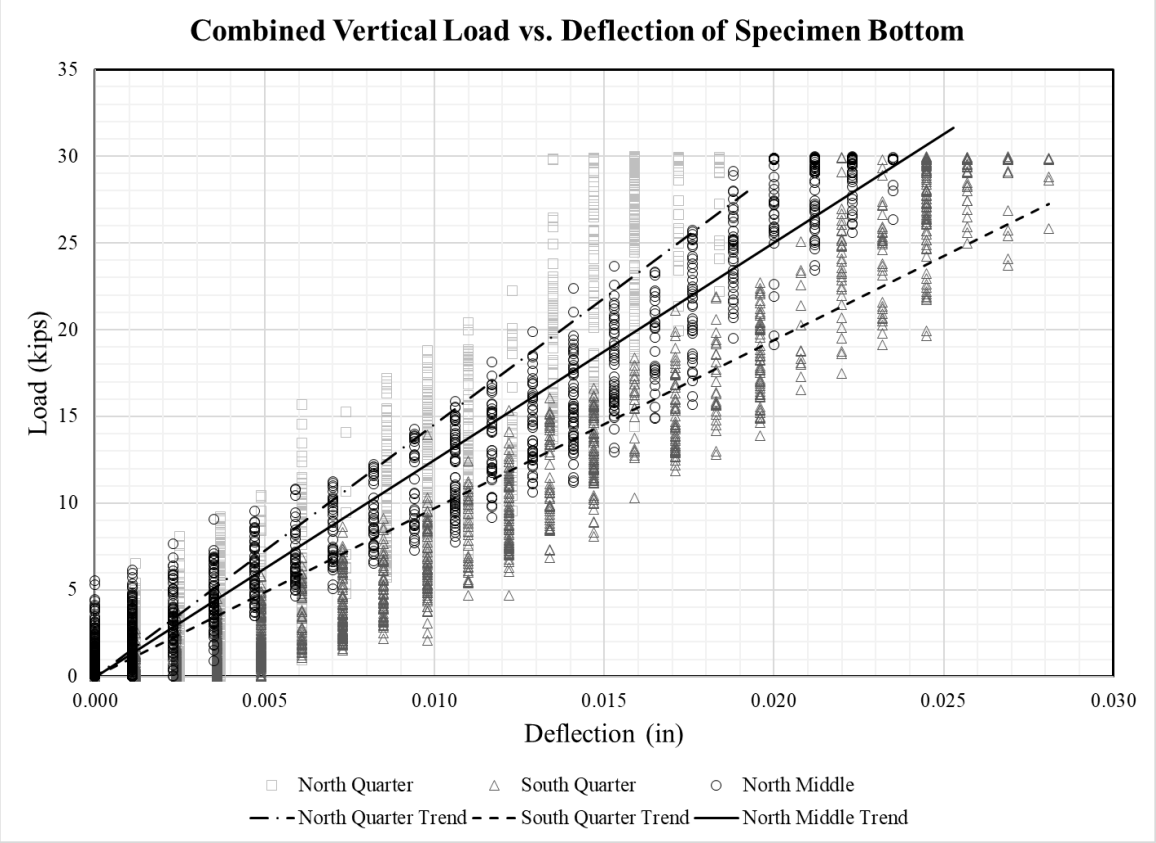
Combined Vertical Load vs. Deflection of Specimen Bottom
Load (kips)
Deflection (in)
0
5
10
15
20
25
30
35
0.000
0.005
0.010
0.015
0.020
0.025
0.030
North Quarter
South Quarter
North Middle
North Quarter Trend
South Quarter Trend
North Middle Trend


Combined Vertical Load vs. Strain in Reinforcement
Load (kips)
Strain (με)
0
5
10
15
20
25
30
35
0
10
20
30
40
50
60
70
80
90
100
Precast South-West
Precast North-West
Cast-in-Place West
Precast South-East
Precast North-East
Cast-in-Place East

Monotonic Test at 300,000 Cycles

Summary	
Number of Cycles Performed Before Test	299999 cycles
Central Deflection of Specimen at 30-kips	0.019 in
Maximum Opening of Joint Between Beams	0.001 in
Maximum Reinforcement Strain in Precast	18 με
Maximum Reinforcement Strain in Cast-in-Place	99 με

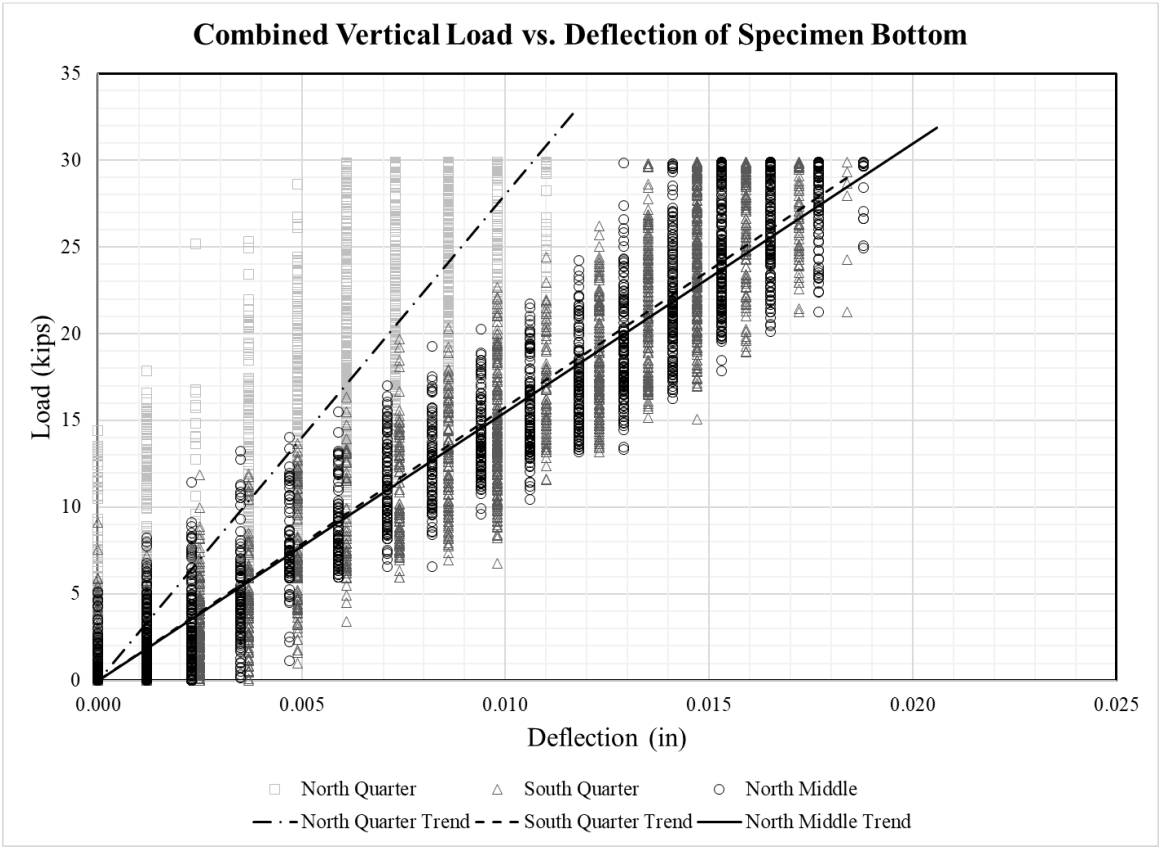
Combined Vertical Load vs. Deflection of Specimen Bottom
Load (kips)
Deflection (in)
0
5
10
15
20
25
30
35
0.000
0.005
0.010
0.015
0.020
0.025
North Quarter
South Quarter
North Middle
North Quarter Trend
South Quarter Trend
North Middle Trend

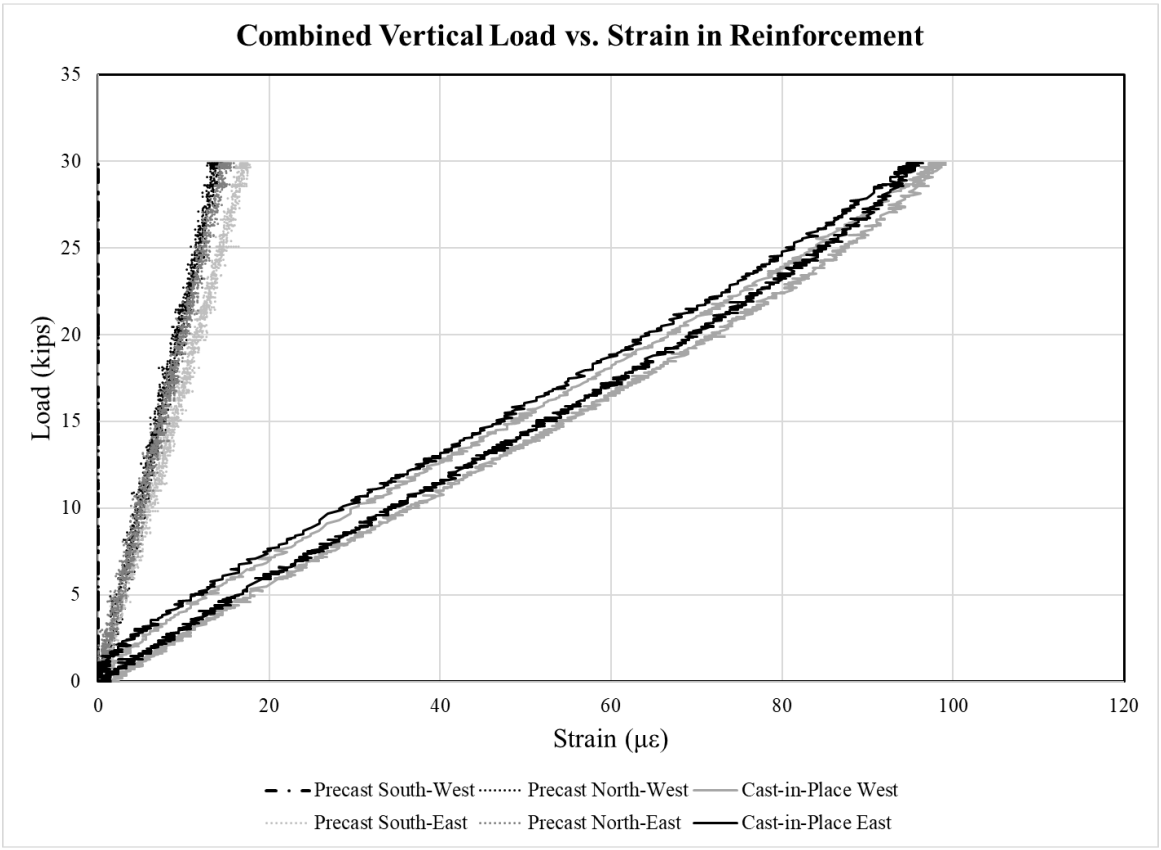
Combined Vertical Load vs. Strain in Reinforcement
Load (kips)
Strain (με)
0
5
10
15
20
25
30
35
0
20
40
60
80
100
120
Precast South-West
Precast North-West
Cast-in-Place West
Precast South-East
Precast North-East
Cast-in-Place East

Monotonic Test at 500,000 Cycles

Summary	
Number of Cycles Performed Before Test	502737 cycles
Central Deflection of Specimen at 30-kips	0.019 in
Maximum Opening of Joint Between Beams	0.001 in
Maximum Reinforcement Strain in Precast	18 με
Maximum Reinforcement Strain in Cast-in-Place	106 με

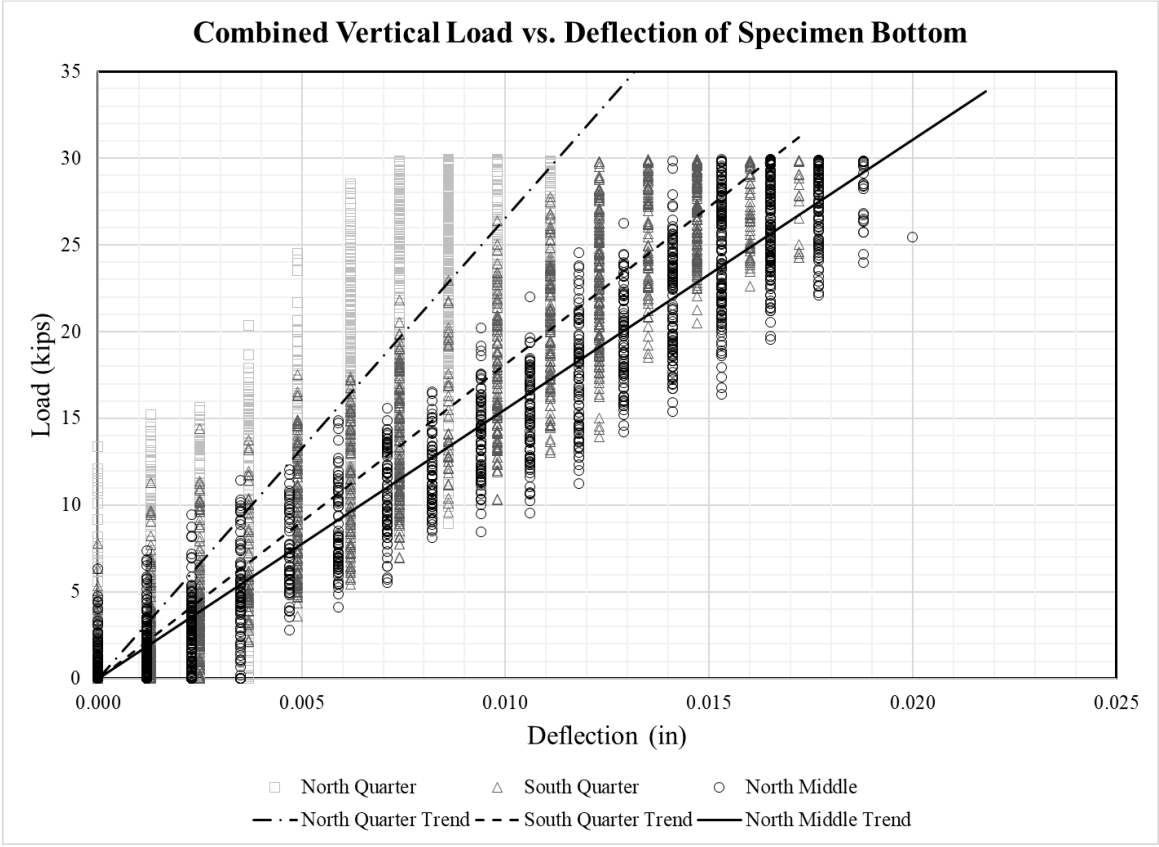
Combined Vertical Load vs. Deflection of Specimen Bottom
Load (kips)
Deflection (in)
0
5
10
15
20
25
30
35
0.000
0.005
0.010
0.015
0.020
0.025
North Quarter
South Quarter
North Middle
North Quarter Trend
South Quarter Trend
North Middle Trend

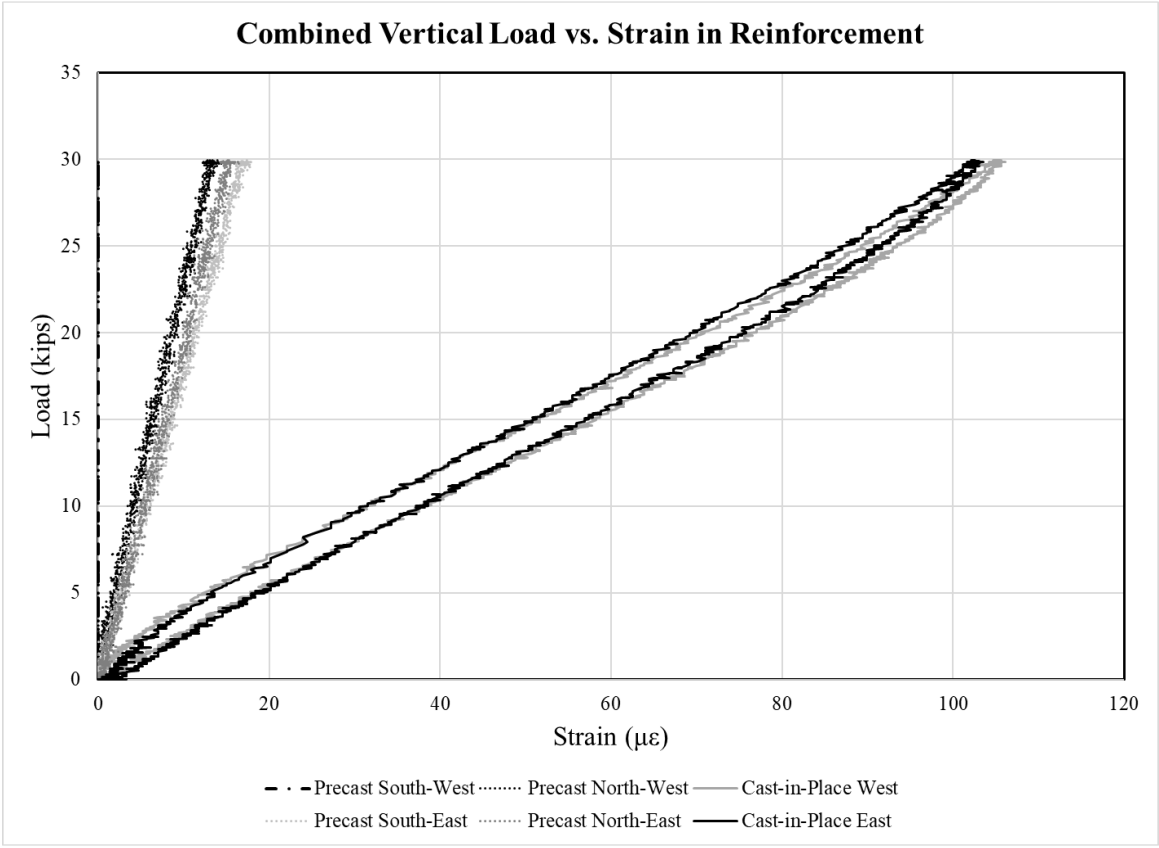
Combined Vertical Load vs. Strain in Reinforcement
Load (kips)
Strain (με)
0
5
10
15
20
25
30
35
0
20
40
60
80
100
120
Precast South-West
Precast North-West
Cast-in-Place West
Precast South-East
Precast North-East
Cast-in-Place East

Monotonic Test at 700,000 Cycles

Summary	
Number of Cycles Performed Before Test	700001 cycles
Central Deflection of Specimen at 30-kips	0.018 in
Maximum Opening of Joint Between Beams	0.001 in
Maximum Reinforcement Strain in Precast	17 με
Maximum Reinforcement Strain in Cast-in-Place	111 με

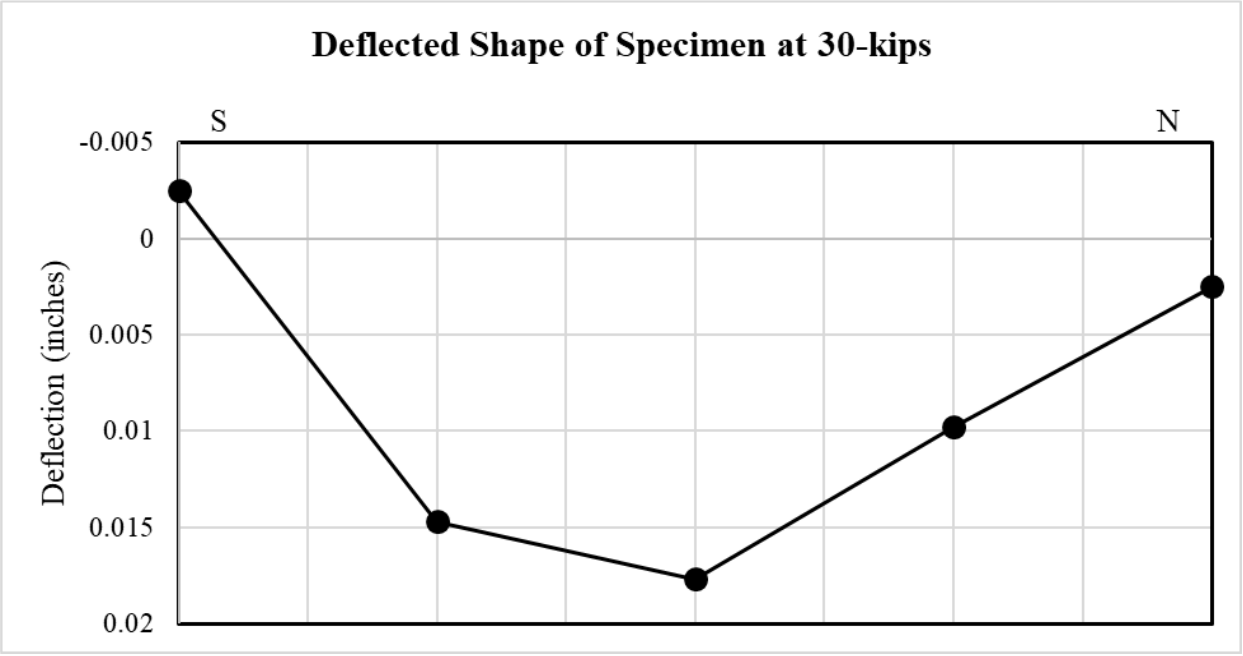

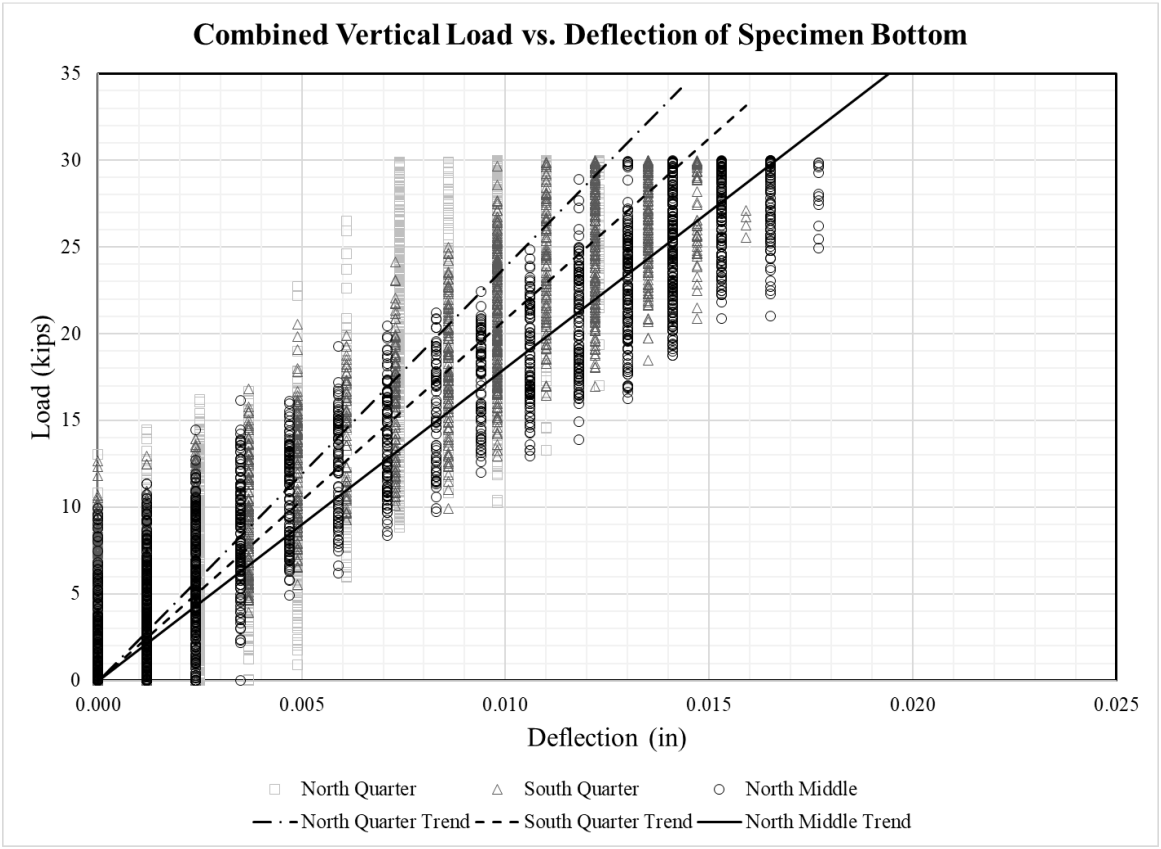
Combined Vertical Load vs. Deflection of Specimen Bottom
Load (kips)
Deflection (in)
0
5
10
15
20
25
30
35
0.000
0.005
0.010
0.015
0.020
0.025
North Quarter
South Quarter
North Middle
North Quarter Trend
South Quarter Trend
North Middle Trend

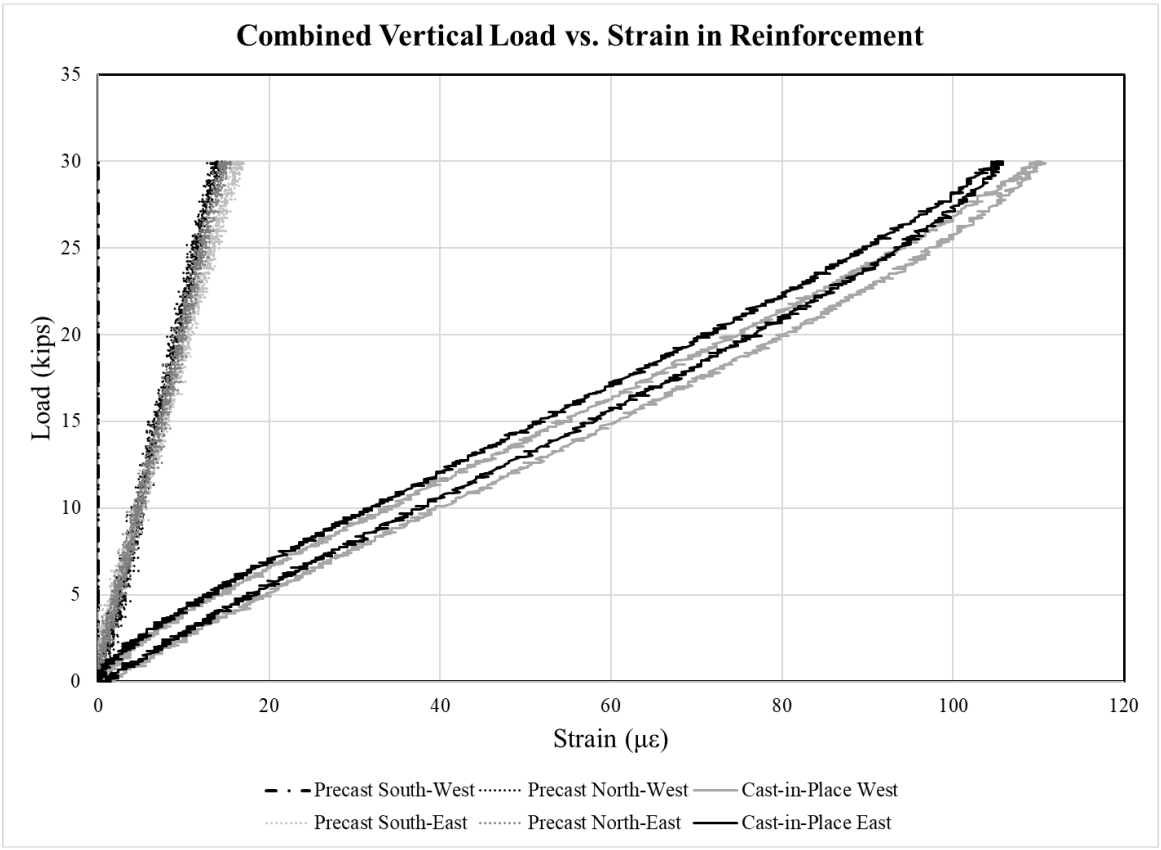
Combined Vertical Load vs. Strain in Reinforcement
Load (kips)
Strain (με)
0
5
10
15
20
25
30
35
0
20
40
60
80
100
120
Precast South-West
Precast North-West
Cast-in-Place West
Precast South-East
Precast North-East
Cast-in-Place East

Monotonic Test at 900,000 Cycles

Summary	
Number of Cycles Performed Before Test	900554 cycles
Central Deflection of Specimen at 30-kips	0.019 in
Maximum Opening of Joint Between Beams	0.001 in
Maximum Reinforcement Strain in Precast	19 με
Maximum Reinforcement Strain in Cast-in-Place	114 με

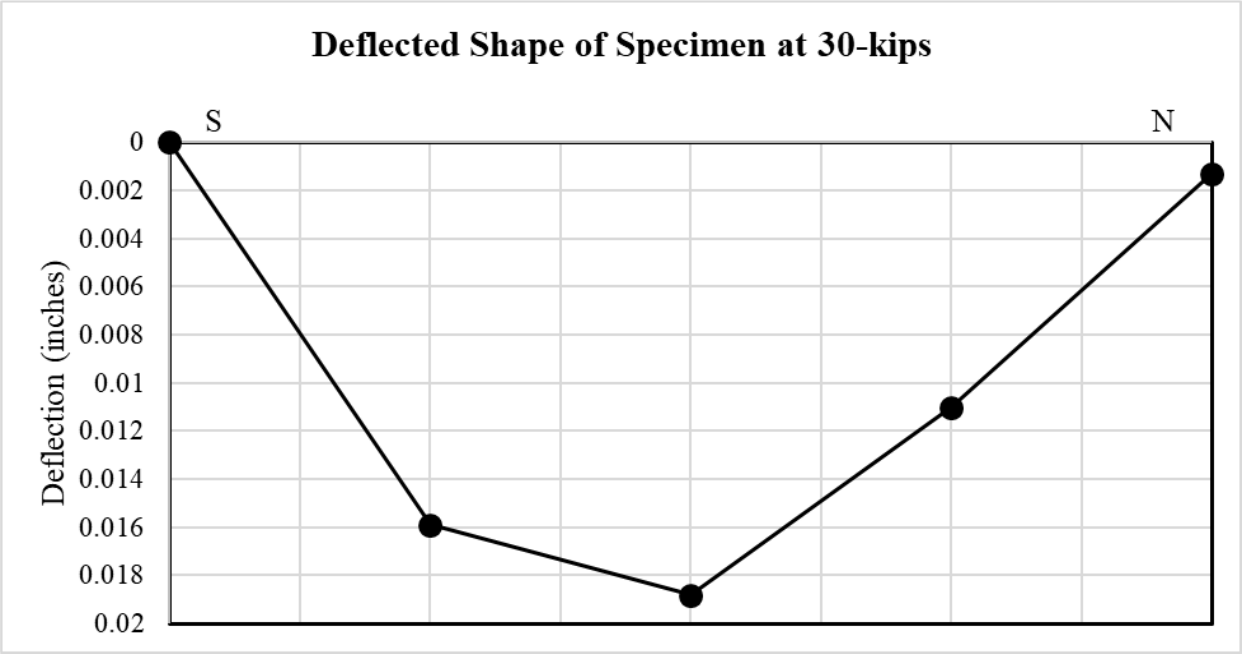

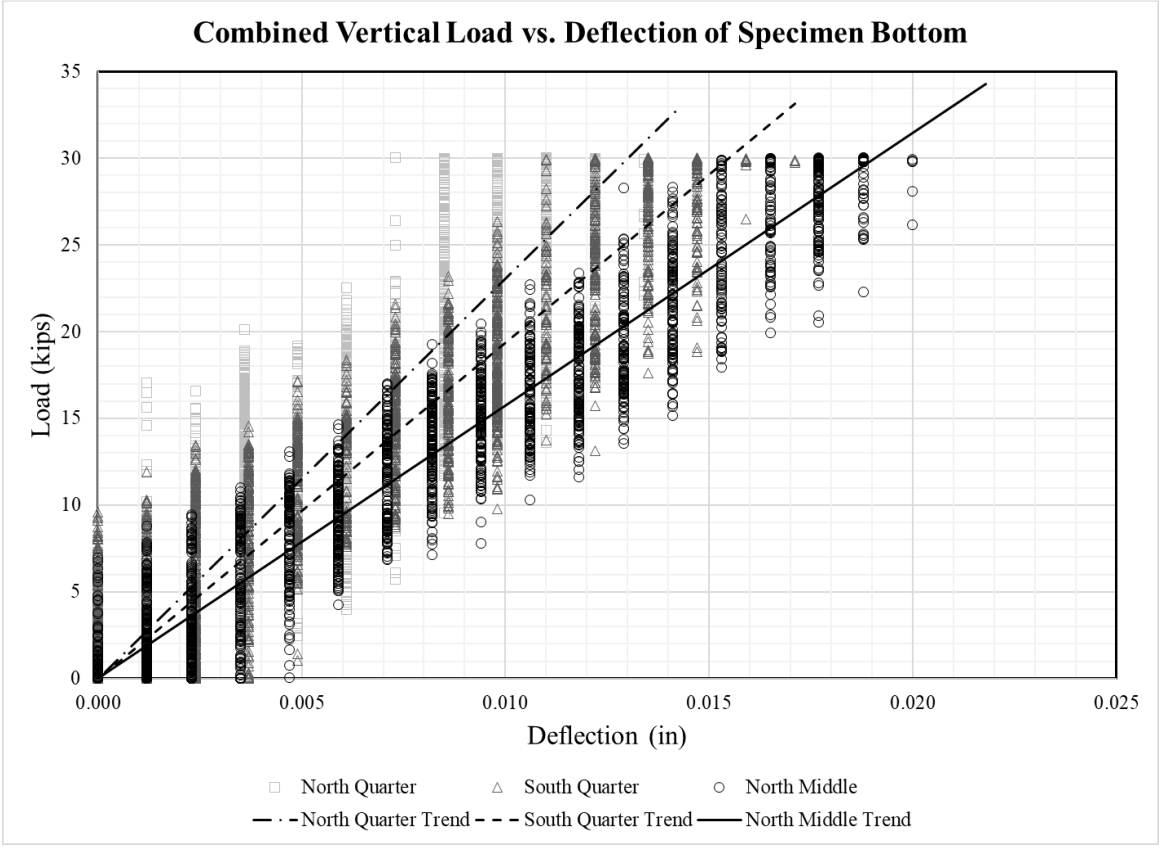
Combined Vertical Load vs. Deflection of Specimen Bottom
Load (kips)
Deflection (in)
0
5
10
15
20
25
30
35
0.000
0.005
0.010
0.015
0.020
0.025
North Quarter
South Quarter
North Middle
North Quarter Trend
South Quarter Trend
North Middle Trend

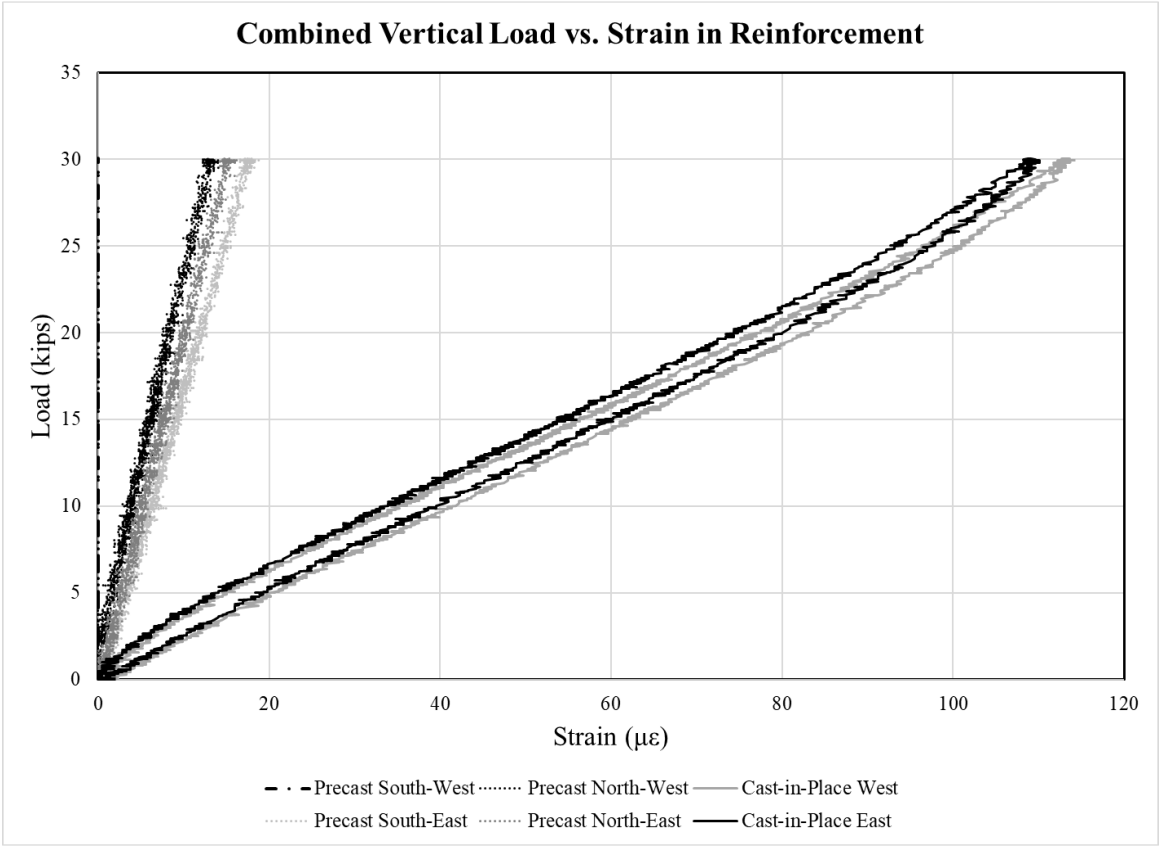
Combined Vertical Load vs. Strain in Reinforcement
Load (kips)
Strain (με)
0
5
10
15
20
25
30
35
0
20
40
60
80
100
120
Precast South-West
Precast North-West
Cast-in-Place West
Precast South-East
Precast North-East
Cast-in-Place East

Monotonic Test at 1,100,000 Cycles

Summary	
Number of Cycles Performed Before Test	1100000 cycles
Central Deflection of Specimen at 30-kips	0.021 in
Maximum Opening of Joint Between Beams	0.001 in
Maximum Reinforcement Strain in Precast	19 με
Maximum Reinforcement Strain in Cast-in-Place	119 με

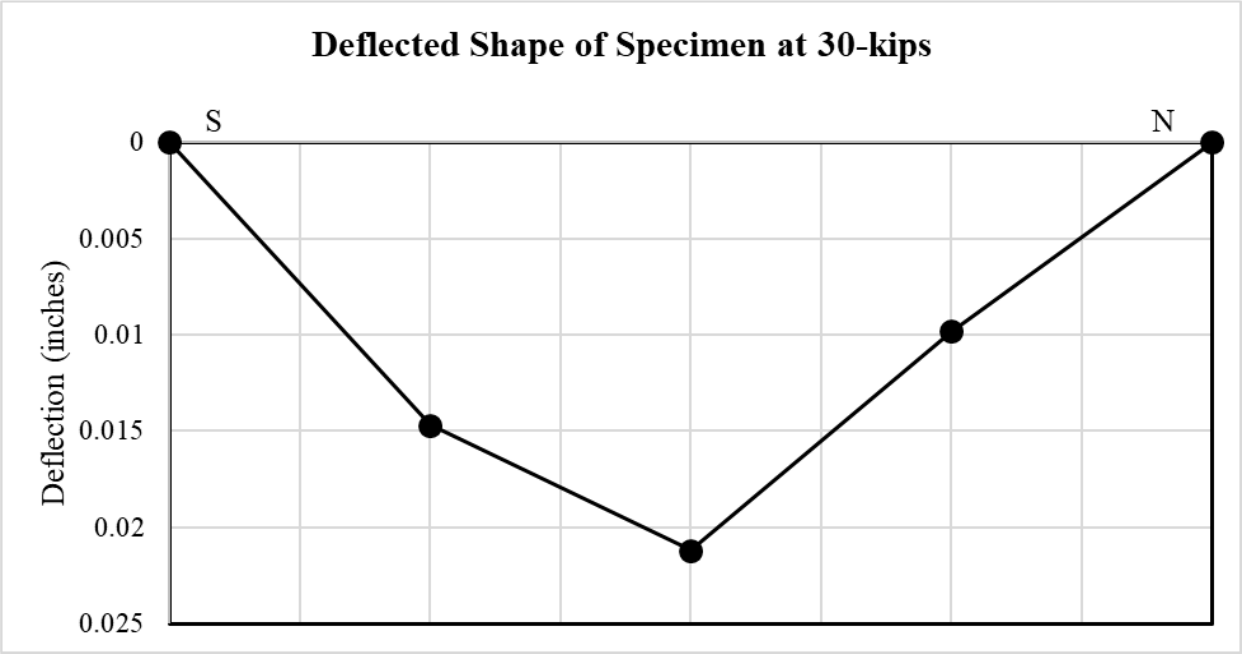

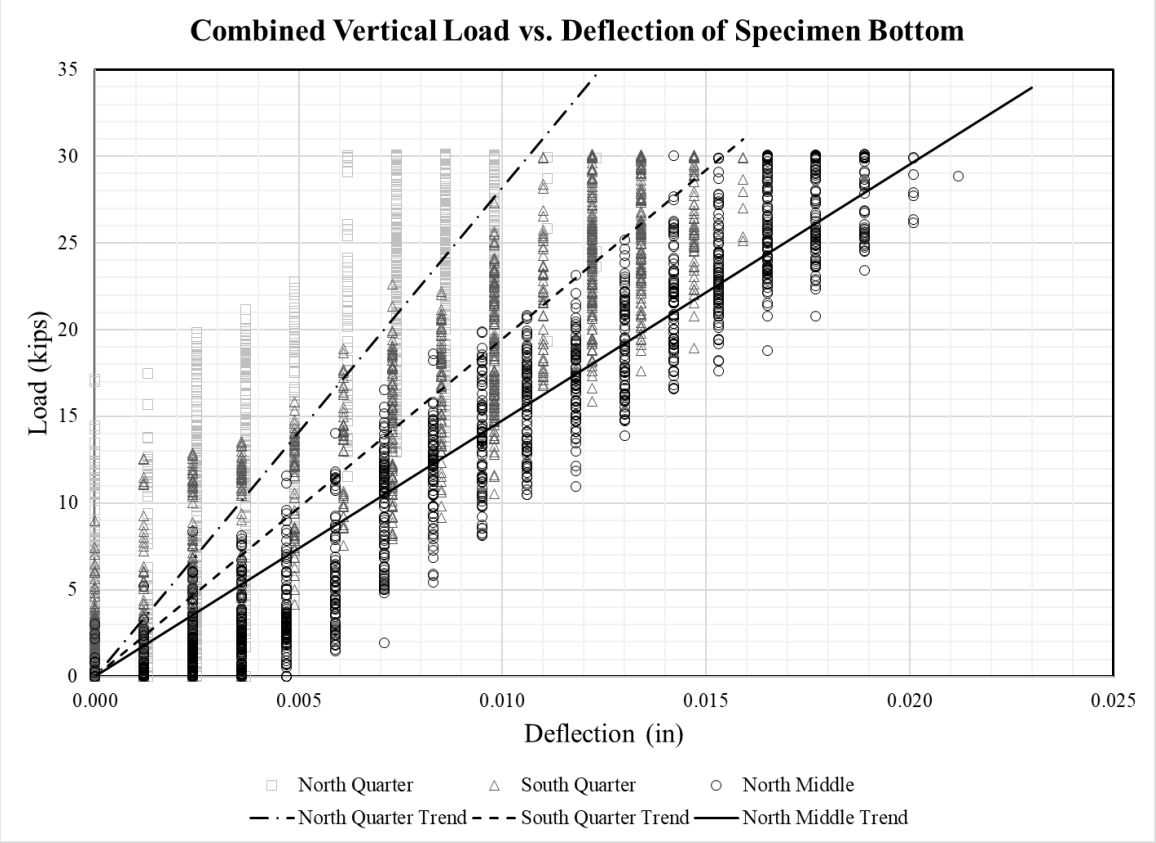
Combined Vertical Load vs. Deflection of Specimen Bottom
Load (kips)
Deflection (in)
0
5
10
15
20
25
30
35
0.000
0.005
0.010
0.015
0.020
0.025
North Quarter
South Quarter
North Middle
North Quarter Trend
South Quarter Trend
North Middle Trend

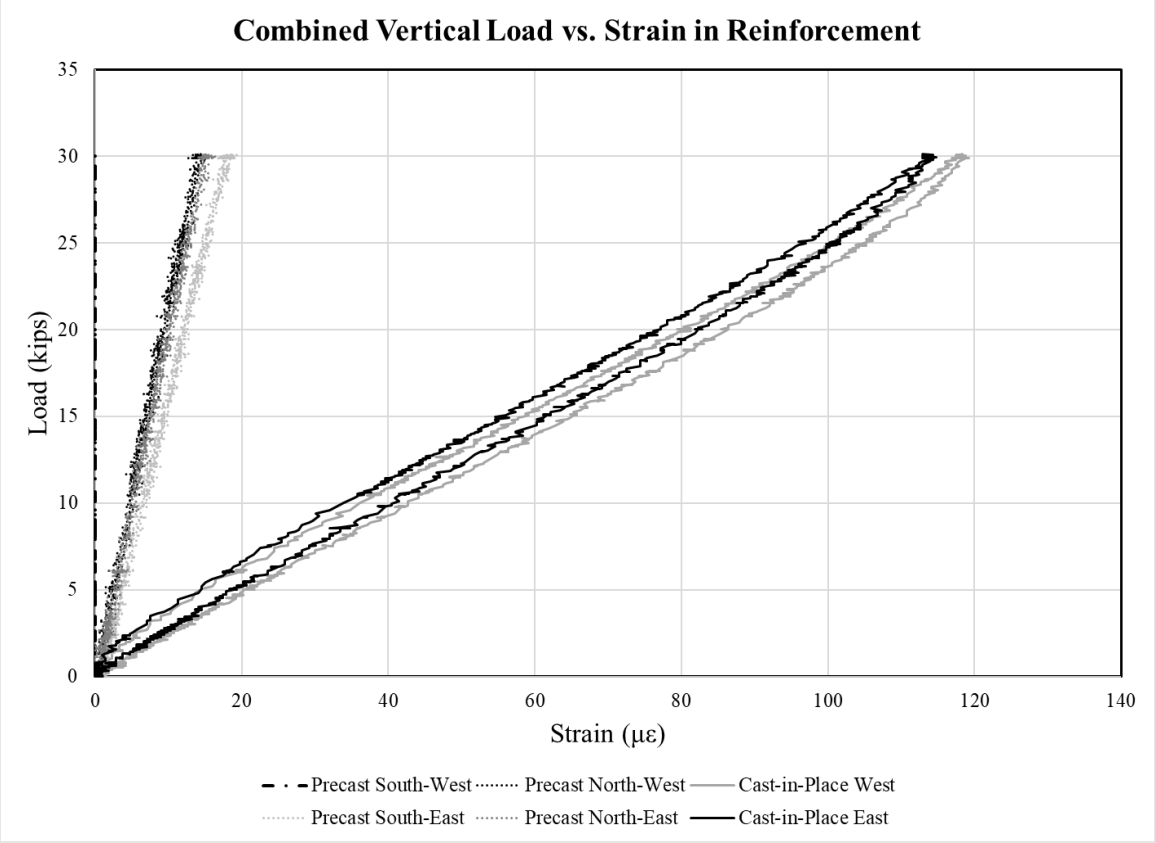
Combined Vertical Load vs. Strain in Reinforcement
Load (kips)
Strain (με)
0
5
10
15
20
25
30
35
0
20
40
60
80
100
120
140
Precast South-West
Precast North-West
Cast-in-Place West
Precast South-East
Precast North-East
Cast-in-Place East

Monotonic Test at 1,300,000 Cycles

Summary	
Number of Cycles Performed Before Test	1301131 cycles
Central Deflection of Specimen at 30-kips	0.019 in
Maximum Opening of Joint Between Beams	0.001 in
Maximum Reinforcement Strain in Precast	18 με
Maximum Reinforcement Strain in Cast-in-Place	123 με

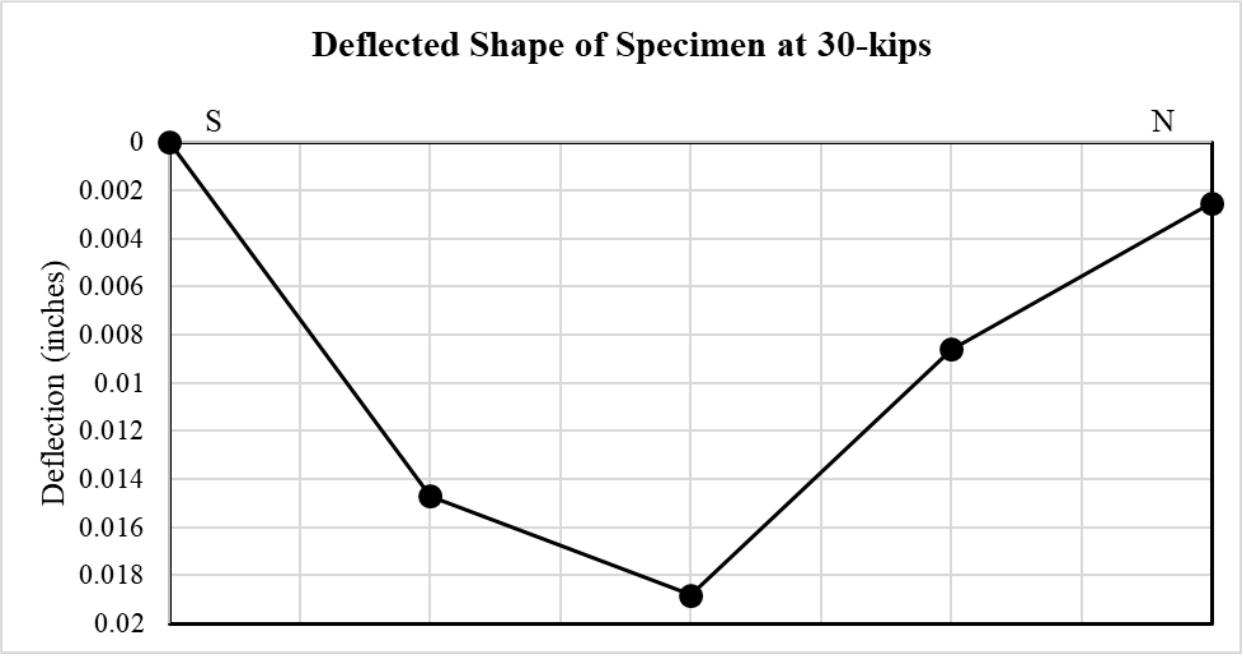

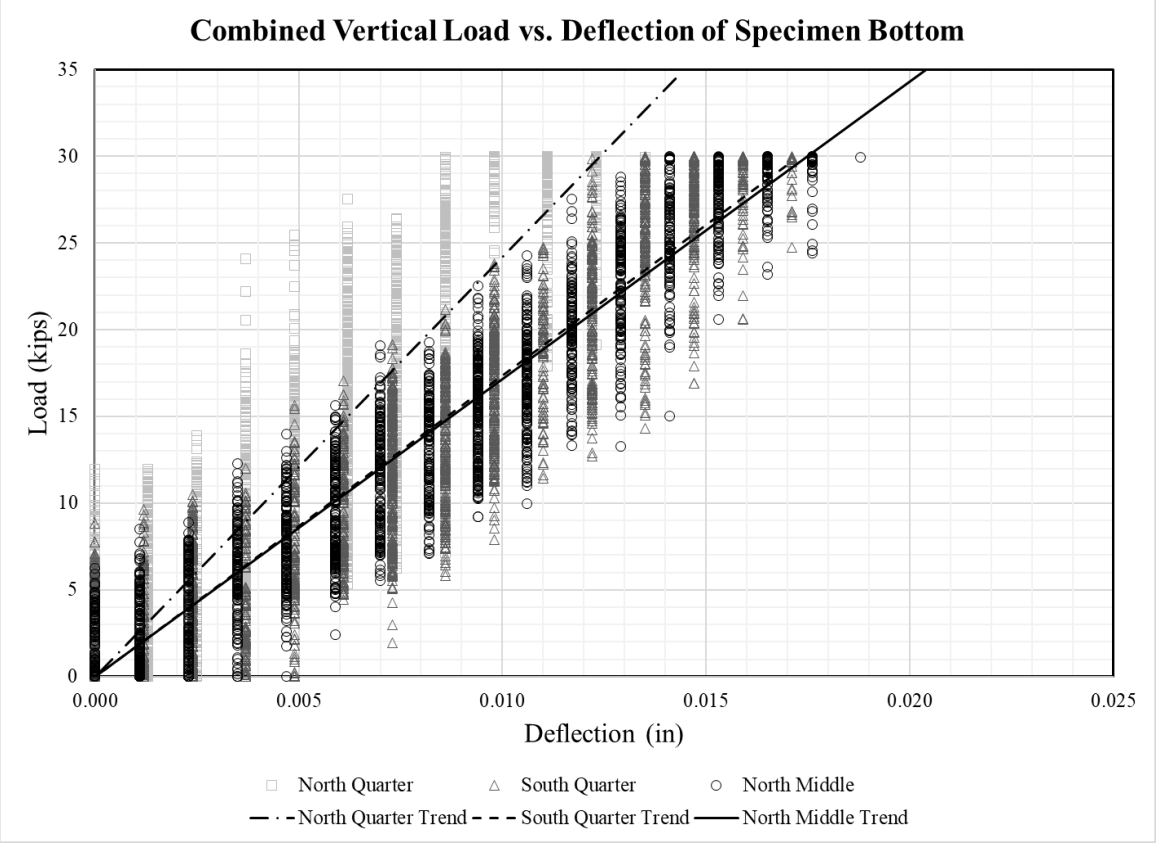
Combined Vertical Load vs. Deflection of Specimen Bottom
Load (kips)
Deflection (in)
0
5
10
15
20
25
30
35
0.000
0.005
0.010
0.015
0.020
0.025
North Quarter
South Quarter
North Middle
North Quarter Trend
South Quarter Trend
North Middle Trend

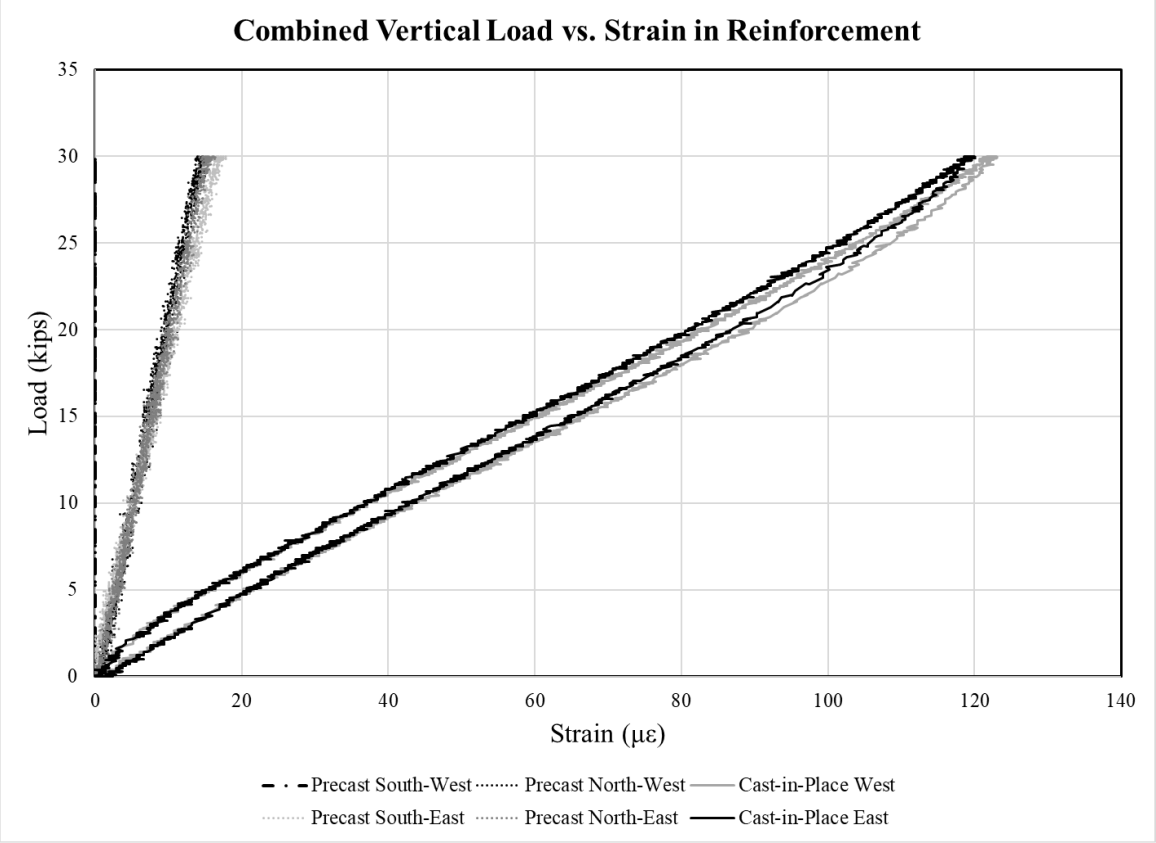
Combined Vertical Load vs. Strain in Reinforcement
Load (kips)
Strain (με)
0
5
10
15
20
25
30
35
0
20
40
60
80
100
120
140
Precast South-West
Precast North-West
Cast-in-Place West
Precast South-East
Precast North-East
Cast-in-Place East

Monotonic Test at 1,500,000 Cycles

Summary	
Number of Cycles Performed Before Test	1500001 cycles
Central Deflection of Specimen at 30-kips	0.015 in
Maximum Opening of Joint Between Beams	0.001 in
Maximum Reinforcement Strain in Precast	18 με
Maximum Reinforcement Strain in Cast-in-Place	125 με

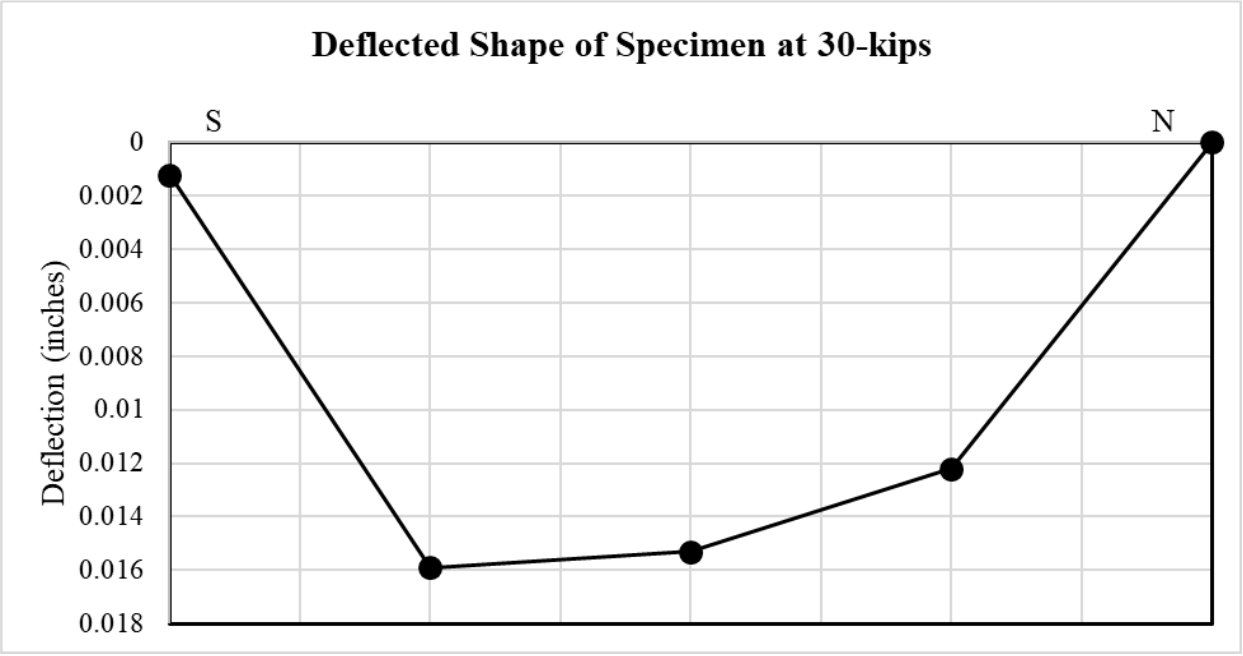

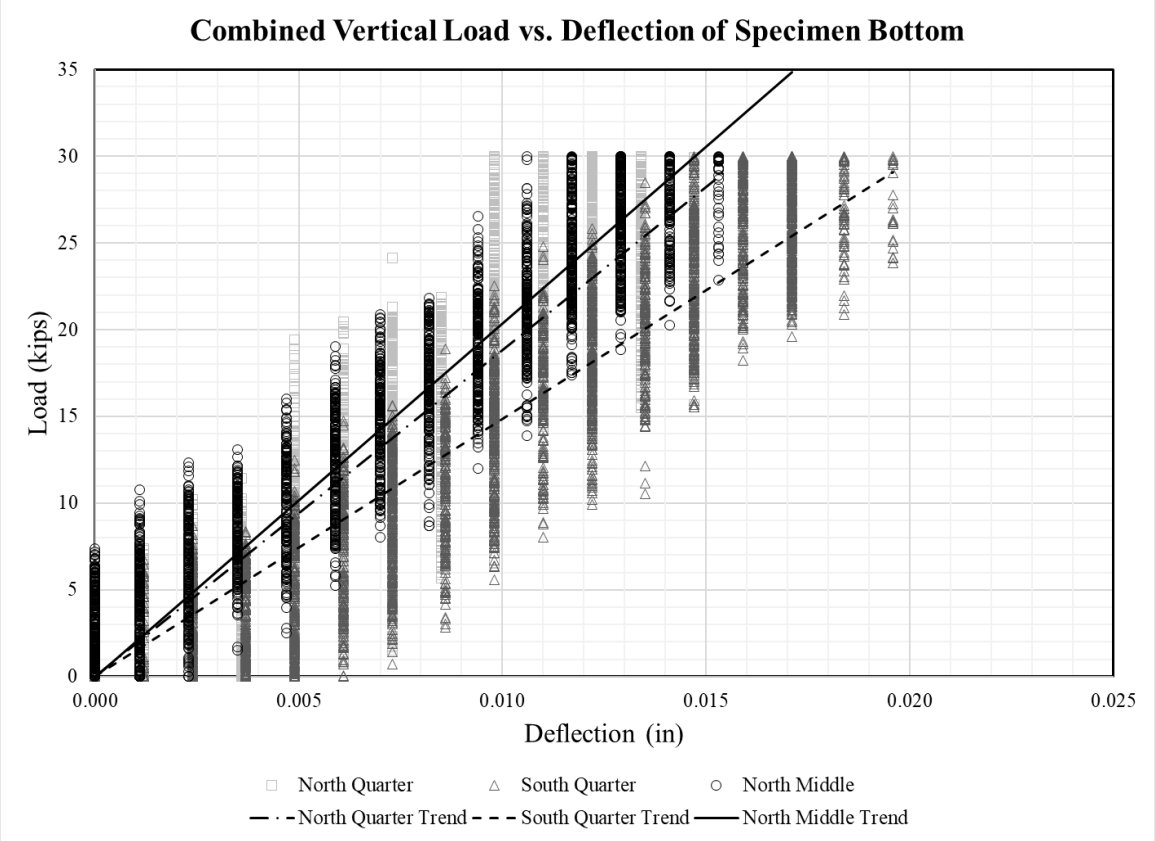
Combined Vertical Load vs. Deflection of Specimen Bottom
Load (kips)
Deflection (in)
0
5
10
15
20
25
30
35
0.000
0.005
0.010
0.015
0.020
0.025
North Quarter
South Quarter
North Middle
North Quarter Trend
South Quarter Trend
North Middle Trend

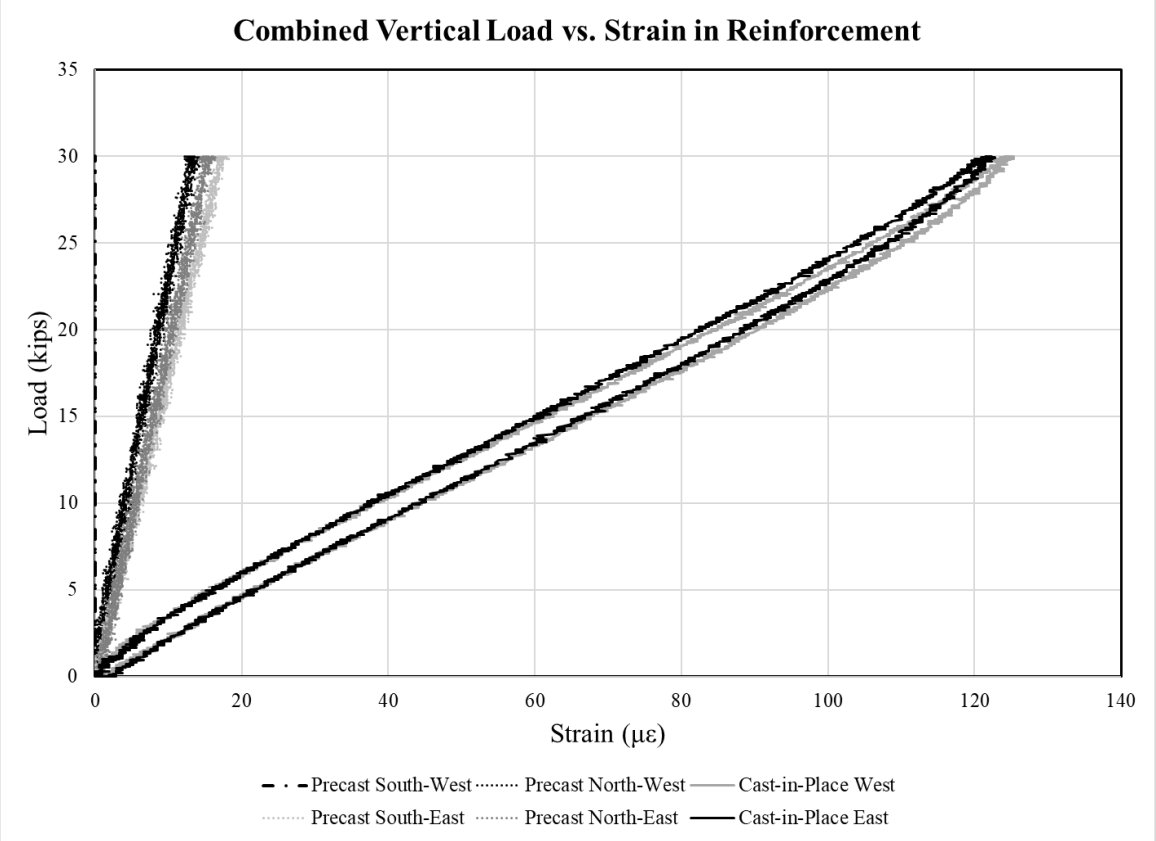
Combined Vertical Load vs. Strain in Reinforcement
Load (kips)
Strain (με)
0
5
10
15
20
25
30
35
0
20
40
60
80
100
120
140
Precast South-West
Precast North-West
Cast-in-Place West
Precast South-East
Precast North-East
Cast-in-Place East

Monotonic Test at 1,700,000 Cycles

Summary	
Number of Cycles Performed Before Test	1700000 cycles
Central Deflection of Specimen at 30-kips	0.018 in
Maximum Opening of Joint Between Beams	0.001 in
Maximum Reinforcement Strain in Precast	19 με
Maximum Reinforcement Strain in Cast-in-Place	128 με

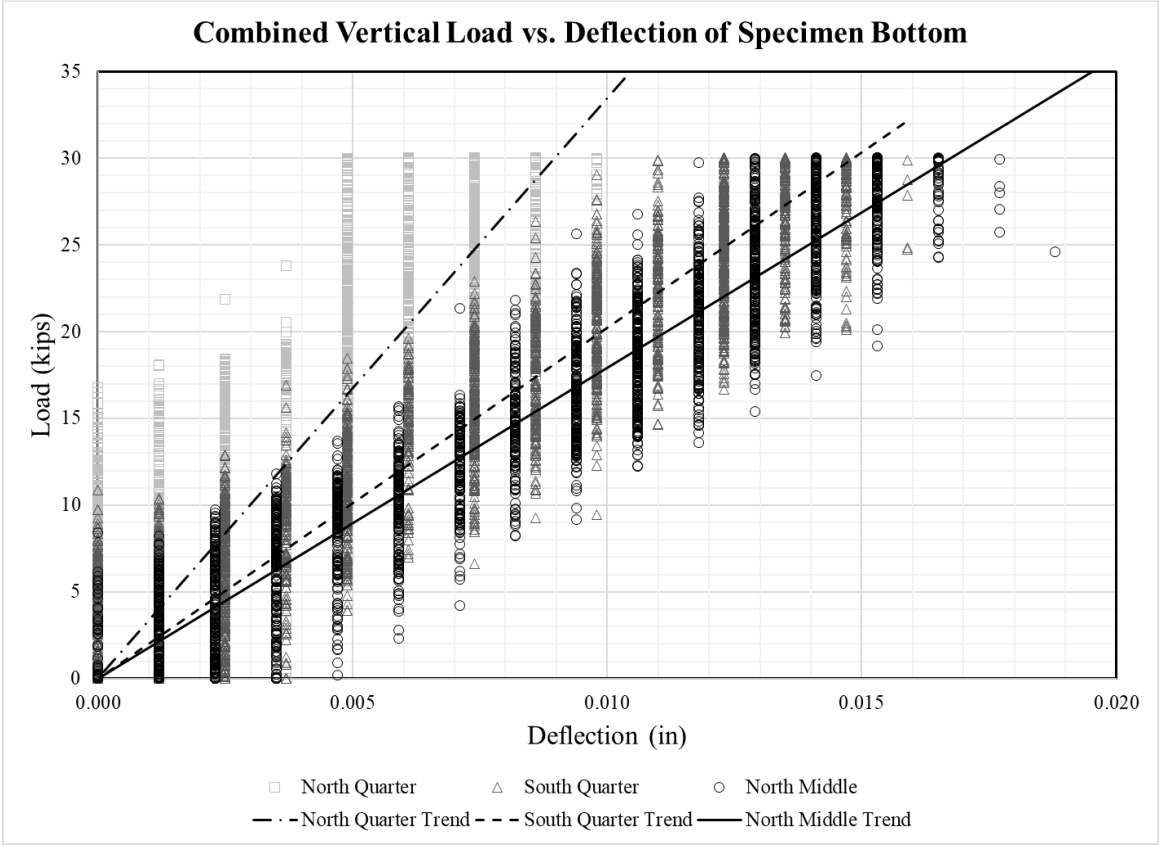
Combined Vertical Load vs. Deflection of Specimen Bottom
Load (kips)
Deflection (in)
0
5
10
15
20
25
30
35
0.000
0.005
0.010
0.015
0.020
North Quarter
South Quarter
North Middle
North Quarter Trend
South Quarter Trend
North Middle Trend

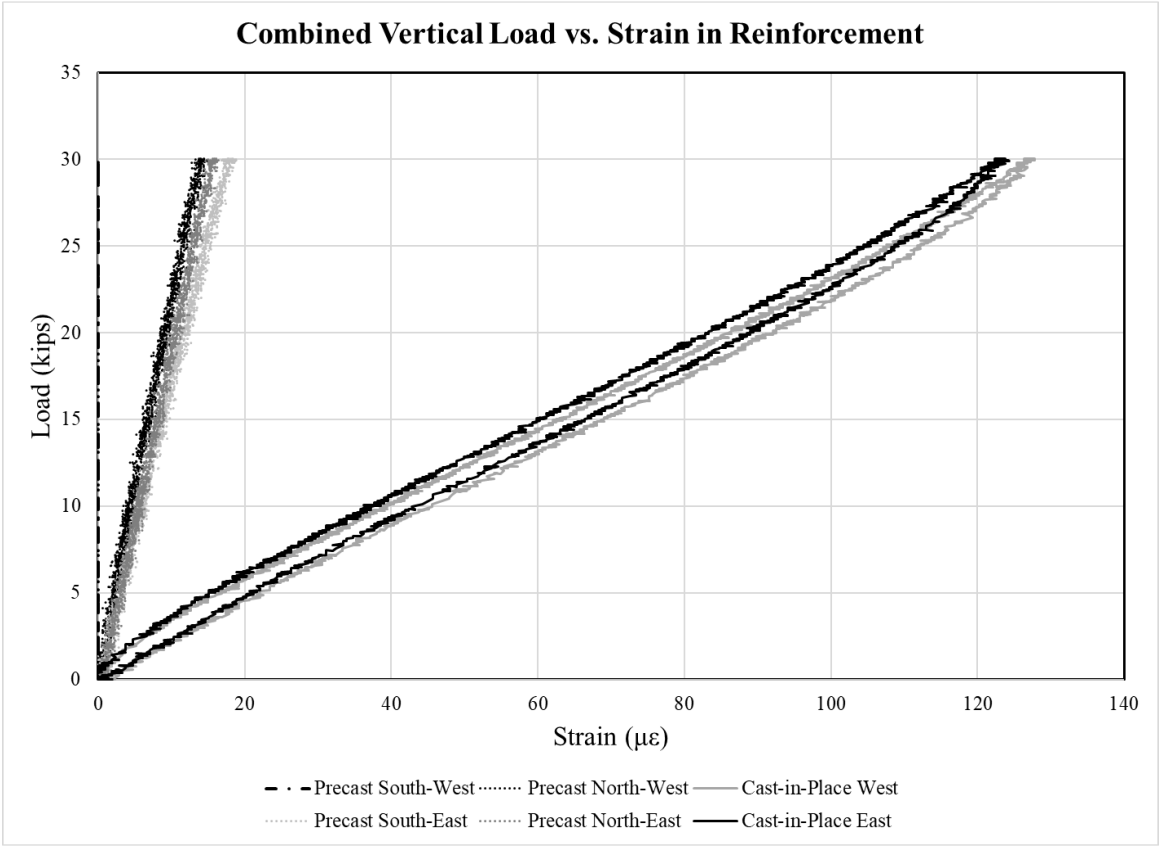
Combined Vertical Load vs. Strain in Reinforcement
Load (kips)
Strain (με)
0
5
10
15
20
25
30
35
0
20
40
60
80
100
120
140
Precast South-West
Precast North-West
Cast-in-Place West
Precast South-East
Precast North-East
Cast-in-Place East

Monotonic Test at 1,900,000 Cycles

Summary	
Number of Cycles Performed Before Test	1901142 cycles
Central Deflection of Specimen at 30-kips	0.018 in
Maximum Opening of Joint Between Beams	0.001 in
Maximum Reinforcement Strain in Precast	19 με
Maximum Reinforcement Strain in Cast-in-Place	130 με

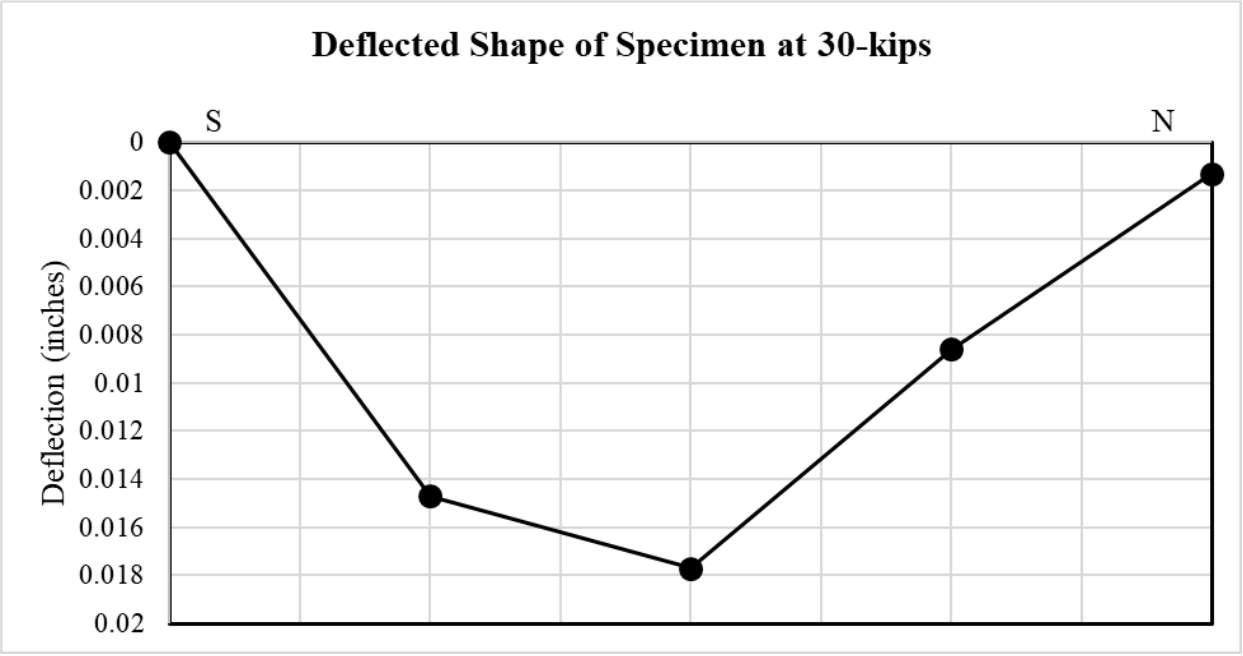

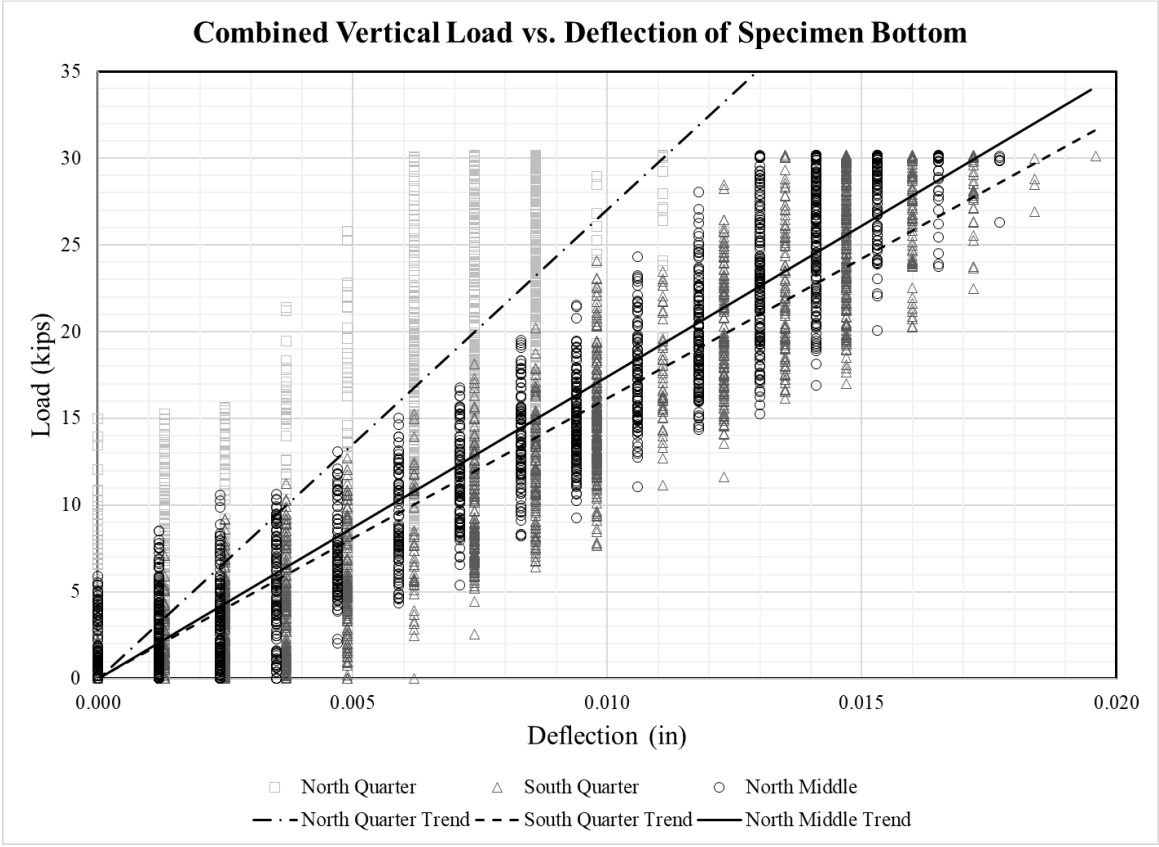
Combined Vertical Load vs. Deflection of Specimen Bottom
Load (kips)
Deflection (in)
0
5
10
15
20
25
30
35
0.000
0.005
0.010
0.015
0.020
North Quarter
South Quarter
North Middle
North Quarter Trend
South Quarter Trend
North Middle Trend

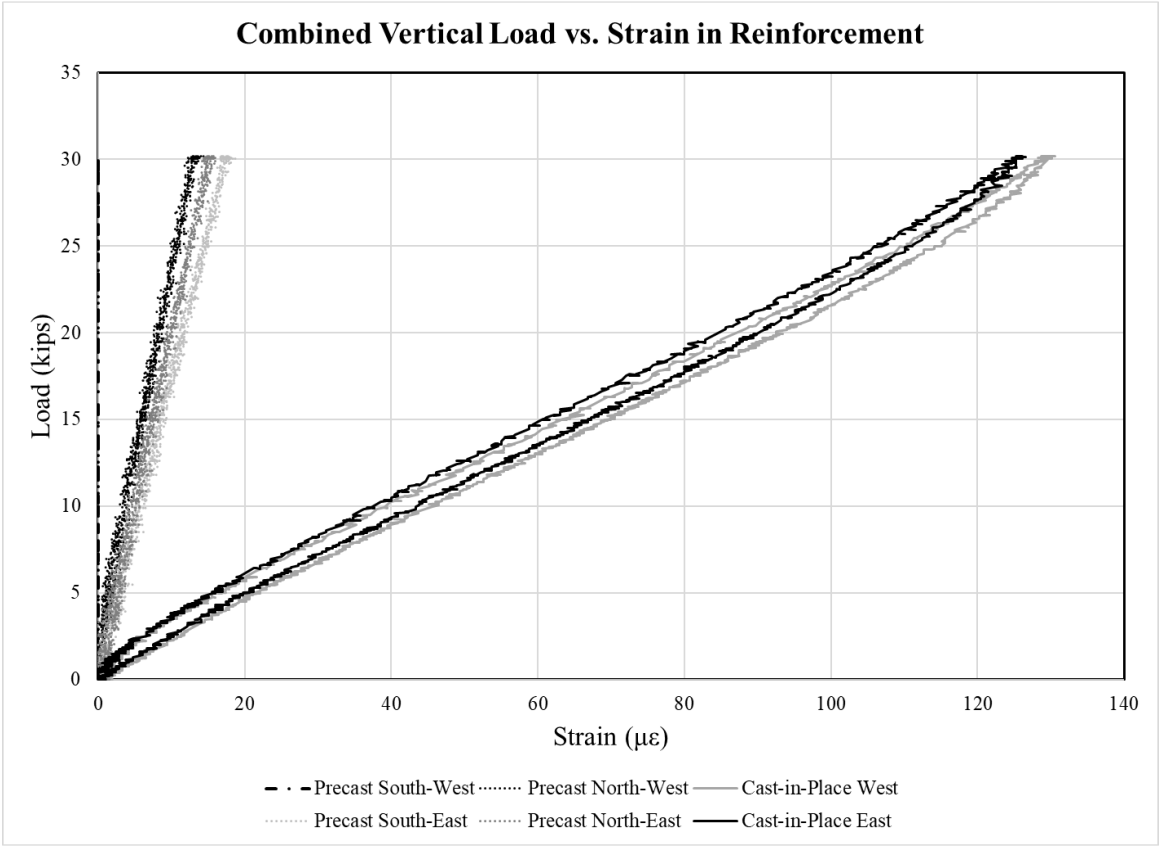
Combined Vertical Load vs. Strain in Reinforcement
Load (kips)
Strain (με)
0
5
10
15
20
25
30
35
0
20
40
60
80
100
120
140
Precast South-West
Precast North-West
Cast-in-Place West
Precast South-East
Precast North-East
Cast-in-Place East

Monotonic Test at 2,100,000 Cycles

Summary	
Number of Cycles Performed Before Test	2100001 cycles
Central Deflection of Specimen at 30-kips	0.016 in
Maximum Opening of Joint Between Beams	0.001 in
Maximum Reinforcement Strain in Precast	20 με
Maximum Reinforcement Strain in Cast-in-Place	134 με

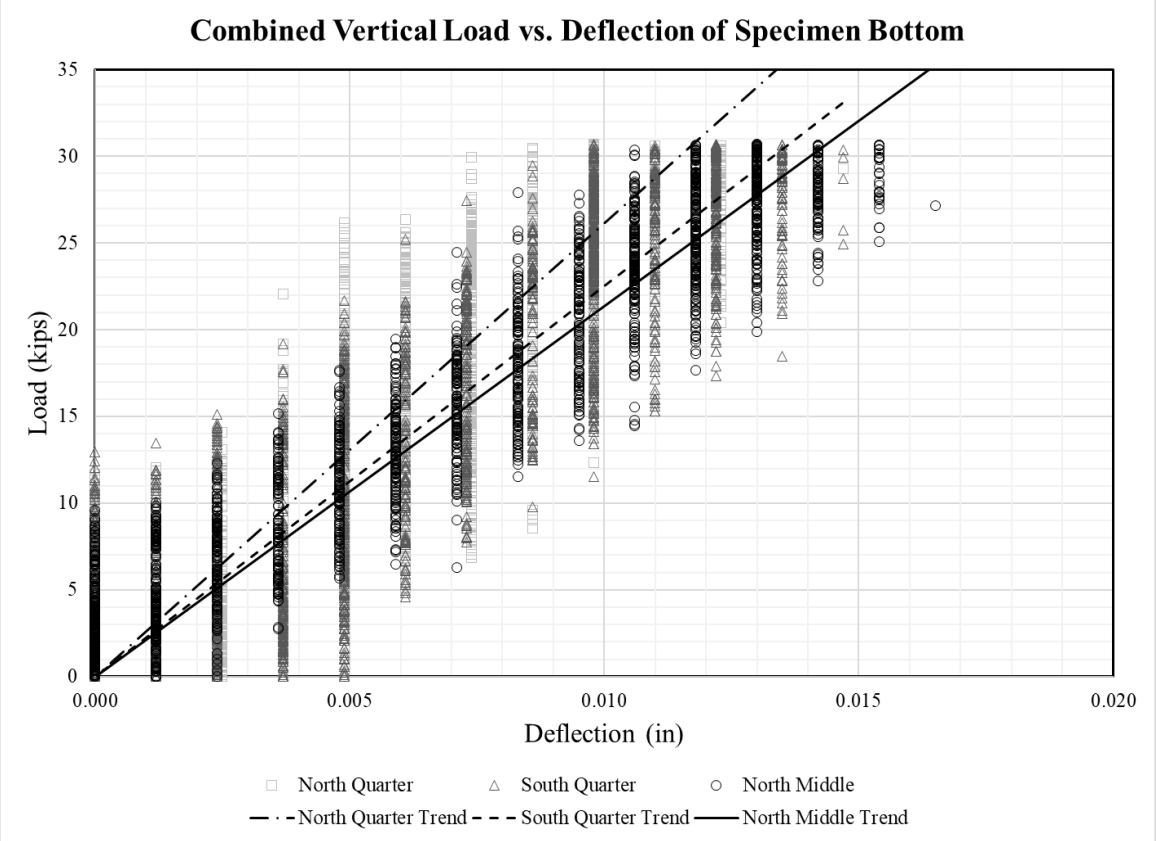
Combined Vertical Load vs. Deflection of Specimen Bottom
Load (kips)
Deflection (in)
0
5
10
15
20
25
30
35
0.000
0.005
0.010
0.015
0.020
North Quarter
South Quarter
North Middle
North Quarter Trend
South Quarter Trend
North Middle Trend

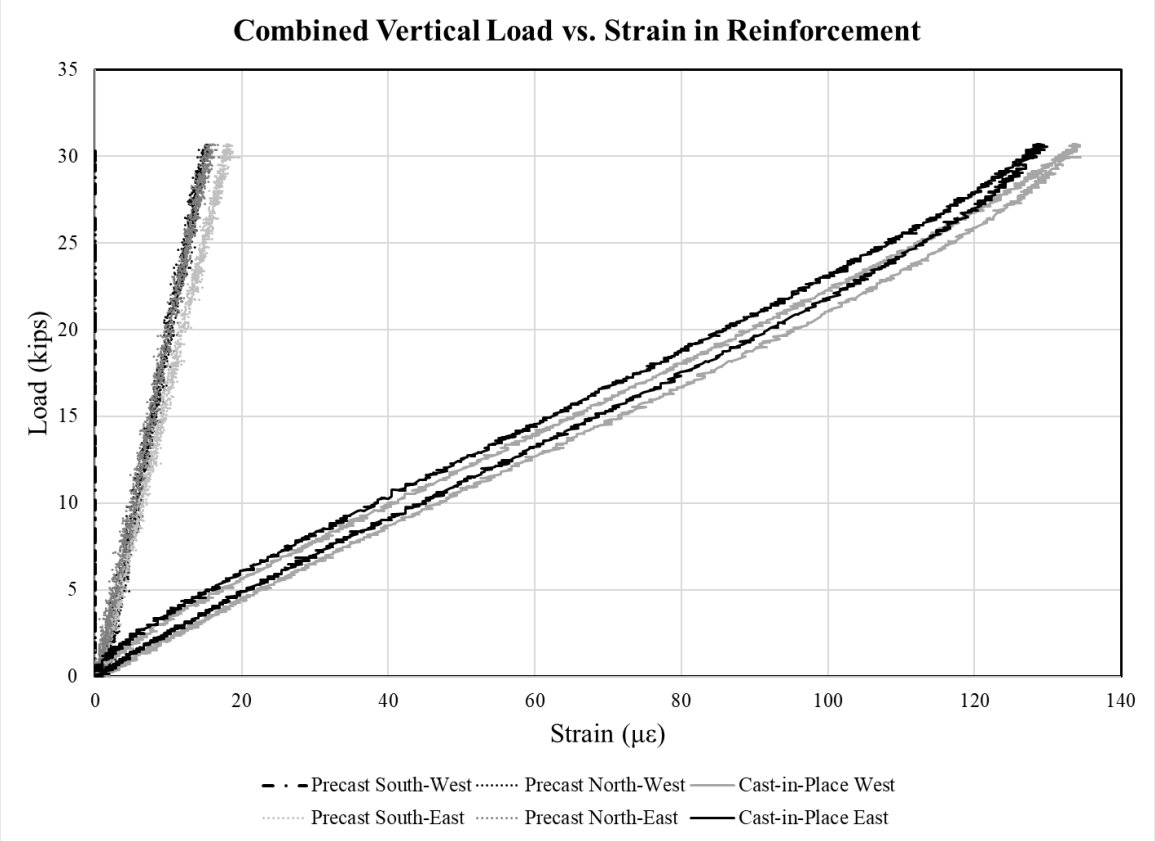
Combined Vertical Load vs. Strain in Reinforcement
Load (kips)
Strain (με)
0
5
10
15
20
25
30
35
0
20
40
60
80
100
120
140
Precast South-West
Precast North-West
Cast-in-Place West
Precast South-East
Precast North-East
Cast-in-Place East

Monotonic Test at 2,300,000 Cycles

Summary	
Number of Cycles Performed Before Test	2300000 cycles
Central Deflection of Specimen at 30-kips	0.018 in
Maximum Opening of Joint Between Beams	0.001 in
Maximum Reinforcement Strain in Precast	18 με
Maximum Reinforcement Strain in Cast-in-Place	135 με

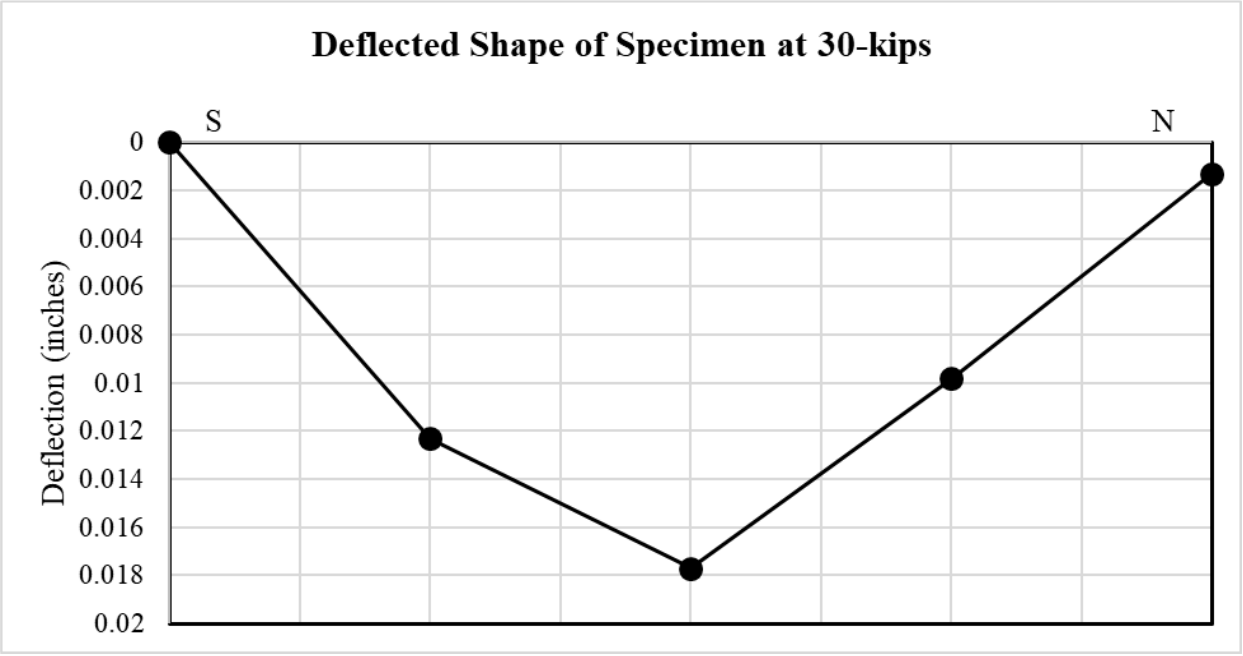

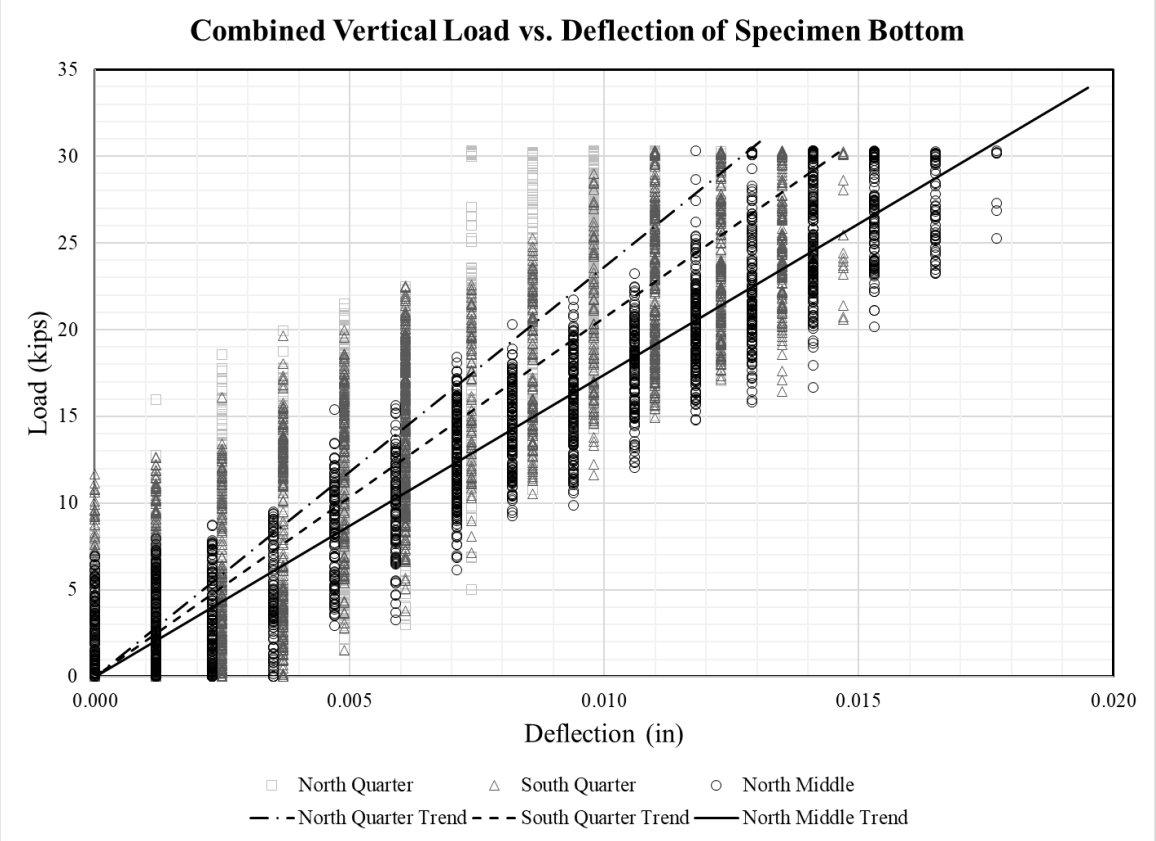
Combined Vertical Load vs. Deflection of Specimen Bottom
Load (kips)
Deflection (in)
0
5
10
15
20
25
30
35
0.000
0.005
0.010
0.015
0.020
North Quarter
South Quarter
North Middle
North Quarter Trend
South Quarter Trend
North Middle Trend

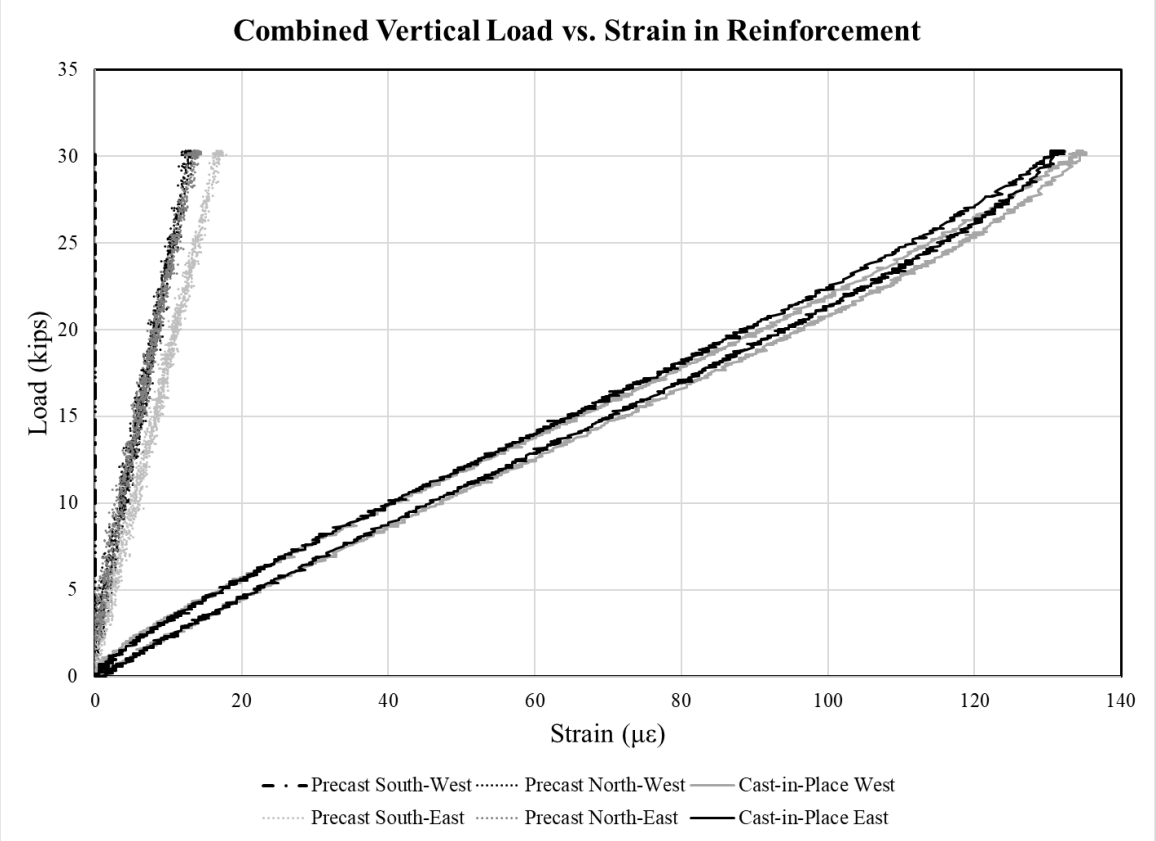
Combined Vertical Load vs. Strain in Reinforcement
Load (kips)
Strain (με)
0
5
10
15
20
25
30
35
0
20
40
60
80
100
120
140
Precast South-West
Precast North-West
Cast-in-Place West
Precast South-East
Precast North-East
Cast-in-Place East

Monotonic Test at 2,500,000 Cycles

Summary	
Number of Cycles Performed Before Test	2500000 cycles
Central Deflection of Specimen at 30-kips	0.018 in
Maximum Opening of Joint Between Beams	0.001 in
Maximum Reinforcement Strain in Precast	17 με
Maximum Reinforcement Strain in Cast-in-Place	139 με

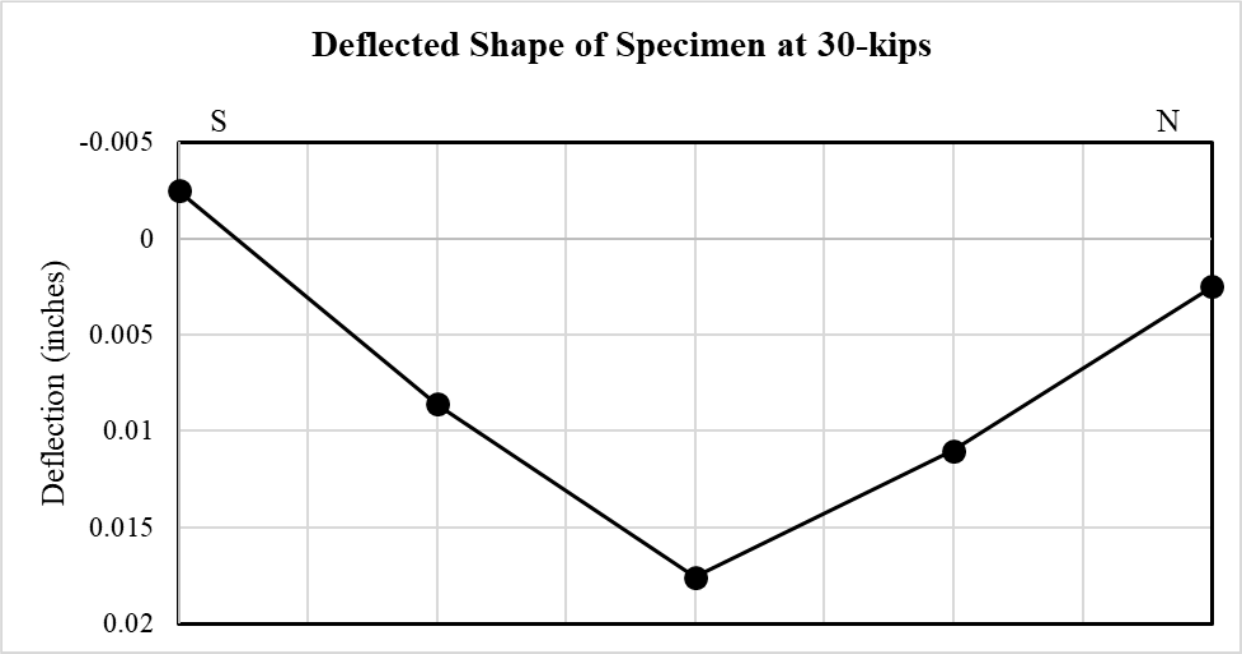

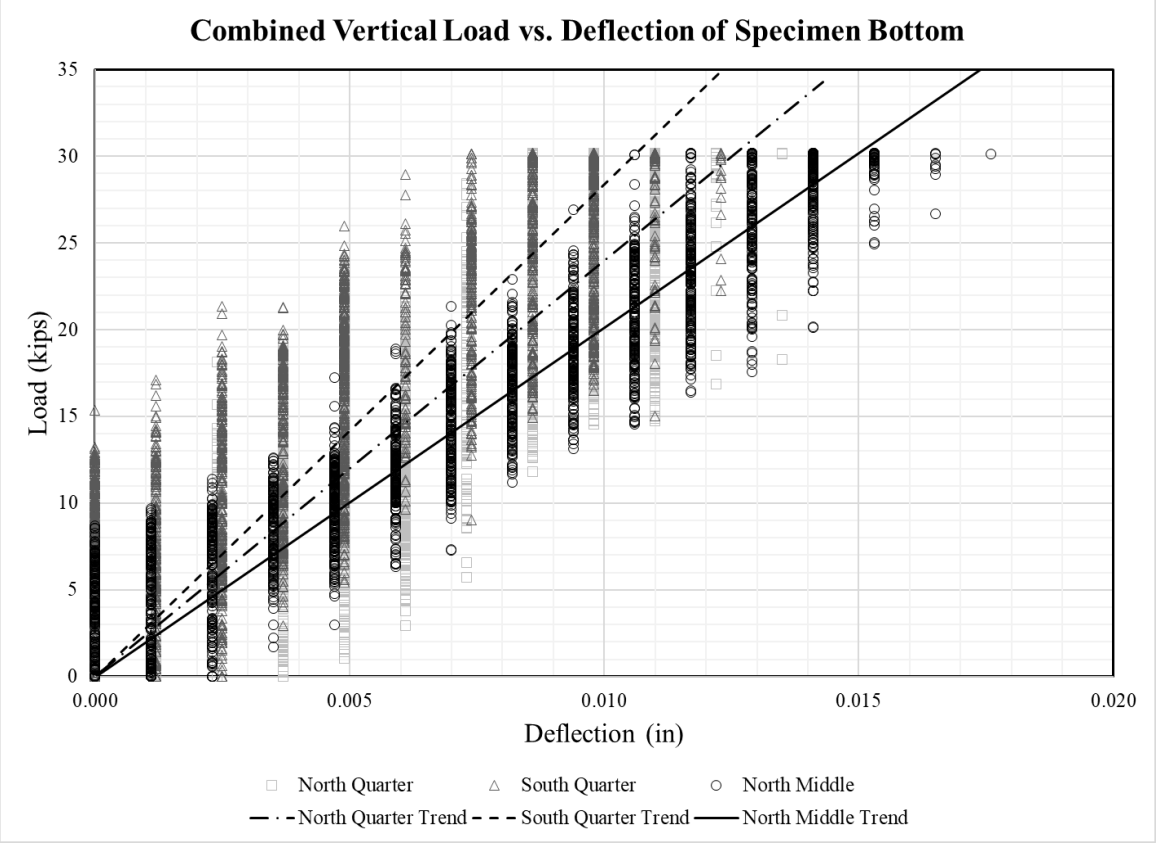
Combined Vertical Load vs. Deflection of Specimen Bottom
Load (kips)
Deflection (in)
0
5
10
15
20
25
30
35
0.000
0.005
0.010
0.015
0.020
North Quarter
South Quarter
North Middle
North Quarter Trend
South Quarter Trend
North Middle Trend

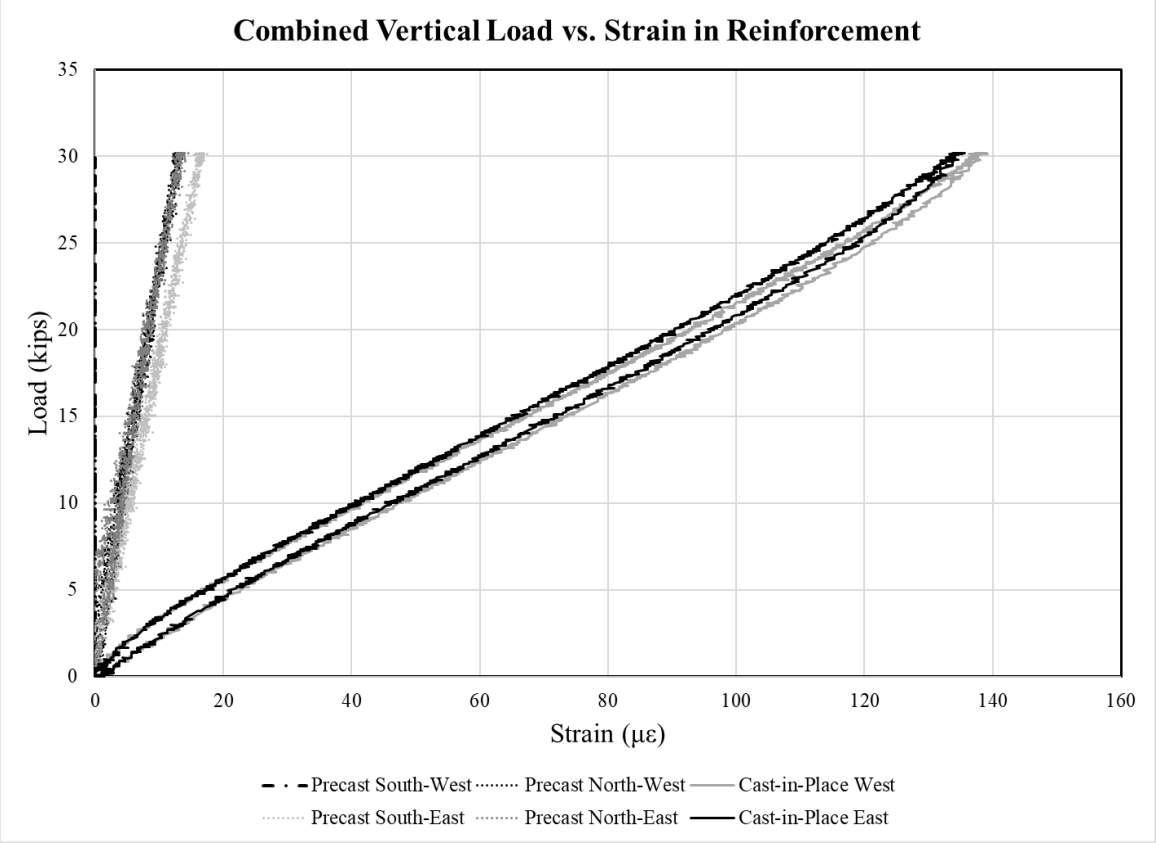
Combined Vertical Load vs. Strain in Reinforcement
Load (kips)
Strain (με)
0
5
10
15
20
25
30
35
0
20
40
60
80
100
120
140
160
Precast South-West
Precast North-West
Cast-in-Place West
Precast South-East
Precast North-East
Cast-in-Place East

Monotonic Test at 2,700,000 Cycles

Summary	
Number of Cycles Performed Before Test	2700000 cycles
Central Deflection of Specimen at 30-kips	0.016 in
Maximum Opening of Joint Between Beams	0.001 in
Maximum Reinforcement Strain in Precast	18 με
Maximum Reinforcement Strain in Cast-in-Place	154 με

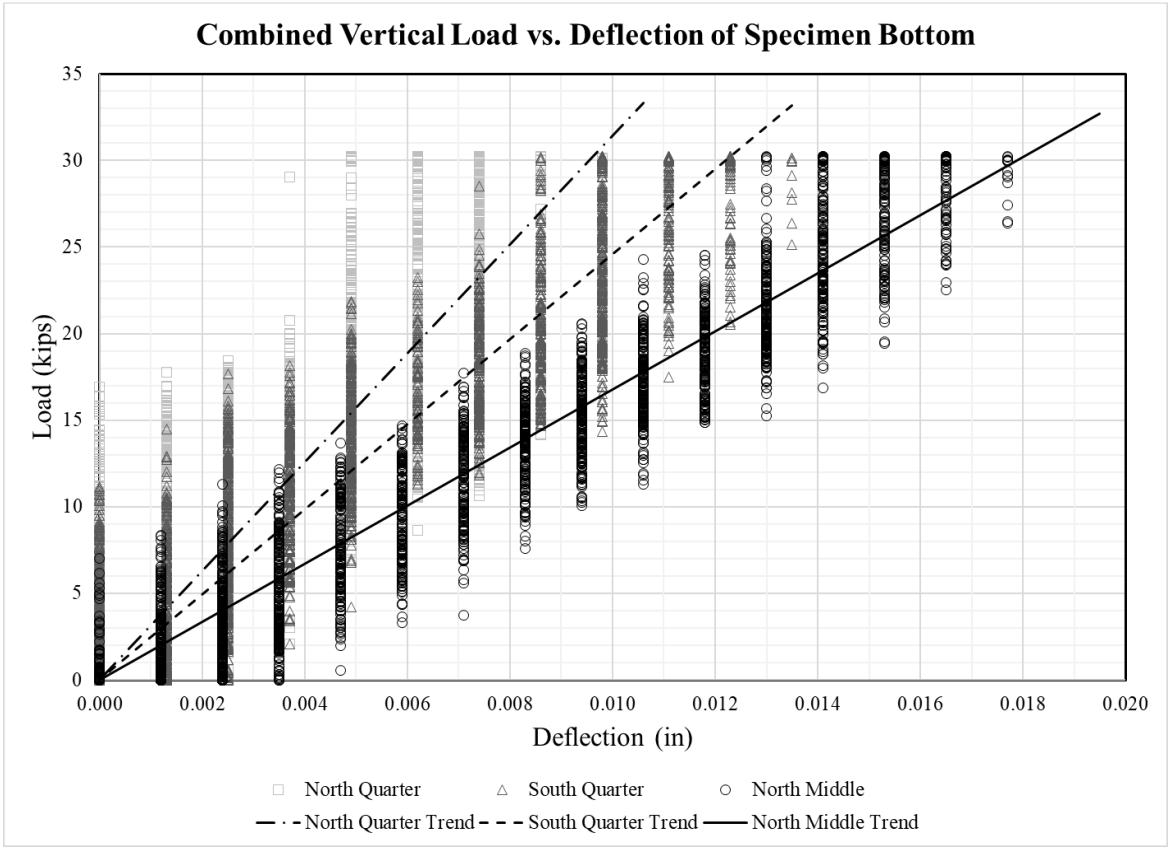
Combined Vertical Load vs. Deflection of Specimen Bottom
Load (kips)
Deflection (in)
North Quarter
South Quarter
North Middle
North Quarter Trend
South Quarter Trend
North Middle Trend

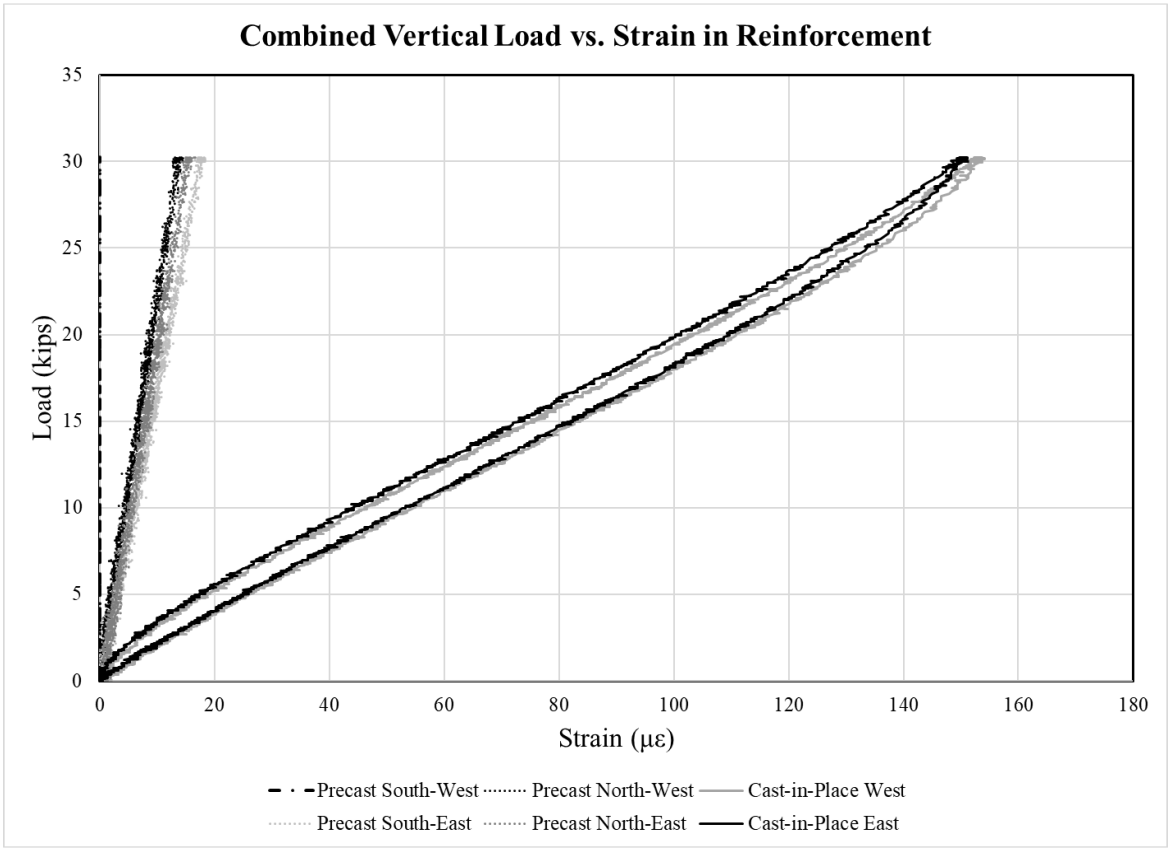
Combined Vertical Load vs. Strain in Reinforcement
Load (kips)
Strain (με)
Precast South-West
Precast North-West
Cast-in-Place West
Precast South-East
Precast North-East
Cast-in-Place East

Monotonic Test at 2,900,000 Cycles

Summary	
Number of Cycles Performed Before Test	2900001 cycles
Central Deflection of Specimen at 30-kips	0.018 in
Maximum Opening of Joint Between Beams	0.001 in
Maximum Reinforcement Strain in Precast	17 με
Maximum Reinforcement Strain in Cast-in-Place	170 με

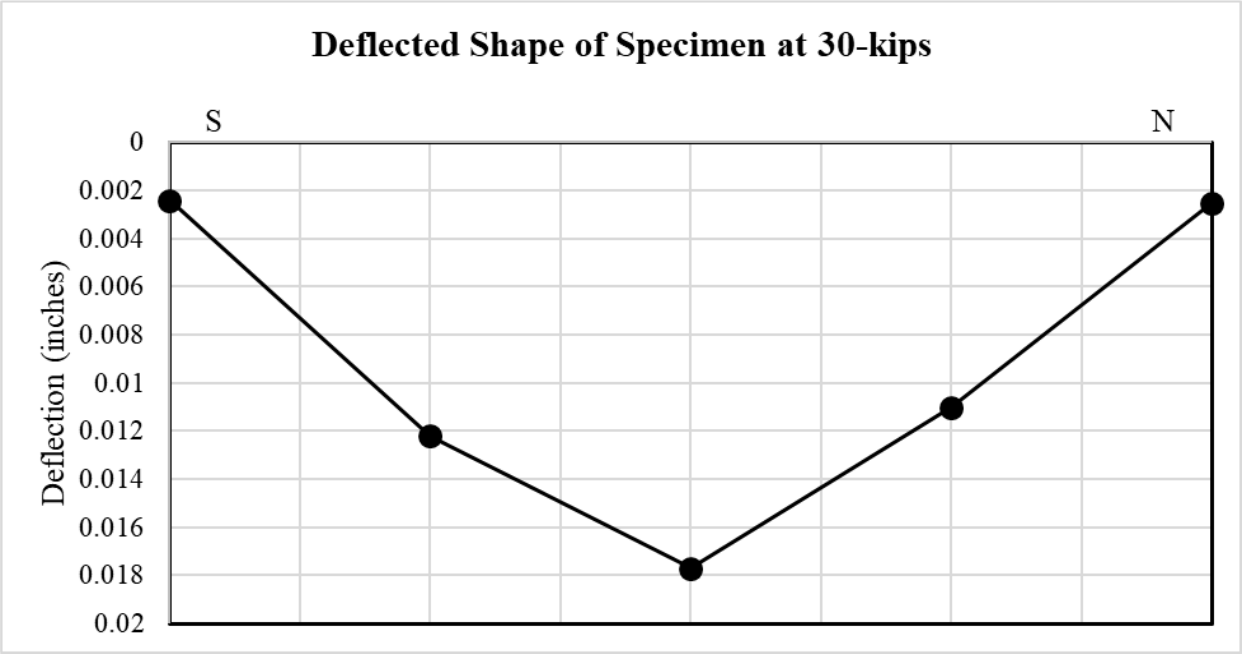

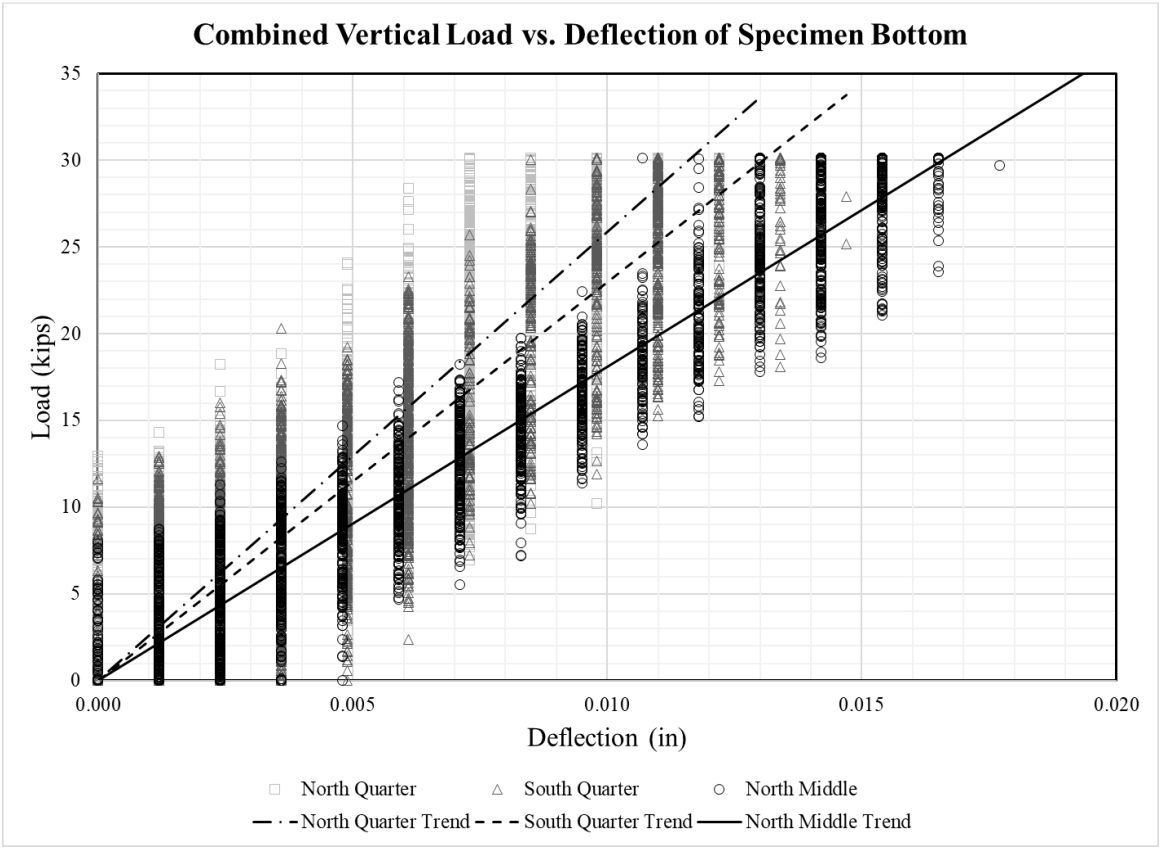
Combined Vertical Load vs. Deflection of Specimen Bottom
Load (kips)
Deflection (in)
0
5
10
15
20
25
30
35
0.000
0.005
0.010
0.015
0.020
North Quarter
South Quarter
North Middle
North Quarter Trend
South Quarter Trend
North Middle Trend

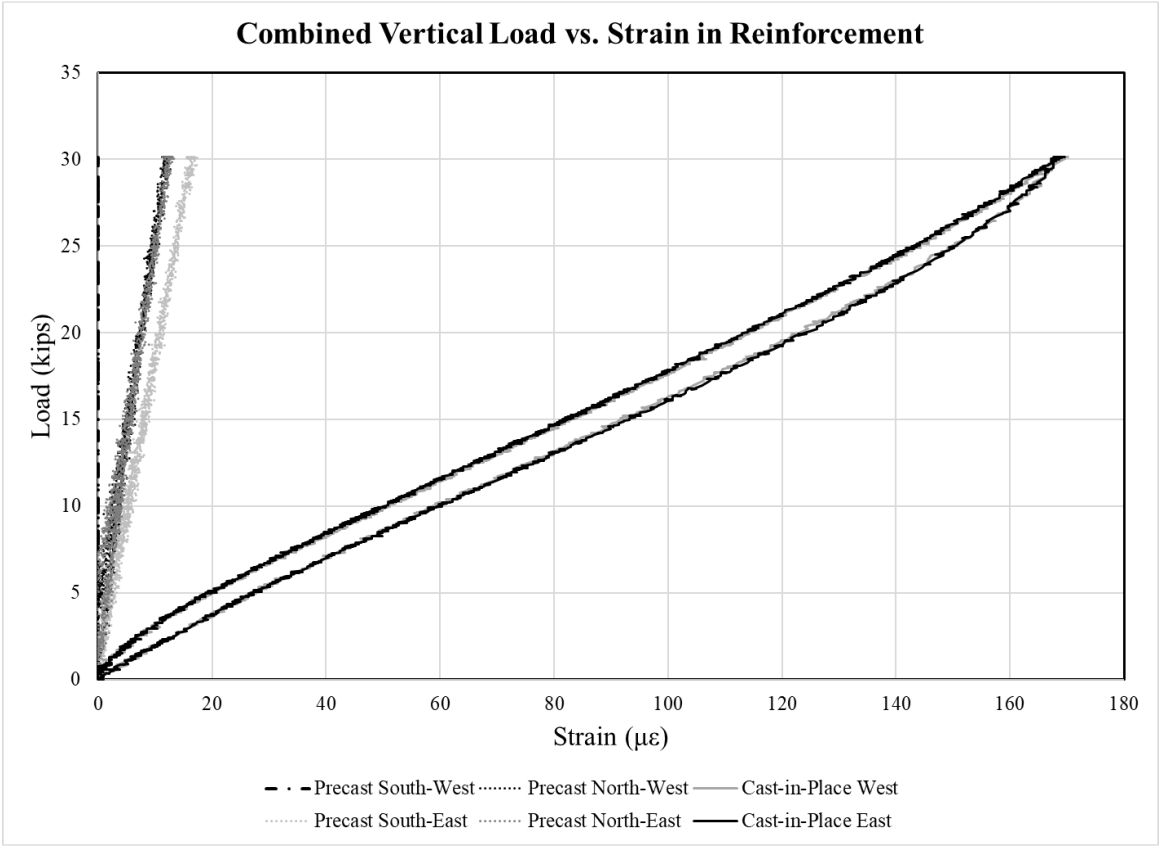
Combined Vertical Load vs. Strain in Reinforcement
Load (kips)
Strain (με)
0
5
10
15
20
25
30
35
0
20
40
60
80
100
120
140
160
180
Precast South-West
Precast North-West
Cast-in-Place West
Precast South-East
Precast North-East
Cast-in-Place East

Monotonic Test at 3,100,000 Cycles

Summary	
Number of Cycles Performed Before Test	3100001 cycles
Central Deflection of Specimen at 30-kips	0.014 in
Maximum Opening of Joint Between Beams	0.002 in
Maximum Reinforcement Strain in Precast	18 με
Maximum Reinforcement Strain in Cast-in-Place	237 με

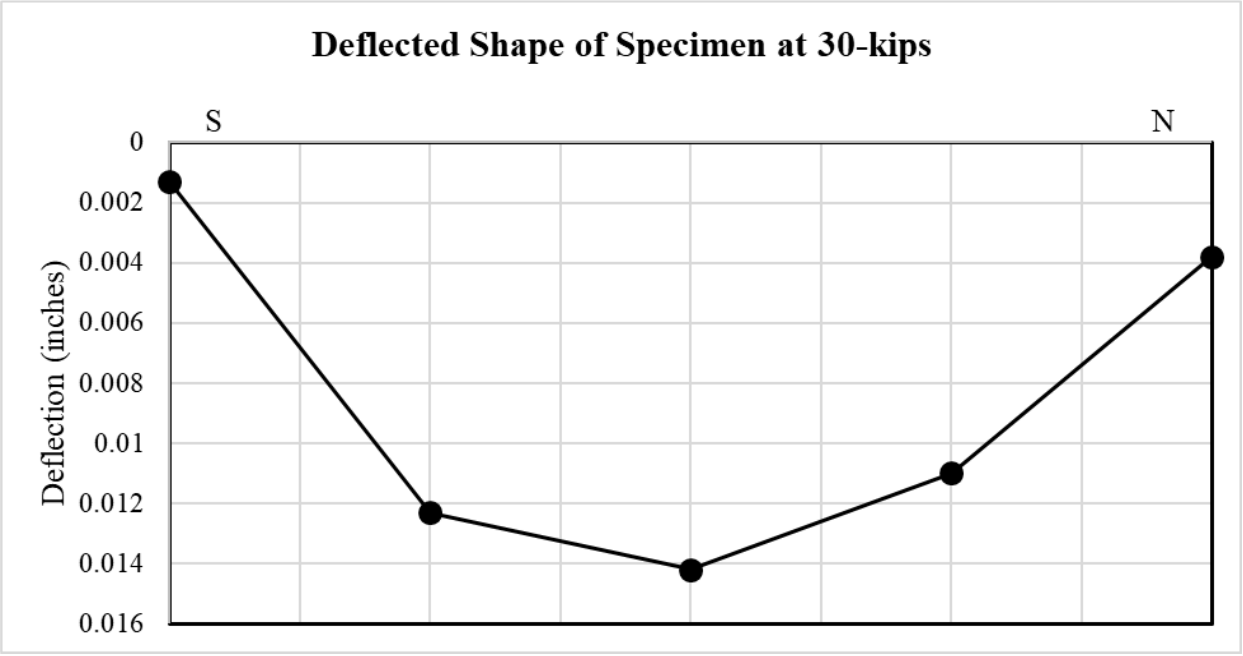

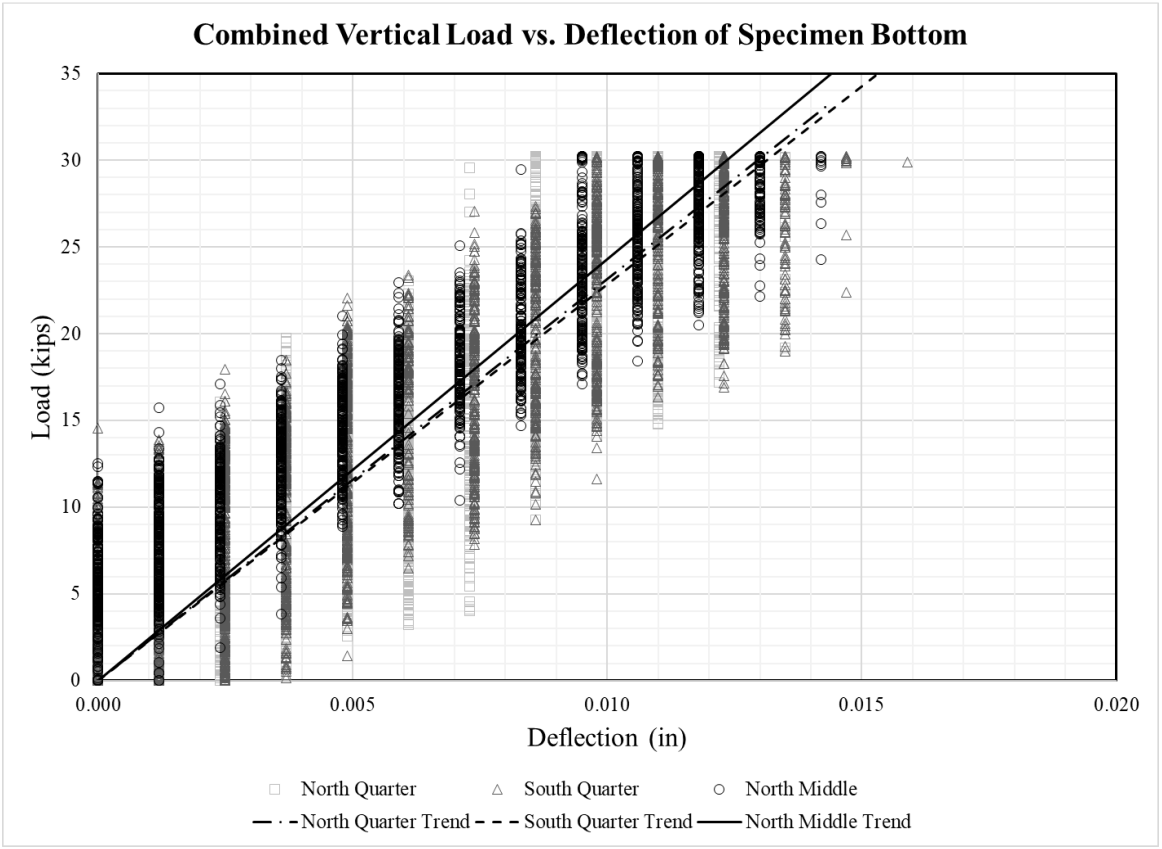
Combined Vertical Load vs. Deflection of Specimen Bottom
Load (kips)
Deflection (in)
0
5
10
15
20
25
30
35
0.000
0.005
0.010
0.015
0.020
North Quarter
South Quarter
North Middle
North Quarter Trend
South Quarter Trend
North Middle Trend

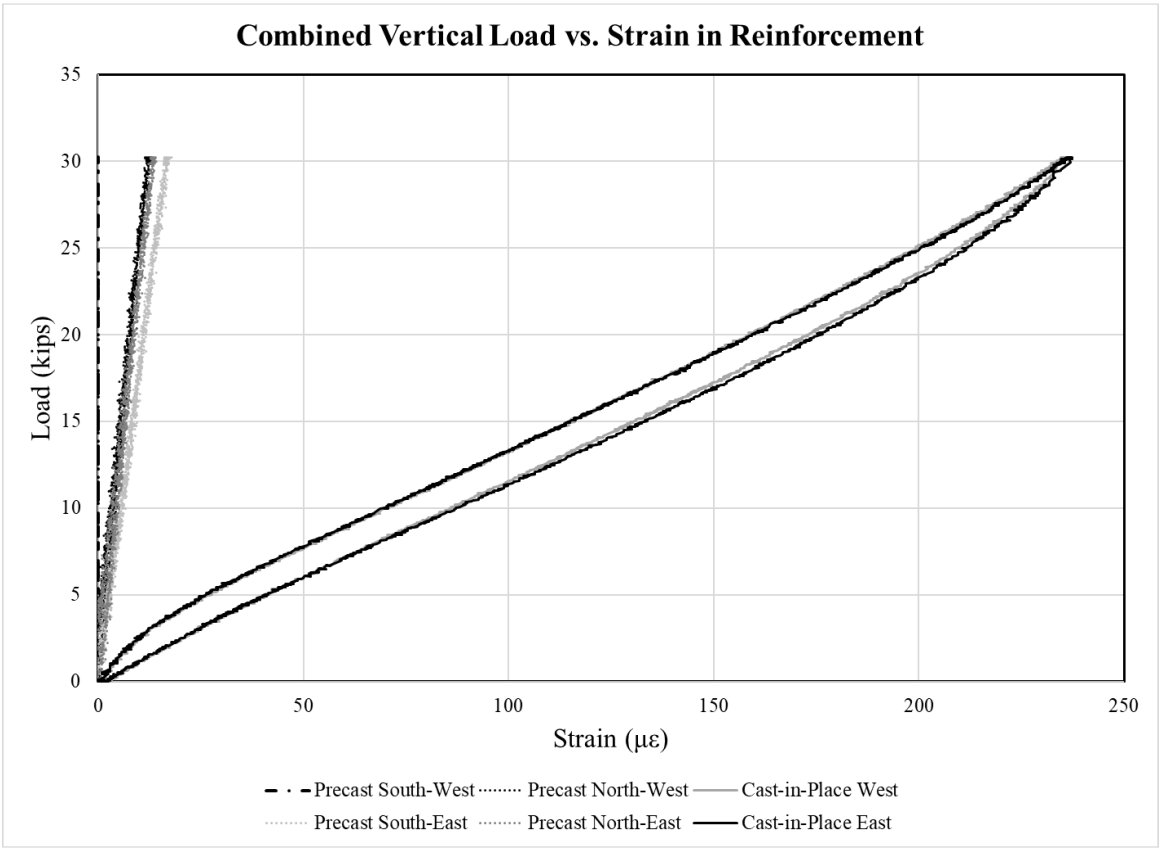
Combined Vertical Load vs. Strain in Reinforcement
Load (kips)
Strain (με)
0
5
10
15
20
25
30
35
0
50
100
150
200
250
Precast South-West
Precast North-West
Cast-in-Place West
Precast South-East
Precast North-East
Cast-in-Place East

Monotonic Test at 3,300,000 Cycles

Summary	
Number of Cycles Performed Before Test	3300000 cycles
Central Deflection of Specimen at 30-kips	0.018 in
Maximum Opening of Joint Between Beams	0.003 in
Maximum Reinforcement Strain in Precast	17 με
Maximum Reinforcement Strain in Cast-in-Place	429 με

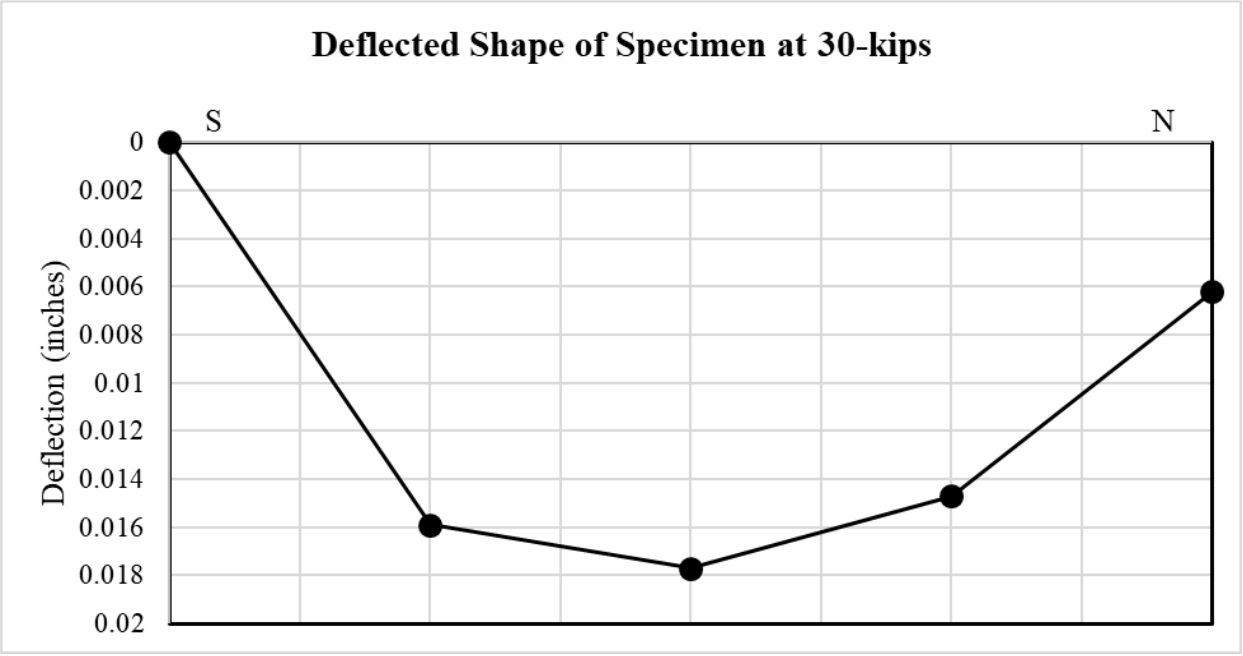

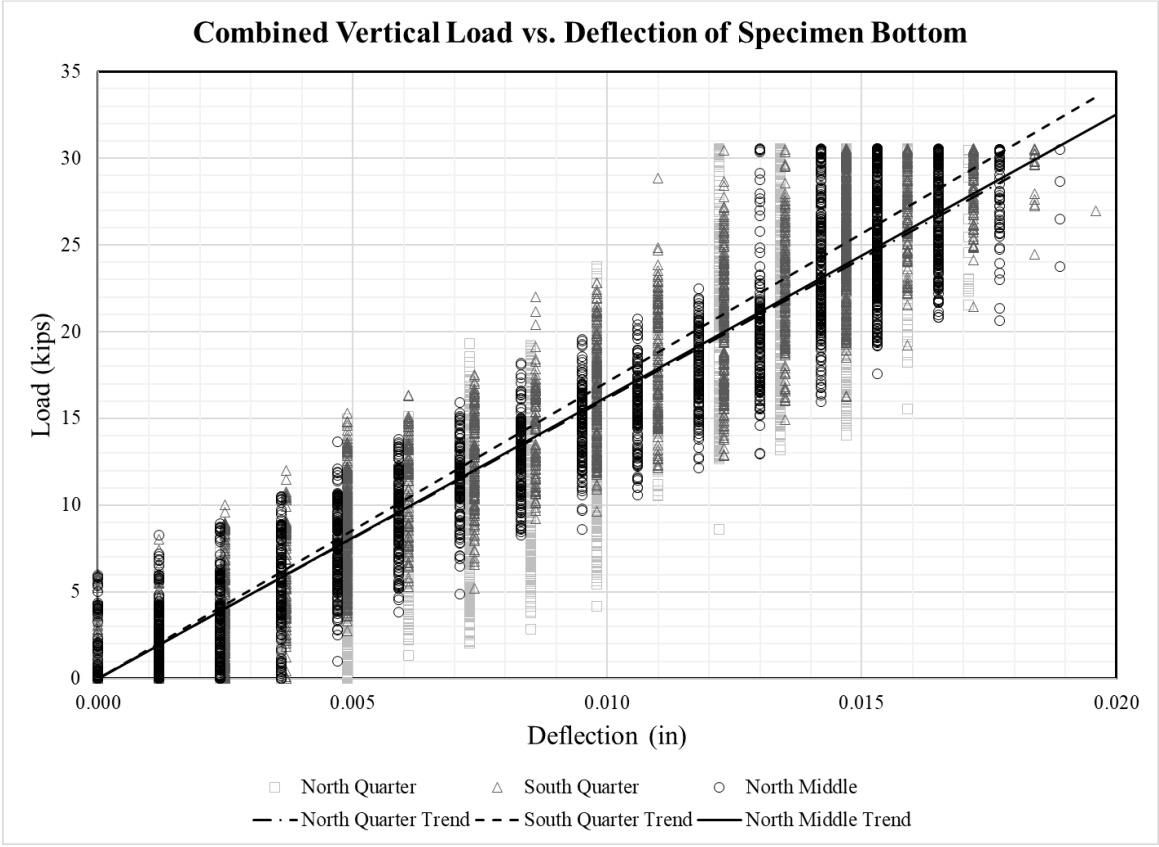
Combined Vertical Load vs. Deflection of Specimen Bottom
Load (kips)
Deflection (in)
0
5
10
15
20
25
30
35
0.000
0.005
0.010
0.015
0.020
North Quarter
South Quarter
North Middle
North Quarter Trend
South Quarter Trend
North Middle Trend


Combined Vertical Load vs. Strain in Reinforcement
Load (kips)
Strain (με)
0
5
10
15
20
25
30
35
0
50
100
150
200
250
300
350
400
450
Precast South-West
Precast North-West
Cast-in-Place West
Precast South-East
Precast North-East
Cast-in-Place East

Monotonic Test at 3,500,000 Cycles

Summary	
Number of Cycles Performed Before Test	3500000 cycles
Central Deflection of Specimen at 30-kips	0.02 in
Maximum Opening of Joint Between Beams	0.004 in
Maximum Reinforcement Strain in Precast	17 με
Maximum Reinforcement Strain in Cast-in-Place	514 με

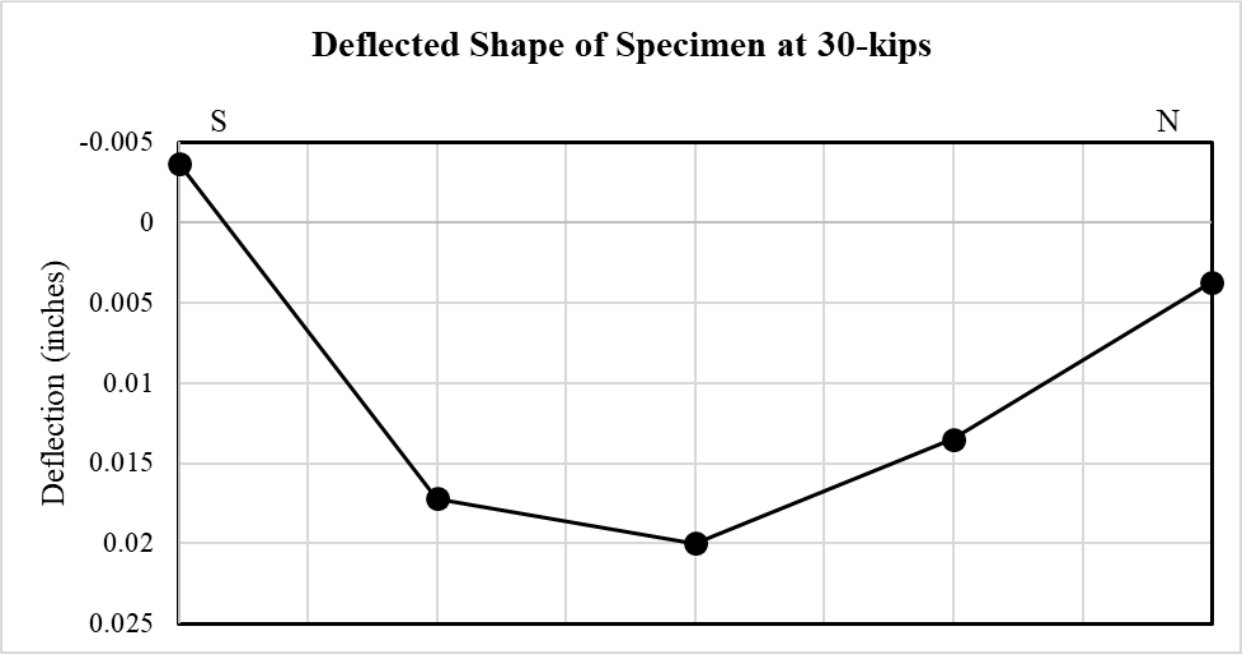

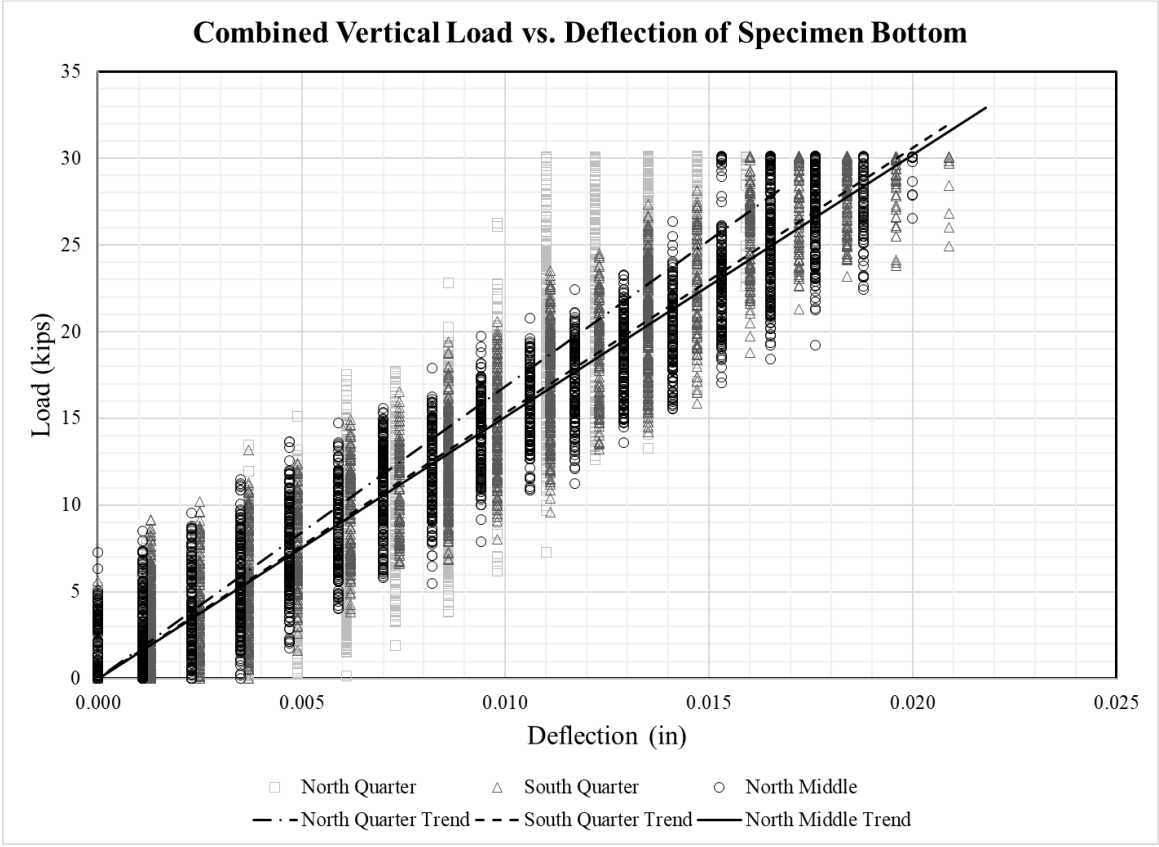
Combined Vertical Load vs. Deflection of Specimen Bottom
Load (kips)
Deflection (in)
0
5
10
15
20
25
30
35
0.000
0.005
0.010
0.015
0.020
0.025
North Quarter
South Quarter
North Middle
North Quarter Trend
South Quarter Trend
North Middle Trend


Combined Vertical Load vs. Strain in Reinforcement
Load (kips)
Strain (με)
0
5
10
15
20
25
30
35
0
100
200
300
400
500
600
Precast South-West
Precast North-West
Cast-in-Place West
Precast South-East
Precast North-East
Cast-in-Place East

Monotonic Test at 3,650,000 Cycles

Summary	
Number of Cycles Performed Before Test	3650001 cycles
Central Deflection of Specimen at 30-kips	0.02 in
Maximum Opening of Joint Between Beams	0.004 in
Maximum Reinforcement Strain in Precast	18 με
Maximum Reinforcement Strain in Cast-in-Place	546 με

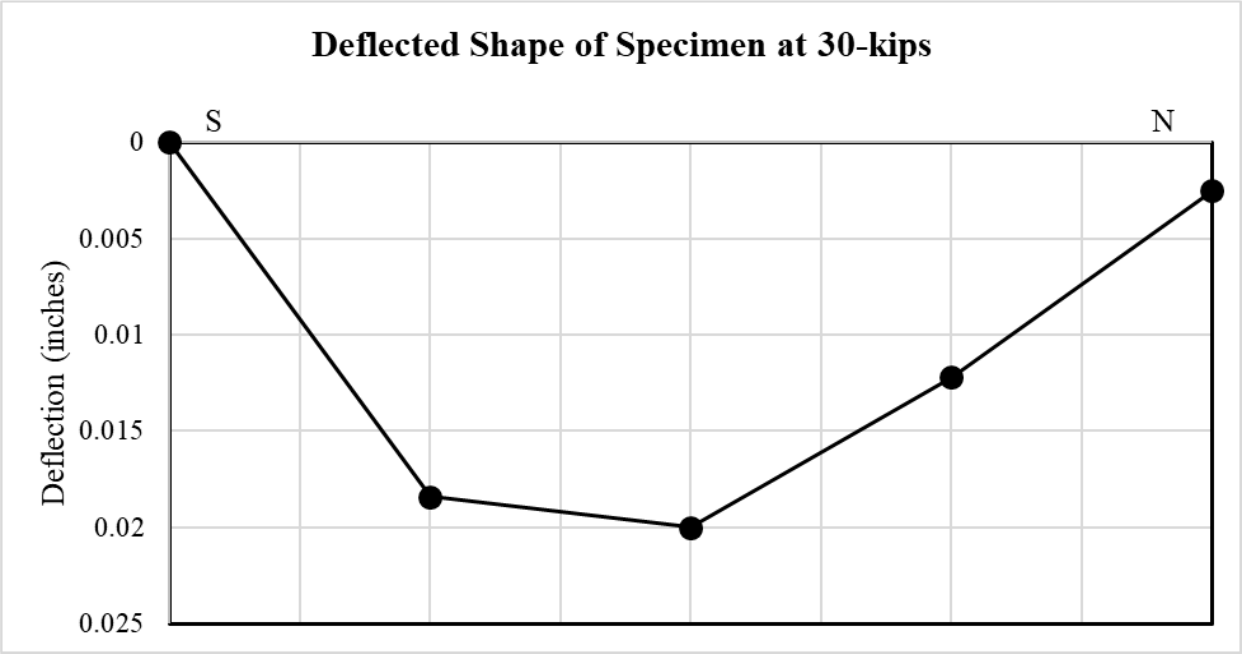

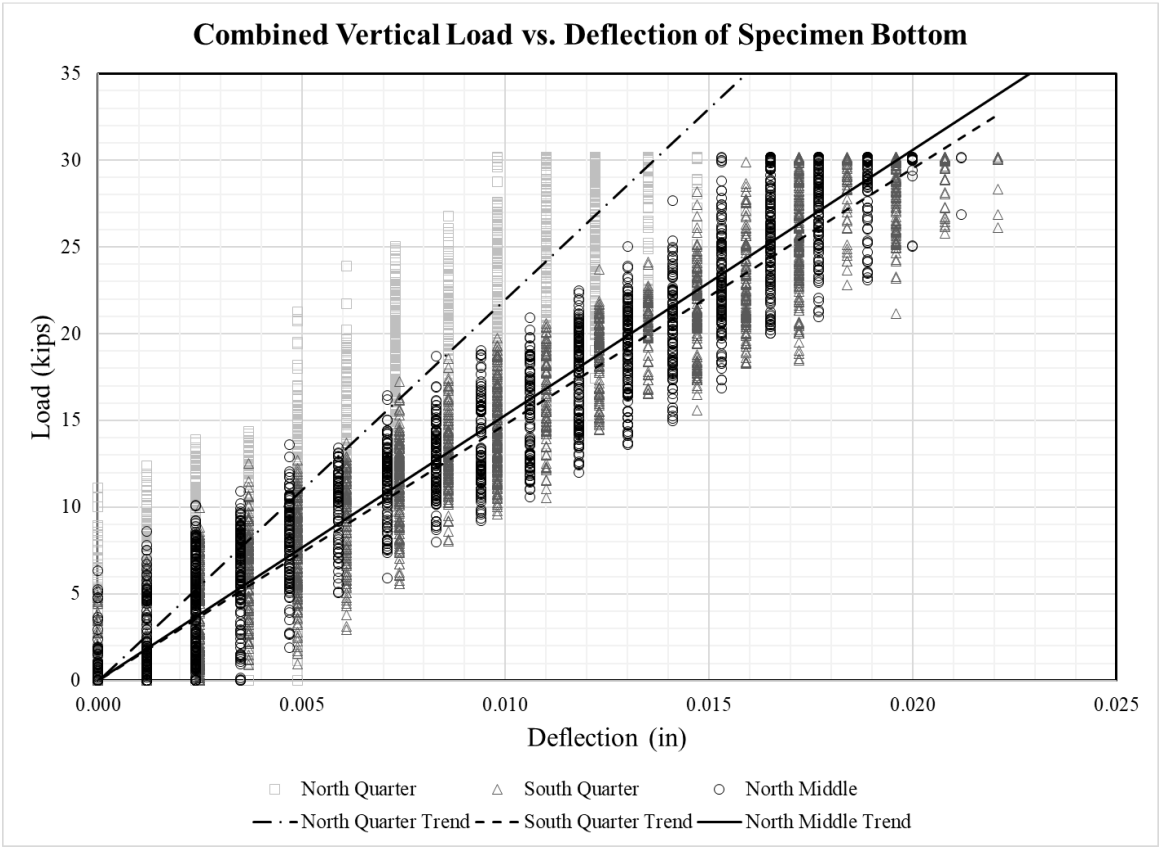
Combined Vertical Load vs. Deflection of Specimen Bottom
Load (kips)
Deflection (in)
0
5
10
15
20
25
30
35
0.000
0.005
0.010
0.015
0.020
0.025
North Quarter
South Quarter
North Middle
North Quarter Trend
South Quarter Trend
North Middle Trend

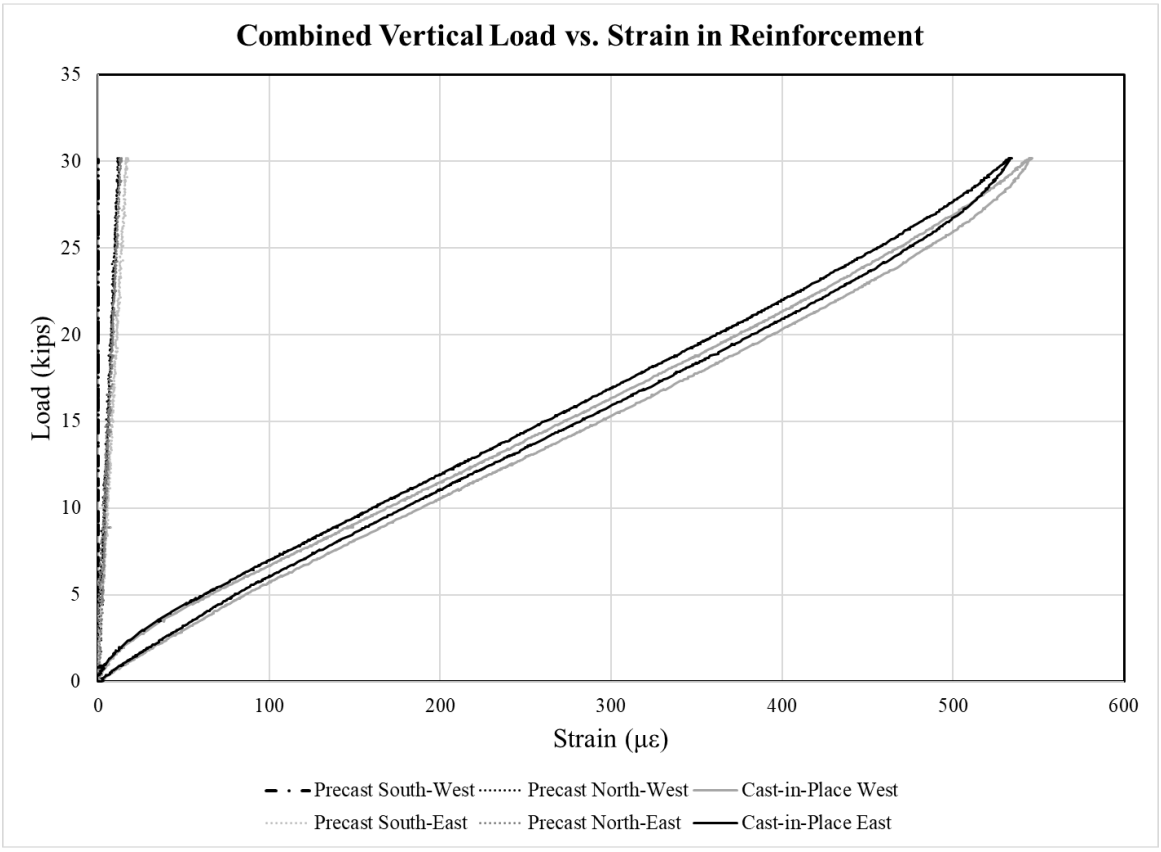
Combined Vertical Load vs. Strain in Reinforcement
Load (kips)
Strain (με)
0
5
10
15
20
25
30
35
0
100
200
300
400
500
600
Precast South-West
Precast North-West
Cast-in-Place West
Precast South-East
Precast North-East
Cast-in-Place East

APPENDIX F: INVERTED T-BEAM CALCULATIONS

Inputs:

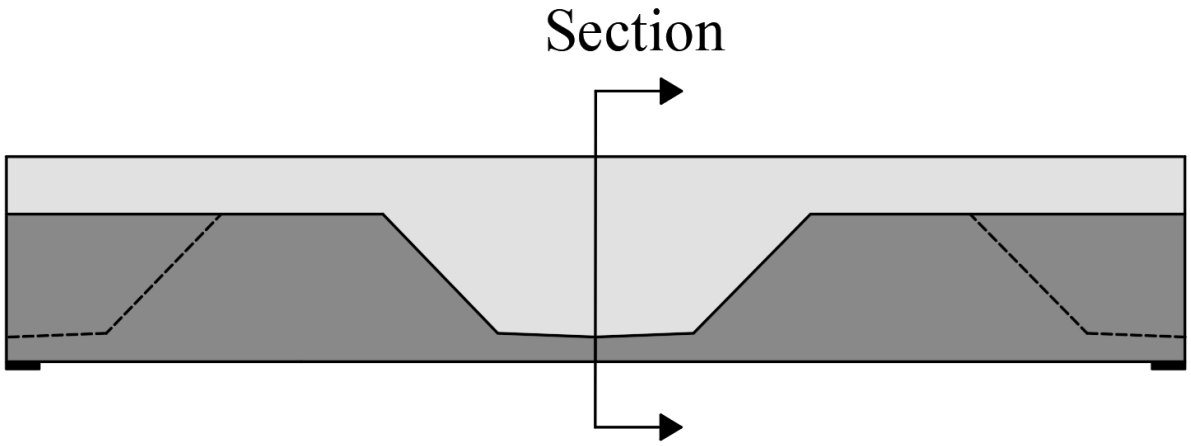

Geometric Properties

	Gross Conc.	Trans (n=8.33)
Area (in^2)	1032.0	1050.8
Inertia (in^4)	39753.5	41257.8
y_t (in)	10.8	10.8
y_b (in)	10.8	10.7
S_t (in^3)	3698.0	3812.9
S_b (in^3)	3698.0	3863.3

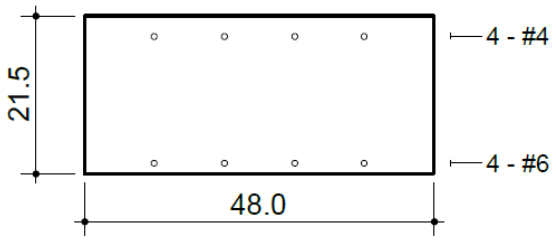

Crack Spacing

2 x dist + 0.1 d_b /ρ

Loading (N,M,V + dN,dM,dV)

0.0 , -0.0 , 0.0 + 0.0 , 1.0 , 0.0

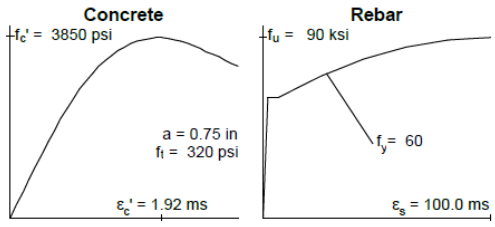

All dimensions in inches
Clear cover to reinforcement = 1.00 in

Inverted T-Beam Specimen

2018/4/18

Cracking:

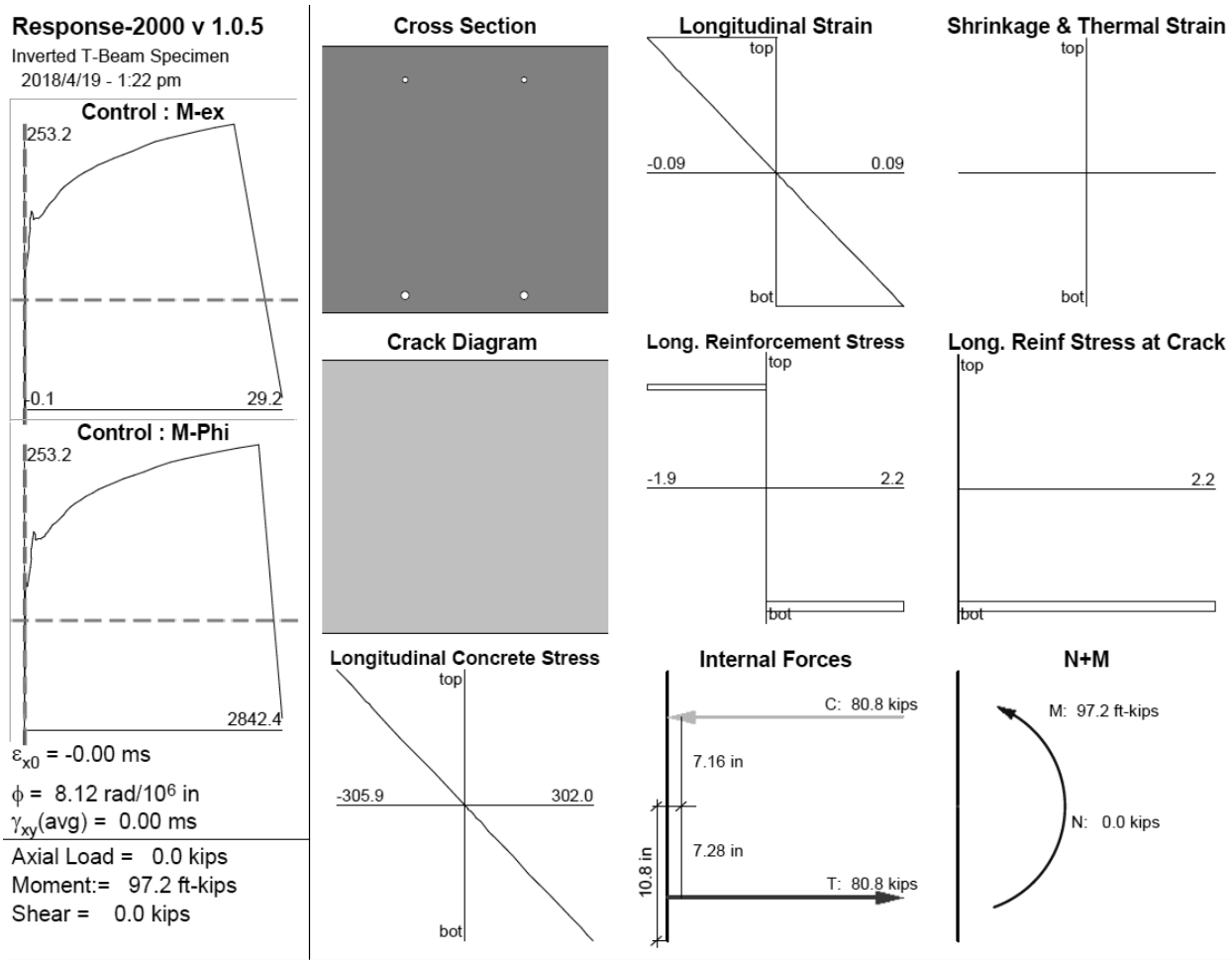
Response-2000 v 1.0.5
Inverted T-Beam Specimen
2018/4/19 - 1:22 pm
Control : M-ex
253.2
-0.1
29.2
Control : M-Phi
253.2
2842.4
ε_{x0} = -0.00 ms
ϕ = 8.12 rad/10^6 in
γ_{xy}(avg) = 0.00 ms
Axial Load = 0.0 kips
Moment:= 97.2 ft-kips
Shear = 0.0 kips
Cross Section
Crack Diagram
Longitudinal Concrete Stress
top
-305.9
302.0
bot
Longitudinal Strain
top
-0.09
0.09
bot
Long. Reinforcement Stress
top
-1.9
2.2
bot
Internal Forces
C: 80.8 kips
7.16 in
7.28 in
10.8 in
T: 80.8 kips
Shrinkage & Thermal Strain
top
bot
Long. Reinf Stress at Crack
top
2.2
bot
N+M
M: 97.2 ft-kips
N: 0.0 kips

Yielding:

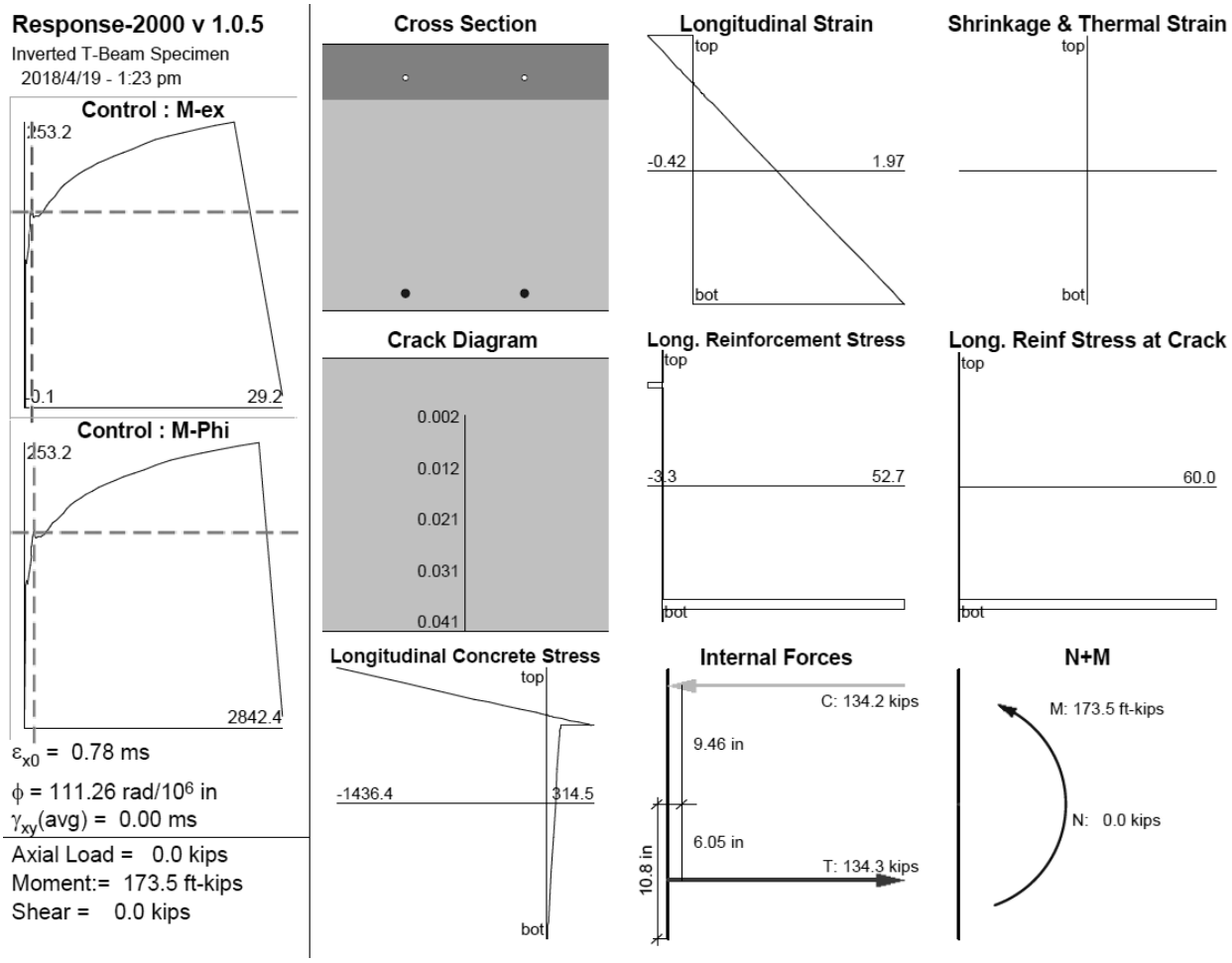
Response-2000 v 1.0.5
Inverted T-Beam Specimen
2018/4/19 - 1:23 pm
Control : M-ex
253.2
-0.1
29.2
Control : M-Phi
253.2
2842.4
ε_{x0} = 0.78 ms
ϕ = 111.26 rad/10^6 in
γ_{xy}(avg) = 0.00 ms
Axial Load = 0.0 kips
Moment:= 173.5 ft-kips
Shear = 0.0 kips
Cross Section
Crack Diagram
0.002
0.012
0.021
0.031
0.041
Longitudinal Concrete Stress
top
-1436.4
314.5
bot
Longitudinal Strain
top
-0.42
1.97
bot
Long. Reinforcement Stress
top
-3.3
52.7
bot
Internal Forces
C: 134.2 kips
9.46 in
6.05 in
T: 134.3 kips
10.8 in
Shrinkage & Thermal Strain
top
bot
Long. Reinf Stress at Crack
top
60.0
bot
N+M
M: 173.5 ft-kips
N: 0.0 kips

Ultimate:

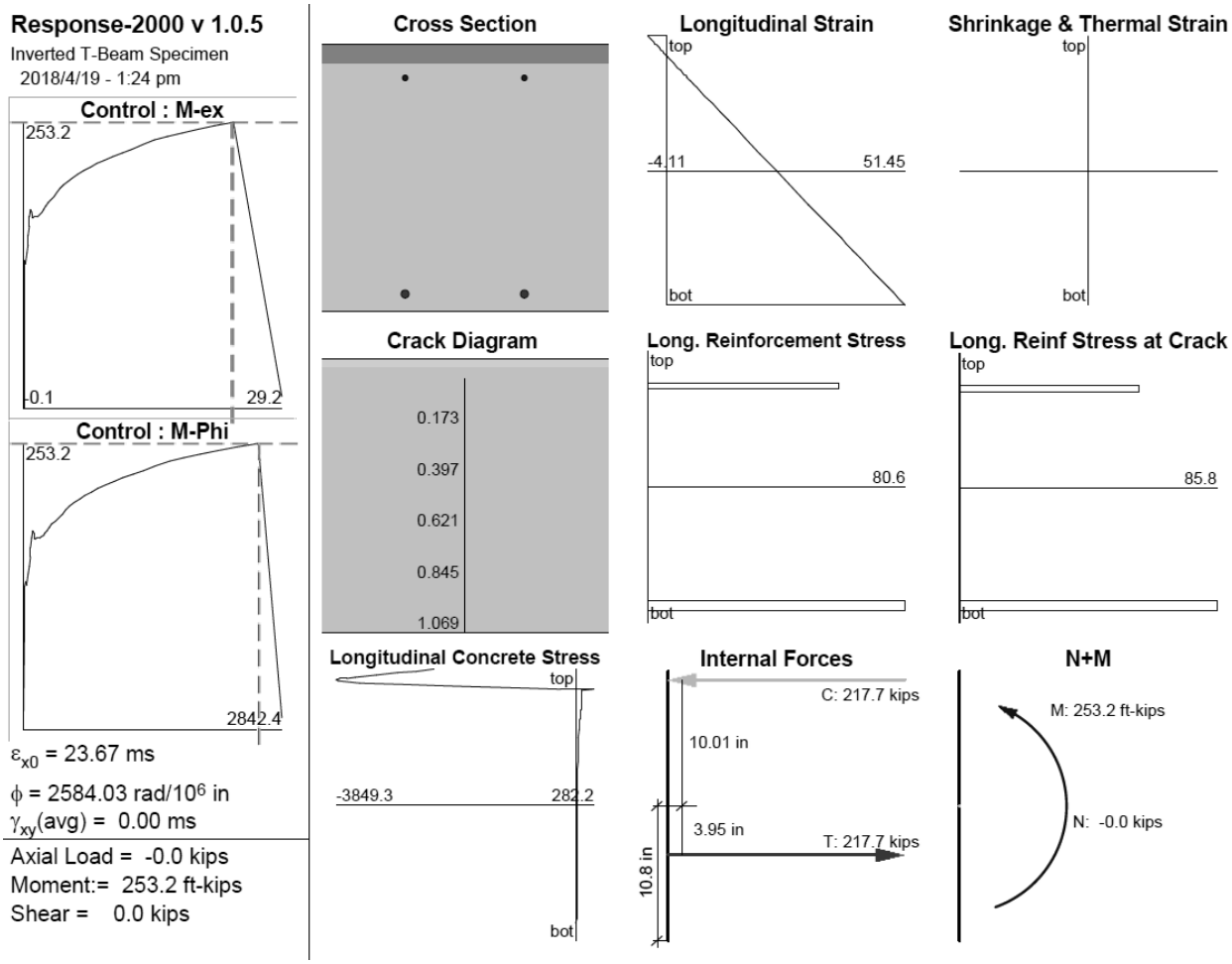
Response-2000 v 1.0.5
Inverted T-Beam Specimen
2018/4/19 - 1:24 pm
Control : M-ex
253.2
-0.1
29.2
Control : M-Phi
253.2
2842.4
ε_{x0} = 23.67 ms
ϕ = 2584.03 rad/10^6 in
γ_{xy}(avg) = 0.00 ms
Axial Load = -0.0 kips
Moment:= 253.2 ft-kips
Shear = 0.0 kips
Cross Section
Crack Diagram
0.173
0.397
0.621
0.845
1.069
Longitudinal Concrete Stress
top
-3849.3
282.2
bot
Longitudinal Strain
top
-4.11
51.45
bot
Long. Reinforcement Stress
top
80.6
bot
Internal Forces
C: 217.7 kips
10.01 in
3.95 in
T: 217.7 kips
10.8 in
Shrinkage & Thermal Strain
top
bot
Long. Reinf Stress at Crack
top
85.8
bot
N+M
M: 253.2 ft-kips
N: -0.0 kips